Acta Biologica Szegediensis

Volume 62(1):1-6, 2018
Acta Biologica Szegediensis
http://abs.bibl.u-szeged.hu/index.php/abs
DOI:10.14232/abs.2018.1.1-6

ARTICLE

'Sensory pad'- A novel chemoreceptive device in Hilsa (*Tenualosa ilisha*) to support its amphihaline attribute

Subhendu Kumar Chatterjee[1,2], Chandan Malick[1,3], Samir Bhattacharya[2], Rakesh Kundu[3], Vettath Raghavan Suresh[4], Surjya Kumar Saikia[1*]

[1]Aquatic Ecology and Fish Biology Laboratory, Department of Zoology, Visva-Bharati University, Santiniketan-731235, India
[2]Molecular Endocrinology Laboratory, Department of Zoology, Visva-Bharati University, Santiniketan-731235, India
[3]Cell Signaling Laboratory, Department of Zoology, Visva-Bharati University, Santiniketan-731235, India
[4]Riverine Ecology and Fisheries Division, Central Inland Fisheries Research Institute, Barrackpore, Kolkata-700120, India

ABSTRACT Hilsa, *Tenualosa ilisha* is an amphihaline migratory fish that performs spawning migration to selected freshwater rivers in Indo-Pacific region. It is not clear what force triggers its migration. In this paper, we attempted to describe the features of outer integument from its head region as chemosensory site which appears to play significant role in its upstream migration. We found that this area (termed as snout) has very soft and scale less tissue oriented with pit like grooves named as 'epidermal pit'. Around these pits, odorant receptor G-protein subunits (Gαq, Gαs/olf and Gαo) have been substantially localized. Use of DASPEI also traced this area with neuronal existence. These features in the snout likely to contribute for chemosensory requirements of the fish during upstream migration. Considering such findings, we named this area of snout as 'sensory pad'. Its position at the forefront of olfactory organ and brain may have important role in facilitating sensory reception by the fish swimming upstream to the river.

Acta Biol Szeged 62(1):1-6 (2018)

KEY WORDS
chemosensory
epidermis
fish migration
odorant receptor

ARTICLE INFORMATION
Submitted
30 January 2018.
Accepted
11 April 2018.
***Corresponding author**
E-mail: surjyasurjya@gmail.com

Introduction

The Indian shad of hilsa, *Tenualosa ilisha* (Order: Clupeiformes; Family: Clupeidae) is an amphihaline migratory fish with remarkable commercial importance in the Indo-Pacific region, especially in India, Bangladesh and Myanmar. This anadromous fish migrates to freshwater rivers of India and Bangladesh from sea during the south-west monsoon and consequent flooding of the rivers for spawning and breeding (Ahsan et al. 2014). The major migratory period of this fish has been classified as 'summer spawning migration' (a long upstream migratory period during July-October) every year. After their preparative hauls near the coastal areas for some time (body weight 450-1200 g), shoals of sexually matured adults enter into estuarine habitat heading towards riverine freshwater for breeding. They breed in certain selected stretches of riverine freshwater identified as suitable breeding zones. This is completed within 3-4 months. The immature juveniles grow in river channels and return to the sea where they spend 1-1.5 years for feeding and growth. Most likely, the anadromous stocks that ascend from sea to the river during the breeding season also return to sea after spawning (Panhwar et al. 2011). In marine water, the juveniles grow to adults and resume upstream migration once they attain sexual maturity. This is in brief the 'migratory cycle' of hilsa.

It is known that amphihaline migratory fish like salmon tracks odour from the natal river during spawning migration. For example, adults of Arctic charr are attracted to water quality and can discriminate between odours from different charr populations (Døving et al. 1974; Selset and Døving 1980). Hasler and Wisby (1951) proposed olfactory imprinting hypothesis for such odour discrimination, where various chemosensory receptor cells of olfactory system can identify natal odours for

Abbreviations: DAPI: 4',6-diamidino-2-phenylindole; DASPEI: 2-(4-(dimethylamino)styryl)-N-ethylpyridinium iodide; EP: epidermal pits; FITC: fluorescein isothiocyanate; PB: phosphate buffer; PBS: phosphate buffer saline; PFA: paraformaldehyde; SEM: scanning electron microscopy; SCCs: solitary chemosensory cells; ORs: odorant receptors;

migration. During spawning migration, they are guided to their natal habitat with the help of such odours. However, in hilsa being a successful migratory fish, such information on migration are not available. Although, olfactory organ is a common player for migration in fish, in hilsa, we observed a soft and scale less outer integument area just above the neurocranium, the function of which is not known. We assume that this area might have significant relevance to its migration and therefore an attempt was made to reveal chemosensory details from this area of hilsa.

Materials and Methods

Study sites and sample collection

Freshwater adult hilsa (25-30 cm in total length) were collected from Hooghly, a natural freshwater habitat of hilsa, and also a distributary channel of river Ganga that flows through West Bengal, India and empties to Bay of Bengal. A total of 30-35 samples were collected and preserved immediately in ice avoiding any physical aberrations to its body. We collected tissues from the outer integument from the area above the neurocranium. This portion on the head is soft and scale less with identifiable outline (Figs. 1a, b). For our convenience, we termed it as 'snout'.

Sample preparation and SEM

The tissue sections collected from snout of at least four fishes were washed with 0.1 M PB (pH 7.4) with the help of fine brush under a binocular microscope (Fig. 1c). This was followed by removal of mucus contents through treating the sample with 0.1 M sucrose solution for 15-20 min. After repeated washing, the samples were kept in 2.5-3.0% glutaraldehyde in cacodylate buffer for 24 hours at 4 °C. Subsequently, samples were washed with 0.1 M PBS to remove external fixative, and preceded to standard dehydration steps with graded acetone each with two changes for 15 min. These were dipped in acetone (acetone was passed through $CuSO_4$ and filtrate was taken for use) for 15 min and followed by critical point drying and gold plating. SEM was done in a JEOL electron microscope (NEHU, Shillong, India).

Sample preparation and immunofluorescence study

From the preserved stock of fishes, tissue samples (3 replicates) from snout were treated with physiological saline, followed by fixation in a solution of 4% PFA in 0.1 M PB (pH 7.2) for 18-20 h at 4 °C, rinsed with 0.1 M PBS dehydrated through a graded ethanol series and embedded in paraffin (Sigma-Aldrich, USA). Serial sections at ~7 μm thickness were prepared using a rotary microtome, mounted on glass slides (Riviera Matsunami, Osaka, Japan), air-dried at 4 °C and used for immunofluorescence. Deparaffinized and hydrated sections from snout were washed in chilled PBS and permeabilized with 0.5% Triton X-100 in PBS for 20 min at room temperature. These sections were incubated in blocking buffer (0.5% Triton X-100 and 1% bovine serum albumin in PBS) for one hour at room temperature and then probed overnight at 4 °C with respective mammalian polyclonal G-protein subunits (Gαq, Gαs/olf, Gαo, Gαi; Santa Cruz Biotechnology) primary antibody diluted in blocking buffer (1:100). Simultaneously, a small piece of tissue (whole mount) was also processed along with the sections. After 3 washes in PBS, slides were incubated with the secondary antibody (FITC conjugated goat anti-rabbit IgG, Thermo Scientific) in diluted blocking buffer (1:100) for 1 h at room temperature in the dark. Slides were then washed 4 times in PBS. Vectashield mounting medium with DAPI (Vector Labs) was applied to mount glass cover slips onto the slides.

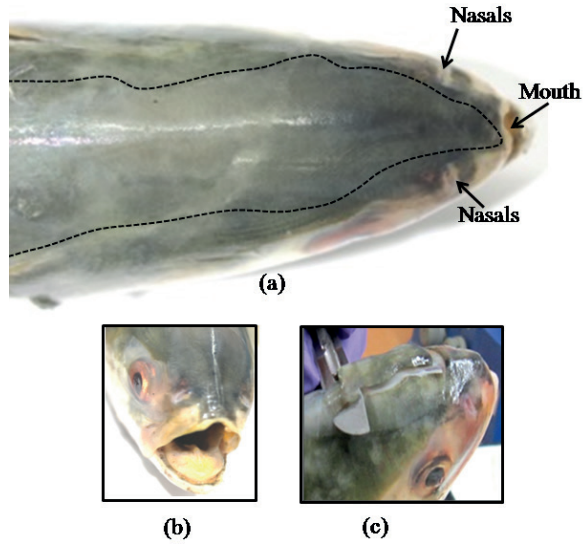

Figure 1. Sensory pad on snout region of *Tenualosa ilisha*. (a) The sensory pad on snout (marked with dotted line) showing positions for nasal pairs and mouth, (b) Frontal view of sensory pad and (c) Collection of tissues from sensory pad.

We used DASPEI that stains different type of chemosensory neurons (Leise 1996). At least three sections from the snout tissues were rinsed with 25 μg/ml DASPEI, washed in distilled water and kept in room temperature in the dark.

Processed sections were observed under Leica inverted microscope (DMi8) and Leica confocal microscope (DMi8).

Results

The SEM of snout showed that the snout is decorated

with numerous openings, described as 'epidermal pits' (EPs) and arranged in a more or less regular fashion in hilsa (Fig. 2a). The average diameter of each EP is 5-10 μm with uniformly oval or round in shape and opens into the epidermal surface through a circular mouth with slightly elevated rim from the surface. The positive labelling of these pits with DASPEI also showed their neural zones around EPs under fluorescent microscope (Fig. 2b). SEM further showed numerous SCCs around the adjacent areas to the openings of EP (Fig. 2c). Histologically, EPs are spread up to the dermal tissue proper as long groove (Fig. 2d).

On treating with FITC and DAPI, the odorant receptors, Gαq and Gαs/olf were found highly immunoreactive with Gαq and Gαs/olf antibodies. The Figs. 3(a-c) and Figs. 3(d-f) represent Gαq labelled and Gαs/olf labelled areas on the snout respectively. The Gαq proteins are expressed close to the surroundings of the EP, whereas, the Gαs/olf proteins expressed not only around EP, but beyond the EPs on the epidermal surface. Similarly, in Figs. 4(a-c) and Figs. 4(d-f), the Gαq and Gαi3 labelled areas are shown. It is clear, that Gαo was expressed around the EPs, whereas, Gαi3 did not show remarkable expression around EP in the snout. All the DAPI and FITC conjugated regions were merged and found to be localized to ensure their cellular expression in the snout.

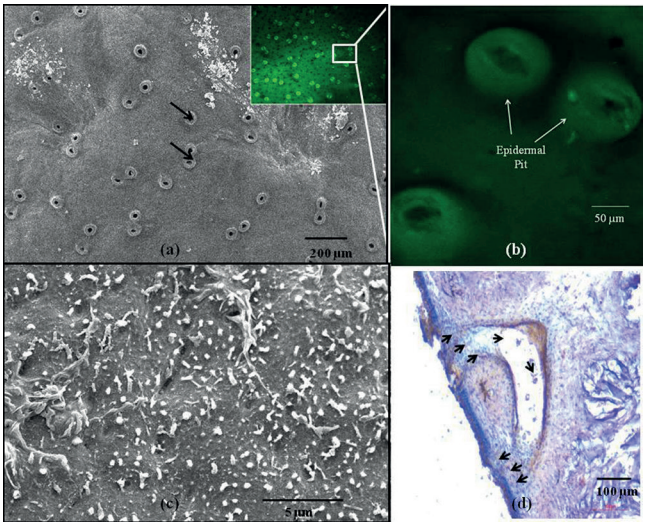

Figure 2. Structural and functional relevance of sensory pad in the snout region of *Tenualosa ilisha*. (a) Scanning electron microscopic view of epidermal pits. Two of such pits marked with dark arrows. DASPEI labelled epidermal pits (from Malick et al. 2018) are shown in inset. (b) Enlarged view of DASPEI labelled epidermal pits (from Malick et al. 2018). (c) Solitary chemosensory cells (SCCs) on the sensory pad of snout. (d) Groove of epidermal pit traversed to tissue proper. Black arrows show the openings of epidermal pits. (Revised figures from Malick et al. (2018) have been included to clarify the structural relevance of snout. The figures were added with due permission from authors).

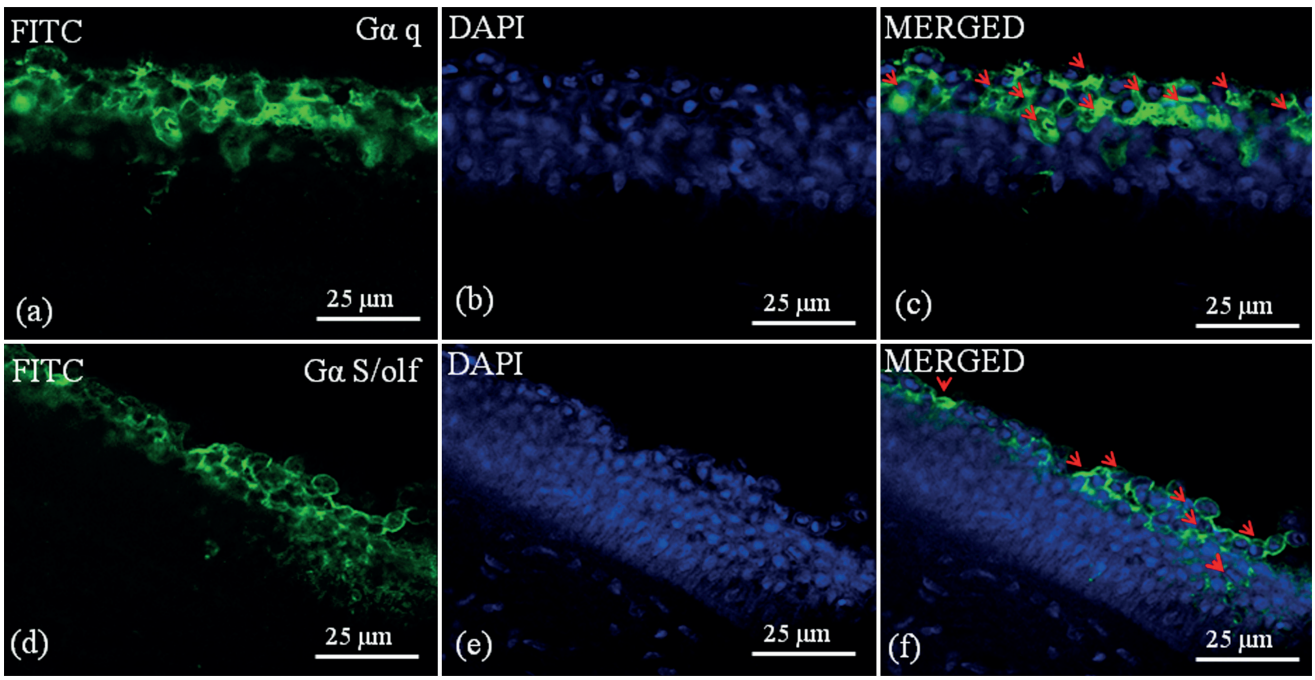

Figure 4. Expression of Gαq and Gαs/olf in sensory pad of snout region of *Tenualosa ilisha*. (a-c) Immunofluorescence of snout against Gαq and (d-f) Gαs/olf antisera using FITC and DAPI. FITC and DAPI are merged to localize cells and antibody labelled proteins. Arrows indicate areas where Gαq and Gαs/olf are highly expressed.

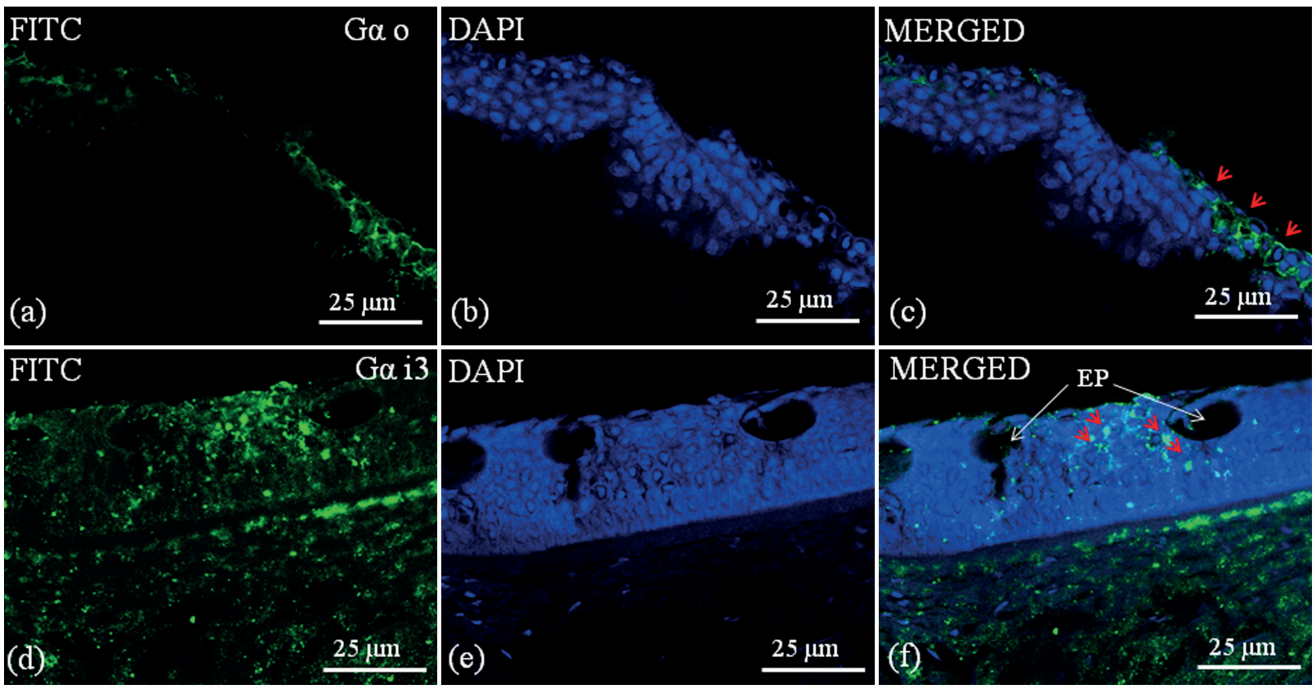

Figure 3. Expression of Gαo and Gαi3 on sensory pad of snout region in *Tenualosa ilisha*. (a-c) Immunofluorescence of snout epidermis against Gαo and (d-f) Gαi3 antisera using FITC and DAPI. FITC and DAPI are merged to localize cells and antibody labelled proteins. Arrows indicate areas where Gαo and Gαi3 are highly expressed.

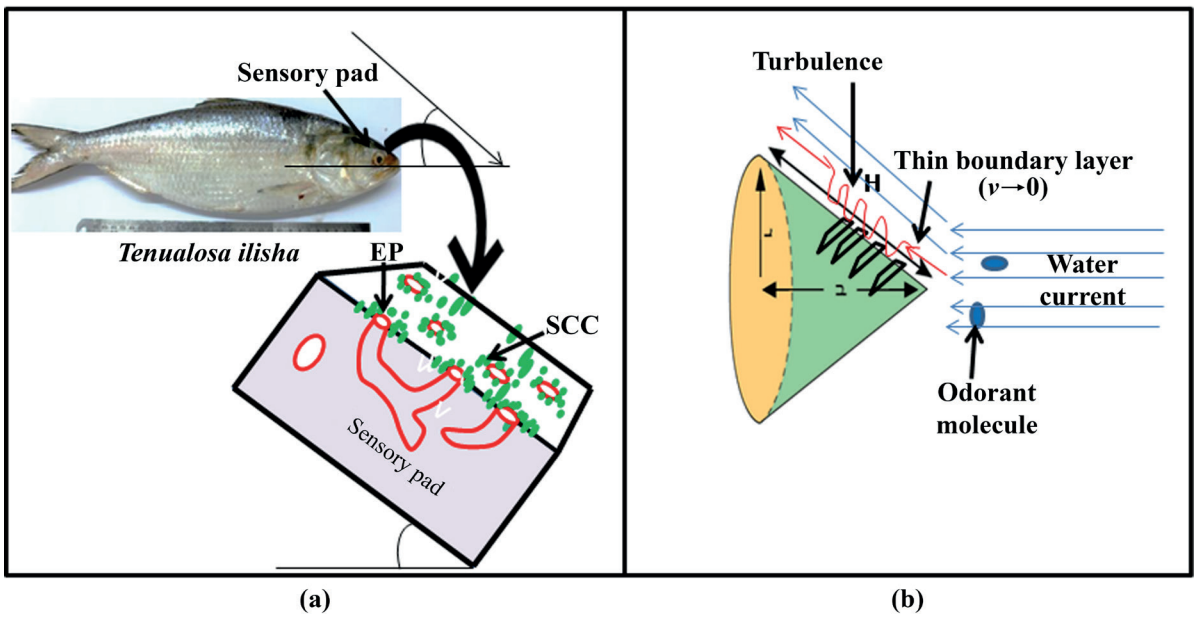

Figure 5. Hypothetical explanation on the interaction between sensory pad and natural ambience in *Tenualosa ilisha*. (a) Schematic diagram showing the slope of the sensory pad with sensory arrangement on the snout of hilsa (b) Possible explanation of the role of the cone shaped head with sensory arrangement in hilsa. This arrangement may create turbulence and thin boundary layer while swimming against water current to facilitate odorant reception. (EP: epidermal pit; SCC: solitary chemosensory cells).

Discussion

In this study, the structures of the snout of hilsa from freshwater habitat were studied. It was evident that snout of adult hilsa has a soft and dark fleshy area of about 12 mm^2 above the neurocranium. This area seems to face the water current when the fish swims upstream. The pit-like structure, called 'the epidermal pit' is oriented in such a way that the mouth of the pit opens to the exterior against the water current. Histological studies also confirmed that the grooves originating from epidermal pits traverse through tissue proper and open into the exterior, probably allowing water to pass through it. This is a unique arrangement not reported from any other fishes (Fig. 5a). What is more, the areas around the pit are found to be rich in SCCs. These cells are also widely scattered throughout this soft pad in the snout. From the morphological point of view, this kind of arrangement is assumed to be associated to sensory functions. Kotrschal (1992) reported that SCCs occur scattered within the epidermis of lampreys, a successful migratory fish. In amphibian, these were reported to be present in ventral skin and used to sense salt (Nagai et al. 1999). Mammals have it in their oral cavity (Sbarbati et al. 2000) as well as in respiratory epithelium of nasal passage (Saundersa et al. 2014) to sense odour. In hilsa, therefore, its presence in this area justifies the feature of chemosensory function carried out by SCCs. This is further supported by DASPEI labelling indicating existence of neuronal functions in this area.

To ascertain the chemosensory role, we have attempted to trace G-proteins subunits associated with odorant receptor or olfaction. Four of them, namely, Gαs/olf, Gαq, Gαo and Gαi-3 were tested. Of these, the Gαs/olf is activated by odorant receptors at cell/outer environment interface (Li et al. 2013), whereas Gαo and Gαi3 (and also Gαq) mediate vomeronasal olfaction on activation by ORs in vertebrates (Luo et al. 1994). Interestingly, all these G-protein subunits are found to be expressed around the epidermal pit of hilsa. Recently, Malick and co-workers (2018) also reported the expression of Gαs/olf and Gαq from the epidermal cell from this area, both in adults from marine and freshwater habitats. Thus, in this fish, the expression of G-protein subunits associated with chemosensory function recognized the snout as a specially designed 'sensory pad' to facilitate upstream migration. The incoming water current probably flushes the epidermal pits and its surrounding and flows through the grooves to optimize the sensory interaction between the odorant molecules and the receptor proteins.

Hypothetically, this is acceptable that the cone shaped head of hilsa has sufficiently inclined surface with snout to enable it to create 'thin boundary layer', closure to it with turbulent water flow through grooves of EPs in the integument, thereby facilitating enough time and surface to maximize the process of odorant reception during upstream migration (Fig. 5b). Being such an efficient facilitator, it plays its role as an extraordinary 'sensory pad' for the spawning migration of the fish from sea to river.

Acknowledgements

Authors are highly thankful to National Agriculture Science Fund, Indian Council of Agriculture Research, New Delhi for their financial support to the work. The instrumental support of DST-FIST and CAS (UGC) of the Department of Zoology, Visva-Bharati to the present work is also acknowledged.

References

Ahsan DA, Naser MN, Bhaumik U, Hazra S, Bhattacharya SB (2014) Migration, Spawning Patterns and Conservation of Hilsa Shad *(Tenualosa ilisha)* in Bangladesh and India: Ecosystems for Life: A Bangladesh-India Initiative (in association of IUCN), Academic Foundation, Darya Ganj, New Delhi, India.

Døving KB, Nordeng H, Oakley B (1974) Single unit discrimination of fish odours released by char (*Salmo alpines* L.) populations. Comp Biochem Physiol A. 47:1051-1063.

Hasler AD, Wisby WJ (1951) Discrimination of stream odors by fishes and its relation to parent stream behavior. Am Nat 85(823):223-238.

Kotrschal K (1992) Quantitative scanning electron microscopy of solitary chemoreceptor cells in cyprinids and other teleosts. Env Biol Fish 35:273-282.

Leise EM (1996) Selective retention of the fluorescent dye DASPEI in a larval gastropod mollusc after paraformaldehyde fixation. Microsc Res Tech 33(6):496-500.

Li F, Ponissery-Saidu S, Yee K K, Wang H, Chen ML, Iguchi N, Zhang G, Jiang P, Reisert J, Huang L (2013) Heterotrimeric G protein subunit Gγ13 is critical to olfaction. J Neurosci 33:7975-7984.

Luo Y, Lu S, Chen P, Wang D, Halpern M (1994) Identification of chemoattractant receptors and G-proteins in the vomeronasal system of Garter snakes. J Biol Chem 269:16867-16877.

Malick C, Chatterjee SK, Bhattacharya S, Suresh VR, Kundu R, Saikia SK (2018) Evidence of putative sensory receptors from snout and tongue in an upstream amphihaline migratory fish hulas *Tenualosa ilisha*. Ichthyol Res 65:42-55.

Nagai T, Koyama H, Hoff KS, Hillyard SD (1999) Desert toads discriminate salt taste with chemosensory function of the ventral skin. J Comp Neurol 408:125-136.

Panhwar SK, Siddiqui G, Zarrien A (2011) Reproductive pattern and some biological features of anadromous fish *Tenualosa ilisha* from Pakistan. Ind J Geo-Mar Sci 40(5):687-696.

Selset R, Døving KB (1980) Behaviour of mature anadromous char (*Salmo alpinus* L.) towards odorants produced by smolts of their own population. Acta Physiol Scand 108(2):113-122.

Saundersa CJ, Christensenc M, Fingera TE, Tizzanoa M (2014) Cholinergic neurotransmission links solitary chemosensory cells to nasal inflammation. PNAS 111(16):6075-6080.

Sbarbati A, Crescimanno C, Bernardi V, Benati V, Merigo V, Osculati V (2000) Postnatal development of the intrinsic nervous system in the circumvallate papilla-von Ebner gland complex. Histochem J 32:483-488.

Acta Biologica Szegediensis

Volume 62(1):7-15, 2018
Acta Biologica Szegediensis
http://abs.bibl.u-szeged.hu/index.php/abs
DOI:10.14232/abs.2018.1.7-15

ARTICLE

Restoration of uterine redox-balance by methanolic extract of *Camellia sinensis* in arsenicated rats

Arindam Dey, Sandip Chattopadhyay*, Suryashis Jana, Mukul Kumar Giri, Shamima Khatun, Moumita Dash, Hasina Perveen, Moulima Maity

Department of Biomedical Laboratory Science and Management and Clinical Nutrition and Dietetics Division, (UGC Innovative Department), Vidyasagar University, Midnapore, West Bengal 721102, India

ABSTRACT Arsenic, an environmental and industrial pollutant causes female reproductive disturbances and female infertility. Several researchers found that the use of *Camellia sinensis* (CS) (green tea) is effective as an alternative therapeutic strategy in the management of several health ailments. This study explores the role of CS extract against arsenic-induced rat uterine tissue damage. Methanolic extract of CS (10 mg/kg BW) was tested concomitantly in arsenic-treated (10 mg/kg BW) rats for a duration of two-oestrous cycle length (8 days). CS effectively attenuated arsenic-induced antioxidant-depletion and necrosis in uterine tissue. Rats treated with sodium arsenite showed significantly reduced activities of enzymatic antioxidants like superoxide dismutase (SOD), catalase (CAT) and glutathione peroxidase (GPx) in uterine tissue as evidenced by the results of spectrophotometric and electrozymographic analysis. Co-administration of CS significantly reversed the above oxidative stress markers in uterine tissue along with the histopathological changes in ovarian and uterine tissue. Moreover, an increase in the level of transcription factor NF-κB in the uterine tissue in association with reduced serum levels of vitamin B_{12} and folic acid were mitigated in arsenic fed rats following CS co-administration.
Acta Biol Szeged 62(1):7-15 (2018)

KEY WORDS
arsenic
uterine oxidative stress
steroidogenesis
Camellia sinensis
metallothionein
B_{12} and folate
NF-κB

ARTICLE INFORMATION
Submitted
11 December 2017.
Accepted
9 April 2018.
***Corresponding author**
E-mail: sandipdoc@mail.vidyasagar.ac.in
sandipdoc@yahoo.com

Introduction

Arsenic a heavy metal and toxic element widely distributed in the environment. Arsenic in drinking water is being a major health problem all over the world (Drličková et al. 2013). Long term exposure to arsenic causes lung, skin, liver and kidney cancer (IARC Working Group et al. 2004). Arsenic intoxication during pregnancy may cause stillbirth. Damage of DNA and chromosomal aberration has been also reported during arsenic toxicity (Mazumder and Dasgupta 2011). Previous studies revealed that long term arsenic exposure in animal exhibited reproductive hazards, including the changes of ovarian and testicular steroidogenesis, arrestation of spermatogenesis and folliculogenesis (Sarkar et al. 2003; Chattopadhyay and Ghosh 2010). Reactive oxygen species (ROS) may lead to DNA strand breaks, deletion mutation, micronuclei formation and chromatid exchange (Bau et al. 2002; Kitchin and Wallace 2008). Chronic exposure in humans elevates the necrotic indicator lactate dehydrogenase (LDH) (Calderon et al. 2001). Management of arsenic-mediated chronic health hazards primarily depends on the chelation therapy where British Anti Lewisite (BAL) and Dimercaptosulfonic acid (DMSA) are extensively used. But the long-term treatment strategy with these chelating agents is questionable because of its painful intramuscular mode of treatment. These agents also generate several moderate to severe side effects (Flora et al. 2007) among the patients. Hence, the mitigation of arsenic toxicity with the use of a safe, non-invasive strategy is becoming a new challenge. Several investigators used different antioxidants and plant products to counteract arsenic toxicity. Vitamin C, vitamin E, selenium and reduced glutathione (GSH) play pivotal role in maintaining normal ovarian and uterine activities in arsenic-treated rats (Chattopadhyay et al. 2001). Seed extract of *Moringa oleifera* (Sajina seed) has been proven to actively strengthen the hepatoprotective and antioxidative efficiencies in rats exposed to arsenic (Chattopadhyay et al. 2011). *Camellia sinensis* (CS), belonging to Theaceae family, contains polyphenolic compound such as epicatechin (EC), epicatechin-3-gallate (ECG), epigallocatechin (EGC) and epigallocatechin-3-gallate (EGCG) and these polyphenols have anti-carcinogenic and anti-mutagenic activities (Yang et al. 1998). The most abundant CS polyphenol, EGCG has antioxidant capac-

ity, which attenuates arsenic-induced cardiotoxicity in rats (Sun et al. 2016). EGCG also protects doxorubicin induced cardiotoxicity by suppressing oxidative stress, inflammation and apoptosis signals (Saeed et al. 2015).

Aqueous extract of CS leaves showed protective effects against arsenic-induced toxicity and lipid peroxide production in experimental rats (Messarah et al. 2013). Green tea strongly prevents arsenic-induced apoptosis, degeneration and mutagenic DNA damage in liver cells of experimental animal (Acharyya et al. 2014). Considering the above benefits, here we planned to investigate the defensive role of methanolic extract of *C. sinensis* on arsenic-induced uterine disorder in experimental animal model.

Materials and Methods

Chemicals

Green tea was collected from local market. The standard rat pellet was obtained from the SAHA Enterprise (Kolkata, India). Vitamin B_{12}, folic acid, NF-κB and metallothionine ELISA kit were purchased from the Wuhan fine test, China. Sodium arsenite, chloroform, cyclohexane, hydrogen peroxide, phenol, ethanol and methanol were obtained from SDFCL India. Nitro-blue tetrazolium, nicotinamide adenine dinucleotide, agarose, Tris-base, sodium acetate, nicotinamide adenine dinucleotide phosphate, potassium phosphate and sodium lactate were supplied by SRL (Mumbai, India). Riboflavin was obtained from Loba Chemical (Mumbai, India). Potassium ferricyanide and ethidium bromide were supplied by Merck (Mumbai, India). Ferric chloride, hematoxyline and eosin were obtained from Qualigens (India). Testosterone was obtained from Himedia (India).

Preparation of green tea methanolic extract

Collected green tea leaves were allowed to dry in an incubator for two days at 40 °C. Dry leaves were crushed and powdered in an electric grinder. This tea powder (500 g) was dissolved in 1000 ml solvent containing 80% methanol and 20% distilled water and followed by mixing in a shaker for two days. After two days the liquid extract was filtered and transferred in a beaker. The liquid deep brown extract was evaporated and preserved in dry powdered form. This dry powder was dissolved in distilled water before treatment in rat.

Animal selection and care

In this experiment 24 adult female albino rats (6 weeks of age and 90-110 g body weight) were acclimatized for 8 days at 12 h light-dark cycle with 32 ± 2 °C temperature and 50-70% humidity in the institutional animal house. Animals were purchased from approved animal provider 'Saha Enterprise' (Kolkata, West Bengal). This study was approved by the Institutional Ethics Committee (IEC/7-4/C-4/16), and all assay procedures were executed by following the guidelines of the Committee for the Purpose of Control and Supervision of Experiments on Animals (CPCSEA), India. Rats were placed in polycarbonate cages and fed with a standard pellet diet (Saha Enterprise, India) and water ad libitum. Rats were equally distributed in four groups. Control group received distilled water as vehicle. Arsenic treated rats received 10 mg of sodium arsenite /kg body weight by gavage. Another group was administered with only CS extract by gavage at a dose of 100 mg/kg body weight. Remaining group of rats was co-administered with the same dose of CS extract along with sodium arsenite for 8 days. Prior to the experiment, the estrous cycle of the rats was synchronized by ethynyl oestradiol and the experiment was started at estrous phase. During the entire schedule of treatment body weight of all rats and pattern of estrous cycle were noted. On day nine, rats were sacrificed, and different organs were dissected out for biochemical and histological examinations. All biological samples, including collected serum, were preserved at -20 °C in several aliquots for further analysis.

Assessment of malondialdehyde (MDA) and conjugated dienes (CD) levels

MDA was determined by the reaction against thiobarbituric acid. The amount of MDA formed was measured (Devasagayam et al. 2003) at the absorbance at 530 nm ($\varepsilon = 1.56 \times 10^5$ mol^{-1} cm^{-1}).

The CD was measured by standard technique where lipids were extracted in presence of chloroform and methanol at the ratio of 2:1 and centrifuged at 1000 g for 5 min. Lipid residues were then dissolved in 1.5 ml of cyclohexane and the absorbance was then measured at 233 nm to determine the amount of hydroperoxides formed (Kumar 2012).

Assessment of uterine, non-protein, soluble thiol (NPSH)

Uterine tissue was homogenized in ice cold PBS (0.1 M, pH 7.4) and centrifuged at 10 000 g for 10 min at 4 °C. The supernatant was then used for the determination of NPSH by standard DTNB (5, 5"-dithiobis-2-nitrobenzoic acid) method with a slight change. Here, precipitation of protein was obtained by sulfosalicialic acid and supernatant was mixed with 0.1 M sodium phosphate buffer containing DTNB. Finally, the absorbance was taken at 412 nm (Mieyal et al. 2008).

Assessment of superoxide dismutase (SOD), catalase (CAT), peroxidase and lactate dehydrogenase (LDH) in native gel

To determine SOD activity, homogenized uterine tissue in ice cold PBS (1.0 mM pH 7.4) was centrifuged at 10 000 g for 20 min at 4 °C. The 40 μg of the tissue protein extract was added to the 12% PAGE. Achromatic bands were achieved against a dark blue background following light exposure in the presence of nitro-blue tetrazolium and riboflavin (Weydert and Cullen 2010).

Proteins (60 μg) were electrophoresed on 8% PAGE to measure catalase activity in uterine tissue extract. Gels were kept at 0.003% H_2O_2 solution for 10 min and stained with 2% potassium ferricyanide and 2% ferric chloride. Bluish yellow bands were observed against a blue, green background (Lewis et al. 2005).

For the determination of GPx activity, native PAGE (8%) was used. The level of GPx was determined by the removal of peroxide for the transformation of potassium ferricyanide to ferrocyanide between samples. Elimination of peroxide by GPx inhibited the combination with ferric chloride, which allowed the appearance of the achromatic clear band on the green-blue gel where GPx was present (Liu et al. 2006).

A 8.0% agarose gel in 50 mM Tris-HCl buffer (pH 8.2) was used for the detection of serum LDH enzyme. Serum (20 μl) was loaded into the gel to electrophorese at 170 volts. Agarose gel was stained by using a cocktail of 1.0 M Tris, tetrazolium blue, phenazine methosulphate, Na-lactate and NAD. And then incubated at 37 °C to mature the colour reaction following rinsing the gels under water in the presence of light (Brandt et al. 1987).

DNA fragmentation study

Uterine tissue was used: it was lysed with 500 μl of lysis buffer and centrifuged (12 000 rpm) at 4 °C for 15 min. Supernatant was then mixed with 1:1 mixture of phenol and chloroform with a gentle agitation for 5 minutes, followed by centrifugation and precipitation in two parts of cold ethanol and one-tenth part of sodium acetate. After spinning down and decanting, the precipitate was resuspended in 30 μl of deionized water, 5 μl of RNA-ase solution and 5 μl of loading buffer followed by an incubation for 30 min at 37 °C. Then the samples were run in 0.8% agarose gel with ethidium bromide at 65 V and visualized in the BioRad gel documentation system (Garcia-Martinez et al. 1993).

Comet assay

Glass slides were precoated with 1% agarose. A combination of 7.5 ml of low melting point agarose (0.6%) in PBS at 37 °C and 2.5 ml of uterine cell suspension was prepared before placing the cell suspension on the agarose coated glass slide and electrophoresed with alkaline electrophoresis buffer (0.3 M NaOH and 1 mM EDTA) for 30 min at 25 V. Then the slides were stained with ethidium bromide and observed under a fluorescence microscope (Nikon Eclipse LV 100 POL), with the VisComet Impuls Bild Analyse software (Singh et al. 1988).

Assay of ovarian 17beta- hydroxysteroid dehydrogenase (17β-HSD) activity

Assessment of ovarian 17β-HSD activity was performed by the homogenization of ovarian tissue at 4 °C in 20% spectroscopic grade glycerol containing 5 mM potassium phosphate and 1 mM EDTA at a tissue concentration of 10 mg/ml. Residual supernatant was mixed with 25 mg of crystalline BSA, 0.3 μM of testosterone and 1.1 μM of NADP and the absorbance was read at 340 nm against blank (Jarabak et al. 1962).

Analysis of vitamin B_{12}, folic acid and NF-κB and metallothionein (MT-I)

The serum levels of vitamin B_{12} (Cat no. ER1579), folic acid (Cat no. EU0381), NF-κB (Cat no. ER1579) and metallothionein (Cat no. ER0447) were measured by ELISA technique according to the procedure recommended by the manufacturer (Wunhan Fine Test, China).

Serum hormone levels and histology of ovary and uterus

Serum level of oestradiol was measured by ELISA kits (Cat no. ER1507), according to the procedures recommended by the manufacturer (Wunhan Fine test, China).

Uterine and ovarian tissues were embedded in paraffin, sectioned with 5 μm thickness, and then stained with haematoxylin (Harris) and eosin and observed under a light microscope (Olympus, CX21i; magnification x 400).

Statistical analysis

Data were expressed in terms of mean ± SE, where n = 6 in all groups. Arsenic and CS co-administered groups were compared with the control by utilizing ANOVA followed by post-hoc Dunnett's multiple comparison test. Statistical significance was considered at the level of $p<0.05$.

Results

General observations

No significant difference was found in their body weight between the control, arsenic-treated and CS co-administered group before and after treatment (Table 1). Here, organo-somatic indices are expressed by the weight of the organs in terms of the percentage of body mass. In case of arsenic-treated group, the weight of the reproductive organs was significantly decreased in comparison

Table 1. Effect of methanolic extract of CS on final body weights and organo-somatic indices in arsenic ingestion rats. The data represent mean ± SE, N=6, ANOVA followed by post-hoc Dunnett's multiple comparison test. Statistical significance was considered at the level of *p<0.05.

	Body weight (g)		Organo-somatic indices (g %)	
	Initial	Final	Ovary in pair	Uterus
Control	118.71 ± 8.21	129.6 ± 7.95	0.0504 ± 0.003	0.181 ± 0.020
Arsenic	108.87 ± 5.53	110.8 ± 5.35	0.0329* ± 0.002	0.099* ± 0.010
CS	115.5 ± 3.85	117 ± 5.13	0.0498 ± 0.001	0.159 ± 0.022
As^{III} + CS	110.5 ± 4.83	110 ± 5.11	0.0491 ± 0.001	0.166 ± 0.022

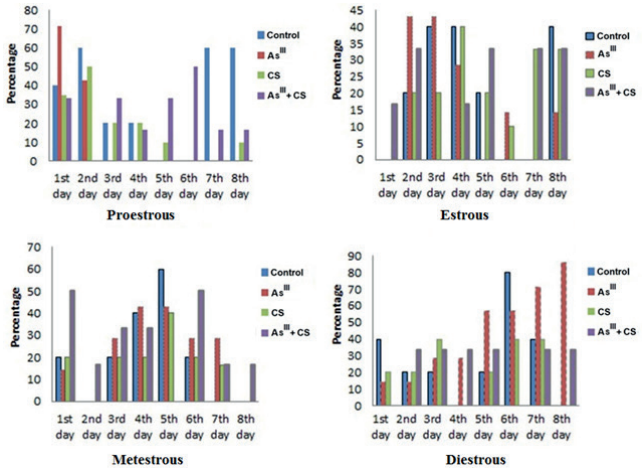

Figure 1. Effect of arsenic and methanolic extract of CS on pattern of estrous cycle of arsenic treated rats.

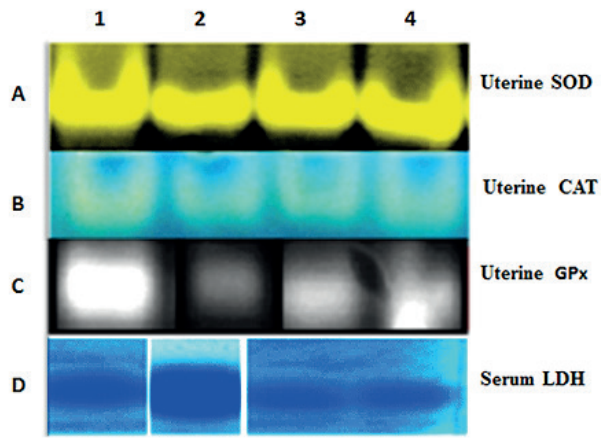

Figure 2. Protective effect of methanolic extract of CS on uterine tissue SOD, CAT, GPx and serum LDH in As^{III} intoxicated rats. Panel A, B, C and D: SOD, CAT, GPx and LDH activity on native gel. Lane 1: control; lane 2: arsenic; lane 3: CS; lane 4: arsenic + CS.

to control (Table 1). Co-treatment with *C. sinensis* (CS) attenuated this deleterious effect of arsenic.

Pattern of vaginal smear

The pattern of estrous cycle was noticed during the entire experimental schedule. Vaginal fluid was collected regularly, and was stained with Leishman stain. Results showed that rats continuously shifted towards consistent metestrous or diestrous phase after the first 4 days of treatment with arsenic (Fig. 1). Maintenance of normal estrous cycle was achieved by application of methanolic extract of CS in arsenic ingested rats (Fig. 1).

Status of oxidative stress markers

Uterine MDA and CD showed a significant elevation in rats fed with sodium arsenite (Table 2). Adminsitration of methanolic extract of CS to the arsenic treated rats caused a significant improvement of this lipid peroxidation state in the uterus (Table 2). NPSH was significantly reduced following the ingestion of arsenic whereas CS co-administration in arsenic fed rats caused significant reverseal of this parameter (Table 2).

Electrozymogram of SOD, catalase and GPx in uterine tissue showed comparatively weaker band strength in the arsenic treated group compared to control (Fig. 2). On the other hand, intense band strength was seen in CS and arsenic treated rats. Serum LDH zymogram was obtained to assess the necrotic risk factor. In arsenic-treated group a very strong band of LDH was observed in contrast to

Table 2. The defensive role of methanolic extract of CS on arsenic affected rats on the status of free radical generation and NPSH. Data represent mean ± SE where N=6 evaluated by ANOVA followed by post-hoc Dunnett's multiple comparison test. Statistical significance was considered at the level of ***p<0.001, and **p<0.01.

	Control	As^{III}	CS	CS+ As^{III}
MDA (nmol/mg of tissue)	29.37 ± 3.09	67.91 ± 3.87***	28.85 ± 1.51	23.77 ± 1.54
CD (nmol/mg of tissue)	14.33 ± 0.88	27.8 ± 1.09***	15.54 ± 0.66*	18.43 ± 0.59**
NPSH (µg/g of protein)	15.46 ± 0.33	6.12 ± 0.31***	14.58 ± 0.35	14 ± 0.66

Table 3. Defensive effect of methanolic extract of CS against arsenic-induced ovarian steroidogenesis. The data represent mean ± SE, N=6, ANOVA followed by post-hoc Dunnett's multiple comparison test. Statistical significance was considered at the level of ***p<0.001 , and **p<0.01.

	Control	As^{III}	CS	CS+ As^{III}
17â HSD (unit/mg of tissue)	0.0344 ± 0.004	0.0052 ± 0.002***	0.032 ± 0.001	0.022 ± 0.003*
Oestradiol (ng/ml)	27 ± 0.45	4.0 ± 0.40***	23 ± 0.81**	16 ± 0.90***

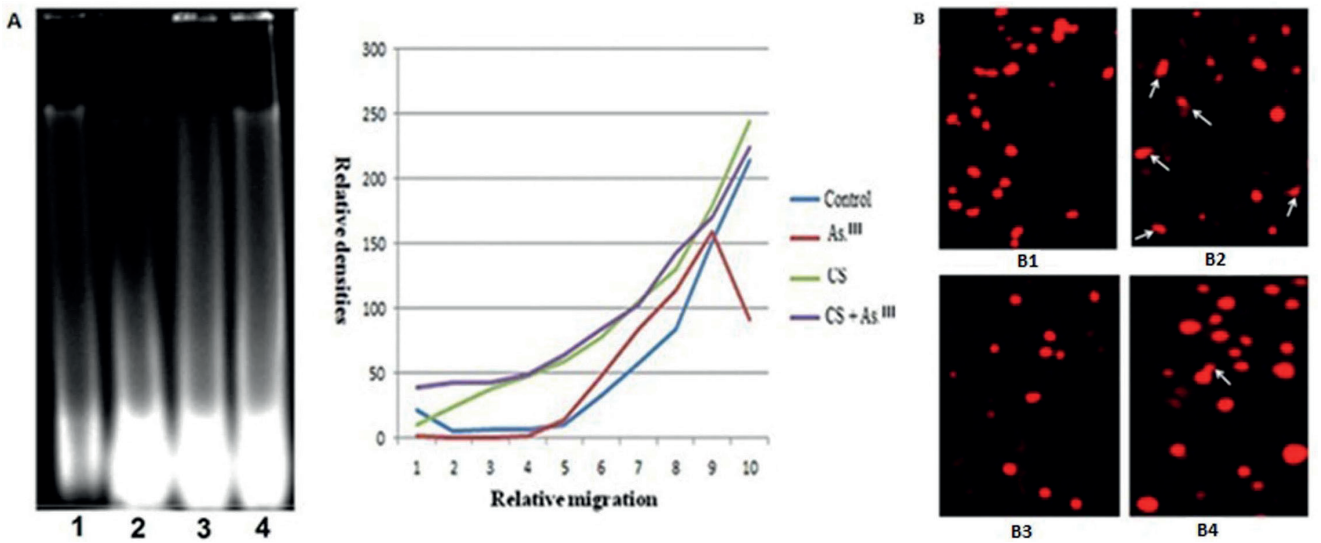

Figure 3. Effect of methanolic extract of CS on the DNA fragmentation (Panel A) with graphical representation and the comet assay (Panel B) in uterine cells of female rats treated with arsenic. Lanes in panel A: 1: control; 2: arsenic; 3: CS; 4: arsenic + CS. Panels in B: B1: control; B2: arsenic; B3: CS; B4: arsenic + CS. Arrows indicate comet formation.

control group (Fig. 2). This nature of the band was substituted by a weaker expression pattern when arsenic-treated rats were co-ingested with CS extract (Fig. 2).

Status of uterine DNA

Arsenic exposure lead to DNA damage, but supplementation of CS extract had a beneficial effect against this damage (Fig. 3A). The DNA degradation was more prominent in arsenic-treated rats compared to control rats (Fig 3A). Migration of the exposed DNA occurred with the less intense band in arsenic-treated rats in comparison to control DNA as evidenced from densitometric analysis (Fig. 3A). However, this damage recovered successfully in the CS supplemented group (Fig. 3A). Comet assay showed that arsenic-treated uterine DNA cells were degraded and broken (Fig. 3B). This was finally restrained by the supplementation of CS extract as demonstrated from the comparatively less number of comets in this group (Fig. 3B).

Ovarian steroidogenesis and histopathology of ovary and uterus

A notable inhibition in the activity of ovarian 17β HSD was observed in arsenic exposed rats compared with control, while co-administration of CS extract significantly protected the activity of this steroidogenic enzyme (Table 3).

A diminished oestradiol level was observed following 8 days of arsenic treatment in comparison with control (Table 3). On the contrary, CS co-treatment in arsenic fed rats increased this hormonal signalling (Table 3).

Table 4. Effect of methanolic extract of CS on vitamins, NF-κB, and metallothionein level of arsenic-treated rats. The data represent mean ± SE, N=6, ANOVA followed by post-hoc Dunnett's multiple comparison test. Statistical significance was considered at the level of, ***p<0.001, and **p<0.01.

	Control	As^{III}	CS	CS + As^{III}
Vitamin B_{12} (ng/ml)	23.32 ± 1.05	10.71 ± 0.39**	22.47 ± 0.80	18.23 ± 0.42*
Folic acid (ng/ml)	1231.5 ± 43.71	918 ± 16.01***	1125.1 ± 34.70	1047 ± 29.50**
NF-κB (ng/ml)	6.11 ± 0.285	9.42 ± 0.311***	5.77 ± 0.223	6.72 ± 0.166
Metallothionine (MT-I) (ng/ml)	12.5 ± 0.28	31±0.92***	14±1.03*	17±1.12***

Normal uterine histology is composed of three layers, the inner one is endometrium, middle layer is myometrium and the outer layer is serosa (Fig. 4). Following the exposure of arsenic there was a thinning of the uterine layer along with a remarkable loss of uterine secretory glands in the arsenic ingested group (Fig. 4). CS supplementation reverts back the above degeneration of the uterine layers towards normalcy (Fig. 4).

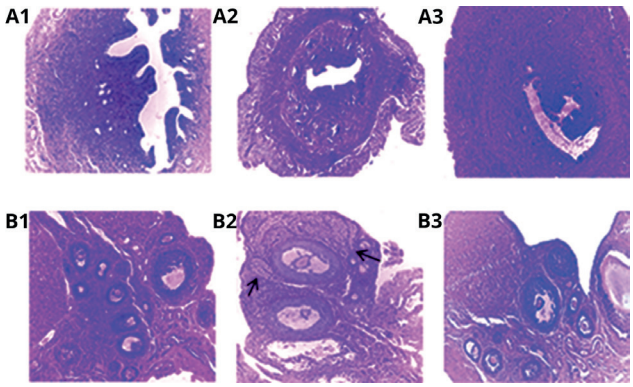

Figure 4. Effect of methanolic extract of CS on uterine (A) and ovarian (B) histo-architecture. Panels A1 and B1: vehicle treated control; A2 and B2: arsenic; A3 and B3: arsenic + methanolic extract of CS. Arrow indicates follicular atresia.

Significant shrinkage or decrease in the number of graafian follicles, with a higher degree of follicular regression and follicular atresia, was seen in the arsenic treated rats compared to the controls (Fig. 4). Supplementation with CS extract resulted in significant reappearance of a growing number of developing follicles followed by lesser number of immature follicles (Fig. 4).

Status of vitamin B_{12}, folic acid, NF-κB and metallothionein (MT-I)

There was a decreased level of vitamin B_{12} and folic acid in arsenic-treated group when compared to the control rats (Table 4). Methanolic extract of CS significantly reversed this effect. A notable elevation of uterine NF-κB was also noted in arsenic-treated group (Table 4) while co-administration of the CS methanolic extract significantly reduced the level of this transcription factor towards normalcy. We also assessed metallothionein in the liver to bio-monitor the deposition of this metalloid in tissue. The result showed an increase level of MT-1 in As^{III} treated group compared to control group (Table 4). Supplementation with CS methanolic extract significantly decreased this elevation of hepatic MT-1 level.

Discussion

Our results showed a low-level expression of SOD, catalase and GPx as faint bands in Figure 2 in arsenic fed rats compared to the control. SOD, catalase and GPx are considered as the first line of defense against oxidative injury at the cellular level. The NPSH, precursor of GSH, was significantly deprived by arsenic and was returned towards control level when the arsenicated rats received methanolic extract of CS (Table 2). Hence, increased level of free radical generation and diminished enzymatic antioxidant activity in arsenic exposed rats may lead to DNA damage due to the formation of H_2O_2 and arsenic peroxyl radicals (Maiti et al. 2012). Elevated uterine MDA and CD levels (Table 2) indicated an increase in lipid peroxidation. Endometrium is the potential site in the female reproductive organ for the generation of superoxide anions (Akram et al. 2010), and arsenic has been shown to induce endometrial carcinogenicity or cellular toxicity that may lead to cell death (Du et al. 2012).

In our experiment arsenic-treated rats lost their normal estrous cyclicity (Fig. 1) and moved towards consistent diestrous phase along with the reduced weight of ovary and uterus (Table 1). Reduced activity of steroidogenic enzyme 17β-HSD may result in suppression of oestradiol (E_2) signalling (Table 3). Suppression of E_2 (Table 3) and deterioration of follicular maturation (Fig. 4) in response to As^{III} lead to cellular degeneration in uterine layers (Fig. 4). Several studies demonstrated that during ovarian aging high level of ROS is responsible for DNA damage (Gore-Langton and Daniel 1990). Reactive oxygen species play a critical role in the alteration of physiological and reproductive functions like oocyte maturation and luteolysis. Arsenic probably binds to estrogen receptor (ER) and inhibits E_2 binding to the estrogen receptor alpha (ERα) (Bae-Jump et al. 2008). Exposure to arsenic caused a degradation of circulating levels of vitamin B_{12} and folate, (Table 4). These two vitamins are indispensable to protect the reproductive organs from necrosis and have a protective role by diminishing serum LDH level (Fig 2D) as a consequence of an inverse relationship between the serum LDH activities and serum vitamin B_{12}-folate levels (Maity et al. 2017). LDH expression was noticeably elevated (Fig. 2D) in arsenic fed rats since As^{III} is directly linked to the development of necrosis (Karim et al. 2010).

The liver is the most sensitive to arsenic and is the site of the synthesis of low molecular weight, cysteine rich metal binding antioxidant, MT, in response. MT-1 is required to ensure protection against arsenic toxicity and has an important role in heavy metal detoxification as well as essential metal homeostasis (Cai et al. 2006). The maintenance of cellular MT-I level is regulated by IKK-NF-κB pathway which suspends the generation of

ROS. ROS driven apoptosis is attributed to the failure of IKK-NF-κB (Peng et al. 2007). A high uterine NF-κB in arsenic exposed group (Table 4) was in accordance with reports on arsenic damaging the tissue via activation of NF-κB signalling pathway (Felix et al. 2005). The level of MT-I was normalized in presence of CS co-administration (Table 4). There is apparently an inverse correlation between MT and ER (Ioachim et al. 2000), as MT gene is potentially down-regulated by ERα (Surowiak et al. 2005), and arsenic trioxide has been supposed to exert anti-estrogenic activity by down regulating the expression of ERα (Bae-Jump et al. 2008).

Co-administration of methanolic CS extraction can reverse uterine ROS production with a concomitant repairing of the anti-oxidant enzyme activities (Fig. 2) in arsenic treated rats. The methanolic CS extract significantly reduced uterine DNA degradation in arsenic fed rats (Fig. 3A-B). The mechanism of counteracting arsenic-mediated uterine damage might be linked to the antioxidant, scavenging and chelating properties of *C. sinensis* (CS) (Cao et al. 2015). It was established that methanolic and water extracts of *C. sinensis* contain an enormous amount of catechins and flavonoids (Noor 2016). Catechins, present in green tea, have a strong scavenging capacity against superoxide, hydrogen peroxide, hydroxyl radicals. They have the ability to chelate with metals because of the presence of catechol structural motif (El-Shahat et al. 2009). EGCG-3 and EGC are the most abundant and important polyphenols scavenging a wide range of free radicals including the active hydroxyl; and the chemical structure of catechins play a crucial role in their antioxidant effect (Skrzydlewska et al. 2005). The anti-oxidative, anti-apoptotic, and metal chelating properties of EGC are helpful to suppress the generation of arsenic-induced oxidative stress (Rice-Evans et al. 1996; Guo et al. 1996). However, our experiment showed that green tea protects uterine tissue from a state of redox imbalance by up regulating enzymatic antioxidants (Fig. 2).

Co-administration with CS could significantly normalize the activity of LDH (Fig. 2). CS supplementation may effectively rescue the uterus from apoptotic degeneration and this was indicated from the weakened band intensity of serum LDH compared to arsenic-treated rats (Fig. 2). The presence of the pyrogallol motif in EGCG conveys its strong metal chelating ability. Supplementation with CS extract resulted in comparatively lower level of NF-κB, similar to control. EGCG 3 can block NF-κB activation by downregulation of NF-κB kinase in the intestinal epithelial cell line IEC-6 (Yang et al. 2001). In this study arsenic-mediated apoptotic and necrotic processes were detected by single cell DNA assay and DNA fragmentation picture (Fig. 3, lane 2). CS co-treatment significantly reduced DNA degradation and this may highlight the efficacy of CS polyphenols to protect the cells from arsenic-mediated mutagenic DNA breakage and tissue necrosis (Ndiaye et al. 2005). Supplementation with CS was able to maintain the circulating level of vitamin B_{12} and folic acid in arsenicated rats (Table 4). Previous studies showed that vitamin B_{12} is present in green tea (Kittaka-Katsura et al. 2004) Vitamin B_{12} and folate maintain the level of endogenous methionine where folic acid acts as methyl group donor and vitamin B_{12} act as co-factor for the synthesis of methionine (Sahin et al. 2003). Therefore, CS mediated maintenance of these vitamins contributes to the attenuation of arsenic toxicity, and so, to the prevention of reproductive organ necrosis. It is confirmed from the above information that CS has a protective effect against oxidative stress induced ovarian and uterine damage by the rebuilding the normal uterine and ovarian histological structure. Co-administration with CS significantly increased plasma oestradiol level and ovarian 17β-HSD activity and that was helpful for the restoration of normal histoarchitecture of ovary and uterus (Fig. 4).

From the above study, we may conclude that green tea methanolic extract has a potential role to improve uterine anti-oxidant defense system and restore normal ovarian-uterine histoarchitecture either by its chelating action with arsenic or by sustaining B vitamins.

Acknowledgement

The authors acknowledged the funding from the Department of Science and Technology, Government of West Bengal for this investigation (1212(Sanc.)/ST/P/S&T/1G-13/2015).

References

Acharyya N, Chattopadhyay S, Maiti S (2014) Chemoprevention against arsenic-induced mutagenic DNA breakage and apoptotic liver damage in rat via antioxidant and SOD1 upregulation by green tea (*Camellia sinensis*) which recovers broken DNA resulted from arsenic-H2O2 related in vitro oxidant stress. J Environ Sci Health (Part C) 32:338-361.

Akram Z, Jalali S, Shami SA, Ahmad L, Batool S, Kalsoom O (2010) Adverse effects of arsenic exposure on uterine function and structure in female rat. Exper Toxicol Pathol 62:451-459.

Bae-Jump VL, Zhou C, Boggess JF, Gehrig PA (2008) Arsenic trioxide (As_2O_3) inhibits expression of estrogen receptor-alpha through regulation of the mitogen-activated protein kinase (MAPK) pathway in endometrial cancer

cells. Reprod Sci 15:1011-1017.
Bau DT, Wang TS, Chung CH, Wang AS, Wang AS, Jan KY (2002) Oxidative DNA adducts and DNA-protein cross-links are the major DNA lesions induced by arsenite. Environ Health Perspect 110(S3):753-756.
Brandt RB, Laux JE, Spainhour SE, Kline ES (1987) Lactate dehydrogenase in rat mitochondria. Arch Biochem Biophys 259:412-422.
Calderon J, Navarro ME, Jimenez-Capdeville ME, Santos-Diaz MA, Golden A, Rodriguez-Leyva I, Díaz-Barriga F (2001) Exposure to arsenic and lead and neuropsychological development in Mexican children. Environ Res 85:69-76.
Cao SQ, Hu YH, Zhang L, Liu, SN, Wang F, Shu-Hua XI. (2015) Effects of dimethylarsinic acid on expression levels of IKKα and p65 in bladder epithelial cells of rats. Chin J Ind Med 2:95-97.
Chattopadhyay S, Ghosh D (2010) The involvement of hypophyseal-gonadal and hypophyseal-adrenal axes in arsenic-mediated ovarian and uterine toxicity: modulation by hCG. J Biochem Mol Toxicol 24:29-41.
Chattopadhyay S, Ghosh S, Debnath J, Ghosh D (2001) Protection of sodium arsenite-induced ovarian toxicity by coadministration of L-ascorbate (vitamin C) in mature Wistar strain rat. Arch Environ Contam Toxicol 41:83-89.
Chattopadhyay S, Maiti S, Maji G, Deb B, Pan B, Ghosh D (2011) Protective role of *Moringa oleifera* (Sajina) seed on arsenic-induced hepatocellular degeneration in female albino rats. Biol Trace Elem Res 142:200-212.
Devasagayam TPA, Boloor KK, Ramasarma T (2003) Methods for estimating lipid peroxidation: an analysis of merits and demerits. Ind J Biochem Biophys 40:300-308.
Drličková G, Vaculík M, Matejkovič P, Lux A (2013) Bioavailability and toxicity of arsenic in maize (*Zea mays* L.) grown in contaminated soils. Bull Environ Contam Toxicol 91:235-239.
Du J, Zhou N, Liu H, Jiang F, Wang Y, Hu C, Li Z (2012) Arsenic induces functional re-expression of estrogen receptor α by demethylation of DNA in estrogen receptor-negative human breast cancer. PLOS ONE 7:1-10.
El-Shahat AER, Gabr A, Meki AR, Mehana ES (2009) Altered testicular morphology and oxidative stress induced by cadmium in experimental rats and protective effect of simultaneous green tea extract. Int J Morphol 27:757-764.
Felix K, Manna SK, Wise K, Barr J, Ramesh GT (2005) Low levels of arsenite activates nuclear factor-κB and activator protein-1 in immortalized mesencephalic cells. J Biochem Mol Toxicol 19:67-77.
Flora SJS, Bhadauria S, Kannan GM, Singh N (2007) Arsenic-induced oxidative stress and the role of antioxidant supplementation during chelation: a review. J Environ Biol 28:333-347.
Garcia-Martinez V, Macias D, Ganan Y, Garcia-Lobo JM, Francia MV, Fernandez-Teran MA, Hurle JM (1993). Internucleosomal DNA fragmentation and programmed cell death (apoptosis) in the interdigital tissue of the embryonic chick leg bud. J Cell Sci 106:201-208.
Gore-Langton RE, Daniel SA (1990) Follicle-stimulating hormone and oestradiol regulate antrum-like reorganization of granulosa cells in rat preantral follicle cultures. Biol Reprod 43:65-72.
Guo Q, Zhao B, Li M, Shen S, Xin W (1996) Studies on protective mechanisms of four components of green tea polyphenols against lipid peroxidation in synaptosomes. BBA- Lipid Lipid Met 1304:210-222.
IARC Working Group on the Evaluation of Carcinogenic Risks to Humans, World Health Organization, & International Agency for Research on Cancer (2004) Some drinking-water disinfectants and contaminants, including arsenic. 84:14-20.
Ioachim EE, Kitsiou E, Carassavoglou C, Stefanaki S, Agnantis NJ (2000) Immunohistochemical localization of metallothionein in endometrial lesions. J Pathol 191:269-273.
Jarabak J, Adams JA, Williams-Ashman HG, Talalay P (1962) Purification of a 17β-hydroxysteroid dehydrogenase of human placenta and studies on its transhydrogenase function. J Biol Chem 237:345-357.
Karim MR, Salam KA, Hossain E, Islam K, Ali N, Haque A, Himeno S (2010) Interaction between chronic arsenic exposure via drinking water and plasma lactate dehydrogenase activity. Sci Total Environ 409:278-283.
Kitchin KT, Wallace K (2008) Evidence against the nuclear in situ binding of arsenicals–oxidative stress theory of arsenic carcinogenesis. Toxicol Appl Pharmacol 232:252-257.
Kittaka-Katsura H, Watanabe F, Nakano Y (2004) Occurrence of vitamin B_{12} in green, blue, red, and black tea leaves. J Nutr Sci Vitaminol 50:438-440.
Kumar A (2012) Effect of simvastatin on paraxonase 1 (PON1) activity and oxidative stress. In Kumar A (ed.), Significance of Lipid Profile Assay as Diagnostic and Prognostic Tool. Create Space Independent Publishing Platform, California, 105-109.
Lewis A, Du J, Liu J, Ritchie JM, Oberley LW, Cullen JJ (2005) Metastatic progression of pancreatic cancer: changes in antioxidant enzymes and cell growth. Clin Exp Metastasis 22:523-532.
Liu J, Du J, Zhang Y, Sun W, Smith BJ, Oberley LW, Cullen JJ (2006) Suppression of the malignant phenotype in pancreatic cancer by overexpression of phospholipid hydroperoxide glutathione peroxidase. Hum Gene Ther 17:105-116.
Ma J, Stampfer MJ, Christensen B, Giovannucci E, Hunter DJ, Chen J, Rozen R (1999) A polymorphism of the methionine synthase gene: association with plasma folate, vitamin B_{12}, homocyst(e)ine, and colorectal cancer risk.

Cancer Epidemiol Biomark Prev 8:825-829.

Maiti S, Chattopadhyay S, Deb B, Samanta T, Maji G, Pan B, Ghosh D (2012) Antioxidant and metabolic impairment result in DNA damage in arsenic-exposed individuals with severe dermatological manifestations in Eastern India. Environ Toxicol 27:342-350.

Maity M, Perveen H, Dash M, Jana S, Khatun S, Dey A, Mandal AK, Chattopadhyay S (2017) Arjunolic acid improves the serum level of vitamin B_{12} and folate in the process of the attenuation of arsenic-induced uterine oxidative stress. Biol Tres Elem Res 182:78-90.

Mazumder DG, Dasgupta UB (2011) Chronic arsenic toxicity: studies in West Bengal, India. Kaohsiung J Med Sci 27:360-370.

Messarah M, Saoudi M, Boumendjel A, Kadeche L, Boulakoud MS, Feki AE (2013) Green tea extract alleviates arsenic-induced biochemical toxicity and lipid peroxidation in rats. Toxicol Ind Health 29:349-359.

Mieyal JJ, Gallogly MM, Qanungo S, Sabens EA, Shelton MD (2008) Molecular mechanisms and clinical implications of reversible protein S-glutathionylation. Antioxid Redox Signal 10:1941-1988.

Ndiaye M, Chataigneau M, Lobysheva I, Chataigneau T, Schini-Kerth VB (2005) Red wine polyphenol-induced, endothelium-dependent NO-mediated relaxation is due to the redox-sensitive PI3-kinase/Akt-dependent phosphorylation of endothelial NO-synthase in the isolated porcine coronary artery. FASEB J 19:455-457.

Noor S. Latteef (2016) Phytochemical, antibacterial and antioxidant activity of *Camellia sinensis* methanolic and aqueous extracts. IOSR J Pharm Biol Sci 11:113-119.

Peng Z, Peng L, Fan Y, Zandi E, Shertzer HG, Xia Y (2007) A critical role for IκB kinase β in metallothionein-1 expression and protection against arsenic toxicity. J Biol Chem 282:21487-21496.

Refsum H (2001) Folate, vitamin B_{12} and homocysteine in relation to birth defects and pregnancy outcome. Br J Nutr 85:S109-S113.

Rice-Evans CA, Miller NJ, Paganga G (1996) Structure-antioxidant activity relationships of flavonoids and phenolic acids. Free Radic Biol Med 20:933-956.

Saeed NM, El-Naga RN, El-Bakly WM, Abdel-Rahman HM, ElDin RAS, El-Demerdash E (2015) Epigallocatechin-3-gallate pretreatment attenuates doxorubicin-induced cardiotoxicity in rats: a mechanistic study. Biochem Pharmacol 95:145-155.

Sahin K, Onderci M, Sahin N, Gursu MF, Kucuk O (2003) Dietary vitamin C and folic acid supplementation ameliorates the detrimental effects of heat stress in Japanese quail. J Nutr 133:1882-1886.

Sarkar M, Chaudhuri GR, Chattopadhyay A, Biswas NM (2003) Effect of sodium arsenite on spermatogenesis, plasma gonadotrophins and testosterone in rats. Asian J Androl 5:27-32.

Singh NP, McCoy MT, Tice RR, Schneider EL (1988) A simple technique for quantitation of low levels of DNA damage in individual cells. Exp Cell Res 175:184-191.

Skrzydlewska E, Augustyniak A, Michalak K, Farbiszewski R (2005) Green tea supplementation in rats of different ages mitigates ethanol-induced changes in brain antioxidant abilities. Alcohol 37:89-98.

Smid-Koopman E, Kuhne LC, Hanekamp EE, Gielen SC, De Ruiter PE, Grootegoed JA, Blok LJ (2005) Progesterone-induced inhibition of growth and differential regulation of gene expression in PRA-and/or PRB-expressing endometrial cancer cell lines. J Soc Gynecol Investig 12:285-292.

Sun TL, Liu Z, Qi ZJ, Huang YP, Gao XQ, Zhang YY (2016) (-)-Epigallocatechin-3-gallate (EGCG) attenuates arsenic-induced cardiotoxicity in rats. Food Chem Toxicol 93:102-110.

Surowiak P, Matkowski R, Materna V, Gyorffy B, Wojnar A, Pudelko M, Zabel M (2005) Elevated metallothionein (MT) expression in invasive ductal breast cancers predicts tamoxifen resistance. Histol Histopathol 20:1037-1044.

Yang CS, Chen L, Lee MJ, Balentine D, Kuo MC, Schantz SP (1998) Blood and urine levels of tea catechins after ingestion of different amounts of green tea by human volunteers. Cancer Epidemiol Biomark Prev 7:351-354.

Yang F, Oz HS, Barve S, De Villiers WJ, McClain CJ, Varilek GW (2001) The green tea polyphenol (–)-epigallocatechin-3-gallate blocks nuclear factor-κB activation by inhibiting IκB kinase activity in the intestinal epithelial cell line IEC-6. Mol Pharmacol 60:528-533.

Acta Biologica Szegediensis

Volume 62(1):17-23, 2018
Acta Biologica Szegediensis
http://abs.bibl.u-szeged.hu/index.php/abs
DOI:10.14232/abs.2018.1.17-23

ARTICLE

Nephroprotective efficacy of *Asparagus racemosus* root extract on acetaminophen-induced renal injury in rats

Suchismita Roy[1], Shrabani Pradhan[1], Shreya Mandal[2], Koushik Das[2], Dilip Kumar Nandi[2]*

[1]Department of Biological Sciences, Midnapore City College, Kuturia, Bhadutala, Midnapore- 721129, West Bengal, India
[2]Research Unit, Developed by Department of Nutrition, Physiology & Microbiology, Raja N. L. Khan Women's College, Midnapore, West Bengal, India

ABSTRACT Acetaminophen-induced renal necrosis and insufficiency occurs in patients with acetaminophen overdose. Renal failure is rapidly assuming epidemic proportions globally. In absence of reliable and effective nephroprotective drugs, strategies towards exploring alternative therapies for treatment of kidney diseases are essential. *Asparagus racemosus* is a medicinal plant used for treatment of various ailments. This research was undertaken to investigate the protective effect of ethanol fraction of *A. racemosus* roots extract in acetaminophen-induced uraemia and renal failure in rats. Rats were co-administered with acetaminophen injection and oral administration of *A. racemosus* roots extract in an attempt of protection against renal failure. Uremic biomarkers significantly decreased, and elevated levels of antioxidant enzymes were found, in the animals treated with ethanol fraction of *A. racemosus* when compared with acetaminophen treated uremic animals. Also, histology of kidneys showed control like structure in animals treated with this extract but severe damage in the uremic animals. HPLC analysis of the ethanol fraction of *A. racemosus* roots extract revealed eight compounds out of which one had a retention time near to the quercetin standard. It may be concluded that this extract of *A. racemosus* has therapeutically useful nephroprotective potential.
Acta Biol Szeged 62(1):17-23 (2018)

KEY WORDS
acetaminophen
nephroprotection
renal failure

ARTICLE INFORMATION
Submitted
9 February 2018.
Accepted
21 May 2018.
***Corresponding author**
E-mail: dilipnandi2004@yahoo.co.in

Introduction

Acetaminophen (N-acetyl-p-aminophenol; APAP), also known as paracetamol, is one of the most effective over-the-counter analgesic-antipyretic chemotherapeutic agents belonging to the para-aminophenol class of the non-steroidal anti-inflammatory drugs (NSAIDs) (Hardman et al. 2001) and is considered safe at therapeutic dosages. Acute and chronic high doses of APAP are known to cause hepatic necrosis in both animals and humans (O'Grady 1997), but impairment of renal function by acetaminophen as the main untoward effect is also becoming increasingly reported (McLaughlin et al. 1998; Fored et al. 2001).

Different research work done on the anti-uremic and nephroprotective phytochemicals from different plant extracts such as methanolic bark extract of *Terminalia arjuna* (Das et al. 2010a), methanolic root extract of *Withania somnifera* (Das et al. 2010b) which had been effective to reduce uremic toxins in experimentally induced renal failure in rats. Other research work, undertaken on nutraceuticals like alpha lipoic acid (Pradhan et al. 2013) and on probiotic therapy (Mandal et al. 2013c) as an alternative; both the work was shown to have excellent nephroprotective activity against acetaminophen-induced renal failure in male rats.

In Indian system of medicine, *Asparagus racemosus* (Liliaceae) is an important medicinal plant having a wide range of biological activities (Goyal et al. 2003). The therapeutic components present in the root of *A. racemosus* are phytosterols, saponins, polyphenols, flavonoids and ascorbic acid (Visavadiya and Narsimhacharya 2005). The aim of the present study was to evaluate the protective effect of the ethanol fraction of *A. racemosus* roots (AR) against acetaminophen-induced nephrotoxicity in male albino rats by evaluating biochemical and histological alterations. HPLC analysis of phytochemicals to search out most active compounds in this plant was also performed.

Table 1. Grouping of animals with the treatment

Groups	Number of rats	Treatments
Group I	6 rats	Served as untreated control and was provided normal food and water.
Group II	6 rats	Ethanol fraction of AR at 500 mg/kg body weight/day for 10 days was orally feeding to rats through gavage for 10 days. One g of ethanol fraction of AR was dissolved in 1 ml of deionized water.
Group III	6 rats	Uremic animals were treated with intraperitoneal APAP injection at 500 mg/kg body weight/day once in every day for 10 consecutive days. One g of APAP was dissolved in 1 ml of deionized water.
Group IV	6 rats	Orally feeding with ethanol fraction of AR at the dose of 500 mg/kg body weight/day with co administration of intraperitoneal APAP injection at 500 mg/kg body weight/day once in every day for 10 consecutive days.

Materials and methods

Drug and chemicals

Acetaminophen (paracetamol, *N*-acetyl *p*-aminophenol; APAP) was purchased from AshChemie India (Thane, India). It was administered intraperitoneally with saline. All other chemicals and kits were obtained from Merck (Mumbai, India) and HiMedia Laboratories (Mumbai, India).

Plant materials

The root of *A. racemosus* was collected from Gopali, Indian Institute of Technology, Kharagpur (Paschim Medinipur district, West Bengal). Plant material was identified by taxonomist at the Department of Botany, Raja N. L. Khan Women's College, Midnapore. The voucher specimens were deposited at the Department of Botany (Raja N. L. Khan Women's College).

Animal care and selection

The study was conducted on 24 healthy adult male albino rats of Wistar strain (Ghosh Animal, Kolkata 54, India) having a body weight of 90 ± 10 g. They were acclimatized to laboratory conditions for two weeks prior to experimentation. The animals were grouped and housed in polyacrylic cages (38 x 23 x 10 cm) three rats/cage in a temperature-controlled room (22 ± 2 °C) with 12-12 h dark-light cycles (8.00- 20.00 h light, 20.00-8.00 h dark) at a humidity of 50 ± 10%. They were provided with standard food and water *ad libitum*. Animal care (NIH 1985) was provided according to the guiding principle for the care and use of animals (Olfert et al. 1993). This experiment was approved by our Institutional Animal Ethical Committee according to the CPCSEA guidelines (CPCSEA Registration No- 1905/PO/Re/S/2016/CPCSEA).

Preparation of ethanol fraction of AR

Roots of *A. racemosus* were washed and cut into small pieces then shade dried and crushed in an electrical grinder. A total of 100 g powdered root material was washed in 400 ml of hexane for 24 h to remove the greasy non-polar components. The hexane was discarded, and residue was dissolved in hydromethanol (methanol and water mixture 4:6) for 2 h in a Soxhlet apparatus. Then the extract was filtered through Whatman No. 1 filter paper and the filtrate was evaporated in a rotary vacuum evaporator. Of this hydromethanol extract residue, 25 g was dissolved in 500 ml ethyl acetate for 2 h in a Soxhlet apparatus. The extract was filtered, and the resulting filtrate was dried in the air. The ethyl acetate extract was then dissolved in 250 ml ethanol for 2 h in a Soxhlet apparatus. Then it was filtered, and the resulting filtrate was dried under reduced pressure at 40 °C on a rotary evaporator (Das et al. 2010b; Roy et al. 2014b; Roy et al. 2014a). The fraction was named as ethanol fraction of *A. racemosus* (AR) and it was stored in refrigerator for further study.

Grouping of animals

Twenty-four rats were divided into four groups. The dose of acetaminophen and AR was established in our laboratory according to OECD guidelines (Roy et al. 2015; Roy et al. 2014a), by acute and main toxicity study. The details of groups with the 10-days treatment are given in Table 1.

Animal scarification, plasma and organ collection

This experimental design was continued for 10 days. On the 11th day, the animals were sacrificed by exsanguinations method and using chloroform anaesthesia. Blood was collected from the aorta for biochemical and haematological analysis, after which the liver was collected for liver glutathione content and histopathological analysis. Blood was centrifuged at 10 000 g for 20 min at 4 °C and then plasma was collected.

Measurement of biochemical parameters

Plasma urea and creatinine level were measured by standard kit method (Pradhan et al. 2013; Burtis and Ashwood 1999). Quantification of plasma sodium and potassium was done by standard kit methods using electrolyte analyser (Systronics, India) by using plasma samples (Sunderman 1959; Roy et al. 2013). Activity of the antioxidant enzymes catalase (CAT; Pradhan et al. 2013; Beers and Sizer 1952),

Table 2. Effect of ethanol fraction of *A. racemosus* on body weight in rats with acetaminophen-induced renal failure. Data were expressed as mean ± SE (n = 6) and data with different superscripts (a, b and c) in a specific vertical column differ from each other significantly ($p < 0.05$).

Groups	Initial body weight (g)	Final body weight (g)	Increase or decrease in body weight (g)
I	104.2 ± 2.5[a]	120.3 ± 5.3[a]	16.1
II	106.4 ± 3.8[a]	126.3 ± 4.7[c]	19.9
III	105.6 ± 3.6[a]	109.2 ± 3.2[b]	3.6
IV	106.7 ± 3.1[a]	122.5 ± 6.2[a]	15.8

and superoxide dismutase (SOD; Marklund and Marklund 1947; Roy et al. 2015), and GSH level (Elkarib 2014) were measured spectrophotometrically from plasma and kidney samples. SOD and CAT are the most important enzymes involved in ameliorating the effects of oxygen metabolism (Linares et al. 2006). The oxidative stress marker MDA was determined by UV-VIS spectrophotometer (Systronics, India) as described in Roy et al. (2015) and Ohkawa et al. (1976). Histology of kidney tissue was performed by standard method (Roy et al. 2015; Mukherjee 2010).

Table 3. Effect of ethanol fraction of *A. racemosus* on plasma and kidney catalase in rats with acetaminophen-induced renal failure. Data were expressed as mean ± SE (n = 6) and data with different superscripts (a and b) in a specific vertical column differ from each other significantly ($p < 0.05$).

Groups	Plasma catalase (mmol of H_2O_2 consumption/dl of plasma/min)	Kidney catalase (mmol of H_2O_2 consumption/mg of tissue/min)
I	0.92 ± 0.08[a]	0.97 ± 0.05[a]
II	0.94 ± 0.17[a]	0.96 ± 0.07[a]
III	0.13 ± 0.03[b]	0.26 ± 0.04[b]
IV	0.88 ± 0.06[a]	0.92 ± 0.07[a]

Statistical analysis

Analysis of variance (ANOVA) followed by a multiple two-tail t-test with Bonferroni modification was used for statistical analysis of the collected data.

HPLC analysis

HPLC analysis of AR was carried out on a Thermo Fisher HPLC system equipped with an ODS-2 250 x 4.6, 5 µm (Thermo Scientific, UK) reverse phase chromatographic column using UV detector at 254 nm. For the separation, 4.6 mM, pH 7.2 phosphate buffer (A) and acetonitrile (B) were applied in the ratio of 1:1. The flow rate was 1.5 ml/min at 37 °C and the injection volume was 20 µl. Concentration of test solution used for this study was 50 mg dry weight/ml dissolved in methanol. The run time was 45 min and quercetin was used as a standard for HPLC analysis.

Results

Body weight (BW)

BW was measured prior to experiment and final BW was taken before animal sacrification. Due to acetaminophen-induced uraemia and oxidative stress, there was a decreased rate of body weight gain in uremic group in comparison to Group I, II and IV. Also, in Group IV, the animals' BW was significantly ($P < 0.05$) increased when compared with Group III animals and it was similar to control group of animals as shown in Table 2.

Antioxidants and lipid peroxidation

Activity of CAT and SOD, as well as GSH levels, were significantly ($P < 0.05$) decreased in the acetaminophen-induced uremic Group III animals comparing control group of animals (Table 3 and 4). But on co administration of AR at 500 mg/kg BW/day for 10 days to the Group IV animals these antioxidant enzyme levels shifted towards control group of animals and increased significantly ($P < 0.05$) when compared with Group III.

Table 4. Effect of ethanol fraction of *A. racemosus* on SOD and GSH level in rats with acetaminophen-induced renal failure. Data were expressed as mean ± SE (n = 6) and data with different superscripts (a, b and c) in a specific vertical column differ from each other significantly ($p < 0.05$).

Groups	Plasma SOD (mmol of H_2O_2 consumption/dl of plasma/min)	Kidney SOD (mmol of H_2O_2 consumption/mg of tissue/min)	Kidney GSH (µmol/g of tissue)
I	0.95 ± 0.06[a]	1.31 ± 0.08[a]	19.53 ± 2.43[a]
II	0.98 ± 0.04[a]	1.38 ± 0.08[a]	20.03 ± 3.17[a]
III	0.48 ± 0.05[b]	0.55 ± 0.08[b]	5.44 ± 0.83[b]
IV	0.92 ± 0.07[a]	1.32 ± 0.07[a]	13.66 ± 1.58[c]

Table 5. Effect of ethanol fraction of *A. racemosus* on plasma and kidney MDA level in rats with acetaminophen-induced renal failure. Data were expressed as mean ± SE (n = 6) and data with different superscripts (a and b) in a specific vertical column differ from each other significantly (p < 0.05).

Groups	Plasma MDA (nmol/dl of plasma)	Kidney MDA (nmol/mg of tissue)
I	20.9 ± 6.27[a]	26.9 ± 3.5[a]
II	23.5 ± 8.5[b]	26.7 ± 2.03[b]
III	49.02 ± 5.2[b]	63.4 ± 1. 9[a]
IV	23.8 ± 3.5[a]	42.1 ± 0.32[a]

Plasma and kidney MDA levels were increased significantly (P < 0.05) in Group III animals in comparison to Group I, II and IV (Table 5). On oral administration of AR to Group IV animals, the levels of MDA decreased significantly (P < 0.05) in comparison to Group III (Table 5) and the values were very near to the control. So, the ethanol fraction of AR significantly resettled the MDA value near to the control and prevented lipid peroxidation.

Renal function effects

There was a significantly (P < 0.05) higher plasma sodium, and lower plasma potassium, level in Group III animals in comparison to other groups (Table 6), indicating that electrolyte balance was hampered due to nephrotoxicity. In Group IV, co administered with AR and acetaminophen for 10 days, electrolyte imbalance was prevented.

There was also a significant (P < 0.05) increase in the plasma urea and creatinine concentrations in the Group III. In Group IV, urea and creatinine level was significantly (P < 0.05) decreased and was very close to the controls (Table 7). Administration of AR apparently exerts maximum antioxidative and antiuremic effects on APAP-induced uremic and oxidative damage in rats.

Table 6. Effect of ethanol fraction of *A. racemosus* on plasma sodium and potassium level in rats with acetaminophen-induced renal failure. Data were expressed as mean ± SE (n = 6). Data with different superscripts (a and b) in a column differ from each other significantly (p < 0.05).

Groups	Plasma sodium (mmol/l)	Plasma potassium (mmol/l)
I	132.3 ± 3.5[a]	4.76 ± 0.42[a]
II	134.2 ± 4.22[a]	4.87 ± 0.58[a]
III	182.72 ± 2.53[b]	2.67 ± 0.37[b]
IV	138.5 ± 6.3[a]	4.68 ± 0.47[a]

Table 7. Effect of ethanol fraction of *A. racemosus* on plasma urea and creatinine level in rats with acetaminophen-induced renal failure. Data were expressed as mean ± SE (n = 6). Data with different superscripts (a and b) in a column differ from each other significantly (p < 0.05).

Groups	Plasma urea (mg/dl)	Plasma creatinine (mg/dl)
I	22.5 ± 2.27[a]	0.36 ± 0.05[a]
II	20.08 ± 3.6[b]	0.37 ± 0.03[b]
III	66.2 ± 4.2[b]	1.27 ± 0.09[a]
IV	34.8 ± 2.5[a]	0.39 ± 0.02[a]

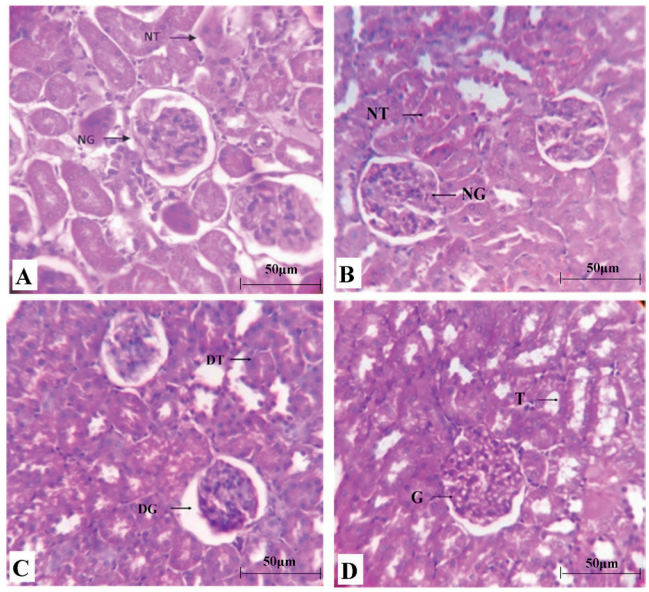

Figure 1. Histology of kidney tissues stained with hematoxylin and eosin magnified using a 40X objective. Figure 1A showing normal histology of kidney of control group of rats with normal glomerulus (NG) and renal tubules (NT) are well organized in histoarchitecture. Figure 1B showing normal histology of kidney of AR treated control group of rats with normal glomerulus (NG) and renal tubules (NT) are well organized in histoarchitecture. Figure 1C showing severe disorganization of rat kidney after acetaminophen injection of 500 mg/kg body weight to Group II rats, where damaged glomerulus (DG) and dilated renal tubules (DT) are seen. Figure 1D showing acetaminophen induced nephrotoxic rat kidney (500 mg/kg body weight) with treatment by AR (500 mg/kg) for 10 days to group IV rats showing control like histology with normal glomerulus (G) and renal tubule (T).

Histology

The histological pattern of the kidney in control and AR-treated rats showed normal tubular brush borders and intact glomeruli and Bowman's capsule (Fig. 1A, B). APAP-induced uremic Group III animals showed kidney tissues with severe tubular necrosis and degeneration in the renal tissues (Fig. 1C): dilation in tubules (DT), damaged glomeruli with a mild degree of swelling, necrosis and degranulation were present. Coadministration of AR for 10 days in Group IV ameliorated the toxic manifestations of acetaminophen in the kidney, normal glomerulus (G) with organized normal tubules (T) were seen (Fig. 1D).

HPLC analysis

Analysis of AR revealed two major and six minor peaks in the HPLC chromatogram; the two major peaks were

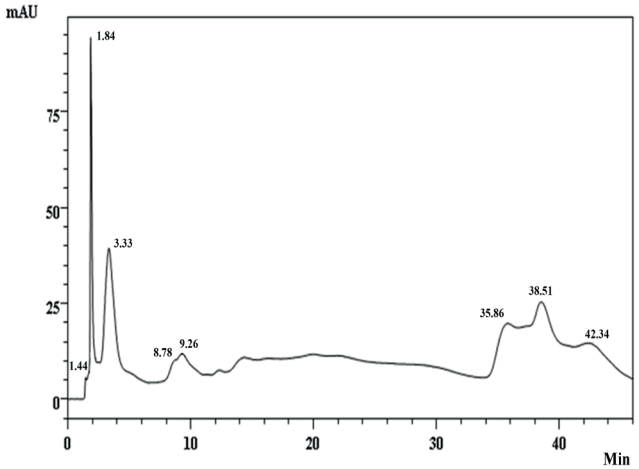

Figure 2. HPLC chromatogram of ethanol fraction of AR showing eight separate peaks.

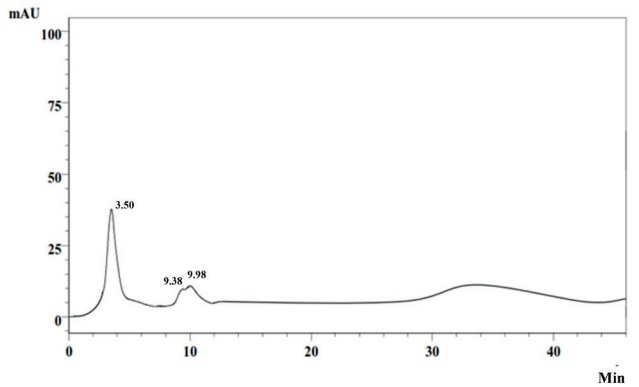

Figure 3. HPLC chromatogram of standard quercetin with one distinct peak and other minor peaks.

found at retention times of 1.849 and 3.334, respectively (Fig. 2). The quercetin standard had a HPLC chromatogram with three peaks (Fig. 3). The major compound of AR had a similar retention time (3.334) as found for the major compound of quercetin standard (3.507).

Discussion

Body weight gain decreased in uremic animals by repeated dose of acetaminophen due to oxidative stress, but co administration of ethanol fraction of AR brought the body weight back towards control.

Generation of reactive oxygen species has been proposed as a mechanism by which different chemicals can induce nephrotoxicity (Somani et al. 2000). During kidney injury, superoxide radicals were generated in body and modulate SOD and CAT, resulting in the loss of activity and accumulation of superoxide radical, which damages kidney. Several pathways are known for acetaminophen metabolism. By sulfation and glucoronidation 90% of APAP is metabolized and about 5% via cytochrome P-450 enzyme system (Slitt et al. 2005; Prescott 2005). Metabolism by cytochrome P-450 produced *N*-acetyl-*p*-benzoquinone imine (NAPQI) which is a toxic metabolite to liver and kidney. At therapeutic doses, NAPQI is conjugated with reduced glutathione, an antioxidant compound, in the liver and NAPQI is excreted by the kidneys (da Silva Melo et al. 2006). At high doses, depletion of cellular GSH allows NAPQI to bind with cellular proteins and initiate lipid peroxidation which leads to renal and hepatic injury. The high antioxidant enzyme levels in AR-treated animals might play a significant role in the mechanism of the nephroprotective effect of *A. racemosus* root extract.

Oxidative stress and lipid peroxidation are early events related to free radicals generated in the metabolism of APAP. Free radical mediated chain reactions damage cell membrane, and MDA is the most important indicator for the degree of lipid peroxidation. Earlier studies have clearly demonstrated that acute APAP overdose increases the lipid peroxidation and suppresses the antioxidant defence mechanisms in renal tissues (Roy et al. 2013; Roy et al. 2014a). On oral administration of AR to Group IV animals, the levels of MDA decreased significantly in comparison to uremic animals (Group III). It was likely that the action of compounds present in this plant fraction is mainly related to its ability to scavenge lipid peroxidation-initiating agents.

The most important biochemical alteration in APAP-induced nephrotoxicity is inhibition of Na^+/K^+-ATPase. This enzyme regulates intracellular electrolytes and cell volume. Its damage may lead to enhancement of the electrolyte imbalance across the tubular cell membrane leading to the cellular lysis and tissue injury. Furthermore, nephrotoxicity and oxidative stress causes interference in ADH secretion. This may result in loss of large volumes of dilute urine and consequent rise in plasma osmolality and serum sodium concentration.

Elevations in blood urea, serum creatinine and acute tubular necrosis were often associated with drug-induced nephrotoxicity (Pradhan et al. 2013; Roy et al. 2015). The therapeutic components present in the root of *A. racemosus,* i.e. phytosterols, saponins, polyphenols, flavonoids and ascorbic acid (Visavadiya and Narsimhacharya 2005; Roy et al. 2014b) may be responsible for reduction of the APAP-induced toxicity.

Treatment with *A. racemosus* roots could have enhanced detoxification of APAP thereby maintaining the kidney architecture. The biochemical estimations were confirmed

by the histological study of kidney tissues. Kidney sections of control groups (Fig. 1A, B) reveal normal kidney architecture with normal tubules and organized glomerulus. Kidney tissues of animals treated with APAP (Group III; Fig. 1C) showed loss of renal tubular architecture with dilated tubules and damages in glomeruli, and diffuse degenerative changes. In the renal tubules, massive cellular swelling and narrowing of lumen was evident. There were focal areas of necrosis with accumulation of protein casts in the tubular lumen. Rats treated with AR for 10 days (Group IV; Figure 1D) showed normal renal tubular architecture with organized glomeruli, very near to normal animals, there was only a very low degree of cellular swelling. The protective effects of this plant could have been due to presence of flavonoids and antioxidants (Roy et al. 2014b). These findings suggest the nephroprotective potentials of AR against acetaminophen-induced uraemia and oxidative stress.

A. racemosus roots contain phenols and flavonoids, chiefly responsible for antioxidant activity (Roy et al. 2014b). Also, the HPLC analysis of the ethanol fraction of AR showed that there was a major compound, which have similar retention time as quercetin, a flavonol from the flavonoid group of polyphenols. This compound may have comparable properties as quercetin, though further studies are necessary to identify this specific compound.

In conclusion, result suggests that the ethanol fraction of *A. racemosus* roots has a nephroprotective potential which reduces biochemical and histological damages associated with APAP toxicity. Further studies are required to find out the active principles and their possible mechanisms of action to aid the discovery of new therapeutic agents for the treatment of renal diseases.

Acknowledgements

The author thanks for financial help provided by Department of Science and Technology (DST), New Delhi in form of INSPIRE Fellowship to first author and also acknowledges to Dr. Pradip Ghosh, Director, Midnapore City College, Kuturiya, Paschim Medinipur for providing research facilities.

References

Beers RF, Sizer IW (1952) A spectrophotometric method for measuring the breakdown of hydrogen peroxide of catalase. J Biol Chem 195:133-140.

Burtis CA, Ashwood ER (1999) Tietz Textbook of Clinical Chemistry. 3rd ed, W. B. Saunders Co., Philadelphia. pp. 809-861.

Das K, Chakraborty PP, Ghosh D, Nandi DK (2010a) Protective effect of aqueous extract of *Terminalia arjuna o*n dehydrating induced oxidative stress and uremia in male rat. Iran J Pharm Res 9:153-161.

Das K, Tulsian T, Samanta P, Nandi DK (2010b) Effect of extract of *Withania sominifera* on dehydration induced oxidative stress related uremia of male rat. Saudi J Kidney Dis Transpl 21:75-80.

Elkarib AO (2014) Impact of dehydro epiandrosterone in prevention of paracetamol induced nephrotoxicity in rats. Am Med J 5:16-27.

Fored CM, Ejerblad E, Lindbland P, Fryzek JP, Dickman PW, Signorello LB, Lipworth L, Elinder CG, Blot WJ, McLaughlin JK, Zack MM, Nyren O (2001) Acetaminophen, aspirin, and chronic renal failure. New Eng J Med 345:1801-1808.

Goyal RK, Singh J, Lal H (2003) *Asparagus racemosus* - An update. Indian J Med Sci 57:408-414.

Hardman JG, Limbird LE, Gilman AG (2001) Goodman and Gilman's The Pharmacological Basis of Therapeutics, 10th ed. Chapter 4. McGraw-Hill Medical Publishing Division, New York.

Linares V, Belles M, Albina ML, Sirvent JJ, Sanchez DJ, Domingo JL (2006). Assessment of the pro-oxidant activity of uranium in kidney and testis of rats. Toxicol Lett 167:152-161.

Mandal A, Mandal S, Roy S, Patra A, Pradhan S, Das K, Paul T, Mondal KC, Nandi DK (2013c) Assessment of efficacy of a potential probiotic strain and its antiuremic and antioxidative activities. e-SPEN J 8:155-163.

Mansour HH, Hafez HF, Fahmy NM (2006) Silymarin modulates cisplatin-induced oxidative stress and hepatotoxicity in rats. J Biochem Mol Biol 39:656-661.

Marklund S, Marklund G (1947) Involvement of superoxide anion radical in autotoxidation of pyrogallol and a convenient assay of superoxide dismutase. Eur J Biochem 47:469-474.

McLaughlin JK, Lipworth L, Chow WH, Blot WJ (1998) Analgesic use and chronic renal failure: a critical review of the epidemiologic literature. Kidney Int 54:679-686.

Mukherjee KL (2010) Medical Laboratory Technology. 2nd ed. Chapter 4. New Delhi, Tata McGraw-Hill Education.

NIH (1985) NIH Guide for the Care and Use of Laboratory Animals. NIH Publication No.85-23. Bethesda MD: US Department of Health, Education and Welfare, National Institute of Health.

O'Grady JG (1997) Paracetamol-induced liver failure: prevention and management. J Hepatol 26:41-46.

Ohkawa H, Ohishi N, Yagi K (1976) Assay for lipid peroxidation in animal tissues by thiobarbituric acid reaction. Anal Biochem 95:351-358.

Olfert ED, Cross BM, McWilliam AA (1993) Guide to Care and Use of Experimental Animals, 2nd ed. Chapter 2.

Ottawa, CCAC.

Pradhan S, Mandal S, Roy S, Mandal A, Das K, Nandi DK (2013) Attenuation of uremia by orally feeding alpha-lipoic acid on acetaminophen induced uremic male rats. Saudi Pharm J 21:187-192.

Prescott L (2005) Oral or intravenous N-acetylcysteine for acetaminophen poisoning? Ann Emerg Med 45:409-413.

Roy S, Das K, Mandal S, Pradhan S, Patra A, Nandi DK (2013) Crude extract from root of Asparagus racemosus ameliorates acetaminophen induced uremic rats. Int J Pharm Sci Res 4: 3004-3012.

Roy S, Pradhan S, Das K, Mandal A, Mandal S, Patra A, Samanta A, Sinha B, Nandi DK (2015) Acetaminophen induced kidney failure in rats: a dose response study. J Biol Sci 15:187-193.

Roy S, Das K, Mandal S, Pradhan S, Patra A, Samanta A, Mandal A, Kar S, Nandi DK (2014a) *Asparagus racemosus* roots ameliorates acetaminophen induced hepatotoxicity in rats: an experimental, biochemical and histological study. Int J Recent Sci Res 5:1192-1197.

Roy S, Pradhan S, Mandal S, Das K, Patra A, Samanta A, Sinha B, Kar S, Nandi DK (2014b). Phytochemical analysis, antimicrobial activity and assessment of potential compounds by thin layer chromatography of ethanol fraction of *Asparagus racemosus* roots. Int J Pharm Pharm Sci 6:367-370.

da Silva Melo DA, Saciura VC, Poloni JA, Oliveira CS, Filho JC, Padilha RZ, Reichel CL, Neto EJ, Oliveira RM, D'avila LC, Kessler A, de Oliveira JR (2006) Evaluation of renal enzymuria and cellular excretion as a marker of acute nephrotoxicity due to an overdose of acetaminophen in Wistar rats. Clin Chim Acta 373:88-91.

Slitt AML, Dominick PK, Roberts JC, Cohen SD (2005) Effects of ribose cysteine pretreatment on hepatic and renal acetaminophen metabolite formation and glutathione depletion. Basic Clin Pharmacol Toxicol 96:487-494.

Somani SM, Husain K, Whitworth C, Trammell GL, Malafa M, Rybak LP (2000) Dose-dependent protection by lipoic acid against cisplatin-induced nephrotoxicity in rats: antioxidant defense system. Pharmacol Toxicol 86: 234-241.

Sunderman FW (1959) Studies on the serum proteins. IV. The dye-binding of purified serum proteins separated by continuous-flow electrophoresis. Clin Chem 5:171-185.

Visavadiya NP, Narsimhacharya AV (2005). Hypolipidemic and antioxidant activities of *Asparagus racemosus* in hypercholesteromic rats. Indian J Pharmacol 37:376-380.

Youdin KA, Deans SG, Finlayson HJ (2002) The antioxidant properties of thyme (*Thymus zygis* L.) essential oil: an inhibitor of lipid peroxidation and a free radical scavenger. J Essen Oil Res 14: 210-215.

Acta Biologica Szegediensis

Volume 62(1):25-36, 2018
Acta Biologica Szegediensis
http://abs.bibl.u-szeged.hu/index.php/abs
DOI:10.14232/abs.2018.1.25-36

ARTICLE

Aspects of ecological anatomy of *Traganum nudatum* Del. (Amaranthaceae) from the Northeast of the Algerian Sahara

Mohamed Elhafed Kherraze[1,2*], Mohamed Belhamra[3], Marius-Nicuşor Grigore[4]

[1]Department of Ecology and Environment, Faculty of Science and the Natural and Life Science and Sciences of Earth and the Universe, University of Abou Bakr Belkaid, Tlemcen 13000, Algeria
[2]Scientific and Technical Research Center of Arid Areas (CRSTRA), Biophysical Station, 3240 Nezla, Touggourt, Algeria
[3]Department of Agronomy, Faculty of Science and the Natural and Life Sciences, University of Mohamed Kheider, Biskra, Algeria
[4]Alexandru Ioan Cuza University, Faculty of Biology, Iaşi, Romania

ABSTRACT This study focuses on the anatomical strategies developed by the *Traganum nudatum* Del., prevalent in the Algerian Sahara, particularly in the region of Oued Righ, which allows to this species to survive in a harsh environment (aridity and salinity). The anatomical structure of this species was studied using fresh materials (roots, stems and leaves). These materials have been collected from several individuals in different saline habitats. Some interesting features such as successive cambia phenomenon, calcium oxalate crystals, Kranz anatomy (salsoloid subtype), succulence, low stomata density, low stomata index, the presence of the papillae, paracytic stomata and other structures have been noticed. We can conclude that the ecological significance of evidenced adaptations by *T. nudatum* is supported in this article by the analysis of adaptations of other species belonging either to the Amaranthaceae or to other botanical families; and that this adaptation has no link with botanical families. In these species, the key adaptation is the ability to maintain growth processes and water saving under difficult living conditions (high summer temperatures or salty soils), regardless of the evolutionary level of the taxon.

KEY WORDS
Kranz anatomy
photosynthesis C4 strategy
successive cambia
succulence

ARTICLE INFORMATION
Submitted
25 December 2017.
Accepted
30 March 2018.
***Corresponding author**
E-mail: kherrazetggt@gmail.com

Introduction

Natural rangelands in North Africa cover an area of 130 million hectares (Ben M'hamed 1990). The flora of these rangelands, important for its specific and infraspecific diversity, is typically Mediterranean with a highly developed Ibero-Maghreb element (Le Houérou 1980). Iranian-Turanian and Saharan-Sindien species are restricted to arid and desert regions. A number of genera of Amaranthaceae family are important components of the flora and vegetation of the arid to semi-arid saline environments as well as agricultural habitats in temperate and subtropical regions (Keshaavrzi and Zare 2006; Grigore 2012; Grigore et al. 2014; Safiallah et al. 2017). Amaranthaceae includes 110 to 166 genera with 1700 species (Cuenoud et al. 2002; Safiallah et al. 2017). It is one of the most interesting families in terms of having species with a great diversity the structure of carbon assimilating organs with different types of photosynthesis C_3 or C_4 (Grigore and Toma 2007; Grigore et al. 2014; Grigore and Toma 2017). The genus *Traganum* Delile, which belongs to the subfamily Salsoloideae, is represented in Amaranthaceae family by a perennial plant species, *Traganum nudatum* Delile (Fig. 1).

Traganum nudatum Del. is a Saharan-Sindien species, non-threatened, classified as "C" (IUCN 2005) and is listed on the floristic list of several protected sites listed by the UNEP World Conservation Monitoring Center (UNEP), (United Nations Environment Programme). It is a xerohalophyte species, chamaephyte (Nedjimi et al. 2012), cosmopolitan (Mroczek 2015), widespread throughout North Africa and Asia (IUCN 2005). Beside other plants belonging to the Amaranthaceae family that have a therapeutic use, such as *Cornulaca monacantha* Del., and *Haloxylon articulatum* Boiss. *Traganum nudatum* is a plant used in the traditional medicine of southern Algeria against diarrhea, wound, rheumatism, dermatitis, otitis, hemorrhoids and back pain especially low back pain. The used part is the leaf, and its mode of use is by

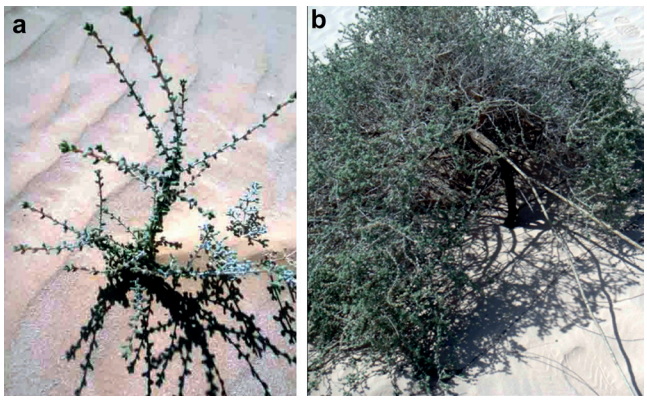

Figure 1. General view of *T. nudatum*. (a) young plant (flexible); (b) adult plant (curved and rigid).

compressed maceration, powder, or pomade (Ould El Hadj et al. 2003; Kalla 2012). Thus, the *Traganum nudatum* with other species such as *Aristida pungens*, *Zilla spinosa*, *Calligonum comosum*, *Anabasis articulata* and *Limoniastrum guyonianum* are considered to be among the most palatable species in previous studies conducted in the camel rangeland (Chehma 2006; Longo-Hammouda et al. 2007; Chehma et al. 2010; Lakhdari et al. 2015). The consumed parts are leaves and tender twigs (Bouallala et al. 2011).

The pastoral areas are dominated by steppes with variable physiognomy (grasses, chamaephyte, halophytes) (Le Floc'h 1995). Several ecological constraints of Mediterranean ecosystems can influence the physiognomy and physiology of plants. The appearance and structures that characterize certain groups of plants summarize to a large extent their ecological and physiological adaptations. *Traganum nudatum* is no exception to this rule, because of the typical structural features of the lands that distinguishes it from other groups of plants. It develops almost all important xerophytic devices to cope with the various hazards of nature such as water scarcity, heat and salt stress. These constraints are extremely detrimental to plant growth and development. Morphological and anatomical modifications of the plant organs can minimize the harmful effects of salt stress (Poljakoff-Mayber 1988; Grigore and Toma 2017).

Morphological, micromorphological and anatomical characteristics are important features, which can be implicated in taxonomical diagnosis, as well as in explaining ecological conditions (Safiallah et al. 2017). Despite the pastoral and medicinal importance of *Traganum nudatum* mentioned above, few anatomical studies have been conducted on this plant species, which led us to perform an anatomical study on the roots, stems and leaves in order to gain a global understanding of the adaptation strategy adopted by *T. nudatum*, facing the hostility of the Saharan habitats, by defining some anatomical characters all by referring in the explanation to previous studies that have been carried out on species.

Materials and Methods

Study area

The study area is located in the region of Oued Righ in the north-east of the Algerian Sahara (between 32° 54' to 39° 9' N, and 05° 50' to 05° 75' E; Fig. 2). The climate is described as Mediterranean hyperarid. The average annual rainfall does not exceed 70.3 mm (1975-2013). These insufficient rains are associated with a significant irregularity of the rains regime and a considerable inter-annual variability, which lead to a period of severe and long drought (Fig. 3). The average annual temperature is 28.47 °C. The average annual relative humidity is around

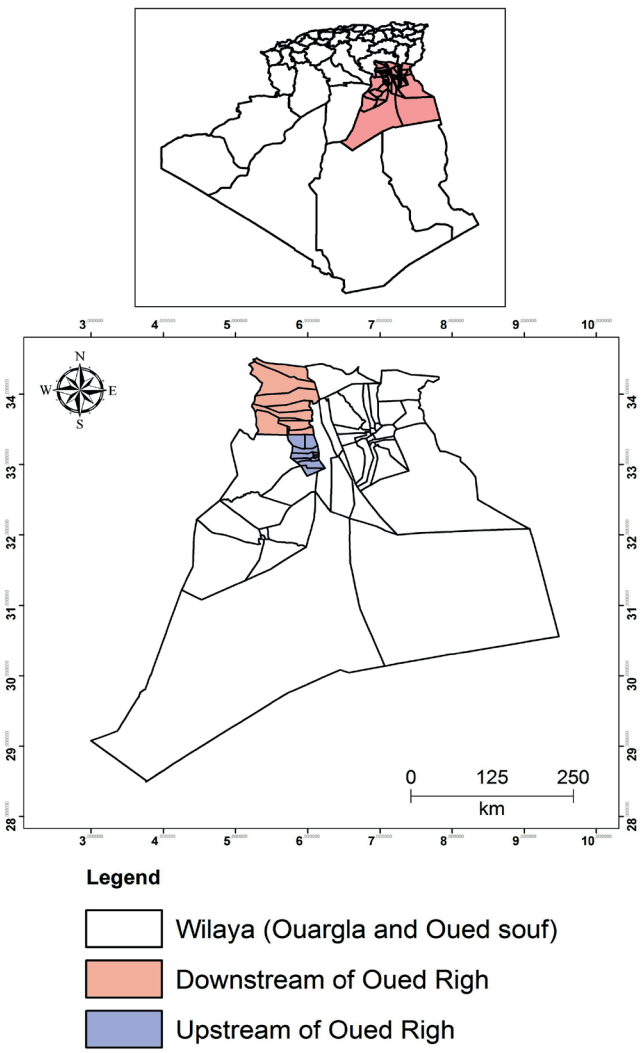

Figure 2. Map indicating the study region.

48%. The average annual evaporation is 237.96 mm, a Saharan bioclimatic stage with a mild winter. Due to the low cloudiness, sunlight in the Sahara is relatively strong and has a drying effect by increasing the temperature (Ozenda 2004).

The soils of the Saharan zone of Algeria contain significant amounts of soluble salts. Their accumulation is due to the rarity of rains that do not penetrate deeply into the soil to cause appreciable infiltration (Halilet 1998). Sogreah (1971) and Abid (1995) define the origin of soils in the Oued Righ region as alluvial, colluvial and Aeolian. The upstream portion (Touggourt) of Oued Righ is composed of shallow Aeolian sandy soils with gypsum crust and the downstream part (Djamaa) of aebral sandy soils deeper with encrustation of more recent gypsum (Mtimet and Hachicha 1998) the soils become hydromorphic all go down (El M'ghiar) in the super-salty depressions composed of fine alluvium.

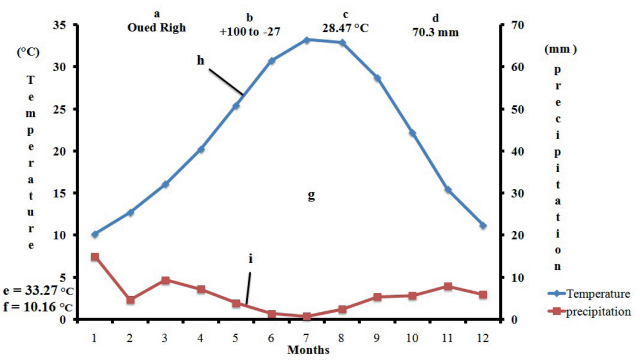

Figure 3. The climatic diagram of Oued Righ. (a) region; (b) the altitude changes gradually from + 100 m to El Goug (the upstream of Oued Righ) to - 27 m in the middle of the chott Méroune (the downstream of Oued Righ); (c) mean annual temperature (°C); (d) mean annual precipitation (mm); (e) the highest temperature average for the hottest month (°C); (f) the lowest temperature average for the coldest month (°C); (g) dry period; (i) temperature curve; (h) precipitation curve.

Sample collection and processing

In the basis of representativity, indicating the presence of several individuals of the same species at the same place (Gounot 1969), we have chosen a most dominant and abundant spontaneous species (Ozenda 1991), known by the dromedary breeders of the region under the name "Damrane", it is *T. nudatum*, belonging to the Amaranthaceae family. To carry out the various observations, cuts and analysis, we collected the plant material on about ten individuals developed in saline soil during the year 2016-2017.

The fresh material (roots, stems and leaves) was fixed and stored in alcohol (70%), according to the usual procedures. A freehand and with a sharp blade, we made very thin cross-sections on the stem in the middle part and on the roots 2 cm from the root apex, also on leaves located at the median of the twigs. These materials were treated with sodium hypochlorite for 10-15 min to empty the cells of their contents, followed by extensive washing with water, followed by rapid washing in 1% diluted acetic acid. The staining was performed in duplicate with methyl green (10 min), followed by water washing and Congo red (for 15 min), followed by washing with water (Ben Dob and Khouildat 2016). Once stained, the preparations were observed and photographed using Motic Digital light microscope (DMB1-2 MP, Motic Instruments, Xiamen, China).

Stomatal density (DS) was calculated according to Timmerman (1927) by the ratio of the number of stomata per unit area on the lower or upper faces of the leaves. By the formula: DS (Stomata per mm^2) = Number of stomata/area. Stomatal index (IS) was calculated according to the method described by Meidner and Mansfield (1968) using the value of (IS) per unit area given: IS (%) = [S/(S + E)] * 100, where, (S) is the number of stomata per unit area and (E) the number of epidermal cells for the same unit. The number of stomata and the number of epidermal cells on both sides of the leaf were counted in a 1 mm^2 area.

Results and Discussion

The observation of anatomical sections made at the root level of the species shows a successive cambia (additional) phenomenon, which is formed of incomplete concentric rings of xylem tissue, phloem tissue and cambia (Fig. 4a). This formation gives to the root the lignified aspect and it offers an ecological advantage in the conditions of water stress. Grigore and Toma (2007; 2017) found in halophytic chenopods, especially in the tertiary structure of organs that are affected by the successive cambia phenomenon, a huge amount of lignin. They have also suggested that lignin may be an element of cellular resistance against high osmotic pressure within the body of the plant (Grigore and Toma 2007; 2017). Robert et al. (2011) state that successive cambia is an important anatomical feature of wood, partially explaining the distribution of ecological species, also the appearance of species in extremely high salinity conditions such as the species of *Avicennia marina*. This phenomenon has also been recorded in stems and roots of the species *Sesuvium portulacastrum*, *Trianthema portulacastrum* and *Boerhaavia diffusa* (Patil et al. 2016).

The stele (central cylinder) of the root is wider than the cortex (Fig. 4b), it is a characteristic of the roots of the plants vegetating in salty deserts, and they seem to reduce their cortex in order to obtain a short distance between the epidermis and the central cylinder (Wahid 2003). This pattern was similar to some of the Amaranthaceae

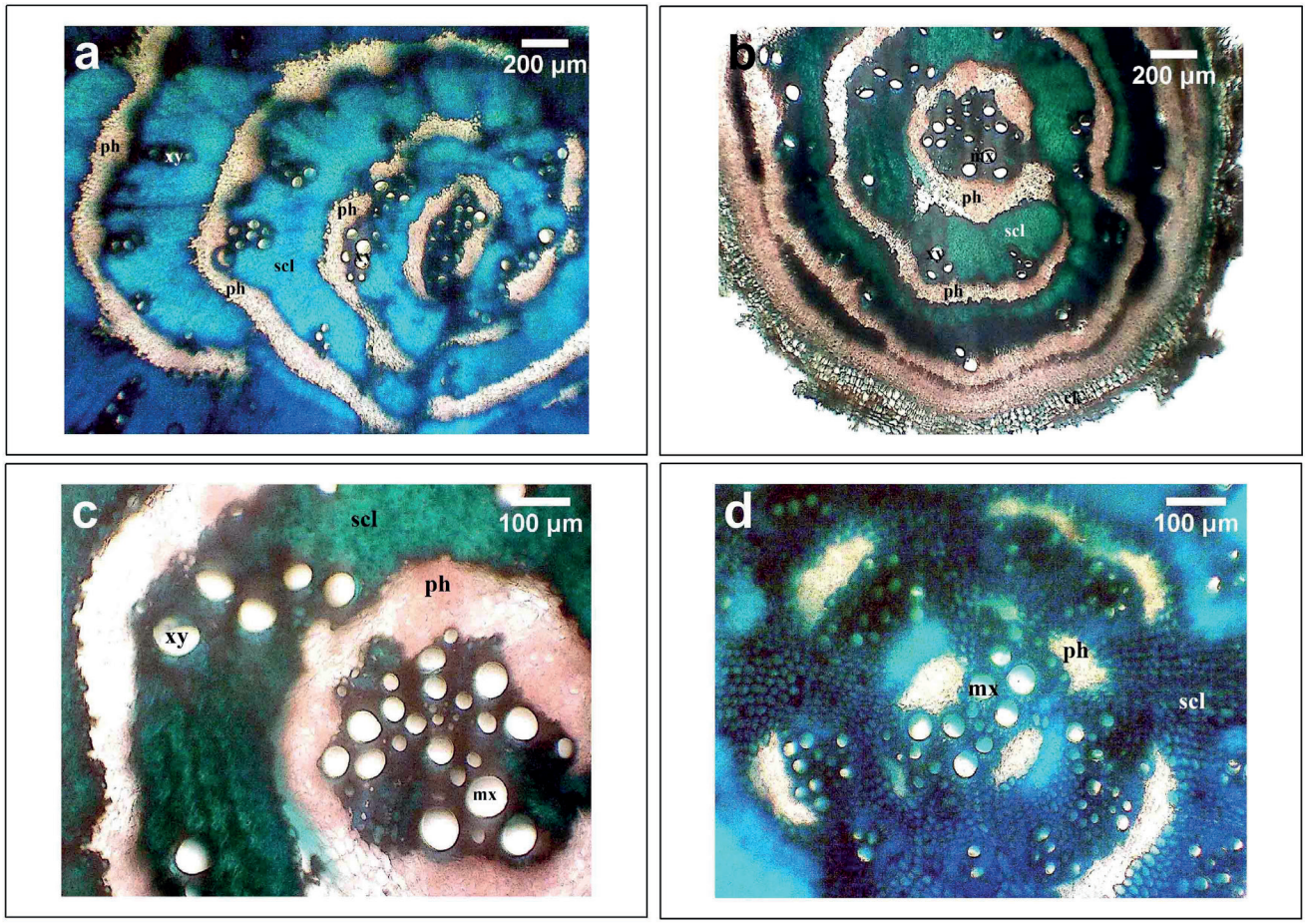

Figure 4. Cross-sections through the root of *T. nudatum*. (a) showing the successive cambia; (b) showing a wider central cylinder; (c) showing larger and more numerous metaxylem vessels; (d) showing the massive sclerification of the central cylinder (stele). xy: xylem; ph: phloem; ck: cork; mx: metaxylem; scl: sclerenchyma.

halophytes such as *Atriplex tatarica*, *Suaeda maritima* and *Camphorosma annua* (Grigore and Toma 2007). On the analyses slide (Fig. 4b), there is an interesting disposition of additional cambia products in a continuous spiral-like ring, with conjunctive tissue located between it.

The vessels of the metaxylem which are in fact the xylem vessels carrying the sap appear at the same time more widened in diameter and more numerous (Fig. 4c), which could facilitate the circulation of the water, as has been reported by Zhu et al. (2000) in *Puccinellia tenuiflora*, a highly salt tolerant species. Hameed et al. (2010) suggested that increasing the surface of metaxylem plays an important role in water conduction, and assimilates, especially in adverse salt conditions. This has been confirmed in rice (Datta and Som 1973), *Kandelia candel* (Hwang and Chen 1995), *Ziziphus lotus* (Awasthi and Pathak 1999), and *Arabidopsis thaliana* (Baloch et al. 1998). The same appearance was also observed in the genera of *Atriplex* (larger in *A. halimus*, narrower and numerous in *A. nummularia*, and wider and more numerous in *A. canescens* subjected to salt stress) (Mâalem 2011). It should also be underlined that a sclerification invades the entire mass of the central cylinder, where it can be observed that its center was previously completely occupied by metaxylem vessels (Fig. 4d). The cell walls of the sclerenchyma have thick secondary layers. This thickness was based on cellulose, hemicellulose and lignin, which will give our species hardness and rigidity (Jarvis 2012). The analyses of Chehma et al. (2010), which were carried out on the chemical composition of 21 spontaneous perennial plants from the northern Algerian Sahara, as well as the chemical analyzes of Bouallala et al. (2011) on the main plants grazed by the dromedary of the Algerian Western Sahara confirms our observation. According to Chehma et al. (2010), the dry matter percentage of crude cellulose in *T. nudatum* was 32.8% DM and 27.33% DM found by Bouallala et al. (2011) in the same species. According to Bouallala et al. (2011) the raw cellulose richness of Sa-

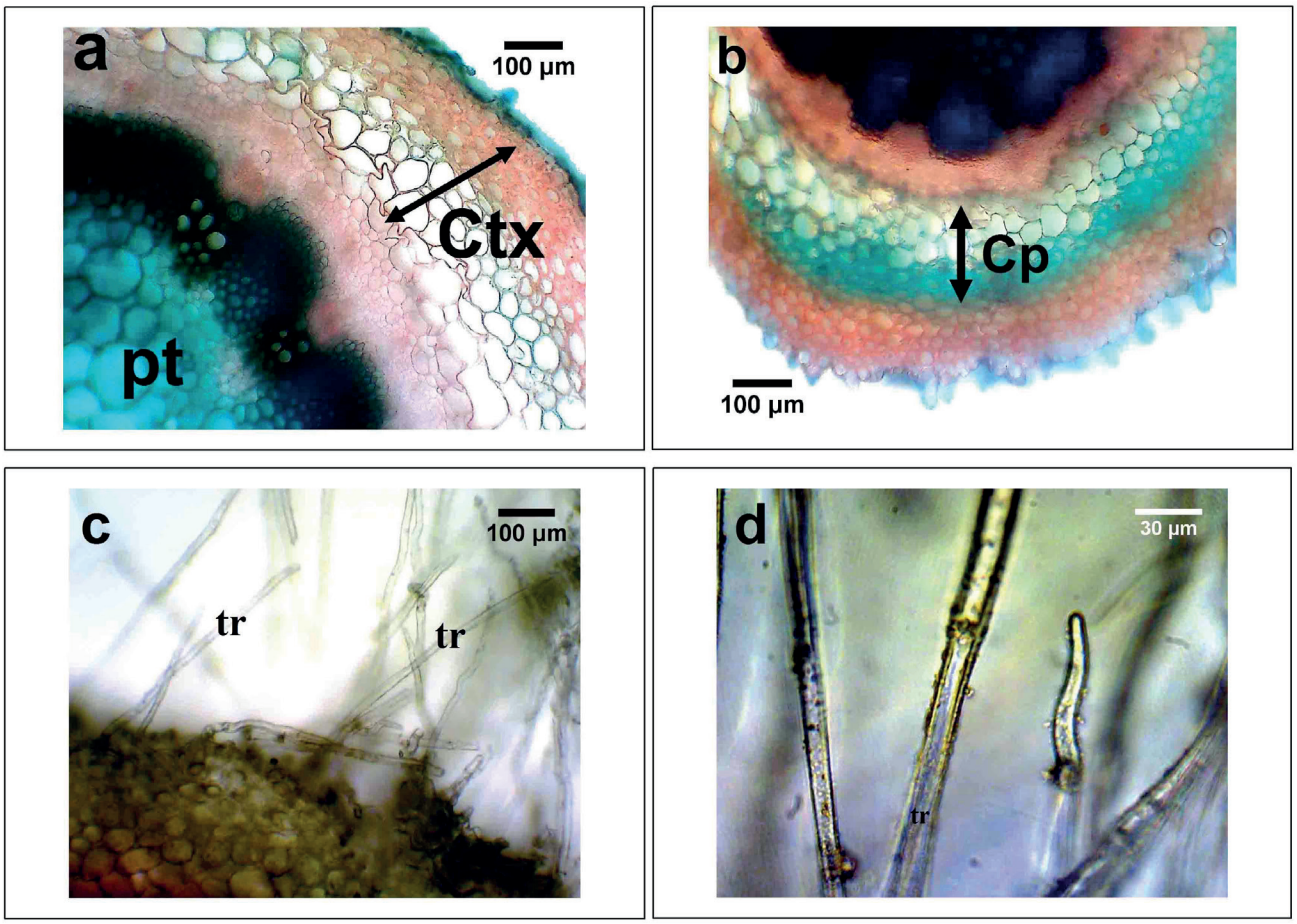

Figure 5. Cross-sections through the stem of *T. nudatum*. (a) showing the reduction of the cortex compared to the central cylinder (stele) and lignification of the pith; ctx: cortex; pt: pith; (b) showing the lignification of cortical parenchyma; cp: cortical parenchyma; (c, d) showing the multicellular trichomes, thread-like, on the epidermis of the stem; tr : trichome.

haran plants is related to their adaptation mechanism. Jarrige (1981) and Demarquilly (1982) point out that the increase in temperature stimulates the lignifications of supporting tissues. Grigore and Toma (2017) consider that all implications related to successive cambia could be related to an increased internal surface, if considering only the high capacity of retention and "storage" of the saltwater in root and stem. On the other hand, the cork outward the root could also delay water absorption. Therefore, salts penetrate slowly in roots, but once arrived there, they would be dispersed in this increased surface. Literally, the water distribution to the rest of the plant's organs seems to be "delayed." Increasing this surface would inevitably mean a dispersion area for salts, which are also diluted, thus these being ultimately less harmful to the plant. Undoubtedly, the number and diameter of xylem vessels may play a role in this mechanism.

We found well developed collenchyma tissue under the epidermis of the stem; it may confer to the stem good elasticity, great resistance to flexion, traction, and good support, since the cells of the collenchyma have very thick cellulosic walls (Zaffran 1998). This anatomical observation corresponds perfectly to the state of aspect of the studied species. The plant is more erect and more flexible in the case of young plants and becomes curved and lignified in adulthood, which confers a form ranging from large tufts to that of a shrub. The elasticity may be advantageous for young plants facing intense wind usually existing in the spring period. The cortex of the stem appears to be reduced in thickness, this corresponding to an adaptive value (Fig. 5a). In fact, this adaptation has been observed in the twigs of *Salsola vermiculata*, *Rhanterium adpressum* (Houari et al. 2012) and even in the alfalfa stem (Zaffran 1998). However, in some halophytic species such as *Euphorbia guyoniana* and *Petrosimonia oppositifolia*, the cortex is very broad with a cortical parenchyma consisting of large water storage cells which gives to these species a succulent appearance (Houari et al. 2012; Grigore

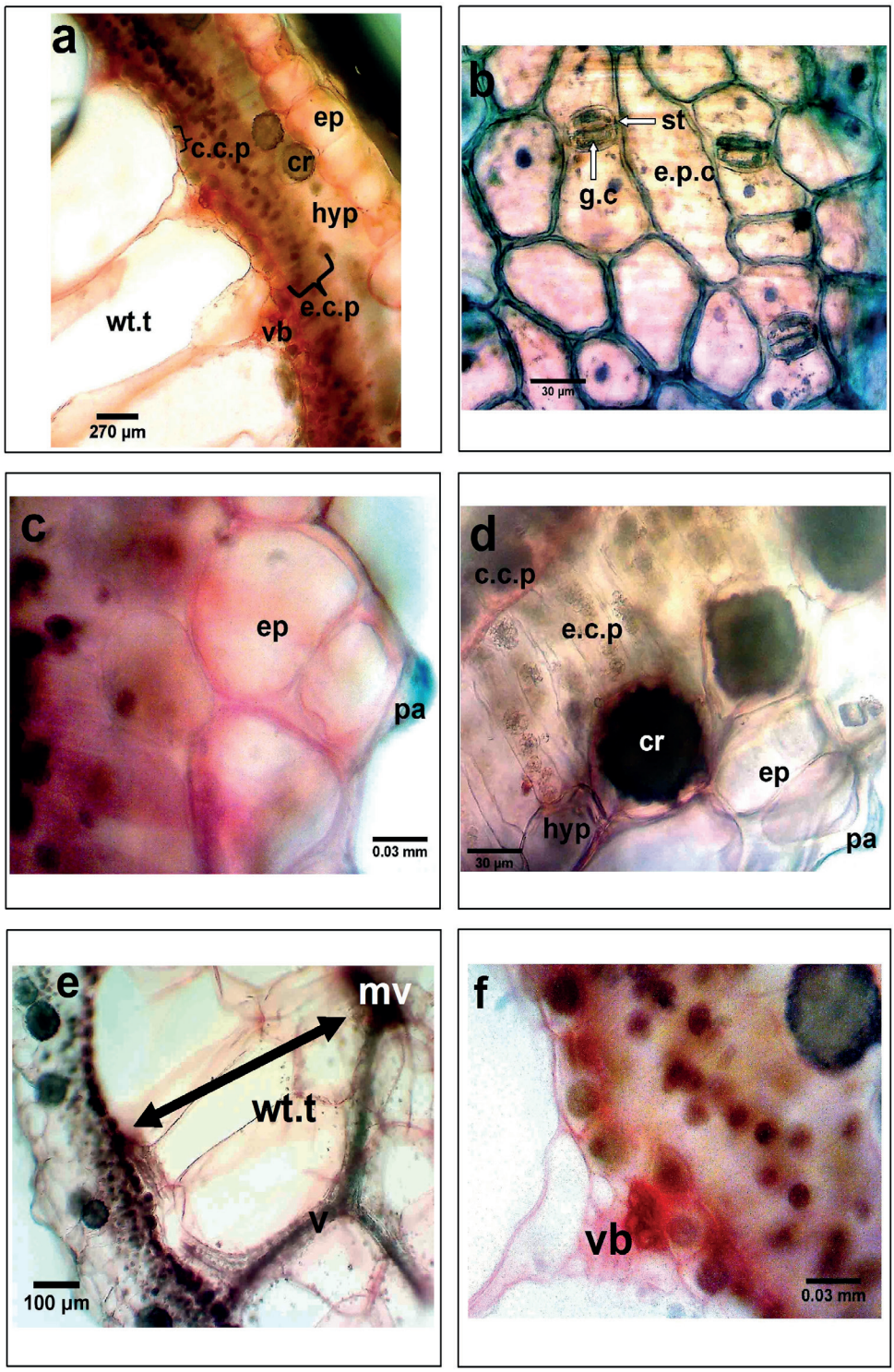

Figure 6. Cross-sections of C4 leaf in *T. nudatum*. Fig. 6a. general view (arrangement of cellular tissues in the lamina); Fig. 6b. shows the arrangement of stomata (paracytic type); Fig. 6c. papilla non aiguë in the epidermis; Fig. 6d. shows the organization of the chlorenchymatic (assimilative) parenchyma in two layers (external (e.c.p) and internal (c.c.p) and the presence of a hypodermis rich in crystals of calcium oxalate (twin form); Fig. 6e. shows large cells of water storage tissue occupying the central area of the leaf and the arrangement of the ribs; Fig. 6f. shows the contact of a vascular bundle with the inner layer (c.c.p) (structural model - known as Kranz anatomy of salsoloid type). ep: epidermis; hyp: hypodermis; e.c.p: elongated cell parenchyma; c.c.p: cubic cell parenchyma; cr: calcium oxalate crystals; vb: vascular bundle; wt.t: water storage tissue; st: stoma; g.c: guard cells; ep.c: epidermal cells; pa: papilla; mv: main vein; v: vein.

and Toma 2007). Another adaptive trait that appears to strengthen the organ in question (stem) is the lignification of cortical parenchyma. This lignification makes the tissues rigid and therefore provides mechanical support to the stem (Fig. 5b). According to Wang et al. (1997), under saline stress, the lignification of the apex of the stems becomes more and more pronounced in *A. prostrata*. The lignification of the pith also appears to give mechanical support to the stem (Fig. 5a). This same aspect was also observed in the pith of the American species *Atriplex canescens* subjected to salt stress (Mâalem 2011) and in the species *Smilax aspera* (Zaffran 1998).

We also evidenced the presence of multicellular trichomes, thread-like, on the surface of the epidermis of the stem of young plants (*T. nudatum*) (Figs. 5c, d). However, the stems of adult plants are completely hairless. These trichomes could have a protective function against environmental changes (*e.g.,* excessive heat). Thus, the presence of *T. nudatum* in open habitats, hot and dry in the study area may be one reason for the presence of these trichomes in young plants (*T. nudatum*) to protect the most sensitive tissues. Some authors such as Grigorev (1955) cited by Weryszko-Chmielewska and Chernetskyy (2005), Agren and Schemske (1993), Nabors (2008) reported that these trichomes protects plants against drought (reducing the intensity of transpiration), prevent the increase in temperature, maintain moisture at surface level (stem or leaf), also they have a defensive function (insect attack or herbivores), it may be a reason more to the presence of these trichomes in young seedlings. In addition to these previous observations on the stem and the root, the anatomical characteristics of the *T. nudatum* leaf are expressed by several criteria related to the mode of adaptation to the Saharan environment (Fig. 6a). A structure evidenced at the level of the epidermis, presence of a paracytic-type stomata arrangement, where two lateral secondary cells oriented parallel to the guard cells (Fig. 6b), as described by Carpenter (2005) based on the work of Dilcher (1974). This paracytic type reflects the xerophytic features of the species (Smail-Saadoun 2005a; Kadi-Bennane et al. 2005). Kadi-Bennane et al. (2005) have reported that the increase in paracytic type frequency is influenced by climatic conditions, this fact is demonstrated with the species of the genus *Pistacia*, where the authors found a positive correlation between the increase of the frequency of the paracytic type and the increase of the degree of aridity of the station. The higher the degree of aridity of the station, the more the frequency of the paracytic type increases (the Emberger coefficient of the stations: Ain Oussera, Messaad and Taissa respectively 23, 16 and 10). We compare these coefficients with those of the region of Oued Righ which is 6.63; we see that these results of these authors support our observation. This type of stomata arrangement (paracytic) has also been found in spontaneous species of the northern Sahara such as *Limoniastrum guyonianum* (Plumbaginaceae), *Anabsis articulata* (Amaranthaceae) and *Pituranthos chloranthus* (Apiaceae) (Benghersallah 2013). Other anatomical features evidenced in the leaf can be correlated with the peculiarities of the environment (very long dry period and very high summer temperature) where the plant grows, which would explain the required presence of a low stomatal density (01-03 stomata/mm²) with a low stomatal index (by means of 11.6%). This observation was supported by the work of Finsinger et al. (2013), who suggested that variation in stomatal frequency (stomatal density and stomatal index) was related to regional environmental conditions (climatic). Kadi-Bennane et al. (2005) have reported that stomatal density is influenced by climatic conditions, this fact is demonstrated with species of the genus *Pistacia* where the authors found a correlation between stomatal density and aridity degree of the station. Other authors such as Flowers et al. (1986), Bray and Reid (2002) reported decreasing the number of stomata and stomatal index at increased salinity of the soil. Indeed, the plant by using this strategy of reducing the number of stomata decreases the loss of water by evaporation (Gorenflot 1980).

In addition, we were able to evidence at the level of the leaf, the presence of an eminence in the form of a papilla, non-acute of a length varying between 0.02 mm and 0.50 mm at the level of the epidermis (Fig. 6c). A subepidermal layer, hypodermis, rich in calcium oxalate crystals in the form of twins (Fig. 6d) has been evidenced. There are two types of chlorenchyma located under the epidermis and hypodermis: an external chlorenchyma consisting of elongated cells of cylindrical form, and an internal chlorenchyma made of cubic cells (Fig. 6d). A developed water storage tissue occupies the central zone (Figs. 6e, 7a), and it is formed of large cells with thin wall, in which the nervures radiate in all directions, which observed to anastomose in a network under the inner layer of cubic cells (Figs. 6f, 7b).

The observation of the papillae was also recorded at a cross section of the stem in a hygro-halophytic species collected from different salt marshes of Iran: the *Halostachys belangeriana* (Moq.). Botch with a length varies between 0.04 mm and 0.06 mm and the stem of *Halocnemum strobilaceum* (Pall.) M. Bieb with a length of about 0.01 mm (Keshaavrzi and Zare 2006). Thus, our observations to other tissues were consistent with the observations of Smail-Saadoun (2005b) at the level of *T. nudatum* leaf harvested in the Béni-Abbès region (Algeria).We note that the presence of the hypodermis was also able to characterize 8 species of *Chenopodiaceae* on the 14 species studied by Saadoun (2005b), and the assimilating parenchyma structure also made it possible

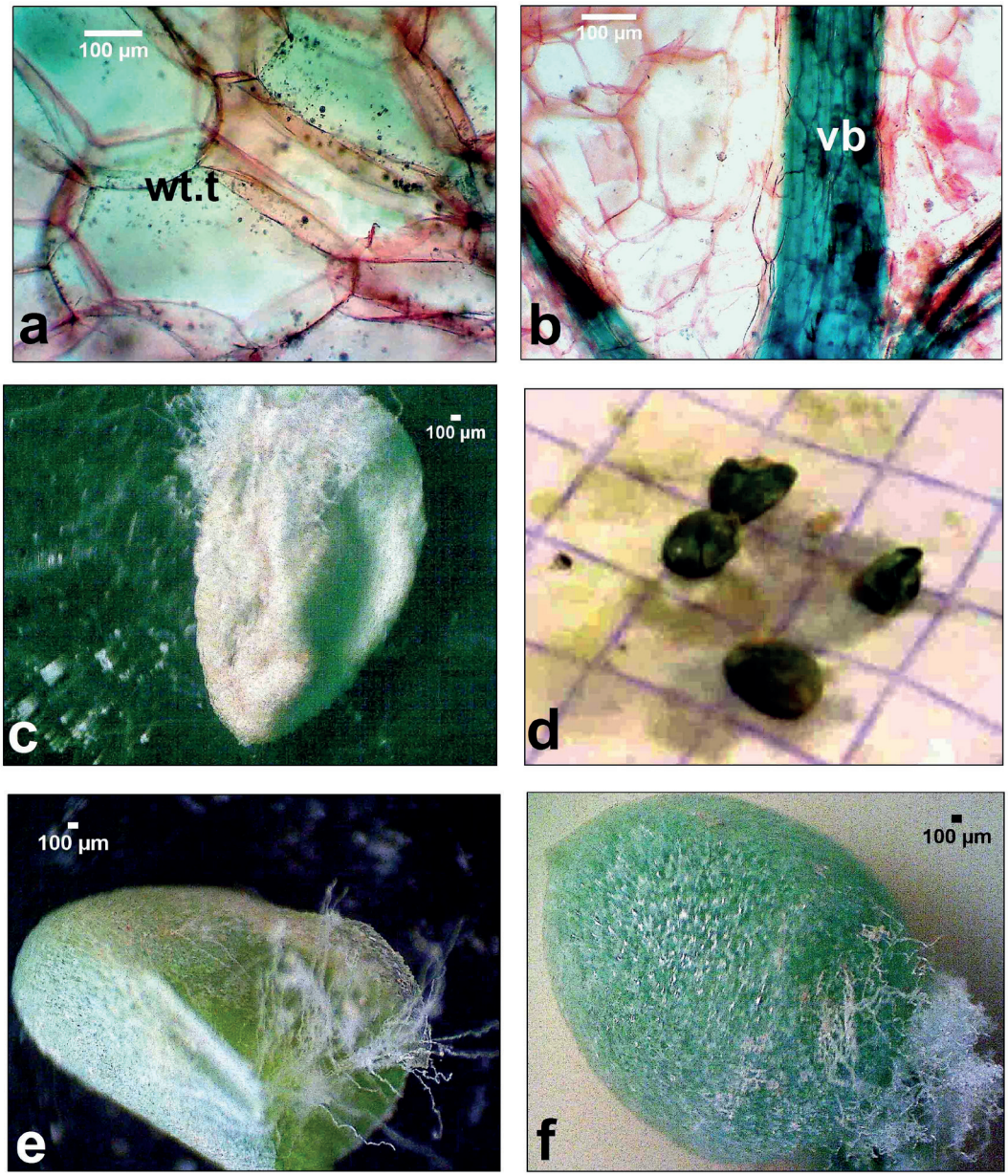

Figure 7. An overview of some morphological and anatomical of the leaf of *T. nudatum*. (a) a cross section shows the water storage tissue; (b) a longitudinal section shows the vascular network; (c) showing a dried leaf; (d) a millimeter paper wet with water sap from compressed leaves; (e, f) showing the succulent appearance of leaves.

to characterize 11 species of Chenopodiaceae studied by the same author. These interesting structures that have been evidenced at the leaf level can be correlated with the peculiarities of the environment, in which the *T. nudatum* grows. Indeed, in the case of excessive heat, the papillae structure of the epidermis of the *T. nudatum* leaf contributes to disseminate the heat. According to Collin (2001), the high heat can have a negative impact on the metabolism of the plant. The same author also argues that the presence of papilla in some cacti (e.g., *Mammilaria* and *Echinopsis*) helps dissipate heat.

The presence of the hypodermis can reinforce the insulating and mechanical characteristics of the epidermis. A particular function of this tissue has been suggested by Pautov and Telepova-Texier (1999) that the hypodermis ensures the absorption of most of the radiation and thus reduces the heat load on the plant, as it participates in the transport of substances in the subepidermal layer of the

mesophyll and also, it protects the foliar blanks against dehydration. Another function of the hypodermis reported by Smail-Saadoun (2005b) is that the hypodermis separates the assimilative parenchyma from the surface of the leaves. The richness of the hypodermis by calcium oxalate crystals could be correlated with plant metabolism. It is an end product of metabolism (Franceschi and Horner 1980) and can also be considered as an effort to maintain ionic balance (Franceschi and Horner 1980; Grigore et al. 2014). Some authors such as Paupardin (1965) and Calmes and Piquemal (1977) cited by Vintéjoux and Shoar-Ghafari (1985) working on other plants, respectively, vine and hawthorn grown *in vitro*, proved that calcium oxalate could be reused in the tissue metabolism of these plants. These last results will encourage us to realize in the future studies in this direction on *T. nudatum*. The organization of assimilating parenchyma in *T. nudatum* in two adjoining and different layers: outer layer with elongated cells (e.c.p) (also called external chlorenchyma) and inner layer with cubic cells (c.c.p) (also called internal chlorenchyma) refer to a specific functional anatomy. This examination is confirmed by the work of Smail-Saadoun (2005b), Muhaidat et al. (2007), Houari et al. (2012), Grigore and Toma (2007), on several genera: *Kochia, Camphorosma, Petrosimonia, Atriplex, Anabasis, Salsola* and *Bassia*.

According to Ting (1975) and Depuit (1978), the species bearing this organization correspond to the photosynthetic pathway of the C_4 type (Figs. 6a, 6d and 6f). According to the work of Smail-Saadoun (2005b), Muhaidat et al. (2007), Houari et al. (2012), the cubic cells of the inner layer are characterized by a greater number of chloroplasts and mitochondria than the elongated cells of the outer layer. In addition, many vascular elements have been observed that anastomose in a network under the cubic layer (presence of vein contact with the inner layer), which seems to be a more specialized layer than the outer layer of elongated cells. According to Muhaidat et al. (2007), this structural model – known as Kranz anatomy – belongs to salsoloid subtype. It has been shown at the level of the species *Salsola kamarovii* (Amaranthaceae) by the same author. This internal architecture physically divides the biochemical events of the C_4 pathway into two stages. (I) Beforehand atmospheric CO_2 is incorporated into four-carbon acids, hence the name C_4 photosynthesis. This incorporation will take place at the level of the external layer (e.c.p), (II) decarboxylation of this C_4 acid and the released CO_2 is re-fixed by Rubisco specific to the internal tissue (c.c.p) (Muhaidat et al. (2007). This bi-phasic system C_4 seems to be a good adaptation to drought since the Calvin cycle and carbohydrate synthesis occur at the level of the internal cells (c.c.p) of the parenchyma assimilator away from the heat and in the vicinity of the vessels, which implies an easier water supply and fast evacuation of carbohydrates (Heller et al. 1993; Sage 2004; Smail-Saadoun 2005b; Houari et al. 2012). In addition to the importance of the successive cambia phenomenon at the root level, or to Kranz anatomy from leaf level, there is also another more important phenomenon at the level of the *T. nudatum* leaf. It is the phenomenon of succulence, which is correlated with local environmental factors. Thus, *T. nudatum* was collected from saline soil, which would explain the necessary presence of water storage tissue at the leaf and its globular form (Fig. 7). This parenchyma tissue appears very thick compared to other tissues of the leaf. This thickening of this tissue could be due to the salinity of the soil. Several published data show that salinity increases succulence in plants such as *Atriplex patula* of the Amaranthaceae family (Longstreth and Nobel 1979), *Cakile maritima* of the Brassicaceae family (Debez et al. 2006), *Nitraria retusa* of the Nitrariaceae family (Boughalleb et al. 2009) and even in glycophytes such as *Gossypium hirsutum* of the Malvaceae family (Longstreth and Nobel 1979) and *Hordeum vulgare* of the Poaceae family (Kiliç et al. 2007), are similar to our observation. This succulence phenomenon makes it possible to slow the rise in temperature of the exposed leaves, because it is more difficult to heat a volume of spherical water than the same volume of water spread as is the case in a non-succulent leaf (Collin 2001). In addition, succulence exerts a dilution effect on salts accumulated in *T. nudatum* leaves, which allows the leaves to cope with higher amounts of salt. Debez et al. (2006) showed that succulence is one of the adaptations to increased salinity. According to Larcher (1986) cited by Mantovani (1999), a plant would be more resistant to drought if it possessed a large capacity of water storage, besides low percentages of transpiration.

Conclusion

The present anatomical study of *T. nudatum*, conducted for the first time in the north-east of the Algerian Sahara, revealed a certain adaptation of the species to a hostile environment (severe aridity and saline soil); thus, *T. nudatum* has shown two very important strategies: tolerance and avoidance. In the case of tolerance, the succulence of the lamina is considered, to be one of the main factors involved in salt tolerance and secondly the presence of calcium oxalate at the level of the hypodermis of the leaf can play a metabolic role conferring salt resistance. In the case of the avoidance strategy, there is a reduction of transpiration, which is an essential element of drought resistance since it allows the maintenance of a high water potential. It is also translated by the reduction of the thermal load of the leaf surface. The reduction of transpiration and the thermal load are obtained by reduction and protection

of the transpiring surface: reduction (density and low stomatal index, assimilative parenchyma distant from the leaf surface, presence of trichomes in the epidermis of the stem) and protection (presence of the papilla and hypodermis and of the globular form due to succulence), in addition, by the specific arrangement of stomata (paracytic type). Other adaptive histological characters appeared at the root and the stem for the reduction of the water and nutrient requirement by the decrease of the density of the living tissues following the presence of successive cambia phenomena and the lignification which also may act against dehydration In addition, the improvement in water uptake is achieved by increasing the number and the diameter of the metaxylem vessels, thus filling the water deficit imposed by the high salinity of the soil solution. Kranz anatomy of salsoloid subtype in *T. nudatum* is necessary for C_4 photosynthesis and contributes to an increased adaptation to drought and salinity.

References

Abid F (1995) Caractérisation des sels des sols de l'Oued Righ. Engineer dissertation, University of Batna, Algeria.

Awasthi OP, Pathak RK (1999) Effect of salinity levels on survival and anatomy of four scion cultivars budded on Indian jujube. Hort J 12(2):53-59.

Agren J, Schemske DW (1993) The cost of defense against herbivores: an experimental study of trichome production in *Brassica rapa*. Am Nat 141(2):338-350.

Ben M'hamed M (1990) Forage shrubs in North Africa-Studies of the green Belt of North Africa. ALESCO, Tunis, Tunisie.

Ben Dob H, Khouildat A (2016) Action de la salinité et de l'acide salicylique sur le comportement physiologique et anatomique des plantules d'*Atriplex halimus* L. et *Atriplex canescens* (Pursh) Nutt. PhD Thesis. Université Kasdi Merbah, Ouargla.

Bouallala M, Chehma A, Bensetti M (2011) Variation de la composition chimique de principales plantes broutées par le dromadaire du Sud-Ouest Algérien. LRRD 23(5):1-9.

Baloch AH, Gates PJ, Baloch GM (1998) Anatomical changes brought about by salinity in stem, leaf and root of *Arabidopsis thaliana* (L.) Heynh (thale cress). Sarhad J Agric Pak 14:131-142.

Benghersallah N, Elhadi K (2013) Réponse anatomique à la sécheresse de quelques plantes spontanées du Sahara septentrional. Master Académique. Université Kasdi Merbah, Ouargla.

Bray S, Reid DM (2002) The effect of salinity and CO2 enrichment on the growth and anatomy of the second trifoliate leaf of *Phaseolus vulgaris*. Can J Bot 80(4):349-359.

Boughalleb F, Denden M, Tiba BB (2009) Anatomical changes induced by increasing NaCl salinity in three fodder shrubs, *Nitraria retusa*, *Atriplex halimus* and *Medicago arborea*. Acta Physiol Plant 31(5):947-960.

Cuénoud P, Savolainen V, Chatrou LW, Powell M, Grayer RJ, Chase MW (2002) Molecular phylogenetics of Caryophyllales based on nuclear 18S rDNA and plastid *rbcL*, *atpB*, and *matK* DNA sequences. Am J Bot 89(1):132-144.

Chehma A (2006) Catalogue des plantes spontanées du Sahara septentrional algérien. Ed Dar El Houda, Algérie 140p.

Chehma A, Faye B, Bastianelli D (2010) Valeurs nutritionnelles de plantes vivaces des parcours sahariens algériens pour dromadaires. Fourrages 204:253-256.

Carpenter KJ (2005) Stomatal architecture and evolution in basal angiosperms. Am J Bot 92(10):1595-1615.

Collin P (2001) L'adaptation au milieu chez les plantes vasculaires. L'Année Biol 40:21-42.

Calmés J, Piquemal M (1977) Variation saisonnière des cristaux d'oxalate de calcium des tissus de Vigne vierge. Can J Bot 55(15):2075-2078.

Datta SK, Som J (1973) Effect of salinity on structural-changes in stem of rice varieties. Indian J Agric Sci 43(6):614-617.

Demarquilly C (1982) Influence des facteurs climatiques sur la composition et la valeur nutritive de l'herbe. In: Actions du climat sur l'animal au pâturage, Séminaire de Theix. Éd., INRA publications, Versailles 49-63.

Dilcher DL (1974) Approaches to the identification of angiosperm leaf remains. Bot Rev 40(1):1-157.

Depuit DJ (1978) Photosynthesis and respiration of plant. In the arid ecosystem. Cambridge: Cambridge University Press, 509-36.

Debez A, Saadaoui D, Ramani B, Ouerghi Z, Koyro HW, Huchzermeyer B, Abdelly C (2006) Leaf H^+-ATPase activity and photosynthetic capacity of Cakile maritima under increasing salinity. Environ Exp Bot 57(3):285-295.

Finsinger W, Dos Santos T, McKey D (2013) Estimating variation in stomatal frequency at intra-individual, intra-site, and inter-taxonomic levels in populations of the *Leonardoxa africana* (Fabaceae) complex over environmental gradients in Cameroon. CR Geoscience 345(7-8):350-359.

Flowers TJ, Hajibagheri MA, Clipson NJW (1986) Halophytes. Q Rev Biol 61(3):313-337.

Franceschi VR, Horner HT (1980) Calcium oxalate crystals in plants. Bot Rev 46(4):361-427.

Grigore MN (2012) Romanian Salt Tolerant Plants. Taxonomy and Ecology Edit. Tehnopress, Iasi.

Grigore MN, Ivanescu L, Toma C (2014) Halophytes. An integrative anatomical study. Springer, Cham, Heidelberg, New York, Dordrecht, London.

Grigore MN, Toma C (2007) Histo-anatomical strategies of Chenopodiaceae halophytes: adaptive, ecological and

evolutionary implications. WSEAS Trans Biol Biomed 4(12):204-218.

Grigore MN, Toma C (2017) Anatomical Adaptations of Halophytes. A Review of Classic Literature and Recent Findings, Springer.

Grigorev JS (1955) Comparative ecological investigations of higher plant xerophilization. AN SSSR, Moscov-Leningrad. (In Russian).

Gounot M (1969) Méthodes d'étude quantitative de la végétation. Masson, Paris.

Gorenflot R (1980) Biologie végétale. Plantes supérieures: appareil végétatif. Masson, Paris.

Halillet MT (1998) Étude expérimentale de sable additionnée d'argile Comportement physique et organisation en condition saline et sodique. PhD Thesis. I.N.A.P.G, Paris.

Hameed M, Ashraf M, Naz N, Al-Qurainy F (2010) Anatomical adaptations of *Cynodon dactylon* (L.) Pers., from the salt range Pakistan, to salinity stress. I. Root and stem anatomy. Pak J Bot 42(1):279-289.

Houari KD, Chehma A, Zerria A (2012) Étude de quelques paramètres d'adaptation anatomique des principales plantes vivaces spontanées dans la région d'Ouargla (Algérie). Sécheresse 23(4):284-288.

Hwang YH, Chen SC (1995) Anatomical responses in *Kandelia candel* (L.) Druce seedlings growing in the presence of different concentrations of NaCl. Bot Bull Acad Sin 36:181-188.

Heller R, Esnault RLC (1993) Physiologie végétale. Vol. I. Nutrition, 5ème éd. Masson. Paris.

IUCN (World Conservation Union) (2005) Guidelines for using the IUCN Red List Categories and Criteria. Prepared by the Standards and Petitions Subcommittee of the IUCN SSC Red list Programme Committee. IUCN, Gland, Switzerland, and Cambridge, United Kingdom. Available: http://www.iucn.org/themes/ssc/red-lists.htm. Accessed September 2006.

Jarvis MC (2012) Sclerenchyma. eLS. Glasbow University, Glasgow, Scotland, UK DOI:10.1002/9780470015902.a0002082.pub2.

Jarrige R (1981) Constituants glucidiques des fourrages: variations, digestibilité et dosage. In Prévision de la valeur nutritive des aliments des ruminants/ouvrage collectif coordonne par C. Demarquilly, éd., INRA publications, Versailles, 13-40.

Keshavarzi M, Zare G (2006) Anatomical study of *Salicornieae dumort* (Chenopodiaceae Vent.) native to Iran. Int J Bot 2(3):278-285.

Kalla A (2012) Étude et valorisation des principes actifs de quelques plantes du sud algérien. Thèse PhD. Université Mentouri-Constantine Algérie.

Kadi-Bennane S, Ait-Said S, Smail-Saadoun N (2005) Adaptation study of three *Pistacia atlantica* Desf. ssp. *atlantica* populations (Ain Oussera - Messaad - Taissa) through stomatal complex**.** In: Oliveira M.M. (ed.), Cordeiro V. (Ed.). XIII GREMPA Meeting on Almonds and Pistachios. Zaragoza: CIHEAM, Opt Méd 63:365-368.

Kılıç S, Çavuşoğlu K, Kabar K (2007) Effects of 24-epibrassinolide on salinity stress induced inhibition of seed germination, seedling growth and leaf anatomy of barley. SDU Fen-Edb Fak Fen Dergisi (E-Dergi) 2(1):41-52

Le Houérou HN (1980) Fourrages ligneux en Afrique du nord. In Les fourrages ligneux en Afrique. État actuel des connaissances. Colloque sur les fourrages ligneux en Afrique, Addis Abeba, Éthiopie, 57-84.

Longo-Hammouda FH, Siboukheur OE, Chehma A (2007) Aspects nutritionnels des pâturages les plus appréciés par *Camelus dromedarius* en Algérie. Agricultures 16(6):477-483.

Lakhdari K, Belhamra M, Mayouf R (2015) Forage species preferred by dromedaries and their chemical composition in arid rangelands of Algeria. LRRD 27(10):1-10.

Le Floc'h E (1995) Les écosystèmes des zones arides du Nord de l'Afrique: orientation pour l'établissement d'un réseau de réserves de biosphère. In: Nabli MA, ed., Ouvrage collectif sur le milieu physique et la végétation. Essai de synthèse sur la végétation et la phytoécologie tunisienne- 5 et 6. Faculté des sciences de Tunis/ Agence de coopération culturelle et technique/ MAB, Tunis, 309-321.

Longstreth DJ, Nobel PS (1979) Salinity effects on leaf anatomy: consequences for photosynthesis. Plant Physiol 63(4):700-703.

Larcher W (1986) Ecofisiologia Vegetal. Curitiba: Editora Pedagógica e Universitária Ltda., São Paulo.

Mroczek A (2015) Phytochemistry and bioactivity of triterpene saponins from Amaranthaceae family. Phytochem Rev 14(4):577-605.

Mtimet A, Hachicha M (1998) Gestion durable de l'eau et du sol dans les oasis tunisiennes. In: Proceedings of the 16th ISSS World Congress. August 1998, Montpellier, France.

Meidner H, Mansfield TA (1968) Physiology of stomata. McGraw-Hill, London.

Mâalem S (2011) Étude de l'impact des interactions entre le phosphore et le chlorure de sodium sur trois espèces végétales halophytes du genre Atriplex (*A. halimus*, *A. canescens* et *A. nummularia*). PhD Thesis, Université Badji Mokhtar-Annaba, Algérie.

Muhaidat R, Sage RF, Dengler NG (2007) Diversity of Kranz anatomy and biochemistry in C_4 eudicots. Am J Bot 94(3):362-381.

Mantovani A (1999) A method to improve leaf succulence quantification. Braz Arch Biol Technol 42(1):9-14.

Nedjimi B, Beladel B, Guit B (2012) Biodiversity of halophytic vegetation in Chott Zehrez Lake of Djelfa (Algeria). Am J Plant Sci 3(11):1527-1534

Nabors MW (2008) Biologie végétale: structures, fonc-

tionnement, écologie et biotechnologies. Pearson Éducation, France, Paris.
Ould El Hadj MD, Hadj-Mahammed M, Zabeirou H (2003) Place des plantes spontanées dans la médicine traditionnelle de la région d'Ouargla (Sahara septentrional Est). Courrier du Savoir (3):47-51.
Ozenda P (2004) Flore et végétation du Sahara, 3ème éd. CNRS Paris.
Ozenda P (1991) Flore de Sahara, 3ème éd. mise à jour et augmentée. CNRS Paris.
Poljakoff-Mayber A (1988) Ecological-physiological studies on the responses of higher plants to salinity and drought. Sci Rev Arid Zone Res 6:163-183.
Patil VS, Rajput KS, Malpathak NP (2016) Comparative study on morpho-anatomy of leaf, stem and root of *Boerhaavia diffusa* L. (Nyctaginaceae) and its adulterant plants. Braz J Pharm Sci 52(3):433-442.
Pautov A, Telepova-Texier M (1999) Structure et développement de l'hypoderme dans les feuilles de Peupliers (Salicaceae). Acta Bot Gallica 146(2):123-137.
Paupardin C (1965) Sur la morphologie des tissus d'Aubépine *(Crataegus monogyllil* Jacq.) cultivés in vitro et la possibilité pour ces tissus d'utiliser l'oxalate de calcium comme substance de réserve. 90ème Congr Nat Soc Sav (Nice). C.R. II. GauthierVillars, Paris 379-389.
Robert EMR, Schmitz N, Boeren I, Driessens T, Herremans K, De Mey J, Van de Casteele E, Beeckman H, Koedam N (2011) Successive cambia: a developmental oddity or an adaptive structure? PLoS One 6(1)e16558.
Safiallah S, Hamdi SMM, Grigore MN, Sara J (2017) Micromorphology and leaf ecological anatomy of *Bassia halophyte* species (Amaranthaceae) from Iran. Acta Biol Szeged 61(1):85-93.
Sogreah S (1971) Participation à la mise en valeur de l'Oued Righ. Étude agro pédologique, Doc Poly MTPC Alger 7-36.
Smail-Saadoun N (2005a) Stomata types of *Pistacia* genus: *Pistacia atlantica* Desf. ssp. *Atlantica* and *Pistacia lentiscus* L. In: Oliveira M.M. (ed.), Cordeiro V. (ed.). XIII GREMPA Meeting on Almonds and Pistachios . Zaragoza : CIHEAM, (Options Méditerranéennes : Série A. Séminaires Méditerranéens). 13. Meeting of the Mediterranean Research Group for Almond and Pistachio, 2003/06/01-05, Mirandela (Portugal), (63):369-371.
Smail-Saadoun N (2005b) Réponse adaptative de l'anatomie des Chénopodiacées du Sahara algérien à des conditions de vie d'aridité extrême. Sécheresse 16(2):121-124.
Sage RF (2004) The evolution of C_4 photosynthesis. New Phytol 161(2):341-370.
Timmerman HA (1927) Stomatal numbers: their value for distinguishing species. Pharm J 118:241-243.
Ting IP (1975) Physiological adaptation to water stress in desert plants. In: Vernberg FJ, ed. Physical Adaptation to the Environment. Intext Educational Publishers, New York, 99-109.
Vintéjoux C, Shoar-Ghafari A (1985) Répartition et ultrastructure comparées des cellules oxalifères en vie latente et en vie active de *Spirodela polyrrhiza* L. (Lemnacées). Bulletin de la Société Botanique de France. Lettres Botaniques 132(1):25-39.
Wahid A (2003) Physiological significance of morpho-anatomical features of halophytes with particular reference to cholistan flora. Int J Agri Biol 5(2):207-212.
Wang L, Showalter A, Ungar I (1997) Effect of salinity on growth, ion content, and cell wall chemistry in *Atriplex prostrata* (Chenopodiaceae). Am J Bot 84(9):1247-1255.
Weryszko-Chmielewska E, Chernetskyy M (2005) Structure of trichomes from the surface of leaves of some species of *Kalanchoë* Adans. Acta Biol Cracov Ser Bot 47(2):15-22.
Zhu Y, Zhang Y, Hu Z, Yan S (2000) Studies on microscopic structure of *Puccinellia tenuiflora* stem under salinity stress. Grassland China (5):6-9.
Zaffran J (1998) Initiation à la biologie végétale. éd. Ellipses, Paris.

Acta Biologica Szegediensis

Volume 62(1):37-43, 2018
Acta Biologica Szegediensis
http://abs.bibl.u-szeged.hu/index.php/abs
DOI:10.14232/abs.2018.1.37-43

ARTICLE

Anatomy study of the genus *Cirsium* Mill. in Iran

Masoud Sheidai, Saeedeh Shojaei, Fahimeh Koohdar*

Faculty of Life Sciences and Biotechnology, Shahid Beheshti University, Tehran, Iran

ABSTRACT The genus *Cirsium* Mill. (Asteraceae) also known as plume thistles with about 250 perennial, biennial or rarely annual spiny species is a phylogenetically unresolved and paraphyletic genus. *Cirsium* species grow in different ecological conditions and tend to form interspecific hybrids. Some species are morphologically very similar and need to be delineated by additional anatomical and molecular characters. About 28 *Cirsium* species have been reported in Flora Iranica; they were classified in five sections. Taxonomic investigation of these species was confined to morphology and molecular study of RAPD and ISSR markers. The present study carried out anatomical investigation (leaf and stem characters) of *Cirsium* species in the country. PCoA analysis of anatomical characters could delimit the studied species and the grouping obtained was almost in agreement with morphological and sectional delineation of the genus. The results obtained are in agreement with several other investigations and all together suggestive of the continued gene flow and introgression between *Cirsium* species that make taxonomy and phylogenetic relationship of the species difficult.
Acta Biol Szeged 62(1):37-43 (2018)

KEY WORDS
anatomy
Cirsium
taxonomy

ARTICLE INFORMATION
Submitted
30 October 2017.
Accepted
30 March 2018.
***Corresponding author**
E-mail: f_koohdar@yahoo.com

Introduction

The genus *Cirsium* Mill. (Asteraceae) contains about 250 perennial, biennial or rarely annual spiny species that grow in different ecological conditions in the Northern hemisphere, Europe, North Africa, Siberia, Central Asia, West and East Africa, as well as Central America (Zwölfer 1994; Bures et al. 2004). The genus *Cirsium* is one of several genera known commonly as thistles. They are more precisely known as plume thistles and differ from other thistle genera (*Carduus*, *Silybum* and *Onopordum*) in having feathered hairs to their achenes. The other genera have a pappus of simple unbranched hairs (Francis 1981). There are about 28 species, 4 subspecies and 10 varieties of *Cirsium* in Iran that have been placed in 5 sections and 7 subsections (Ghoreyshi-Alhosseini et al. 2004).

Cirsium species can adapt to various ecological conditions with variable elevation, temperature and edaphic factors due to their genetic adaptability and plasticity. Their high genetic variability and ecological adaptability partly comes from inter-specific hybridization that frequently occurs in the genus (Bureš et al. 2004; Sheidai et al. 2013). These events cause difficulties in taxonomic delimitation of the *Cirsium* species. For example, *C. arvense* (Bull thistle) exhibits variation in several morphological characteristics that have been described as subspecies by some authors; however, the Flora Europaea does not recognize these taxa, because they lack sufficient morphological or geographical delimitation (Forcella et al. 1994). Moreover, several hybrids of bull thistle have been described in Europe (Klinkhamer and De Jong 1993) and some new varieties have been identified based on morphological and molecular studies in other places (Seif et al. 2012). The occurrence of inter-specific genetic introgression was recognized between *C. aduncum* and *C. haussknechtii* (Sheidai et al. 2016). Taxonomic complication of the *Cirsium* species is also to some degree due to intraspecific genetic and morphological variability. For example, Sheidai et al. (2013) extensively studied different geographical populations in four *Cirsium* species by morphological, cytogenetic and molecular data. They reported extensive morphological variability, genetic admixture, molecular diversity, and variation in chiasma frequency, and also the occurrence of heterozygote translocations. These features all together bring about a high degree of genetic and phenotypic variability in each species.

About 28 *Cirsium* species have been reported in Flora Iranica (Rechinger 1979) and classified in five sections. *C. pyramidale* is endemic species with confined geographical distribution and just growing in Kerman province. The previous studies performed in *Cirsium* species of Iran were mainly concerned with morphometric, cytogenetic and population genetic analysis (Nouroozi et al. 2013; Seif et al. 2012; Sheidai et al. 2012, 2013, 2016). In only one attempt species relationship were investigated by RAPD

Table 1. The species studied their section and locality.

No	Species	Section	Locality
1	*C. pyramidale* Bornm.	*Pseudoepitrachys*	Kerman
2	*C. spectabile* DC.	*Pseudoepitrachys*	Kerman
3	*C. congestum Fisch. & C.A. Mey.* ex *DC.*	*Pseudoepitrachys*	West Azarbaijan
4	*C. vulgare* (Savi) Ten.	*Epitrachys*	West Azarbaijan
5	*C. bornmülleri* Sint. ex Bornm.	*Epitrachys*	Khorassan
6	*C. ciliatum* (Murray) Moench.	*Epitrachys*	West Azarbaijan
7	*C. lappaceum* Lam.	*Epitrachys*	West Azarbaijan
8	*C. bracteosum* DC.	*Epitrachys*	Boyerahmad
9	*C. osseticum* (Adams) Petr.	*Epitrachys*	Mazandaran
10	*C. strigosum* (M.Bieb.) Fisch.	*Epitrachys*	West Azarbaijan
11	*C. arvense* (L.) Scop.	*Cephalonoplos*	West Azarbaijan
12	*C. obvallatum* (M.Bieb.) M.Bieb.	*Cirsium*	West Azarbaijan
13	*C. alatum* (S.G.Gmel.) Bobrov.	*Cirsium*	West Azarbaijan
14	*C. elodes* M.Bieb.	*Cirsium*	Tehran
15	*C. hygrophilum* Boiss.	*Cirsium*	Ardabil
16	*C. libanticum* DC.	*Cirsium*	West Azarbaijan
17	*C. echinus* (M.Bieb.) Hand-Mazz.	*Echenais*	West Azarbaijan

(Random Amplified Polymorphic DNA) and ISSR (Inter Simple Sequence Repeats) molecular markers (Nouroozi et al. 2013). Having in mind above said difficulties and limitations in the published articles on taxonomy of the genus, we carried out detailed population based anatomical investigation of the *Cirsium* species in Iran with the aim produce data for species delimitation and reveal the species relationship.

Materials and Methods

Plant materials

In total, 17 *Cirsium* species (3 individual of each species) could be obtained for the present investigation (Table 1). These species are from all sections of the Iranian *Cirsium*. According to Petrak (1979), the genus *Cirsium* has five sections in Iran, including *Pseudoepitrachys* Petrak, *Epitrachys* DC., *Echenais* (Cass.) Petrak, *Cirsium*, and *Cephalonoplos* (Necker) DC.

Anatomy study

Embedded materials were prepared as follows: Three adult plants samples were excised and immediately fixed in formalin-acetic acid-alcohol (FAA) (formalin: acetic acid:ethanol (90%) = 5:5:50%) (Jensen 1962) for 48 to 72 hours, and stored at 4 °C until sectioning, after dehydrated in a graded ethanol series and embedded in 70% ethanol.

Table 2. Anatomical characteristics of stem in *Cirsium* species.

No	Characters
1	Number of epidermis layers
2	The width of the epidermis layer
3	Cuticle width
4	The length of the pith cells
5	Cortex thickness
6	The number of cortex layers
7	Swinging collenchymatic cells groups
8	Width of lower phloem
9	Width of upper phloem
10	Width of xylem
11	Angular collenchymas thickness
12	Inner sclerenchyma thickness
13	External sclerenchyma thickness
14	Number of stem corners
15	The number of bundles of vascular

Table 3. Anatomical characteristics of leaf in *Cirsium* species.

No	Characters
1	Upper epidermis cell length
2	Upper epidermis cell width
3	Lower epidermis cell length
4	Lower epidermis cell width
5	Mesophile thickness
6	Upper collenchymas thickness
7	Lower collenchymas thickness
8	Xylem thickness
9	Upper phloem thickness
10	Lower phloem thickness
11	Number of vascular of vein
12	Trachea thickness
13	Spongy parenchyma thickness
14	Palisade parenchyma thickness
15	Upper sclerenchyma thickness
16	Lower sclerenchyma thickness
17	Upper cortex thickness
18	Lower cortex thickness

Table 4. Details of stem anatomical characters in *Cirsium* species (species and character numbers are according to Tables 1 and 2).

Character (µm)	Species																
	1	2	3	4	5	6	7	8	9	10	11	12	13	14	15	16	17
1	1	2	2	1	1	2	2	1	2	2	1	2	1	2	2	2	2
2	25.6	15.9	15.1	7.5	3.5	12.3	9.5	5.3	13.3	24.6	5.6	12.0	6.3	27.0	13.3	32.7	23
3	11.0	5.4	2.9	3.5	2.4	3.4	24.6	2.3	2.4	5.8	3.5	2.8	6.2	4.7	2.1	7	6
4	21.4	19.6	18.0	24.8	17.3	25.5	18.2	13.8	11.0	17.3	24.9	27.8	18.8	29.2	25.5	14	24.3
5	219.8	179.5	180.9	94.9	98.5	142.7	232.1	125.5	128.1	100.9	74.1	114.6	124.3	222.2	91.1	141.3	112
6	25	11	22	12	7	12	17	17	14	10	10	15	12	12	11	19	10
7	8	11	8	14	9	11	9	6	7	6	8	13	10	9	8	8	12
8	31.8	30.7	28.5	21.4	30.1	17.0	16.2	13.6	11.9	11.1	15.6	39.2	20.2	22.7	21.3	29.0	15.8
9	85.9	81.1	105.1	47.0	87.1	45.6	49.5	33.9	23.5	42.6	28.9	54.2	48.2	32.5	33.2	33.7	38.2
10	51.0	69.4	65.4	44.9	91.7	43.8	34.8	37.0	23.7	33.7	22.0	52.9	27.3	34.4	34.3	59.7	30.9
11	69.9	33.2	62.2	36.0	16.5	34.9	30.3	35.2	33.8	36.2	29.9	38.5	44.1	46.2	39.1	15.0	22.1
12	23.6	19.7	16.9	9.0	13.9	16.8	12.2	13.2	11.02	12.7	15.02	37.05	6.1	4.5	21.2	13.3	15.4
13	32.4	22.0	15.4	14.1	13.8	19.1	15.9	5.0	12.6	12.2	14.9	14.3	14.0	14.9	17.1	10.0	14.7
14	8	10	8	14	9	10	8	6	7	6	8	12	10	9	8	8	12
15	41	42	72	44	28	42	28	34	27	31	22	38	31	32	35	56	40

Table 5. Details of leaf anatomical characters in *Cirsium* species (species and character numbers are according to Tables 1 and 2).

Character (µm)	Species																
	1	2	3	4	5	6	7	8	9	10	11	12	13	14	15	16	17
1	9.9	6.3	9.3	11.2	9.5	9.3	10.4	9.2	12.3	14.0	11.1	14.5	10.8	11.6	18.33	8.0	8.8
2	12.1	7.2	12.3	13.3	9.0	12.2	13.6	12.0	20.4	12.5	13.3	15.1	10.9	14.1	17.67	8.5	10.2
3	10.5	6.3	7.8	8.7	7.8	11.0	10.7	10.0	9.7	6.5	8.5	12.4	14.0	11.5	19.33	8.0	7.0
4	11.1	7.0	10.0	11.7	9.7	13.5	13.0	16.0	13.9	11.5	9.1	12.6	18.4	12.4	17.01	7.2	8.6
5	239.8	119.5	178.2	90.7	89.1	135.0	108.8	189.5	229.0	271.0	201.9	154.3	195.2	211.0	140	225.0	130.6
6	76.8	57.7	63.2	58.2	28.7	49.0	70.9	38.6	69.8	102.0	24.5	21.1	38.0	29.6	39.57	16.5	26.1
7	56.5	53.7	63.1	66.5	51.0	73.9	50.5	35.4	72.7	60.5	26.6	26.8	47.7	29.1	51.56	13.5	16.1
8	31.6	24.7	38.8	51.5	30.0	55.8	29.0	37.0	84.2	69.5	40.1	38.2	57.8	29.7	55	37.0	43.7
9	36.3	25.0	41.0	33.7	21.0	43.7	27.0	58.0	21.2	77.1	29.9	65.1	29.0	41.6	65	41.0	29.5
10	64.7	28.0	54.2	68.4	34.5	69.8	34.2	69.0	60.8	68.0	58.2	50.6	78.2	39.8	75.67	31.5	38.4
11	1	3	3	6	7	3	1	1	1	2	3	1	3	1	1	3	1
12	52.9	42.1	71.8	79.0	44.0	100.4	53.2	78.0	113.2	86.0	68.5	41.0	86.7	52.4	84	75.0	49.9
13	141.7	57.9	106.3	43.7	65.1	58.0	42.4	92.9	106.0	146.0	100.4	56.6	107.3	112.3	57.42	53.5	48.7
14	98.7	63.3	70.0	49.7	29.7	73.7	50.8	75.5	119.0	117.0	88.7	49.5	110.3	104.9	74.95	43.0	63.3
15	19.8	17.0	18.7	13.8	0.0	18.4	6.3	6.4	16.0	23.0	9.0	6.8	3.7	6.3	35	14.0	9.3
16	20.7	18.0	19.4	22.0	25.0	24.4	5.7	5.5	24.5	52.5	10.0	5.9	16.8	5.8	40	9.0	10.5
17	5.1	2.7	4.3	5.3	4.0	4.2	5.4	1.8	5.6	5.2	4.8	3.5	6.5	3.3	5.41	3.7	4.2
18	9.9	6.3	9.3	11.2	9.5	9.3	10.4	9.2	12.3	14.0	11.1	14.5	10.8	11.6	18.33	8.0	8.8

After preparation of free transverse hand sections of the lamina and stem samples were washed with distilled water and placed in 5% sodium hypochlorite solution for 20 min for clearing and rinsed with distilled water. The sections were stained with methyl blue and carmine and mounted on the slides using Canada balsam. Thin cut sections were observed under a microscope fitted with digital camera. For anatomical studies totally 33 characters were used from which 18 leaf characters were identical and 15 stem ones showed variation (Table 2, 3). Anatomical data were standardized (Mean = 0, Variance = 1) and used for multivariate analyses. Principal coordinate analysis (PCoA) was used for grouping of the species. PCA (Principal Components Analysis) was performed to identify the most variable anatomical characters (Podani 2000). For these analyses, we used PAST (Paleontological Statistical software) version 3 (Hammer et al. 2016).

Results

Anatomy

Details of stem and leaf anatomical characters are given in Figure 1 and Table 4. Cross-section of the stem in all investigated species had multidimensional. Swingeing collenchymatic cells groups, which are 6 (*C. bracteosum*

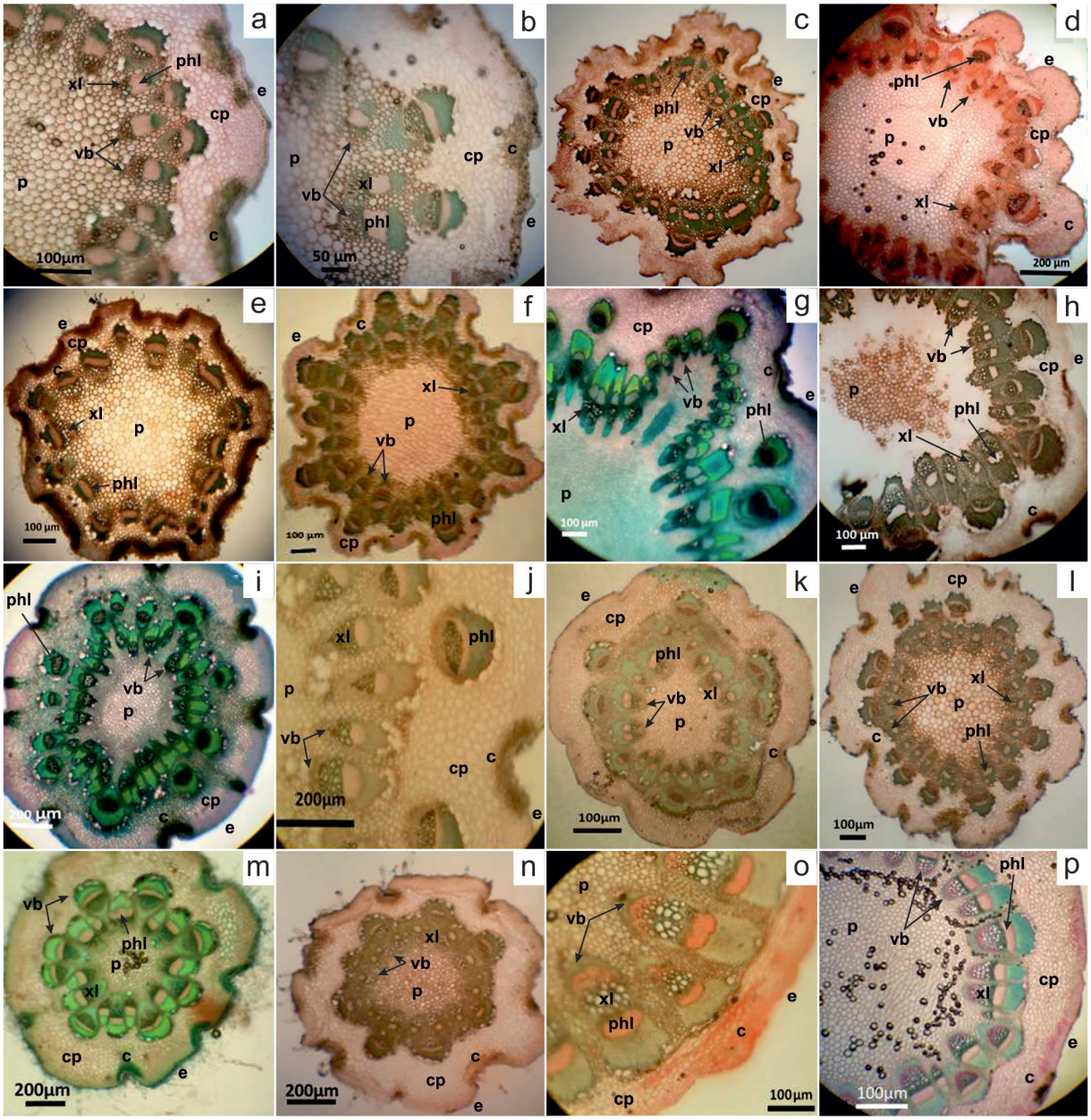

Figure 1. Appearance of stem in *Cirsium* species. a: *C. alatum*; b: *C. elodes*; c: *C. hygrophilum*; d: *C. obvallatum*; e: *C. arvense*; f: *C. echinus*; g: *C. congestum*; h: *C. spectabile*; i: *C. pyramidale*; j: *C. ciliatum*; k: *C. strigosum*; l: *C. vulgare*; m: *C. lappaceum*; n: *C. osseticum*; o: *C. bornmülleri*; p: *C. bracteosum*; e: epidermis; cp: cortex parenchyma; c: collenchymas; phl: phloem; xl: xylem; p: pith.

and *C. strigosum*) to 15 (*C. vulgare*) layered are seen at the protruding sides of the stem.

The highest stem epiderm width was observed in *C. libanticum* (32. 7 µm), while *C. bornmullerii* had the lowest value (3.5 µm). This indicate extensive variation genus. The cortex layer varied from 7 in *C. bornmullerii* to 25 series in *C. pyramidale*. Similarly, the highest value for cortex thickness occurred in *C. lappaceum* (232.1 µm), while *C. arvens* had lowest value of the same (74.1 µm). Details of leaf anatomical characters are given in Figure 2 and Table 5. All of, the leaves in the sections were bifacial (dorsiventral mesophyll) type and are composed of a one or two layered epidermis. The number of vascular of vein varies among different species occurring in either one layer or two to seven layers. The highest value for cortex thickness occurred in *C. bornmülleri* (271 µm), while C. *osseticum* had lowest value of the same (89.1 µm).

PCoA plot of combined anatomical data (Fig. 3) almost

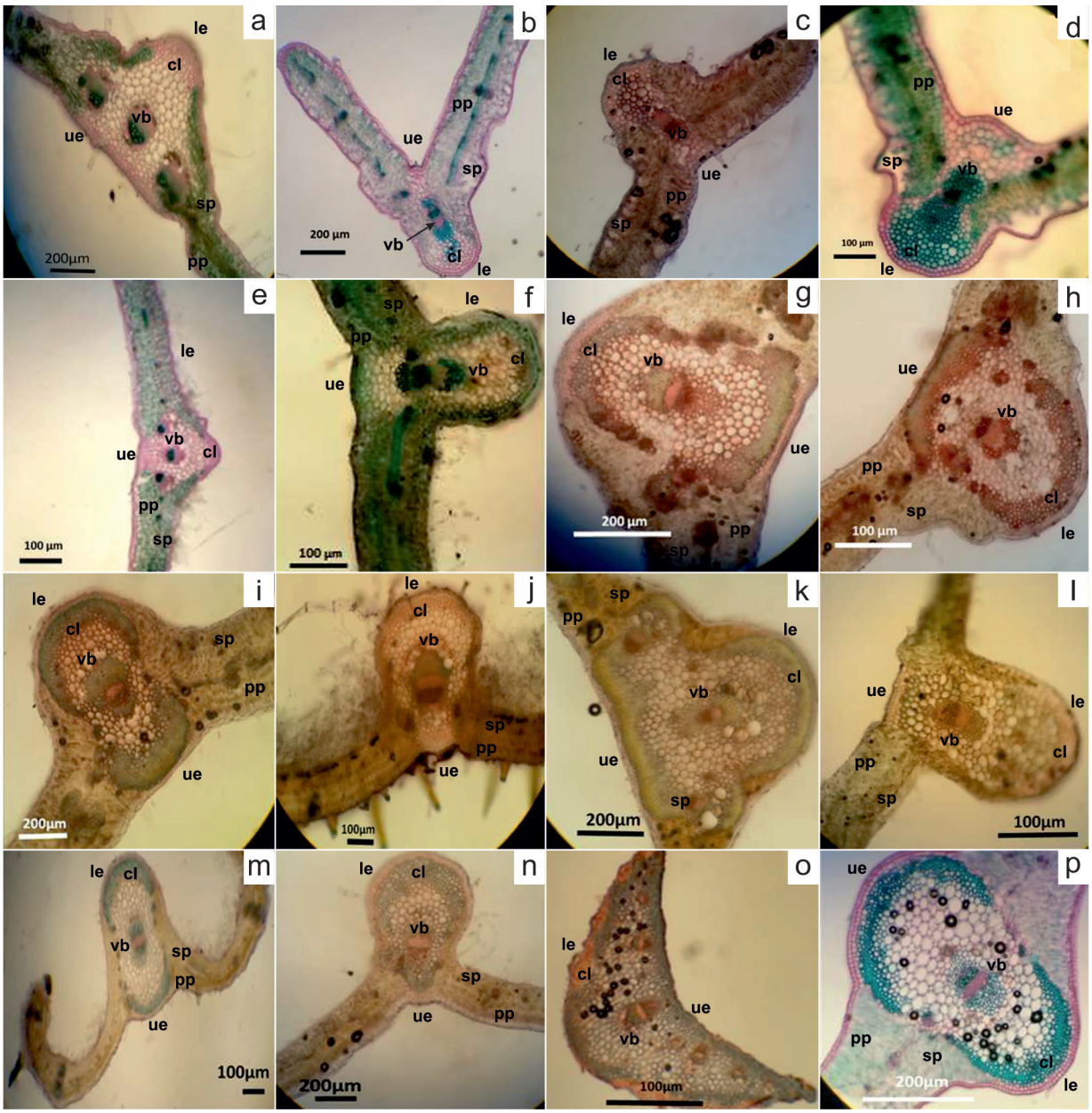

Figure 2. Appearance of stem in *Cirsium* species. a: *C. alatum*; b: *C. elodes*; c: *C. hygrophilum*; d: *C. obvallatum*; e: *C. arvense*; f: *C. echinus*; g: *C. congestum*; h: *C. spectabile*; i: *C. pyramidale*, j: *C. ciliatum*; k: *C. strigosum*; l: *C. vulgare*; m: *C. lappaceum*; n: *C.osseticum*; o: *C. bornmülleri*; p: *C. bracteosum*; le: lower epidermis; cl: collenchyma; vb: vascular bundle; pp: palisade parenchyma; sp: spongy parenchyma; ue upper epidermis.

separated the studied species and indicated the use of anatomical characters in species delimitation.

Considering sectional delimitation of the genus, we find that anatomical data separated the species almost according to their respective sections too. For example, *C. pyramidale*, *C. spectabile*, and *C. congestum* of the sect. *Pseudoepitrachys* Petrak was placed close to each other. Similarly, species of the sect. Epitrachys DC. *viz. C. bracteosum*, *C. bornmülleri*, *C. ciliatum*, *C. osseticum*, and *C. lappaceum* were placed close to each other. Three species studied each from different section *viz. C. echinus* (sect. *Echenais* (Cass.) Petrak), *C. obvallatum* and *C. alatum* (sect. *Cirsium*) and *arvense* (sect. *Cephalonoplos* (Necker) DC. C.) were placed far from the others. PCA analysis revealed that the first two PCA axes, comprised about 85% of total variation and characters like thickness of collenchyma in the lower leaf, thickness of xylem in stem, thickness of inner phloem in stem are the most variable characters

among the studied species. Therefore, these anatomical characters may be used along with morphological characters to delimit *Cirsium* species.

Discussion

The present study revealed taxonomic implication of leaf and stem anatomy in both *Cirsium* species delimitation and sections differentiation. Anatomical characters, like thickness of collenchyma in the lower leaf, thickness of xylem, presence/absence of sclerenchyma, and thickness of inner phloem in stem, may be used along with morphological characters to delimit *Cirsium* species. Ozcan et al. (2015) described the leaf anatomical characters of 26 *Cirsium* taxa of Turkey. These species could be separated based on the midrib and lamina thickness, the height and width of vascular bundle, and number of stomata, and epidermal cell wall patterns in the abaxial and adaxial surfaces. They reported that the species grouping based on leaf anatomy was partly in accordance with their sectional delimitation in the flora of Turkey. In present study also, the species grouping was not in accordance to sectional division.

Ginko et al. (2016) investigated the root and rhizome anatomy implication in taxonomy of 59 species from 34 genera and 12 sub-tribes in Cardueae and Cichorieae They found that anatomical characters used can delineate subtribes Cardueae and Cichorieae. Moreover, combination of morphological, anatomical and molecular data provides efficient data to delimit *Cirsium* species.

References

Bodo Slotta TA, Horvath DP, Foley M (2012) Phylogeny of *Cirsium* spp. in North America: Host specificity does not follow phylogeny. Plants (Basel) 1:61-73.

Bureš P, Wang YF, Horová L, Suda J (2004) Genome size variation in central European species of *Cirsium* (Compositae) and their natural hybrids. Ann Bot 94:353-363.

Francis R (1981) The Wild Flower Key. Frederick Wame & Co, pp. 377-380.

Garcia-Jacas N, Garnatje T, Susanna A, Vilatersana R (2002) Tribal and subtribal delimitation and phylogeny of the Cardueae (Asteraceae): a combined nuclear and chloroplast DNA analysis. Mol Phyl Evol 22:51-64.

Ginko E, Dobeš C, Saukel J (2016) Suitability of root and rhizome anatomy for taxonomic classification and reconstruction of phylogenetic relationships in the tribes Cardueae and Cichorieae (Asteraceae). Sci Pharma 84:585-602.

Ghoreyshi-Alhosseini J, Hosseini J, Amiri-Moghadam D (2004) The systematic study of *Cirsium* species (Asteraceae) in Khorasan of Iran on the base of morphological characters and numerical taxonomy. Iran J Biol 16:60-71.

Hammer Ø, Harper D, Ryan PD (2012) PAST: Paleontological Statistics software package for education and data analysis. *Paleoclimat Res* 4:1-9.

Jump A, Dawson DA, James CM, Woodward FI, Burke T (2002) Isolation of polymorphic microsatellites in the stemless thistle (*Cirsium acaule*) and their utility in other *Cirsium* species. Mol Ecol Notes 2:589-592.

Klinkhamer PGL, De Jong TJ (1993) *Cirsium vulgare* (Savi) Ten.: (*Carduus lanceolatus* L., *Cirsium lanceolatum* L.) Scop., Non Hill). J Ecol 81:177-191.

Kelch DG, Baldwin BG (2003) Phylogeny and ecological radiation of New World thistles (*Cirsium*, Cardueae-Compositae) based on ITS and ETS rDNA sequence data. Mol Ecol 12:141-151.

Lembicz M, Piszczałka P, Grzybowski T, Woźniak M, Jarmołowski A, Borkowska L, Falińska K (2011) Microsatellite identification of ramet genotypes in a clonal plant with phalanx growth: The case of *Cirsium rivulare* (Asteraceae). Flora 206:792-798.

Minaeifar AA, Sheidai M, Attar F, Noormohammadi Z, Ghasemzadeh-Baraki S (2016) Biosystematic study in the genus *Cousinia* Cass. (Asteraceae), section *Cousinia*. Biochem Biochem Syst Ecol 69:252-260.

Nouroozi M, Sheidai M, Seif E, Attar F, Noormohammadi Z (2013) ISSR and RAPD analyses of species and their relationships in the genus *Cirsium* (Asteraceae) in Iran. Phytol Balcan 19:225-232.

Ozcan M, Demiralay M, Kahriman A (2015) Leaf anatomical notes on *Cirsium* Miller (Asteraceae, Carduoideae) from Turkey. Plant Syst Evol 301:1995-2012.

Petrak F (1979) *Cirsium* Miller. In Rechinger KH, Ed., Flora Iranica. Vol. 139a, Compositae III-Cynareae. Akademische Druck-u. Verlagsanstalt, Graz, pp. 231-280.

Podani J (2000) *Introduction to the Exploration of Multivariate Data*. Backhuyes, Leiden, pp. 407.

Rechinger KH (1979) Cousinia. In Rechinger KH, Ed., Flora Iranica, No. 139A. Akademische Druk-u. Verlagsanstalt, Graz, Austria. pp. 108-153.

Seif E, Sheidai M, Norouzi M, Noormohammadi Z (2012) Biosystematic studies of *Cirsium arvense* populations in Iran. Phytol Balcan 18:305-314.

Sheidai M, Seif E, Nouroozi M, Noormohammadi Z (2012) Cytogenetic and molecular diversity of *Cirsium arvense* (Asteraceae) populations in Iran. *J Japan Bot* 87:193-205.

Sheidai M, Zanganeh S, Haji-Ramezanali R, Nouroozi M, Noormohammadi Z, Ghsemzadeh-Baraki S (2013) Genetic diversity and population structure in four *Cirsium* (Asteraceae) species. *Biologia* 68:384-397.

Sheidai M, Naji M, Noormohammadi Z, Nouroozi M, Ghasemzadeh-Baraki S (2016) Contemporary inter-

specific hybridization between *Cirsium aduncum* and *C. haussknechtii* (Asteraceae): Evidence from molecular and morphological data. Genetika 48:497-514.

Tamura K, Peterson D, Peterson N, Stecher G, Nei M, Kumar S (2013) MEGA5: Molecular evolutionary genetics analysis using maximum likelihood, evolutionary distance, and maximum parsimony methods. Mol Biol Evol 28:2731-2739.

Wiens JJ (2014) Character analysis in morphological phylogenetics: Problems and solutions. Sys Biol 50:689-699.

Zwölfer H (1988) Evolutionary and ecological relationships of the insect fauna of thistles. Ann Rev Entomol 33:103-122.

Acta Biologica Szegediensis

Volume 62(1):45-52, 2018
Acta Biologica Szegediensis
http://abs.bibl.u-szeged.hu/index.php/abs
DOI:10.14232/abs.2018.1.45-52

ARTICLE

Comparative anatomical and micromorphological study of some *Rumex* species (Polygonaceae)

Maryam Keshavarzi*, Farzaneh Ebrahimi, Samaneh Mosaferi

Department of Plant Science, Faculty of Biological Sciences, Alzahra University, Tehran, Iran

ABSTRACT *Rumex* (Polygonaceae) is a large genus of annual, biennial and perennial species in temperate regions of the world. In Iran it is represented by 23 species and some hybrids classified in three subgenera. The species identification is difficult due to the importance of fruit features in species separation despite the fact, that plants lose their flower and some other features while bearing fruits. Providing the individuals with the proper set of diagnostic features is very difficult. There are inadequate anatomical studies of *Rumex*. The present study reports the first detailed stem anatomy and epidermis micromorphology of 6 species of *Rumex* in Iran. Main aims of this study were to find the diagnostic value of the adopted features. Cross sections were made by hand and double colored. Dorsal and ventral leaf epidermises were studied by Scanning Electron Microscopy (SEM). Results of stem anatomical study showed that collateral vascular bundle is only present in *R. chalepensis* and oxalate calcium druse crystals were only absent in *R. elbrusensis*. The micro-morphological study of epidermis showed that all species studied had anisocytic stomata type, but there were differences in the epidermis and stomata cell size. Species relationships based on the results have been discussed.
Acta Biol Szeged 62(1):45-52 (2018)

KEY WORDS
Iran
leaf epidermis
Polygonaceae
Rumex
stem anatomy

ARTICLE INFORMATION
Submitted
17 November 2017.
Accepted
4 March 2018.
***Corresponding author**
E-mail: m.keshavarzi@alzahra.ac.ir
neshat112000@yahoo.com

Introduction

Polygonaceae is a complex family with 59 genera and nearly 1200 species in the world (The Plant List 2013). *Rumex* L. is a large genus with 200 species, which are distributed in different habitats of temperate regions of the world (Sanchez and Kron 2008; Chase and Reveal 2009). In Iran it is represented by 23 species and some hybrids classified in three subgenera as subgenus *Acetosella*, subgenus *Acetosa* and subgenus *Rumex* from which the latter is the largest with more species (Rechinger 1968; Mozaffarian 1988).

These are annual, biennial and perennial herbs or rarely suffrutices with basal and cauline leaves. Flowers are hermaphrodite, polygamous or unisexual with 6-segments perianth and 6 stamens arranged in panicle, cyme or axile inflorescences (Rechinger 1968). Rumex species are distributed in different habitats of Iran and are of medicinal importance in folk medicine (Mozaffarian 2015).

The species identification is somehow difficult due to the importance of fruit features in species separation. From the other hand, the plants loss their flower and some other features while bearing fruits so finding individuals with the proper set of diagnostic features is difficult (Rechinger 1968). Anatomical studies in Polygonaceae are mainly focused on leaf anatomy. Leaf anatomical observation provided some diagnostic features in *Polygonum*, *Rumex*, *Persicaria*, *Fagopyrum*, *Pteropyrum* and *Rheum* (Lersten and Curtis 1992; Hameed et al. 2010; Yasmin et al. 2010 a, b; Keshavarzi et al. 2012; Soleimani et al. 2014). Stem anatomy of some *Polygonum* species illustrated that anatomical features can be valuable in species delimitation especially about similar taxa (Nazem Bokaee et al. 2015). Micromorphology of epidermis in Polygonaceae has been studied by different authors. Ronse Decraene and Akeroyd (1988) illustrated the diagnostic value of epidermis. Hong et al. (1998) focused on the tepal micromorphology and found main differences in Polygonaceae. Yasmin et al. (2010 a) studied the leaf epidermis of selected *Persicaria* species. Tahey found variations in size and shape of epidermal cells, stomata, glandular and non-glandular trichomes. They used micro-morphological features of epidermis to elucidate relationship among different taxa.

There are inadequate literatures about the internal structure of *Rumex* (Joschi 1936; Li et al. 2008; Hameed et al. 2010; Sahney and Vibhasa 2012). The present study reports the first detailed stem and epidermis anatomy of six *Rumex* species as: *R. chalepensis* Mill., *R. dentatus* L., *R. elbrusensis* Boiss., *R. conglomerates* Murray, *R. pulcher*

L., and *R. vesicarius* L. Main aims of this study were to illustrate the stem and epidermis anatomical features of the studied species and to discuss diagnostic value of the adopted features.

Materials and Methods

Six different *Rumex* species were studied from the viewpoint of their stem anatomy and epidermis structure (Table 1). Materials were gathered from nature during 2015-2017 in summer and autumn. All studied vouchers are deposited in Herbarium of Alzahra University (ALUH). For each specimen, proper replications were used. Anatomical structures of stem were studied by 4 quantitative features and 8 qualitative ones (Table 2). Anatomical structures were studied in manually sliced cross sections, after double staining with methyl green and Congo red. Cross sections were subsequently observed with an Olympus DP 12 light microscope.

Table 1. Voucher details of *Rumex* species studied (asterisk marks perennial species).

Subgenus	Species	Locality
Rumex	*R. chalepensis* *	Alborz, Karaj, 1202 ALUH
		Guilan, Bandare- Anzali, 1201 ALUH
		Khorasan Razavi, Torbat-e Heydarieh, 1206 ALUH
		Khorasan Razavi, Quchan, 1203 ALUH
		Khuzestan, Masjed Soleyman, 1209 ALUH
		Mazandaran, Amol, 1205 ALUH
		Mazandaran, Sari, 1602 ALUH
		Qom, 20 km of Qom-Kashan, Pasangan, 1207 ALUH
		Tehran, Abali, 1245 ALUH
		Tehran, Darakeh, 1208 ALUH
	*R. conglomeratus**	Guilan, Bandar-e Anzali, 1211 ALUH
		Guilan, Rudsar, 1212 ALUH
		Guilan, Sowme'eh Sara, 122 ALUH
		Mazandaran, Amol, 1217 ALUH
	R. dentatus	Tehran, Vanak, 1502 ALUH
		Khuzestan, Behbahan, 1214 ALUH
	*R. elbrusensis**	Alborz, Mardabad, 1246 ALUH
		Guilan, Rasht, 1223 ALUH
	*R. pulcher**	Alborz, Malard, 2255 ALUH
		Tehran, Taleghani Park, 1229 ALUH
Acetosella	*R. vesicarius*	South Khorasan, Ozbagu, 5241 ALUH
		Fars, Kazerun, 1200 ALUH

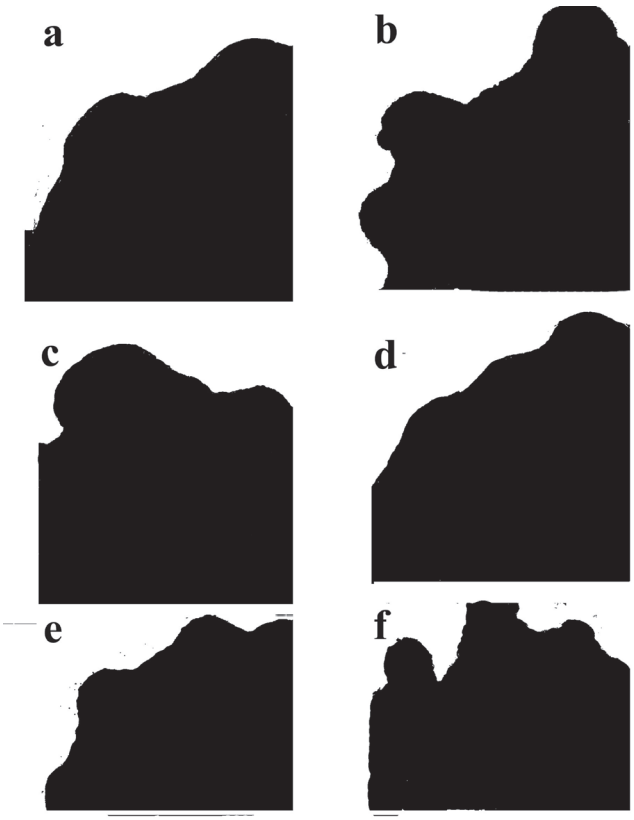

Figure 1. General shape of stem cross section in *Rumex* species studied. a) *R. chalepensis*; b) *R. conglomeratus*; c) *R. dentatus*; d) *R. elbrusensis*; e) *R. pulcher*; f) *R. vesicarius*.

The dorsal and ventral leaf epidermis of all the studied six species were examined by SEM. For SEM studies leaf surface were mounted on stub using double sided cello tape and coated with gold in a sputtering chamber (Sputter Coater BAL-TEC, SCDOOS). Epidermis do not encounter with any pretreatment. Coating with gold by the physical vapor deposition method (PVD) was restricted to 100 Å. The SEM examination was carried out on a TESCAN microscope. The measurements were based on 10-20 readings for each specimen. The terminology of Punt et al. (2007) for leaf micromorphology and Metcalfe and Chalk (1950) for stem anatomy was followed.

In order, to detect significant differences in the studied characters among studied species, Analysis of Variance (ANOVA) was performed. To reveal the species relationships, cluster analysis and principal component analysis (PCA) were used. For multivariate analysis, the mean quantitative characters were applied, while qualitative characters were coded as binary/multi-state characters. Standardized variables were used for a multivariate sta-

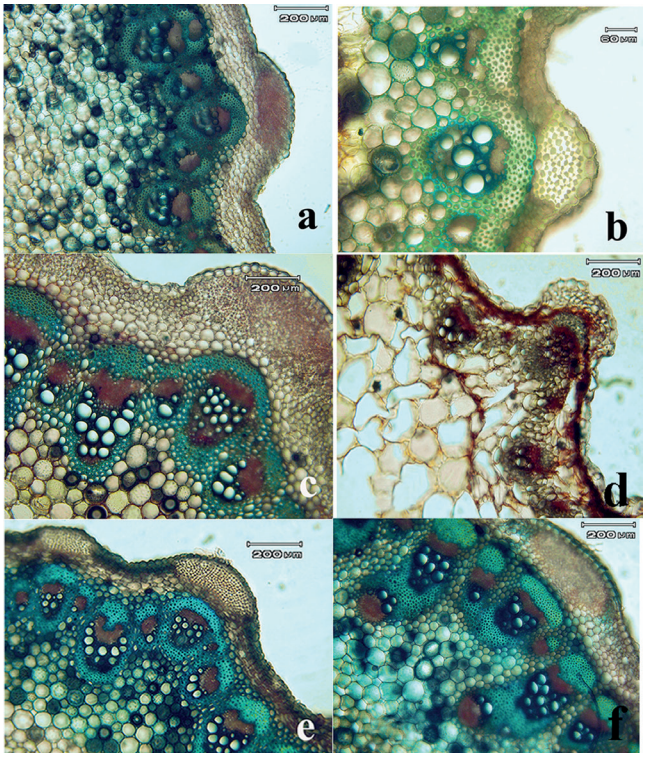

Figure 2. Stem cross section in *Rumex* species studied. a) *R. chalepensis*; b) *R. conglomeratus*; c) *R. dentatus*; d) *R. vesicarius*; e) *R. pulcher*; f) *R. elbrusensis*.

tistical analysis. The average taxonomic distances and squared Euclidean distances were applied as dissimilarity coefficient in the cluster analysis of anatomical data. In order, to determine the most variable anatomical characters among the studied species, a factor analysis based on the principal components analysis was performed. The PAST ver. 2.17c software was used for statistical analyses.

Results

Stem anatomical features

The shape of the cross-section is polygonal-protuberant, with different degree of prominence protuberances (Fig. 1). The epidermis presents cells, with the external wall thicker than the others. Epidermis is covered by a cuticle. A cord of sclerenchymatous fibers is present in the protuberances, under the stem epidermis. The central cylinder has vascular tissues arranged in one ring. Cords of sclerenchymatous fibers are visible at the periphery of each vascular bundle. The medulla is made of spongy parenchyma.

In *R. chalepensis*, ribs are short dome and regularly arranged. Parenchyma is composed of almost 8 layers and vascular bundles are in form of collateral bundles. The sclerenchymatous cap on phloem is arch-shaped (Fig. 2a). In *R. conglomerates* ribs are shaped as large domes with deep groves which are arranged regularly. There are five parenchyma layers and vascular bundles are in form of bicollateral bundles (Fig. 2b). Ribs shapes in *R. dentatus* are in different sized dome, but in *R. vesicarius*, it is in form of deeply groves small ribs (Fig. 2c). Ribs are arranged in *R. dentatus* irregularly but in *R. vesicarius* they are regular. The number of parenchyma layers is less in *R. vesicarius* than *R. dentatus*. Both showed bicollateral vascular bundles and arch-shaped sclerenchymatous cap on phloem (Fig. 2d).

Ribs in *R. pulcher* are in form of large domes which are irregularly arranged. There are 7 parenchyma layers as cortex and oxalate calcium druses crystals are present (Fig. 2e). Vascular bundles are bicollateral and the arch of sclerenchymatous cap on phloem is observed. In *R. elbrusensis* the complete sclerenchymatous sheath was not present. Only on this species medullary vascular bundle was observed. Rib shapes are in form of very short dome with regular arrangement (Fig. 2f). On the outer stem surface trichomes are observed. Cortex parenchyma is composed of 9 layers. In *R. elbrusensis* no oxalate calcium druse crystal was observed. This species has bicollateral vascular bundles. The other difference is the shape of sclerenchymatous cap of phloem, which is not arch-shaped and is in form of horizontal mass. Moreover, internal bundles can be seen in this taxon. There are also quantitative differences which are mentioned in Table 2.

Leaf epidermis micromorphology

The epidermis is made of polygonal cells with straight lateral walls; stomata, often anisocytic, are visible in both epidermis. Numerous druses of calcium oxalate are visible through the transparency. A comparison of

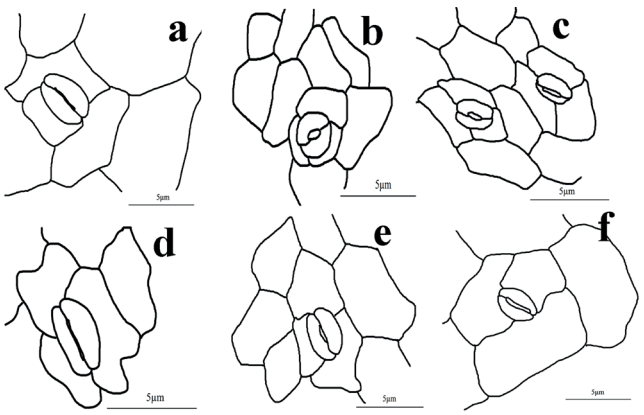

Figure 3. Leaf dorsal epidermis in *Rumex* species studied. a) *R. chalepensis*; b) *R. conglomerates*; c) *R. dentatus*; d) *R. elbrusensis*; e) *R. pulcher*; f) *R. vesicarius*. Scale bar is 5 µm.

Table 2. Results of stem cross section features in *Rumex* species studied.

Character	Taxon					
	R. chalepensis	*R. conglomeratus*	*R. dentatus*	*R. elbrusensis*	*R. pulcher*	*R. vesicarius*
Complete sclerenchyma sheath	present	absent	absent	absent	present	absent
Medullary vascular bundles	absent	absent	absent	present	absent	absent
Rib shape	short dome	large dome with deep groves	different sized dome	very short dome	large dome	deeply grooved small
Rib arrangement	regular	regular	irregular	regular	irregular	regular
Trichome on outer stem surface	absent	absent	present	present	absent	present
Parenchyma layers	8	5	7	9	7	3
Oxalate calcium druse crystals	present	present	present	absent	present	present
Vascular bundle	collateral	bicollateral	bicollateral	bicollateral	bicollateral	bicollateral
Shape of sclerenchyma cap of phloem	arch	arch	arch	horizontal mass	arch	arch
Average epidermis thickness	25.55 µm	14.60 µm	24.41 µm	18.97 µm	17.12 µm	21.14 µm
Average vascular bundles diameter	93.70 µm	105.88 µm	107.50 µm	91.01 µm	95.33 µm	79.34 µm
Average thickness of sclerenchyma fibers over phloem	43.11 µm	61.78 µm	63.24 µm	66.59 µm	50.31 µm	33.48 µm

Table 3. Comparative epidermis features in *Rumex* species studied.

Species	Stomata type		Cell size Adaxial (µm)		Cell size Abaxial (µm)		Stomata average size (µm)
	Ventral	Dorsal	Min	Max	Min	Max	
R. chalepensis	anisocytic	anisocytic	3.8	7.6	3	6.5	4.06
R. conglomeratus	anisocytic	anisocytic	2.28	3.0	2.18	6	1.995
R. dentatus	anisocytic	anisocytic	2.21	3.61	2.78	5.99	2.179
R. elbrusensis	anisoparacytic	anisocytic	4.57	4.9	3.41	5.96	3.778
R. pulcher	anisocytic	anisocytic	3.35	3.61	2.801	7.4	2.98
R. vesicarius	anisocytic	anisocytic	4.03	8.84	3.06	4.907	3.17

epidermis features in species studied in Table 3. Ventral leaf epidermis of all species showed anisocytic stomata type, although, the size of three surrounding cells and their angles are somehow varied in different species (Fig. 3). In *R. elbrusensis* stomata type is similar, to paracytic type in leaf ventral surface. The size of epidermal cells varies from 2.21 to 8.84 µm on adaxial surface and from 2.17 to 7.4 µm on abaxial surface. *R. conglomeratus* had the finest and smallest ventral epidermal cells while *R. vesicarus* has the largest one. In dorsal epidermis, *R. conglomeratus* showed the smallest cells and *R. pulcher* had the largest one. Largest stomata were observed in *R. chalepensis* while the smallest were in *R. conglomeratus* (Fig. 3).

Studying the SEM micrograph of dorsal and ventral leaf epidermis showed some details of the epicuticular wax and epidermis features. *R. chalepensis* has wrinkled cuticle on both surface epidermis. Wax is in form of smooth layers and granules. In some parts of ventral surface, a kind of striate ornamentation is observed (Fig. 4). *R. conglomeratus* showed a dorsal leaf epidermis which is composed of

Table 4. ANOVA results of quantitative anatomical and epidermal characters in *Rumex* species studied.

Source of variation	SS	Df	MS	F	P-value	F crit
Between groups	41695.88	5	8339.175	167.3471	5.75E-21	2.533555
Within groups	1494.949	30	49.83162			
Total	43190.83	35				

Table 5. PCA analysis results of anatomical and epidermal characters in *Rumex* species studied.

PCA	Eigenvalue	Percentage of variance
1	5.38628	33.664
2	4.00992	25.062
3	3.52191	22.012

Table 6. Factor analysis results of anatomical and epidermal characters in *Rumex* species studied.

Characters	Factor 1	Factor 2	Factor 3
Medullary vascular bundle	0.995	-	-
Presence/absence of oxalatecalcium crystals	0.995	-	-
Shape of sclerenchyma cap of phloem	0.995	-	-
Stomata type in ventral epidermis	0.995	-	-
Status of vascular bundle	-	0.747	-
Average vascular bundles diameter	-	0.710	-
Average thickness of sclerenchymafibers over phloem	-	0.766	-
Average size of adaxialepidermal cells	-	0.881	-
Average size of stomata	-	0.855	-
Number of parenchyma layers	-	-	0.815
Average size of abaxial epidermal cells	-	-	0.765

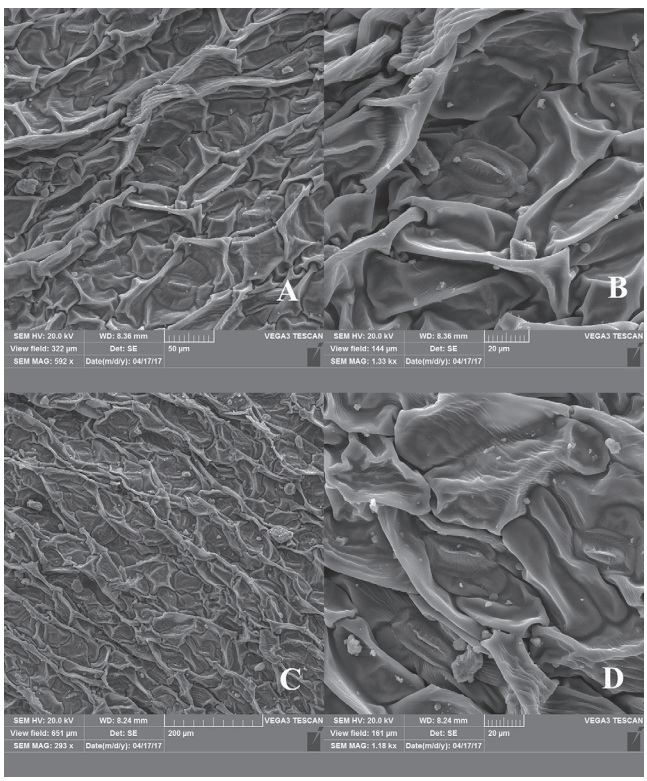

Figure 4. Leaf epidermis in *R. chalepensis*. A & B) dorsal and C & D) ventral epidermis.

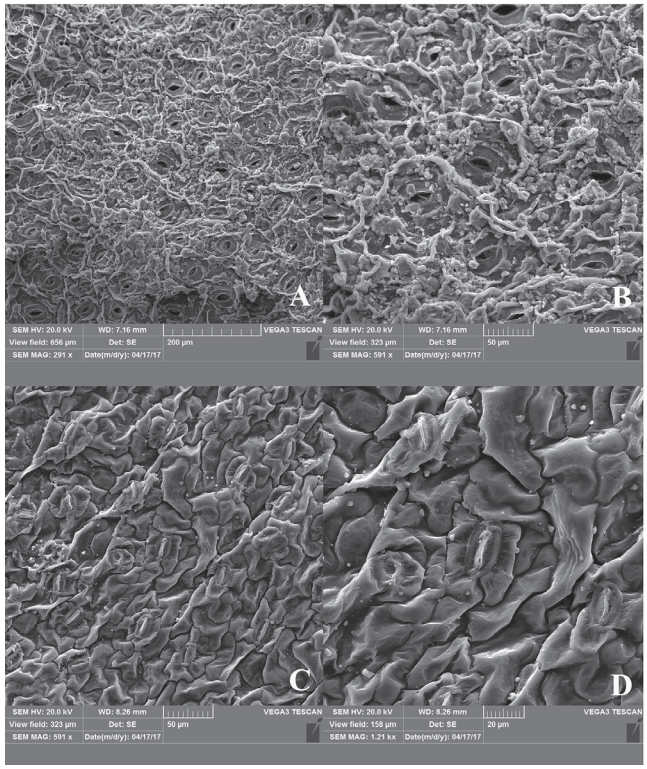

Figure 5. Leaf epidermis in *R. conglomeratus*. A & B) dorsal and C & D) ventral epidermis.

a mass of huge granules of wax and threads. A kind of stomata wax chimney was observed on dorsal epidermis too. Ventral epidermis is composed of wrinkled films of epicuticular wax. The stomata on dorsal epidermis are more frequent than ventral surface (Fig. 5).

Dorsal epidermis in *R. dentatus* demonstrated granules and smooth layer of epicuticular wax while ventral epidermis showed same situation with less granules (Fig. 6). In *R. elbrusensis* dorsal epidermis demonstrated granules and smooth layer of epicuticular wax. Ventral epidermis showed same situation with more granules (Fig. 7). *R. pulcher* showed a kind of stomata wax chimney on dorsal epidermis in addition to a mixture of granules and threads. In ventral epidermis there is no thread or granules and the stomata were less. Some kinds of platelets were observed in ventral surface (Fig. 8). In *R. vesicarius* dorsal and ventral epidermis is composed of wrinkled films of epicuticular wax with some kinds of crusts (Fig. 9).

Statistical analyses

ANOVA showed significant differences in quantitative characters (P<0.01) (Table 4). PCA analysis was done to determine the most variable characters among species studied. First three factors comprised 80.73% of total variation (Table 5). In the first PCA axis, features as

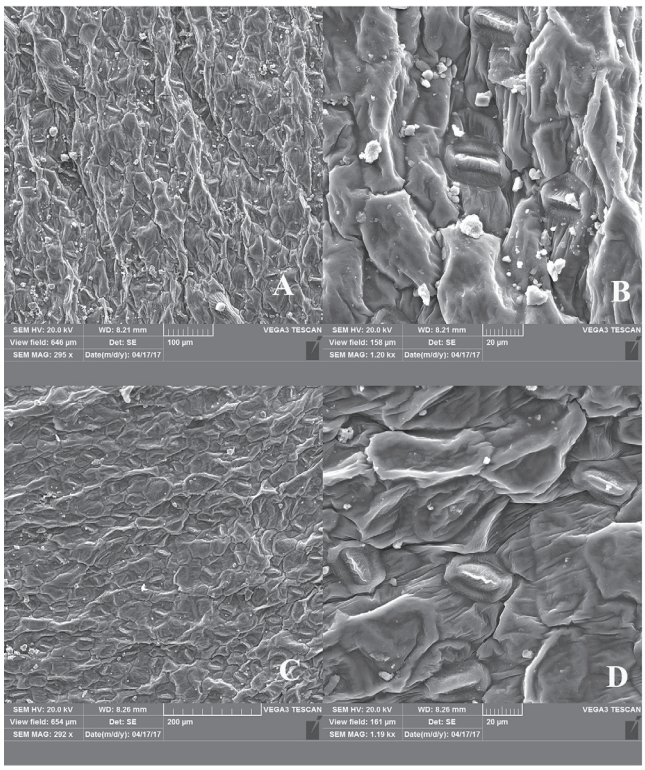

Figure 6. Leaf epidermis in *R. dentatus.* A & B) dorsal and C & D) ventral epidermis.

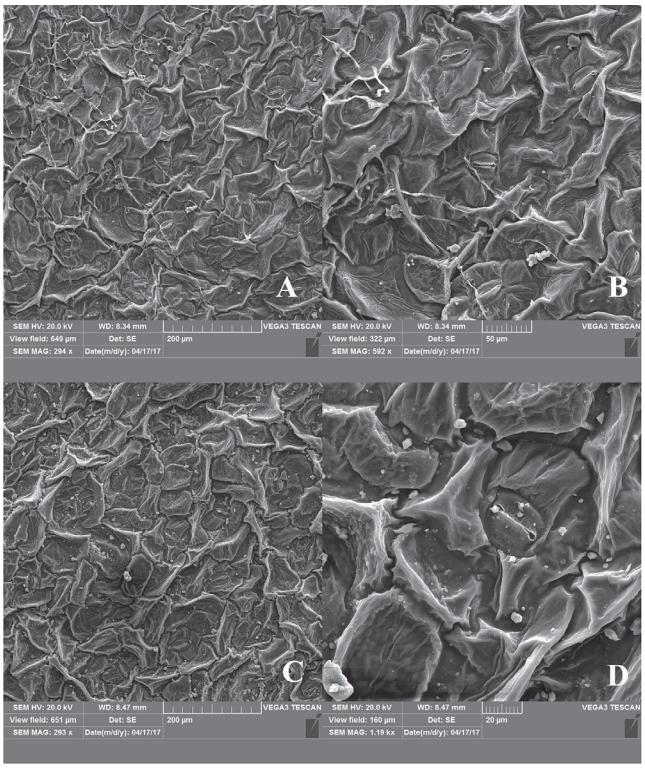

Figure 7. Leaf epidermis in *R. elbrusensis*. A & B) dorsal and C & D) ventral epidermis.

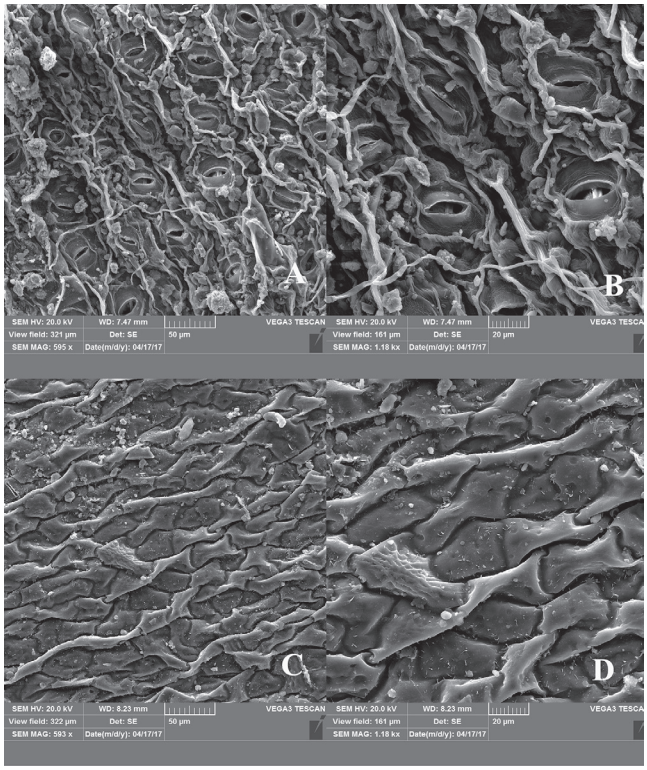

Figure 8. Leaf epidermis in *R. pulcher*. A & B) dorsal and C & D) ventral epidermis.

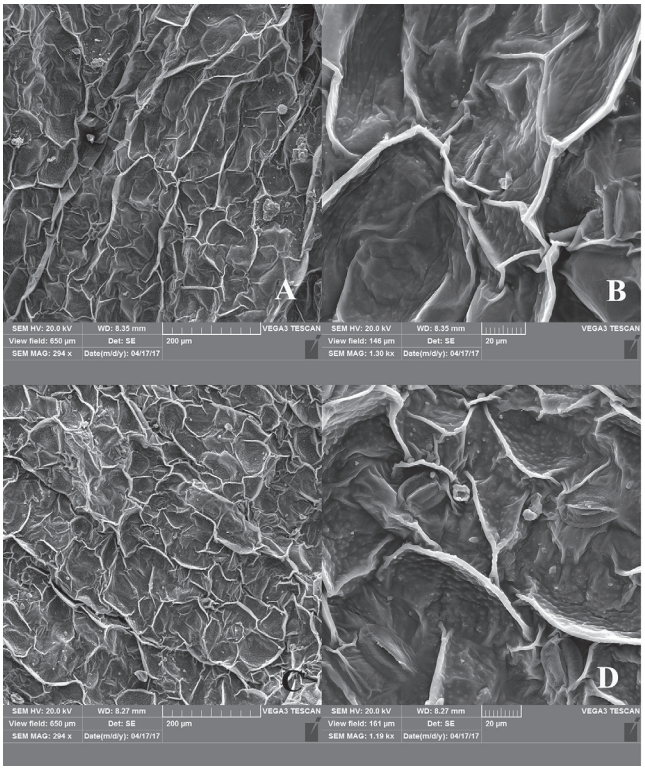

Figure 9. Leaf epidermis in *R. vesicarius*. A & B) dorsal and C & D) ventral epidermis.

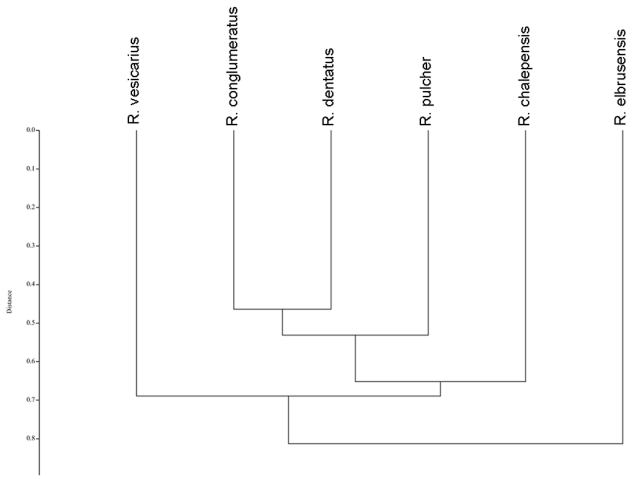

Figure 10. UPGMA tree of anatomical and micromorphological characters in *Rumex* species studies.

medullary vascular bundle, presence/absence of oxalate calcium crystals, shape of sclerenchyma cap of phloem and stomata type in ventral epidermis with 33.66% of total variation showed the highest correlation (>0.7).

Status of vascular bundle, average vascular bundles diameter, average thickness of sclerenchyma fibers over phloem, average size of adaxial epidermal cells, average size of stomata and number of parenchyma layers and average size of abaxial epidermal cells showed the highest correlation in second and third axes, respectively (Table 6).

In UPGMA tree based on all studied characters, *R. elbrusensis* was placed in a separate sub-cluster. In the second sub-cluster, *R. vesicarius* was positioned separately while other taxa grouped together (Fig. 10). Results of PCA ordination was in agreement with UPGMA tree (Fig. 11).

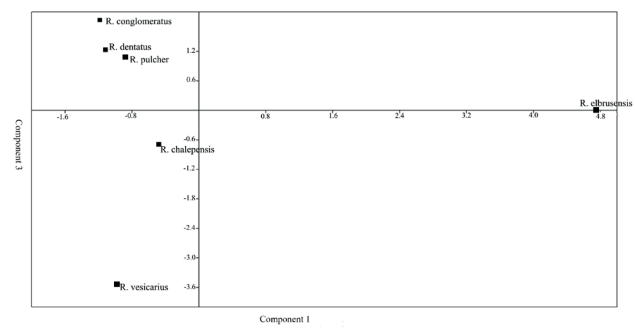

Figure 11. PCA ordination of anatomical and micromorphological characters in *Rumex* species studied.

Discussion

This investigation represents first detailed qualitative and quantitative study of leaf epidermis in *Rumex* species. It indicated the taxonomic importance of leaf epidermis in species delimitation.

Our observations showed anisocytic type of stomata in both surfaces of species studied, except *R. elbrusensis* with aniso-paracytic type in adaxial surface. Ahmad et al. (2009) reported amphianisocytic stomata pattern in *R. vesicarius*. Ayodele and Olwokudejo (2006) mentioned anomocytic and diacytic in other species of *Rumex*. Recently Yasmin et al. (2010 b) reported pericytic type for both leaf surfaces of *R. chalepensis* and *R. vesicarius* and peri-anisocytic type for *R. dentatus* which does not correspond to the present findings for the species studied. Considering epicuticular wax, species studied showed different patterns. In *R. vesicarius* wrinkled films can be seen in both sides, separating *R. vesicarius* from other taxa.

Previous studies on other Polygonaceae elements and different *Rumex* species support the usefulness of stem anatomical features in species delimitation (Hameed et al. 2010; Nazem Bokaee et al. 2015). Our studies showed the diagnostic value of these characters in studied species.

Joshi (1936) worked on the anatomy of *Rumex* with respect to the morphology of the internal bundles and the origin of the internal phloem. He suspected that absence of internal bundles in perennial *Rumex* represent the oldest forms of the genus. Among our perennial species studied (*R. elbrusensis*, *R. conglomeratus*, *R. pulcher*, *R. chalepensis*), only *R. elbrusensis* had these features therefore other perennial taxa are the oldest forms of *Rumex*. Our results were in agreement with other studies (Soleimani et al. 2014).

In both ordination and UPGMA tree, *R. vesicarius* was placed far from other species supporting its position in separate subgenus (Rechinger 1968; Mozaffarian 1988). Generally, our studies showed the taxonomic value of anatomical and micro-morphological characters in differentiation of this problematic genus.

Acknowledgement

The authors wish to thank Iran National Science Foundations (INSF) for the financial support of this research (grant number 95/S/45031).

References

Ahmad K, Khan MA, Ahmad M, Zafar M, Arshad M, Ahmad F (2009) Taxonomic diversity of stomata in dicot flora of a district tank (N.W.F.P.) in Pakistan. AJB 8(6):1052-1055.

Ayodele AE, Olowokudejo JD (2006) The family Polygonaceae in West Africa: Taxonomic significance of leaf epidermal characters. S Afr J Bot 72:442-459.

Chase M, Reveal A (2009) An update of the Angiosperm Phy-

logeny Group classification for the orders and families of flowering plants: APG III. Bot J Linn Soc 161(2):105-121.
Hameed I, Hussain F, Dastagir G (2010) Anatomical studies of some medicinal plants of family Polygonaceae. Pak J Bot 42(5):2975-2983.
Hong SK, Ronse Decraene LP, Smets E (1998) Systematic significance of tepal surface morphology in tribes Persicarieae and Polygoneae (Polygonaceae). Bot J Linn Soc 127:91-116.
Joshi AC (1936) The anatomy of *Rumex* with special reference to the internal bundles and the origin of the internal phloem in the Polygonaceae. Am J Bot 23:362-369.
Keshavarzi M, Mosaferi S, Shojaii M (2012) Leaf anatomical studies of the annual species of *Polygonum* s.l. (*Polygonaceae*) in Iran. Phytol Balcan 18(2):127-133.
Lersten NR, Curtis JD (1992) Foliar anatomy of *Polygonum* (Polygonaceae): Survey of epidermal and selected internal structures. Plant Syst Evol 182(1-2):71-106.
Li B, Zhang WG, Chen SHF, Yang SG (2008) Comparative anatomy of the leaves of *Rumex* in Jiangxi J Wuhan Bot Res 26(5):443-449.
Metcalfe CR, Chalk L (1950) Anatomy of Dicotyledons, Volume 2. Clarendon Press, Oxford.
Mozaffarian V (1988) New species and new plant records from Iran. Iran J Bot 4:61-70.
Mozaffarian V (2015) Identification of Medicinal and Aromatic Plants of Iran. Farhang Moaser Press, Tehran.
Nazem BZ, Keshavarzi M, Gholami A (2015) Stem anatomical study in some annual *Polygonum* L. (Polygonaceae) species in Iran. Pajohes G J 28(3):647-653.
Punt WP, Hoen P, Nilsson S, Thomas L (2007) Glossary of pollen and spore terminology. Rev Paleobot Palyn 143:1-81.
Rechinger K (1968) Polygonaceae. In Rechinger K, Schlman-Czeika H (eds), Flora Iranica, Vol 56. Akademische Druck und Verlagsanstalt, Graz, 2-24.
Ronse DLP, Akeroyd JR (1988) Generic limits in *Polygonum* L., and related genera (Polygonaceae) on the basis of floral characters. Bot J Linn Soc 98:321-371.
Sahney M, Vibhasa (2012) Stem anatomy of medicinally importance *Rumex hastatus* D. Don. (Polygonaceae). Res J Agric Biol Sci 8(2):154-157.
Sanchez I, Kron KA (2008) Phylogenetics of Polygonaceae with an emphasis on the evolution of Eriogonoideae. Syst Bot 33(1):87-96.
Soleimani M, Jafari A, Nejad SKH, Amiri MD (2014) Comparative anatomical and palynological studies on *Rumex* L. species (Polygonaceae) in NE Iran. GJBS 4(4):111-115.
The Plant List (2013) Version 1.1. Available: http://www.theplantlist.org. Accessed 1st January.
Yasmin G, Khan MA, Shaheen N, Qaim HM (2010 a) Taxonomic significance of leaf epidermal anatomy of selected *Persicaria* Mill. species of family Polygonaceae from Pakistan. AJB 9(25):3759-3768.
Yasmin G, Khan MA, Shaheen N, Qaim HM (2010 b) Micro-morphological investigation of foliar anatomy of *Fagopyrum* Mill. And *Rumex* L. of Polygonaceae. Pak J Bot 42(1):47-57.

Acta Biologica Szegediensis

Volume 62(1):53-59, 2018
Acta Biologica Szegediensis
http://abs.bibl.u-szeged.hu/index.php/abs
DOI:10.14232/abs.2018.1.53-59

ARTICLE

Pool of endoglucanase genes in *Schizophyllum commune* Fr.:Fr. (Basidiomycetes) on the territory of Ukraine

Sergiy M. Boiko

Department of Phytoecology, Institute for Evolutionary Ecology, National Academy of Sciences of Ukraine, Kyiv, Ukraine

ABSTRACT Pool of intracellular endoglucanases of the fungus *Schizophyllum commune* on the territory of Ukraine was studied. Two loci of endoglucanase (*Eg1*, *Eg2*) were found. The polymorphic locus *Eg2* controls the expression of four alleles. Alleles $Eg2^{93}$, $Eg2^{96}$ and $Eg2^{102}$ are rare and peculiar to certain populations. Amino acid sequence of the locus *Eg2* in databases of NCBI (XP_003031634.1) and UniProt (D8Q439) was probably identified. It is classified among the family 5 (GH5) and consists of 333 amino acid residues.
Acta Biol Szeged 62(1):53-59 (2018)

KEY WORDS
alleles
amino acid sequence
endoglucanase
Schizophyllum commune

ARTICLE INFORMATION
Submitted
13 December 2017.
Accepted
16 January 2018.
***Corresponding author**
E-mail: bsmbio@gmail.com

Introduction

Wall of a plant cell is the main site where carbon sequestration takes place. In general, it consists of approximately 30% of cellulose, 30% of hemicellulose, 35% of pectin substances and 5% of structural protein. These values vary depending on the type of plant and developmental stage (Albersheim et al. 2011; Hoch 2007; Ochoa-Villarreal et al. 2012). Saprotrophic fungi use this pool of substances as an infinite source of energy for vital activities. Wood-decay fungi cause two main types of wood degradation: white and brown. White rot fungi cause degradation of all wood components including lignin (Baldrian and Valaskova 2008), while brown rot fungi cause complete degradation of polysaccharides of the cell wall and partially of lignin (Worrall et al. 1997; Yelle et al. 2008).

All processes of destruction of the plant cell wall take place with involvement of various fungal enzyme systems, therefore, these are highly favored targets of mycological_(Floudas et al. 2012, 2015; Rytioja et al. 2014) and phytopathological research (Przybył et al. 2006; Simard et al. 2013). Certain fungi cause a transition type of decay (Redhead and Ginns 1985). This group includes *Schizophyllum commune* Fr.:Fr. which has a deficit in peroxidases and laccases (just like brown rot agents) and at the same time has a substantial number of enzyme systems geared to degradation of polysaccharides of a cell wall and crystalline cellulose, just like white rot fungi do (Ohm et al. 2010). Some researchers regarded *S. commune* as a saprophyte, but others recognized the fungus as a plant pathogen that invades living tissues from wounds and potentially causes rot (Latham 1970; Takemoto et al. 2010). The fungus is identified as a pathogen in many deciduous and coniferous tree species. Due to its well-known biology and ubiquitous character, *S. commune* is a frequently studied mycological model organism (Raper 1988; Tsujiyama and Ueno 2011).

One of the main enzymes taking part in the degradation of cellulose is endoglucanase (EC 3.2.1.6), that splits the inner β-1,4-glycosidic bonds (Schmidt and Liese 1980; Kirk and Cullen 1998; Przybył et al. 2006). Literature data show that most of the wood decaying basidiomycetes have several forms of endoglucanases, which makes this enzyme system promising for population genetic research (Baldrian and Valaskova 2008; Rytioja et al. 2014). Genome data of the *S. commune* are available that allow assessing its potentials (Ohm et al. 2010). Currently, important investigations include the research of heterogeneity of enzyme systems and their actual use (Chong et al. 2011; Song et al. 2013; Tovar-Herrera et al. 2015; Lee et al. 2014). Considering the high potential of enzyme systems of *S. commune* in the process of wood degradation and the lack of information regarding their polymorphism, our aim was to investigate the special aspects of endoglucanase pool in *S. commune* on the territory of Ukraine.

Materials and Methods

Organisms and culture conditions

Dikaryotic and monokaryotic cultures of *S. commune* were investigated.

Dikaryotic cultures were obtained from the basidiocarp of fungi collected in different regions of Ukraine (Chernihiv, Crimea, Donets'k, Ivano-Frankivs'k, Kyiv, Vinnytsia, and Zaporizhia region). The isolation of pure cultures from basidiocarps was performed in aseptic conditions under the MBS-10 stereomicroscope by deriving a sample of 1 × 1 mm size from the middle (sterile) part of plectenchyma and subsequently transferring it to the agar containing nutrient medium. After appearing of pure mycelium, it was repeatedly replanted to sterile nutrient.

Monokaryotic cultures were obtained using the spore print method. Water suspension of basidiospores, after multiple dilution procedures were deep plated in Petri dishes on agar medium. Purity and monosporous character of the cultures was controlled by means of microscopy. Monokaryotic cultures were used only to determine the genetic control of the locus. The total number of dikaryotic cultures was 128 (Chernihiv - 10, Crimea - 11, Donets'k - 32, Ivano-Frankivs'k - 12, Kyiv - 43, Vinnytsia - 8, and Zaporizhia - 12), while the number of monokaryotic ones was more than 500. Strains were cultivated in liquid glucose-peptone medium (10 g glucose L^{-1}, 3 g peptone L^{-1}, 0.4 g K_2HPO_4 L^{-1}, 0.5 g $MgSO_4 \times 7\ H_2O$ L^{-1}, 0.001 g $ZnSO_4 \times 7\ H_2O$ L^{-1}, 0.05 g $CaCl_2$ L^{-1}) in a TC-80M thermostat at 28 °C for 15-18 days (Boiko 2011). The initial pH of the medium was 5.0.

Histochemical detection of enzyme activity

Fungal mycelium was flushed out and dried out with the use of vacuum filtration. Subsequently, it was homogenized in Tris-citrate buffer and filtrated. Protein concentration was measured with a ULAB S131UV spectrophotometer (Layne 1957). Electrophoretic separation of proteins was performed in 11.25% polyacrylamide gel (PAAG) with the use of Tris-glycine buffer (pH 8.3). Amount of added protein in each well varied within 40-60 μg.

Detection of activity zones of endoglucanase (EG) in PAAG was performed in the presence of Na-carboxymethylcellulose (C5678, Sigma) (Manchenko 2003). After electrophoresis, the gel was washed in 50 μM phosphate buffer (pH 5.8) for 10 min and incubated at 50 °C for 60 min. Then the gel was rinsed in distilled water and placed in 0.1% Congo Red solution for 10 min at room temperature. Finally, the gel was washed in 1 M NaCl solution for 10 min. Enzyme activity resulted in light yellow bands on the red background of the gel. Electrophoretograms were assessed with the TotalLab TL 120 software.

Statistical analysis

Genetic control of the identified electrophoretic variants of enzymes was studied by analyzing their segregation among monokaryotic cultures. Genetic diversity was characterized using allelic frequency (A_E), Shannon's diversity index (I), expected and observed heterozygosity (H_o та H_e), and Wright's fixation index (Nei 1978). Genetic data were calculated using the POPGENE32 software (Yeh et al. 1999). BLAST searches were conducted on database of the National Center for Biotechnology Information (http://www.ncbi.nlm.nih.gov).

Investigated populations were marked with the name of the closest major settlement.

Results and Discussion

Data processing revealed that intracellular endoglucanase synthesis in *S. commune* is connected to two genetic loci: *Eg1, Eg2* (Fig. 1a). Locus *Eg1* in monokaryotic cultures is visualized in form of two bands with relative mobility (Rf) of 0.74 and 0.77 (Fig. 1b). These may well be two closely linked loci by analogy with the enzyme system of superoxide dismutase in this fungus (Boiko 2015).

Moreover, visualization of the *Eg1* locus is not stable for the most part of dikaryotic cultures (Fig. 1a), it may be illustrative of its dominant type of inheritance and impropriety for population genetic researches. In case of locus *Eg2* we determined four alleles with Rf of 0.53 (93), 0.55 (96), 0.57 (100), and 0.58 (102) (Fig. 1a) and stable visualization regardless of the nuclear status of mycelium.

Studying of genetic diversity of the enzyme system of *S. commune* on the territory of Ukraine with the use of PopGen32 software allowed us to determine that the mean effective number of alleles (A_E) is 1.27, Shannon's index of genetic diversity was high (I = 0.43). Considering the populations, the biggest contributions are made by *Pop2* (I = 0.57), *Pop3* (I = 0.39) and *Pop5* (I = 0.39). Contributions in this data are made by dissimilarity of samples, properties of climatic (e.g., humidity, wind streamline) and anthropogenic factor (e.g., density of traffic roads), which affect the speed of propagation of biological objects (Garcia et al. 2014). Migration processes increase the diversity of populations and cause changes in gene frequencies. Frequency of alleles of the locus *Eg2* that are peculiar to the investigated geographic area are show in Figure 2. The dominant role of $Eg2^{100}$ is noticeable, its frequency is 0.88, the rarest were the alleles $Eg2^{93}$ and $Eg2^{96}$. It should be noted that allele $Eg2^{96}$ is seen only in population *Pop2*, where allele $Eg2^{93}$ is completely absent. In case of populations *Pop1*, *Pop4*, *Pop6* and *Pop7* frequency of allele $Eg2^{100}$ are 1. In case of locus *Eg2* of *S. commune* in separate populations, and in general in the territory of

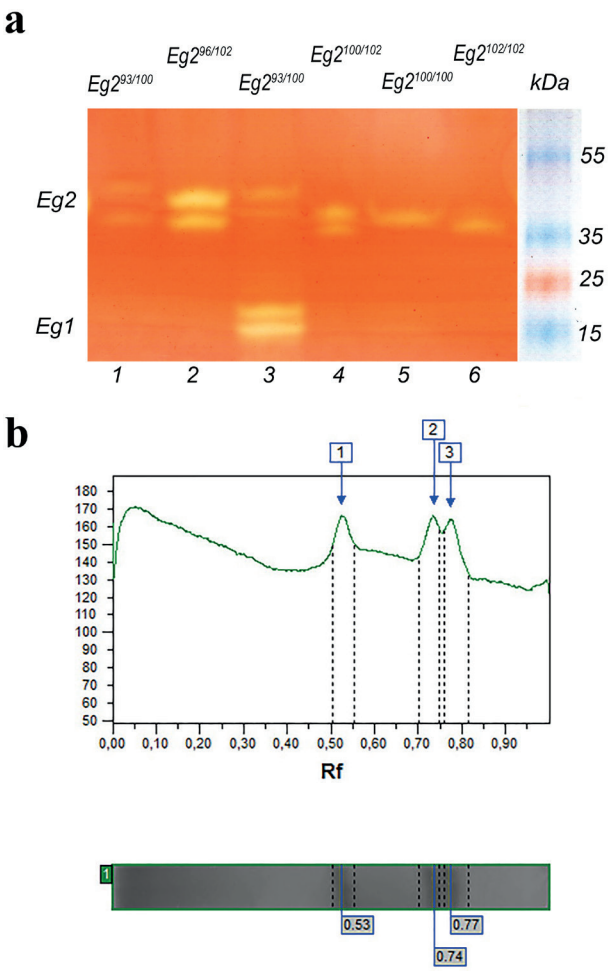

Figure 1. Endoglucanase allozymes of dikaryotic (a) and monokaryotic (b) cultures of *S. commune* (1-6 – patterns of different dikaryotic strains).

Ukraine, we observe deficit in heterozygous genotypes except for population *Pop5* (Table 1). This is also shown by values of Wright's fixation index (Table 2). Such situation may be observable in the absence of random mating in the population which leads to increase in homozygosis in general.

In case of locus *Eg2* of *S. commune*, deviation from the balance of Hardy-Weinberg was found. Such situations are quite frequently observed in populations of fungi and may have different causes (May and Royse 1982; James et al. 1999; Maurice et al. 2014). Thus, in case of a fungus *Serpula lacrymans* deviations in the balance of Hardy-Weinberg were observed both in European and Japanese populations in form of anomalously high level of heterozygosis (Engh et al. 2010). No clear explanation was found, but there have been suggestions of non-random mating or presence of more than two nucleuses in the fungal mycelium. We should also consider the complex tetrapolar system of sexual compatibility that is peculiar to both *S. lacrymans* and *S. commune* and reduces inbreeding. In our case, domination of one allele, $Eg2^{100}$, and low level of heterozygosis of the locus in Ukraine in general (Table 1) could indicate inbreeding in the *S. commune* population. However, data obtained previously regarding other *S. commune* loci indicated abidance by the Hardy-Weinberg principle; and this excludes a significant role of inbreeding in population-genetic processes that take place in this fungus. Obviously, results obtained on one locus only cannot be used as a basis for conclusions regarding the state of populations of *S. commune* particularly or in general in Ukraine, but they raise a question on the causes of the irregular distribution of alleles and give a chance to assess the evolution of this enzyme system. It is fair to assume that alleles $Eg2^{93}$, $Eg2^{96}$ and $Eg2^{102}$ are the "youngest" and, in spite of that, they are concentrated only in some populations in the investigated geographic area. It should be considered that, under stable environmental conditions, selection for decrease in recombination can take place, while under unstable conditions, variation necessarily increases which can lead to appearance of new alleles.

Several authors say that expression of two forms of endoglucanases is peculiar to the species of *S. commune* (Paice et al. 1984; Willick and Seligy 1985). The former determined that molecular weight of extracellular endoglucanases varied within the range of 38-40 kDa. The determined partial amino acid sequence (of 39 amino acids) allowed to define similarity of the two enzymes and assume that *EG2* is a proteolytic product of *EG1,* modified during transport out of the cell. So, most probably, the two are related to the expression of one form of endoglucanase. This data correlates to ours. Taking

Table 1. Observed (H_o) and expected (H_e) heterozygosity of the locus *Eg2* in the investigated *S. commune* populations.

Populations	H_o	H_e
General	0.0394	0.2139
Pop2	0.0263	0.3161
Pop3	0.0364	0.1977
Pop5	0.2000	0.1947

Table 2. Wright's fixation index of the locus *Eg2* in the investigated *S. commune* populations.

Allele	locus *Eg2*
$Eg2^{93}$	-0.0120
$Eg2^{96}$	0.6627
$Eg2^{100}$	0.8488
$Eg2^{102}$	0.9080

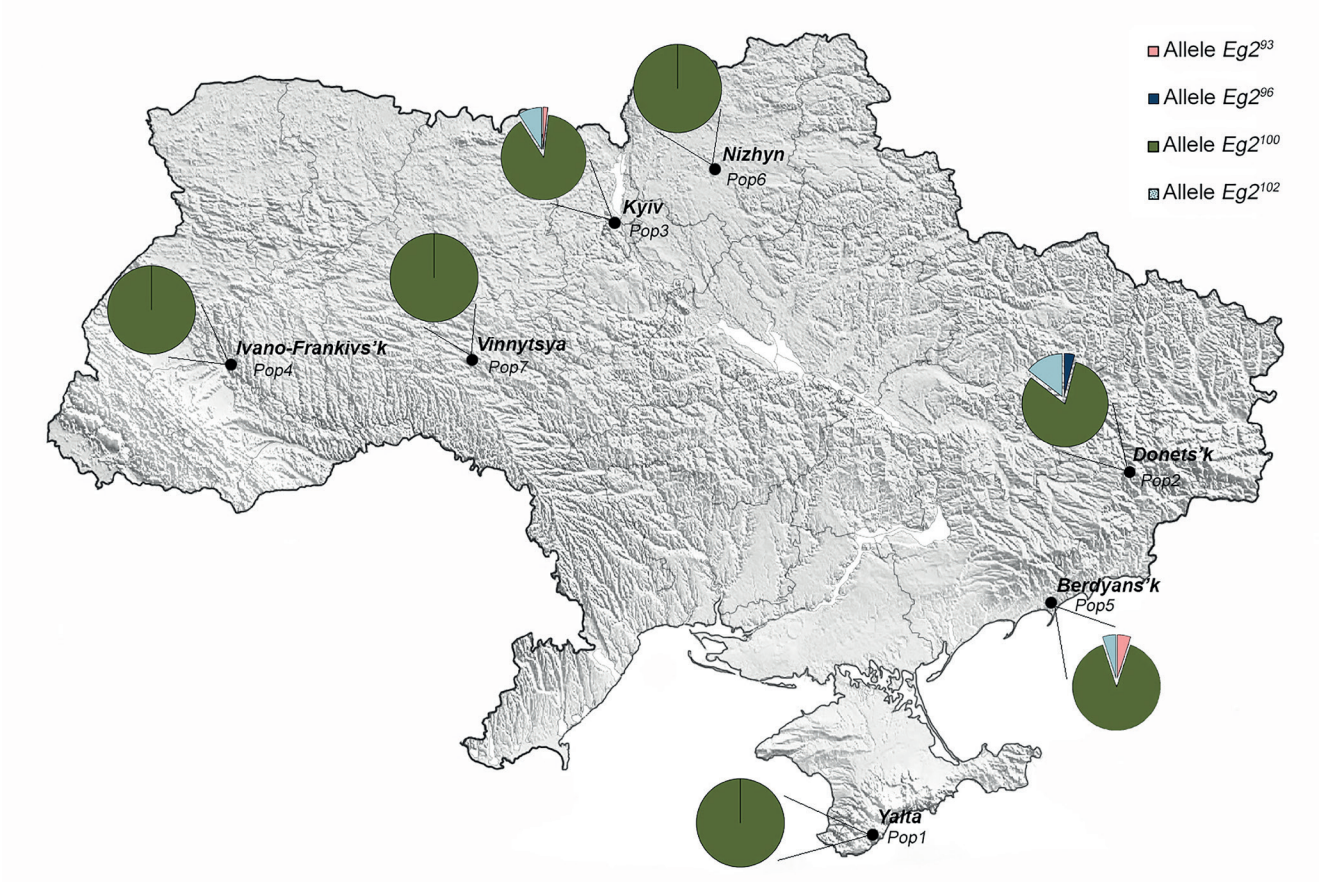

Figure 2. Alleles frequency of the locus *Eg2 S. commune* on the investigated geographic area.

into account that all isoforms of endoglucanase *Eg2* of *S. commune* that we described had a molecular weight of 35 to 40 kDa (Fig. 1), we used this amino acid sequence as a basis for identification. In order to search for homotypes of the initial amino acid sequence (AAECSGATKFDYFGVNESCAEFGNQNIPGVKNTDYTWPS) (Paice et al. 1984) the BLAST software was used (Altschul et al. 1997).

glycoside hydrolase family 5 protein [Schizophyllum commune H4-8]
Sequence ID: XP_003031634.1 Length: 333 Number of Matches: 1
▶ See 1 more title(s)

Range 1: 25 to 63

Score	Expect	Method	Identities	Positives	Gaps
85.9 bits(211)	6e-23	Compositional matrix adjust.	39/39(100%)	39/39(100%)	0/39(0%)

```
Query  1   AAECSGATKFDYFGVNESCAEFGNQNIPGVKNTDYTWPS  39
           AAECSGATKFDYFGVNESCAEFGNQNIPGVKNTDYTWPS
Sbjct  25  AAECSGATKFDYFGVNESCAEFGNQNIPGVKNTDYTWPS  63
```

Figure 3. Resuplts of the search and alignment of the amino acid sequence of *Schizophyllum commune* in the NCBI database.

As a result, we identified the 333 amino acid sequence of the enzyme of glycosidase (family 5) that is present in the database of the NCBI (XP_003031634.1) and is peculiar to *S. commune*. Level of identity of the amino acid sequence was 100% with no gaps (Fig. 3).

According to data from the International Union of Biochemistry and Molecular Biology (http://www.chem.qmul.ac.uk/iubmb/) glycosidase have more than 200 groups of enzymes that differ in activity on substrates. Classification by substrate specificity does not consider evolutionary processes, this is why the preferred classification today is CAZY, that was based on the structural similarity of proteins and that forms families with the similar substrate specificity (http://www.cazy.org) (Henrissat and Bairoch 1993). Glycoside hydrolase family 5 (GH5) includes enzymes with such activities as endoglucanase, β-mannanase, exo-1,3-glucanase, endo-1,6-glucanase, xylanase, endoglycoceramidase. The main peculiarity of this family is that one of the conserved regions contains a glutamic acid residue which potentially takes part in the catalytic mechanism (Py et al. 1991). It should be noted that, according to data from the database of the Universal Protein Resource (UniProt) (Apweiler et al. 2004), the total number of glycoside hydrolases in *S. commune* is over 230, and the only sequence of XP_003031634.1

```
        10         20         30         40         50
SNSAPQGQAP SSTATAPAAT ASSAAAECSG ATKFDYFGVN ESCAEFGNQN
        60         70         80         90        100
IPGVKNTDYT WPSPSSIDYF MQDGLNSFRI PFLLERLAPP ASGITGDFDS
       110        120        130        140        150
TYLADLQSTV EYITGKGGYA IIEPHNFMIY NGSTINSPDE FASFWTNLAT
       160        170        180        190        200
LFIDNTNVIF DLMNEPHDID ASVVYEHMQA AVNAIRAAGA TEQLILVEGT
       210        220        230        240        250
SWTGAWTWTT SGNSDAFAAL TDPNDNIAIE MHQYLDSDGS GTNETCVSAT
       260        270        280        290        300
IGSERLQAAT EWLKANNQRG FLGEMGAGSN ADCISAVSDA LCYLQQQEGT
       310        320        330
WIGALWWAAG PWWGDYFTSI EPPSGVALSD IYP
```

Figure 4. The amino acid sequence of the locus Eg2 S*chizophyllum commune* (UniProtKB – D8Q439).

(UniProtKB - D8Q439) showed complete homology. We can affirm with a high degree of probability that the amino acid sequence found corresponds with one of the alleles of the locus *Eg2* observed by us (Fig. 4).

The molecular weight of the protein (D8Q 439) is 35.660 kDa, which is in agreement with our data (Fig. 1). Research of the amino acid sequence of all allozymes of *Eg2 S. commune* will allow us to examine evolutionary changes of the locus.

Conclusions

In the basidiomycete fungus *S. commune* we found two loci of endoglucanase (*Eg1, Eg2*) on the territory of Ukraine. Polymorphous locus *Eg2* controls the expression of four alleles and despite the low level of heterozygosis on the sampled geographic area in general, it showed perspectives of use in population genetic researches. Alleles $Eg2^{93}$, $Eg2^{96}$ and $Eg2^{102}$ are rare and peculiar to certain populations. The use of a significant amount of *S. commune* samples allowed us to identify the *Eg1* locus, which could not be identified earlier, with molecular weights within the range of 15-18 kDa. A probable amino acid sequence, encoded by the Eg2 locus, was identified in databases of NCBI (sequence XP_003031634.1) and UniProt (D8Q439), which is classified among the family 5 (GH5) and consists of 333 amino acid residues.

References

Albersheim P, Darvill A, Roberts K, Sederoff R, Staehelin A (2011) Plant cell walls: A renewable material source. In Plant Cell Walls, Garland Science, Taylor & Francis Group, LLC, New York, 365-409.

Altschul SF, Madden TL, Schäffer AA, Zhang JZ, Miller W, Lipman DJ (1997) Gapped BLAST and PSI-BLAST: a new generation of protein database search programs. Nucleic Acids Res 25:3389-3402.

Apweiler R, Bairoch A, Wu CH, Barker WC, Boeckmann B, Ferro S, Gasteiger E, Huang H, Lopez R, Magrane M, Martin MJ, Natale DA, O'Donovan C, Redaschi N, Yeh LS (2004) UniProt: The Universal Protein Knowledgebase. Nucleic Acids Res 32: D115-119.

Baldrian P, Valaskova V (2008) Degradation of cellulose by basidiomycetous fungi. FEMS Microbiol Rev 32(3):501-521.

Boiko SM (2011) Change in the isozyme composition of the mushroom *Schizophyllum commune* Fr. (Basidiomycetes) culture depending on the age of mycelium. Ukr Bot J 68(4):598-603.

Boiko S M (2015) Allozyme polymorphism in mono- and dikaryotic cultures of fungus *Schizophyllum commune* Fr. (Basidiomycetes). Cytol Genet 49(1):27-31.

Chong SL, Battaglia E, Coutinho PM, Henrissat B, Tenkanen M, de Vries RP (2011) The alpha-glucuronidase Agu1 from *Schizophyllum commune* is a member of a novel glycoside hydrolase family (GH115). Appl Microbiol Biotechnol 90(4):1323-1332.

Engh IB, Carlsen T, Saetre GP, Hogberg N, Doi S, Kauserud H (2010) Two invasive populations of the dry rot fungus *Serpula lacrymans* show divergent population genetic structures. Mol Ecol 19(4):706-715.

Floudas D, Binder M, Riley R, Barry K, Blanchette RA, Henrissat B, Martínez AT, Otillar R, Spatafora JW, Yadav JS, Aerts A, Benoit I, Boyd A, Carlson A, Copeland A, Coutinho PM, de Vries RP, Ferreira P, Findley K, Foster B, Gaskell J, Glotzer D, Górecki P, Heitman J, Hesse C, Hori C, Igarashi K, Jurgens JA, Kallen N, Kersten P, Kohler A, Kües U, Kumar TK, Kuo A, LaButti K, Larrondo LF, Lindquist E, Ling A, Lombard V, Lucas S, Lundell T, Martin R, McLaughlin DJ, Morgenstern I, Morin E, Murat C, Nagy LG, Nolan M, Ohm RA, Patyshakuliyeva A, Rokas A, Ruiz-Dueñas FJ, Sabat G, Salamov A, Samejima M, Schmutz J, Slot JC, St John F, Stenlid J, Sun H, Sun S, Syed K, Tsang A, Wiebenga A, Young D, Pisabarro A, Eastwood DC, Martin F, Cullen D, Grigoriev IV, Hibbett DS (2012) The paleozoic origin of enzymatic lignin decomposition reconstructed from 31 fungal genomes. Science 336(6089):1715-1719.

Floudas D, Held BW, Riley R, Nagy LG, Koehler G, Ransdell AS, Younus H, Chow J, Chiniquy J, Lipzen A, Tritt A, Sun H, Haridas S, LaButti K, Ohm RA, Kües U, Blanchette RA, Grigoriev IV, Minto RE, Hibbett DS (2015) Evolution of novel wood decay mechanisms in *Agaricales* revealed by the genome sequences of *Fistulina hepatica* and *Cylindrobasidium torrendii.* Fungal Genet Biol 76:78-92.

Garcia RA, Cabeza M, Rahbek C, Araujo MB (2014) Multiple dimensions of climate change and their implications for biodiversity. Science 344(6183):1247579.

Henrissat B, Bairoch A (1993) New families in the classification of glycosyl hydrolases based on amino acid sequence similarities. Biochem J 293:781-788.

Hoch G (2007) Cell wall hemicelluloses as mobile carbon stores in non-reproductive plant tissues. Funct Ecol 21(5):823-834.

James TY, Porter D, Hamrick JL, Vilgalys R (1999) Evidence for limited intercontinental gene flow in the cosmopolitan mushroom *Schizophyllum commune*. Evolution 53(6):1665-1677.

Kirk TK, Cullen D (1998) Enzymology and molecular genetics of wood degradation by white-rot fungi. In Young RA, Akhtar M, eds., Environmentally Friendly Technologies for the Pulp and Paper Industry. John Wiley and Sons, New York, pp. 273-307.

Layne E (1957) Spectrophotometric and turbidimetric methods for measuring proteins. Methods Enzymol 3:447-455.

Latham AJ (1970) Development of apple fruit rot and basidiocarp formation by *Schizophyllum commune*. Phytopathology 60:596-598.

Lee YM, Lee H, Kim JS, Lee J, Ahn BJ, Kim GH, Kim JJ (2014) Optimization of medium components for β-glucosidase production in *Schizophyllum commune* KUC9397 and enzymatic hydrolysis of lignocellulosic biomass. BioResources 9(3):4358-4368.

Manchenko GP (2003) Handbook of Detection of Enzymes on Electrophoretic Gels, CRC Press.

Maurice S, Skrede I, LeFloch G, Barbier G, Kauserud H (2014) Population structure of *Serpula lacrymans* in Europe with an outlook to the French population. Mycologia 106(5):889-895.

May B, Royse DJ (1982) Genetic variation and joint segregation of biochemical loci in the common meadow mushroom *Agaricus campestris.* Biochem Genet 20(11):1165-1173.

Nei M (1978) Estimation of average heterozygosity and genetic distance from a small number of individuals. Genetics 89(3):583-590.

Ochoa-Villarreal M, Aispuro-Hernández E, Vargas-Arispuro I, Martínez-Téllez MÁ (2012) Plant cell wall polymers: function, structure and biological activity of their derivatives. In De Souza Gomes A, ed., Polymerization. InTech 64-89.

Ohm RA, de Jong JF, Lugones LG, Aerts A, Kothe E, Stajich JE, de Vries RP, Record E, Levasseur A, Baker SE, Bartholomew KA, Coutinho PM, Erdmann S, Fowler TJ, Gathman AC, Lombard V, Henrissat B, Knabe N, Kües U, Lilly WW, Lindquist E, Lucas S, Magnuson JK, Piumi F, Raudaskoski M, Salamov A, Schmutz J, Schwarze FW, vanKuyk PA, Horton JS, Grigoriev IV, Wösten HA (2010) Genome sequence of the model mushroom *Schizophyllum commune.* Nat Biotechnol 28(9):957-963.

Paice MG, Desrochers M, Rho D, Jurasek L, Roy C (1984) Two forms of endoglucanase from the basidiomycete *Schizophyllum commune* and their relationship to other beta-1,4-glycoside hydrolases. Biotechnology 2(6):535-539.

Przybył K, Dahm H, Ciesielska A, Moliński K (2006) Cellulolytic activity and virulence of *Ophiostoma ulmi* and *O. novo-ulmi* isolates. Forest Pathol 36:58-67.

Py B, Bortoli-German I, Haiech J, Chippaux M, Barras F (1991) Cellulase EGZ of *Erwinia chrysanthemi*: structural organization and importance of His98 and Glu133 residues for catalysis. Protein Eng 4(3):325-333.

Raper CA (1988) *Schizophyllum commune*, a model for genetic studies of the *Basidiomycotina*. In Sidhu GS, ed., Genetics of Plant Pathogenic Fungi. Academic Press, London, pp. 511-522.

Redhead SA, Ginns JH (1985) A reappraisal of agaric genera associated with brown rots of wood. Trans Mycol Soc Jpn 26:349-381.

Rytioja J, Hildén K, Yuzon J, Hatakka A, de Vries RP, Mäkelä MR (2014) Plant-polysaccharide-degrading enzymes from basidiomycetes. Microbiol Mol Biol Rev 78(4):614-649.

Schmidt O, Liese W (1980) Variability of wood degrading enzymes of *Schizophyllum commune.* Holzforschung 34(2):67-72.

Simard M, Laflamme G, Rioux D (2013) Enzymatic interactions between *Gremmeniella abietina* var. *abietina,* European race, and two resistant hosts, *Pinus banksiana* and *P. contorta*. Forest Pathol 43:29-41.

Song Y, Lee YG, Choi IS, Lee KH, Cho EJ, Bae HJ (2013) Heterologous expression of endo-1,4-beta-xylanase from *Schizophyllum commune* in *Pichia pastoris* and functional characterization of the recombinant enzyme. Enzyme Microb Technol 52(3):170-176.

Takemoto S, Nakamura H, Imamura Y, Shimane T (2010) *Schizophyllum commune* as a ubiquitous plant parasite. Japan Agric Res Quart 44:357-364.

Tovar-Herrera OE, Batista-Garcia RA, Sanchez-Carbente MD, Iracheta-Cardenas MM, Arevalo-Nino K, Folch-Mallol JL (2015) A novel expansin protein from the white-rot fungus *Schizophyllum commune*. PlosOne 10(3):e0122296.

Tsujiyama S, Ueno H (2011) Production of cellulolytic enzymes containing cinnamic acid esterase from *Schizophyllum commune*. J Gen Appl Microbiol 57(6):309-317.

Willick GE, Seligy VL (1985) Multiplicity in cellulases of *Schizophyllum commune* derivation partly from heterogeneity in transcription and glycosylation. Eur J Biochem 151(1):89-96.

Worrall JJ, Anagnost SE, Zabel RA (1997) Comparison of wood decay among diverse lignicolous fungi. Mycologia 89(2):199-219.

Yeh FC, Yang R, Boyle T (1999) POPGENE Version 1.32. Microsoft window-based freeware for population genetic analysis. University of Alberta. Centre for International Forestry Research

Yelle DJ, Ralph J, Lu F, Hammel KE (2008) Evidence for cleavage of lignin by a brown rot basidiomycete. Environ Microbiol 10(7):1844-1849.

Acta Biologica Szegediensis

Volume 62(1):61-66, 2018
Acta Biologica Szegediensis
http://abs.bibl.u-szeged.hu/index.php/abs
DOI:10.14232/abs.2018.1.61-66

ARTICLE

Expression and production optimization of the cationic antimicrobial peptide - indolicidin by the recombinant *E. coli* C41 (DE3) clones

Kanesan Panneer Selvam[1*], Guruvu Nambirajan[1], Balasubramaniam Annamalai[2], Mohammed Alaidarous[3], Bader Mohammed Alshehri[3], Abdul Aziz A. Bin Dukhyil[3], Coimbatore Subramanian Shobana[4], Palanisamy Manikandan[3,5]

[1]PG and Research Department of Microbiology, M. R. Government Arts College, Mannargudi - 614 001, Tamil Nadu, India
[2]Biological E Limited, Genome Valley, Hyderabad - 500 078, India
[3]Department of Medical Laboratory Sciences, College of Applied Medical Sciences, Majmaah University, Saudi Arabia.
[4]Department of Microbiology, PSG College of Arts & Science, Coimbatore - 641 014, Tamilnadu, India
[5]Greenlink Analytical and Research Laboratory India Private Limited, Coimbatore - 641 014, Tamilnadu, India

ABSTRACT The cytoplasmic granules of bovine neutrophils naturally possess indolicidin - a promising cationic antimicrobial peptide as it displays inherent inhibitory activities against a broad type of microbial pathogens. In this study, a shake flask level production and expression optimizations of the indolicidin by the recombinant *Escherichia coli* C41 (DE3) clones (transformed with pET21a(+) plasmid carrying indolicidin gene) were carried out under standard conditions, as to determine the conditions required for maximal production. It was determined that a concentration of 1 mM of IPTG was effective, the 2×YT with salts and LB media at pH 7.5 with 3-6 h of incubation were required for maximal indolicidin expression.
Acta Biol Szeged 62(1):61-66 (2018)

KEY WORDS
cationic antimicrobial peptide
drug resistance
indolicidin
optimization

ARTICLE INFORMATION
Submitted
24 February 2018.
Accepted
28 April 2018.
***Corresponding author**
E-mail: drpanneerselvam.micro@gmail.com

Introduction

The increasing prevalence of drug resistant and multi-drug resistant bacteria has prompted to investigate and produce new compounds against bacterial pathogens as an intervention to ensure efficient infection control measures (Ahmad et al. 1995). Cationic antimicrobial peptides (CAPs) represent an exciting class of drug candidates, particularly because their mechanism of action is unlikely to induce drug resistance. As a kind of humoral immune response, such host defense peptides are synthesized by a wide range of multicellular organisms including bacteria and protect against a wide range of infectious bacteria, viruses, fungi and certain parasites (Zhang and Gallo 2016). Precisely, they are endogenous peptide antibiotics forming important components of the innate immune system (Hancock et al. 2006) of vertebrates and invertebrates. Thus, CAPs can be developed and potentially employed in medicine as new safe antibacterial compounds.

The cationic antimicrobial peptide - indolicidin is a 13-residue peptide (measures less than 2.8 kDa in size) and carries five tryptophan residues that distinguish it from α-helical and β-structured cationic peptides. It is isolated from the cytoplasmic granules of bovine neutrophils possessing a unique amino acid composition (ILPWKWPWWPWRR-NH2-H-Ile-Leu-Pro-Trp-Lys- Trp-Pro-Trp-Trp-Pro-Trp-Arg-Arg-NH_2) with 39% tryptophan, 23% proline, and an amidated carboxyl terminus. The molecular weight of the indolicidin peptide was reported to be 2861 Da with a total of 20 amino acids (MHHHHHHILPWKWPWWPWRR) including `His'-Tag and the start codon. Indolicidin has been noted to be a promising agent since it could target a variety of bacterial and fungal pathogens. It exhibits broad-spectrum antimicrobial activity *in vitro* against Gram positive (*Staphylococcus aureus*) and Gram negative (*Escherichia coli*) bacteria, fungi (*Aspergillus fumigatus, Candida albicans* and *Cryptococcus neoformans*), protozoa (*Leishmania donovani*), and human immunodeficiency virus (HIV-1) (Ahmad et al. 1995; Selsted et al. 1992; Benincasa et al. 2006; Lee et al. 2002; Bertrand-Krajewski et al. 2005). It also possesses

haemolytic and cytotoxic activities towards erythrocytes and human T lymphocytes (Schluesener et al. 1993). Despite the small size and unique composition of indolicidin, it is capable of killing bacteria, by causing disruption of the cytoplasmic membrane by channel formation.

The advent of recombinant DNA technology has conquered the traditional problems of protein research including purification of minute homogenous quantities of desired peptides from tissues (Alberts et al. 1994). It enables isolation of specific genes and to perpetuate them in host organisms besides ensuring higher expression and purity of the compound, safety, decreased cost of production (WHO 2014). Accordingly, many different host/vector systems are being developed to produce antimicrobial peptides through recombinant DNA technology. *E. coli* C41 (DE3) and C43 (DE3) strains have been employed most often due to the low cost of fermentation/expression compared to mammalian cells, and its ability to produce inclusion bodies, which aid in the purification process (Haught et al. 1998; Lee et al. 1998). Industrial biotechnology uses recombinant microbes for producing a commercial product like indolicidin in stages of upstream processing (preparation of raw material/media for fermentation), fermentation (growth of the target microorganism in a large bioreactor with the consequent production of a desired compound) and downstream processing (purification of the desired compound (Glick and Pasternak 1998). The present evaluation has majorly focused on the maximal expression and optimization of indolicidin production by the recombinant *E. coli* C41 (DE3) clone that was earlier cloned in the study to express indolicidin.

Materials and Methods

Competent *E. coli* C41 (DE3) cells (Lucigen, USA) were prepared and transformed with the pET-21a (+) recombinant plasmids (Fig. 1). The optical density (OD) checked transformed cells were subsequently assessed to optimize indolicidin expression with (flasks A & B) and without (flask C) 1 mM IPTG (isopropyl β-D-1-thiogalactopyranoside) induction. After everyone hour, 1 ml of culture was withdrawn from each flask to check the OD and indolicidin expression (Froger and Hall 2007).

Confirmation of indolicidin expression by the recombinant E. coli

Tricine sodium dodecyl sulphate polyacrylamide gel electrophoresis (tricine-SDS-PAGE) was employed for the separation and confirmation of indolicidin. A 20% separating gel (1 cm length) followed by 16% separating gel (5 cm length) was overlaid with 10% 'spacer gel' (to

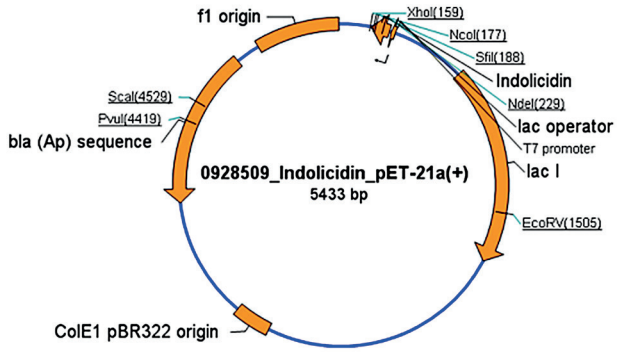

Figure 1. pET-21a (+) expression vector map showing the restriction sites, the gene insert (indolicidin), selectable marker [bla (Ap)] and the origin of replications (f1 origin & ColE1-EMD Biosciences). Gene insert: Indolicidin; Host: *E. coli* K12 XL10 gold (dam+ dcm+); Gene size: 63 bp. Vector backbone: pET-21a (+) Cloning sites: XbaI/XhoI

considerably sharpen the bands for proteins and peptides of 1-5 kDa). The electrophoresis was started after loading 10 µL of the prepared samples at 90 V. After separation, the protein was visualized by directly staining the gel by Coomassie Brilliant Blue (Schägger and von Jagow 1987; Schägger 2006). The culture from A & B flasks (induced) were centrifuged, before and after induction for 10 min, 10 000 rpm at 4 °C. The supernatants were discarded, and the samples of each cell pellet were normalized at appropriate OD, boiled and run on two sets of 16% tris-tricine gels simultaneously. The gels were suitably stained, destained and visualized. The un-induced samples (from the flask C) were also subjected to tricine-SDS-PAGE. The samples possessing the expressed indolicidin of the study were screened for their antimicrobial activity against a set of bacterial pathogens along with un-inoculated media samples as controls so as to determine the presence and antimicrobial activities of the expressed indolicidin of the study.

Effect of the inducer - IPTG on indolicidin production by the recombinant E. coli

A contaminant free, confirmed *E. coli* clone was involved in all the optimization studies. The *E. coli* culture (OD_{600} value of 1.5 - 2.5) in LB medium was induced with different concentrations (0.5 mM, 1.0 mM, 2 mM, 5 mM, and 10 mM) of the IPTG and were incubated at 37 °C in duplicates. Pre and post induction samples were collected and were analyzed quantitatively and qualitatively by electrophoresis.

Primary screening of production media - shake flask studies

A total of eight different media (nutrient broth, min A, Luria Bertani medium, 2×YT medium, 2×YT with salts,

terrific broth (TB) medium, SB medium & SOB medium (Himedia, India) containing varying concentrations of tryptone, yeast extract with different carbon sources like glycerol, glucose and with several salts/buffer combinations were involved in the preliminary screening of a best medium for expression (Sambrook and Russel 2001). Similarly, 1 ml of 100 mg/mL sterile filtered ampicillin was added just before inoculation, 0.5 mL stock culture was inoculated, and all the studies were executed at shake flask level (with 50 ml of the test medium in a 250 ml flask).

To prepare the inoculum for shake flask studies, 0.5 mL of stock culture was inoculated into 50 mL of LB-Amp medium after thawing and incubated at 37 °C, 200 rpm for overnight. From the overnight culture, 5 mL of culture was inoculated into the shake flasks of different media (100 mL) with ampicillin and incubated at 37 °C, 200 rpm. The induction was carried out using 1 mM IPTG at 1.0 ± 0.2 OD after obtaining the desired cell OD. One mL of IPTG induced (also normalized to 10 OD_{600}) culture sample was taken from each flask for 3 h (while a sampling was also done just before induction). The indolicidin peptide expression was checked for both the induced as well as the uninduced cell samples after lysis by tricine SDS-PAGE.

Effect of different pH on indolicidin production by the recombinant E. coli

In order, to study the effect of media pH on indolicidin production, initial media pH was adjusted ranging from 6 to 9 with an increment of 0.5 unit (6, 6.5, 7, 7.5, 8, 8.5 and 9). The experiment was carried out using LB media (with optimized amount of ingredients) in duplicates and indolicidin was extracted after 12 h of incubation and estimated for indolicidin activity.

Effect of incubation time on indolicidin production by the recombinant E. coli

The indolicidin production media was prepared in duplicates with all optimized parameters and inoculated with the *E. coli*. The indolicidin assay was carried out from the 8^{th} h incubation up to 32 h after every 4 h interval (*i.e.* 8, 12, 16, 20, 24, 28, and 32 h) of incubation.

Effect of temperature on indolicidin production by the recombinant E. coli

The incubation - temperature at various ranges (25, 30, 37, 40 and 45 °C) was evaluated and optimized to support a better expression of the indolicidin peptide by the recombinant *E. coli* of the study. Developmental batches were executed at 250 mL flasks with 50 mL of LB medium in duplicates inoculated with the test *E. coli* and were incubated at room temperature as well as at 30, 37, 40 and 45 °C appropriately (Shokri 2003; Schmidt 2005). Precisely, all the indolicidin fermentation processes included simultaneous gearing up of the growing cells to produce the indolicidin protein by inducing them with 1 mM IPTG so that the cellular machinery was mostly engaged in expressing the target protein(s) in abundance from of the start of the inoculation. Finally, the fermentation medium was separated by harvesting the cells, concentrated and then evaluated for the target peptide.

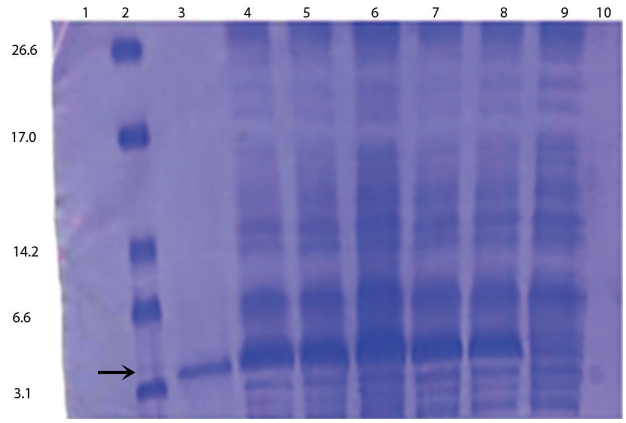

Figure 2. Tricine - SDS-PAGE profile of indolicidin expression check of 10 OD normalized *E. coli* transformants. Band representing the target peptide - indolicidin measuring 2.8 kDa.

Results

In this study, the LB-Amp plates incubated with transformation mixes of host *E. coli* C41 (DE3) cells and pET-21a (+) (EMD Biosciences, USA) with indolicidin gene construct showed a good growth of individual, isolated colonies after overnight incubation. The transformation efficiency was found to be 2.2×10^5 CFU/ng of DNA. The OD values of *E. coli* transformants grown in flasks A & B (with IPTG induction), and flask C (no IPTG induction) at different intervals both before and after induction with the inducer indicated a difference in expression between the IPTG induced and non-induced clones. The SDS-PAGE analysis done for the culture sampled from the flask cultures A & B of the induced clones confirmed the expression of 2.8 kDa indolicidin peptide as a discrete band at the bottom of the gel (Fig. 2) and the expressed peptide was also quantified by densitometry along with a standard. The expression of the peptide by the transformed cells was also confirmed after growing the preliminarily confirmed transformants in shake-flask cultures and was also found that the induction of recombinant protein (indolicidin) in *E. coli* cultures could be best obtained when induced

Table 1. Primary screening - pre and post induction OD patterns of indolicidin expressing *E. coli* clones in different production media.

Test production media	OD600 (time of sampling)			
	JBI	AI (2 h)	AI (3 h)	AI (4 h)
LB medium	0.82	1.73	2.16	2.74
SB medium	0.92	1.72	2.24	2.52
SOB medium	0.74	1.68	2.20	2.46
TB medium	0.86	1.92	2.65	3.00
2×YT medium	0.72	1.82	2.40	2.92
2×YT with salts	1.02	2.06	2.90	3.38

AI - after induction; JBI - just before induction

at OD_{600}value of 0.6 to 1.0.

The standardization of parameters governing the growth of recombinant *E. coli* C41 (DE 3) and production of indolicidin in high yields were studied at shake flask level. The effect of various media, different concentrations of IPTG inducer, suitable temperature, pH of the media, incubation duration brought useful outcomes. Of the eight different media [Nutrient broth, Min A, LB medium, 2×YT medium, 2×YT with salts, Terrific Broth (TB) medium, SB medium and SOB medium] containing varying concentrations of tryptone, yeast extract with different carbon sources like glycerol, glucose and with several salts/buffer combinations involved in the preliminary screening, it was apparent that the growth of *E. coli* was higher 2×YT with salts, TB medium and in LB medium with elevated levels of OD compared to other media. SOB medium was noted to be the least in supporting *E. coli* growth. Similarly, a difference in indolicidin expression by the *E. coli* clone was noted when grown in different media as the OD obviously varied when determined both before and after IPTG induction (Table 1). Although, each medium supported high yield of indolicidin, the 2×YT with salts, TB medium and LB media were found to support higher expressions especially after induction with IPTG. In addition, the difference in indolicidin expression was also evaluated using SDS-PAGE. It was observed that in the presence of 2×YT with salts and LB media as much as 101 mg/L and 90 mg/L of indolicidin was estimated, respectively after four hours from the time of induction.

Discussion

The alarming development of microbial drug resistance has resulted in intensive research and development of alternate antimicrobial compounds in order, to maintain a pool of effective therapeutic agents in real times so as to combat microbial infections. More importantly, these new antimicrobials should preferably possess both unique modes of action as well as different cellular targets compared with the existing antibiotics. Accordingly, good efforts have been made to develop cationic antimicrobial peptides as drugs since they possess broad spectrum ability in killing microbes and act non-specifically by targeting the sites for which development of resistance is difficult. In this line, the peptides like indolicidin is an attractive subject for drug research and hence there has been a lot of commercial interest and effort in developing indolicidin as a potential antimicrobial therapeutic. Though, a large number of antimicrobial peptides have been found in nature and been designed, relatively a few have been investigated for their clinical trials based on their promising *in vitro* and animal studies.

After selection of the expression vector [pET-21a (+)] of the study, several different host strains were identified [*E. coli* C41DE3 derivative of BL21 (Lee et al. 1998; Ponti et al. 1999), HS174DE3 (Lee et al. 2000), BL21DE3 and AD494DE3 (Morin et al. 2006) and JM109 (Taguchi et al. 1994)] from literature and was noted that two mutant strains of *E. coli* BL21 (DE3), C41 (DE3) and C43 (DE3) were frequently used to overcome the toxicity associated with over expressing recombinant proteins using the bacteriophage T7 RNA polymerase expression system. The strains were also reported with properties of proteolytic deficiencies, solubilization of recombinant proteins, or derivation from different cell strains (Miroux and Walker 1996; Dumon-Seignovert et al. 2004). Miroux and Walker (1996) further reported that by using *E. coli* C41 (DE3), cell death during induction of the host could be avoided. Further, *E. coli* has been used successfully for the higher expression of several recombinant antimicrobial peptides like lactoferricin (Feng et al. 2006; Kim et al. 1997), calmodulin (Zheng et al. 1997), CM4 (Zhou et al. 2009) and human beta-defensin 2 (Xu et al. 2006). As has been observed in the present study, Wagner et al. (2008) reported that *E. coli* C41 (DE3) strain is acceptable for convenient over expression of any given novel protein such as indolicidin.

Haught et al. (1998) and Skosyrev et al. (2003) reported a growth maximum of 1.5 OD. Other researchers had reported expression of 0.1 to 310 mg/L of antimicrobial peptide (Haught et al. 1998; Lee et al. 1998; Skosyrev et al. 2003; Hara and Yamakawa 1996; Lee et al. 2002; Hwang et al 2001). The major goal for optimizing production of recombinant proteins is to produce the highest amount of functional product per unit volume per unit time.

In this context, most of the work was only aimed at increasing recombinant protein production in bacterial strains by increasing the biomass production and studies on the expression of recombinant proteins based on the effects of media composition are minimal. Though Swartz (2001) and Balbás (2001) reported that the fermentation and the level of intracellular accumulation of a recom-

binant protein in *E.coli* is dependent on the final cell OD and the specific activity of the protein, it is also known that the production of secondary metabolites in microbial strains can depend on the composition of the medium in which the organism is grown and the expression of all proteins will be not maximal in one medium and it has to be optimized for specific proteins.

Despite this, little attention has been paid to the effects of medium formulation on the accumulation of recombinant proteins (Broedel et al. 2001). As the industrial expression of the eukaryotic peptide - indolicidin is more at the developing stage, the present study included appropriate evaluations so as to formulate an effective medium for the maximal expression of indolicidin. While the available literature played a pivotal role, the prior knowledge on the aspect was of much help in formulating various test media of the study for indolicidin expression in *E. coli*. Further, the expression host of the study - *E. coli* C41 (DE3) that grew rapidly and at high cell densities on inexpensive substrates was an added advantage. Further, the total protein concentration in LB medium was estimated to be higher with 1 mM concentration of IPTG, while the same was noted to be insignificant with further increase in concentration of IPTG. Similarly, from the results obtained, it was evident that the growth rate or doubling time of the indolicidin clone (*E. coli*) was faster in 2×YT with salts, TB medium and LB medium with pH 7.5 at 37 °C than at lesser temperatures, with an incubation ranging from 3-6 h towards a higher production of indolicidin when compared with other tested parameters (Table 2).

Table 2. Post induction OD patterns of *E. coli* clones expressing indolicidin in different production conditions.

Ranges of media pH, incubation temperature/duration and optical density (OD)					
pH	OD	Incubation time (h)	OD (600 nm)	Temperature °C)	OD (600 nm)
6.0	0.608	3	0.485	30	0.598
6.5	0.577	6	0.548	37	0.625
7.0	0.572	12	0.452	40	0.624
7.5	0.670	16	0.512	45	0.588
8.0	0.598	20	0.513	-	-
8.5	0.515	24	0.493	-	-
9.0	0.500	28	0.495	-	-

Conclusion

In this study, lab scale optimization of indolicidin expression determined the ideal parameters for maximal expression of the peptide by pET21a(+) recombinant plasmids in *E. coli* C41 (DE3). Against the fact that industrial production optimization of any novel peptide usually preceded by lab scale production optimization, the outcomes of the present evaluation could be suitably employed during scale up events so as to maximize the indolicidin expression. Further, alternative drugs are viewed to be the remedies to redress the emerging microbial pathogens, and that other potent antimicrobial peptides could also be tried as to develop them in to promising drugs.

Acknowledgement

The authors sincerely thank the University Grants Commission (UGC), New Delhi for having funded this research work [Major Research Project - F. No. 41-1161/2012 (SR)].

References

Ahmad I, Perkins WR, Lupan DM, Selsted ME, Janoff AS (1995) Liposomal entrapment of the neutrophil-derived peptide indolicidin endows it with *in vivo* antifungal activity. Biochim Biophys Acta 26:109-114.

Alberts B, Bray D, Lewis J, Raff M, Roberts K, Watson JD (1994) Molecular Biology of the Cell, 3rd ed. Garland Publishing, New York.

Balbás P (2001) Understanding the art of producing protein and nonprotein molecules in *Escherichia coli.* Mol Biotechnol 19:251-267.

Benincasa M, Scocchi M, Pacor S, Tossi A, Nobili D, Basaglia G, Busetti M, Gennaro R (2006) Fungicidal activity of five cathelicidin peptides against clinically isolated yeasts. J Antimicrob Chemother 58:950-959.

Bertrand-Krajewski JL, Campisano A, Creaco E, Modica C (2005) Experimental analysis of the hydrass flushing gate and field validation of flush propagation modelling. Water Sci Technol 51:129-137.

Broedel SH, Papciak SM, Jones WR (2001) The selection of optimum media formulations for improved expression of recombinant proteins in *E. coli.* Vol 2: Athena Enzyme Systems Technical Bulletin.

Dumon-Seignovert L, Cariot G, Vuillard L (2004) The toxicity of recombinant proteins in *Escherichia coli*: a comparison of overexpression in BL21 (DE3), C41 (DE3), andC43 (DE3). Protein Expr Purif 37:203-206.

Feng XJ, Wang JH, Shan AS, Teng D, Yang YL, Yao Y, Yang GP, Shao YC, Liu S, Zhang F (2006) Fusion expression of bovine lactoferricin in *Escherichia coli*. Protein Expr Purif 47:110-117.

Froger A, Hall JE (2007) Transformation of plasmid DNA into *E. coli* using the heat shock method. J Vis Exp 6:253.

Glick BR, Pasternak JJ (1998) Molecular Biotechnology: Principles and Applications of Recombinant DNA, 2nd ed. SM Press, Washington D.C.

Hara S, Yamakawa M (1996) Production in *Escherichia* of moricin, a novel type antibacterial peptide from the silkworm, *Bombyx mori*. Biochem Biophys Res Commun 220:664-669.

Haught C, Davis GD, Subramanian R, Jackson KW, Harrison RG (1998) Recombinant production and purification of novel antisense antimicrobial peptide in *Escherichia coli*. Biotechnol Bioeng 57:55-61.

Hwang SW, Lee JH, Park HB, Pyo SH, So JE, Lee HS, Hong SS, Kim JH (2001) A simple method for the purification of an antimicrobial peptide in recombinant *Escherichia coli*. Mol Biotechnol 18:193-8.

Kim J, Park JM, Lee BJ (1997) High-level expression and efficient purification of the antimicrobial peptide gaegurin 4 in *E. coli*. Protein Pept Lett 4:391-396.

Lee JH, Hong SS, Kim SC (1998) Expression of an antimicrobial peptide magain in by a promoter inversion system. J Microbiol Biotechnol 8:34-41.

Lee JH, Kim JH, Hwang SW, Lee WJ, Yoon HK, Lee HS, Hong SS (2000) High-level expression of antimicrobial peptide mediated by a fusion partner reinforcing formation of inclusion bodies. Biochem Biophys Res Commun 277:575-580.

Lee JH, Kim MS, Cho JH, Kim SC (2002) Enhanced expression of tandem multimers of the antimicrobial peptide buforin II in *Escherichia coli* by the DEAD-box protein and trxB mutant. Appl Microbiol Biotechnol 58:790-796.

Lee JH, Kim MS, Cho JH, Kim SC (2002) Enhanced expression of tandem multimers of the antimicrobial peptide buforin II in *Escherichia coli* by the DEAD-box protein and trxB mutant. Appl Microbiol Biotechnol 58:790-796.

Miroux B, Walker JE (1996) Over-production of proteins in *Escherichia coli*: mutant hosts that allow synthesis of some membrane proteins and globular proteins at high levels. J Mol Biol 260:289-98.

Morin KM, Arcidiacono S, Beckwitt R, Mello CM (2006) Recombinant expression of indolicidin concatamers in *Escherichia coli*. Appl Microbiol Biotechnol 70:698-704.

Ponti D, Mignogna G, Mangoni ML, De Biase D, Simmaco M, Barra D (1999) Expression and activity of cyclic and linear analogues of esculentin-1, an anti-microbial peptide from amphibian skin. Eur J Biochem 263:921-927.

Sambrook J and Russell DW (2001) Molecular Cloning: A Laboratory Manual, 3rded. Cold Spring Harbor Laboratory Press, New York.

Schägger H (2006) Tricine-SDS-PAGE. Nat Protoc 1:16-22.

Schägger H, von Jagow G (1987) Tricine-sodium dodecyl sulfate-polyacrylamide gel electrophoresis for the separation of proteins in the range from 1 to 100 kDa. Anal Biochem 166:368-379.

Schluesener HJ, Radermacher S, Melms A, Jung S (1993) Leukocytic antimicrobial peptides kill autoimmune T cells. J Neuroimmunol 47:199-202.

Schmidt FR (2005) Optimization and scale up of industrial fermentation processes. Appl Microbiol Biotechnol 68:425-435.

Selsted ME, Novotny MJ, Morris WL, Tang YQ, Smith W, Cullor JS (1992) Indolicidin, a novel bactericidal tridecapeptide amide from neutrophils. J Biol Chem 267:4292-4295.

Shokri A, Sandén AM, Larsson G (2003) Cell and process design for targeting of recombinant protein into the culture medium of *Escherichia coli*. Appl Microbiol Biotechnol 60:654-664.

Skosyrev VS, Kulesskiy EA, Yakhnin AV, Temirov YV, Vinokurov LM (2003) Expression of the recombinant antibacterial peptide sarcotoxin IA in *Escherichia coli* cells. Protein Expr Purif 28:350-356.

Swartz JR (2001) Advances in *Escherichia coli* production of therapeutic proteins. Curr Opin Biotechnol 12:195-201.

Taguchi S, Nakagawa K, Maeno M, Momose H (1994) *In vivo* monitoring system for structure-function relationship analysis of the antibacterial peptide apidaecin. Appl Environ Microbiol 60:3566-3572.

Wagner S, Klepsch MM, Schlegel S, Appel A, Draheim R, Tarry M, Högbom M, vanWijk KJ, Slotboom DJ, Persson JO, de Gier JW (2008) Tuning *Escherichia coli* for membrane protein overexpression. Proc Natl Acad Sci USA 105:14371-14376.

World Health Organization (2014) WHO Expert Committee on Biological Standardization. World Health Organ Tech Rep Ser 987:1-266.

Xu Z, Peng L, Zhong Z, Fang X, Cen P (2006) High-level expression of a soluble functional antimicrobial peptide, human beta-defensin 2, in *Escherichia coli*. Biotechnol Prog 22:382-386.

Zhang LJ, Gallo RL (2016) Antimicrobial peptides. Curr Biol 26:R14-R19.

Zheng CF, Simcox T, Xu L, Vaillancourt P (1997) A new expression vector for high level protein production, one step purification and direct isotopic labeling of calmodulin-binding peptide fusion proteins. Gene 186:55-60.

Zhou L, Lin Q, Li B, Li N, Zhang S (2009) Expression and purification the antimicrobial peptide CM4 in *Escherichia coli*. Biotechnol Lett 31:437-441.

Acta Biologica Szegediensis

Volume 62(1):67-74, 2018
Acta Biologica Szegediensis
http://abs.bibl.u-szeged.hu/index.php/abs
DOI:10.14232/abs.2018.1.67-74

ARTICLE

Optimization of the extraction of natural phenolic antioxidants from the seeds of *Tamarindus indica* L. - an undervalued by product of food processing - using response surface methodology

Atreyi Sarkar, Uma Ghosh*

Department of Food Technology and Biochemical Engineering, Jadavpur University, Jadavpur, Kolkata - 700032, India

ABSTRACT The seeds of *Tamarindus indica* are known to possess a wide range of phenolic compounds with high antioxidant activity as measured by the ferric reducing antioxidant power (FRAP). In the present study, the optimum conditions for the extraction of crude phenolic antioxidants from Tamarind seed were determined using response surface methodology (RSM). A central composite design (CCD) was used to investigate the effects of four independent variables, namely concentration of extractable solids in solvent (g/ml; X_1), extraction time (h; X_2), extraction temperature (°C; X_3) and solvent concentration (%, v/v; X_4) on the responses of total polyphenol content (TPC) and FRAP. The CCD consisted of 30 experimental runs. A second-order polynomial model was used for predicting the responses. Canonical analysis of the surface responses revealed that the predicted optimal conditions for the maximal yield of TPC and FRAP were concentration of extractable solids in solvent of 0.049 g/ml, extraction time of 3.24 h, extraction temperature of 45 °C and a solvent concentration of 50%. The experimental values in the optimised condition coincided with the predicted ones within a 95% confidence interval, hence indicating the suitability of the model and the success of RSM in optimizing the extraction parameters.

KEY WORDS
central composite design
flavonoid
mass transfer
natural antioxidant optimization
solvent extraction

ARTICLE INFORMATION
Submitted
19 January 2018.
Accepted
19 May 2018.
***Corresponding author**
E-mail: ughoshftbe@yahoo.co.in

Introduction

Nature and its diversity have distributed the sources of natural antioxidants in different edible and nonedible parts of the plants. Tamarind pulp is regarded as a popular and well-known condiment in different cuisines across the globe, but the seed of this pulpy fruit is considered a waste item. The seeds of tamarind fruit provide a wide spectrum of natural antioxidants, which principally occur as polyphenols. Polyphenolic compounds namely, 2-hydroxy-3',4'-dihydroxyacetophenone, methyl 3,4-dihydroxybenzoate, 3,4-dihydroxyphenyl acetate, (-)-epicatechin (Tsuda et al. 1995) and procyanidins (Sudjaroen et al. 2005) have been isolated from the seeds. These have therapeutic potential in ameliorating ailments resulting from oxidative stress in human as well as augmenting the nutritive value when added to any food by commuting it into a functional food.

However, the newly emerging need for food safety and food sustainability has built up the concern of food researchers on recovering natural ingredients for application in food. Hence, it is of immense importance to extract natural antioxidants in the active form they are originally present in the source. Extensive studies (Turkmen et al. 2006; Akowuah et al. 2005; Yilmaz and Toledo 2006; Yu et al. 2005) addressing this concern are being executed and the reports generated suggest that effects of individual process parameters along with their composite effects influence the process and efficacy of extraction. Solvent extraction being the most utilised unit operation for mass transfer has been selected here to extract polyphenols from tamarind seed. The first step in solvent extraction is the sorption of the solvent by the solid matrix and consequent swelling up. This operation is followed by diffusion and solubilisation of the extractives into the solvent. The polarity and composition of the solvent medium influence the diffusivity of the solute, hence affects the efficacy of extraction (Treybal 1981). Several other factors such as extraction time, temperature, concentration of extractable solids in solvent and the composition of the solvent influence the process of solvent extraction from milled plant material (Spigno et al. 2007; Pinelo et al. 2005; Cacace and Mazza 2003). The state of the art technologies for recovery of antioxidants from natural sources aim at optimising the influence of

process parameters in order, to maximise the extraction of antioxidants.

Classical optimization studies use the one-factor-at-a-time (OFAT) approach, in which only one factor is a variable at a time while all others are kept constant. Though conventional, this approach is expensive in terms of cost and time resulting in an undesirable cost to benefit ratio. Further, it ignores possible interaction effects between variables and hence the Response Surface Methodology (RSM) comes into play to overcome these difficulties. RSM is a statistical tool for mathematical modelling with the aim to study the individual and interaction effects of several independent variables by varying them simultaneously in designed, limited number of experiments. Central composite design (CCD) needs a bare number of experiments to be performed. This model is composed of a core full factorial, that forms a cube (± 1) which determines the main and interaction effects and axial points (± α) which evaluate the main and quadratic effect. The value of α is calculated as $1/4^{th}$ power to the number of factorial runs. The axial points being outside of the design space confers rotatability to the model (Anderson and Whitcomb 2016).

In view of the above facts, the present study aimed at applying a central composite experimental design by RSM for maximizing the phenolic antioxidant extraction from tamarind seed by means of optimising the effects of four independent variables (extractable solid in solvent, extraction time, extraction temperature and solvent concentration) and their interactions on total antioxidant activity measured by FRAP and total polyphenol content. Finally the work aimed to verify the validity of the proposed model by conducting batch experiments in the experimental range as predicted.

Materials and Methods

Materials

Tamarind seeds were purchased from a local market of Jadavpur. Two kg of raw seeds were procured at once to maintain the uniformity in the composition and characteristic properties of the sample throughout the study. The seeds were frozen at -20 °C until further study. Sodium carbonate, ferric chloride hexahydrate, iron(II)-sulfate-heptahydrate, acetic acid, sodium acetate, hexane, hydrochloric acid and Folin-Ciocalteu's reagent were supplied by Merck (Germany). Other chemicals used for experimental purposes were gallic acid (SDFCL, Mumbai, India) and 2,4,6-Tri(2-pyridyl)-*s*-triazine (HiMedia, Mumbai, India).

Preparation of sample

The seeds were cleaned under running tap water then rinsed with bi-distilled water followed by regular grading and sorting procedures. To remove the superficial moisture, sun drying was done for 4 consecutive days and 7 hours daily by exposing the seeds to direct sunlight at an average atmospheric temperature of 39 °C. Finally, the seeds were dried in a hot air oven (DTC 72S1, International Commercial Traders, Kolkata, India) at 60 °C to attain a constant moisture content of 9%. Dried seeds were disintegrated by crusher grinder (Denver Lab) and were sieved through IS standard ASTM standars sieves to obtain an average sized particle of 0.25 mm. This particle size was found to be effective for extraction by previous studies (Herodež et al. 2003; Laroze et al. 2010). The obtained samples were packaged in dark coloured airtight vacuum saver glass container and stored in dark at 25 °C for further use.

Selection of appropriate extraction conditions

The foremost step of the preliminary experiment was to select an appropriate extraction medium and its corresponding extraction technique for the extraction of phenolics from the sample.

Selection of suitable extraction medium

Previous work (Sarkar and Ghosh 2016) pointed towards better capacity of a binary solvent system than a single solvent extraction medium. Moreover, due to the dehydrating and coagulant effect of absolute alcohol, in the present study aqueous alcohol was selected for solvent extraction. Based on these, three different solvent systems, namely boiling water, 50% ethanol and 50% methanol were tested.

For boiling water extraction, 2 g of sample was put in a muslin cloth sac (Nakchat et al. 2014) and sealed properly. It was immersed in 50 ml of boiling water and held in shaking condition to allow the leaching out of the solute. The red-brown extract was filtered through a Büchner funnel using Whatman filter paper (no 4.1). The filtrate was collected in borosilicate test tube with screw cap and marked as WE (boiling water extract).

A single stage batch processing technique was used for the extraction of sample in two different batches using 50% (v/v) ethanol and 50% (v/v) ethanol as solvents. In a temperature controlled (25 ± 1 °C) water bath shaker (Sicco, Kolkata, India) a constant shaking speed of 60 rpm was set up. Two g of solid sample was extracted in 50 ml of each solvent system and the extracts were collected in borosilicate test tubes with screw cap and marked as EE and ME for aqueous ethanolic and methanolic extracts, respectively.

Table 1. Experimental range of coded and actual values for central composite design (CCD).

Independent variables	Coded levels				
	-α	-1	0	1	+α
Concentration of extractable solids in solvent (g/ml, X_1)	0.03	0.04	0.05	0.06	0.07
Extraction time (h; X_2)	2	2.5	3	3.5	4
Extraction temperature (˚C; X_3)	30	35	40	45	50
Solvent concentration (%, v:v; X_4)	40	45	50	55	60

The extracts obtained from various experimental runs were defatted with hexane in a separating funnel and filtered as described in the previous work by the authors (Sarkar and Ghosh 2016). The freshly prepared extracts were examined for TPC and antioxidant activity by FRAP to determine the best solvent medium.

Selection of experimental ranges of the independent variables

The second step of the preliminary study was to set the ranges of experimental variables namely extractable solid in solvent (g/ml), extraction time (h), extraction temperature (°C) and solvent concentration (%, v/v) for further optimisation studies utilising RSM. Classical single factor optimisation (OFAT) experiments had been performed by the authors previously (Sarkar and Ghosh 2016); in the present study, the optimised values of design variables by OFAT were used as central points for experimental design of RSM. The five levels of the coded design variables are indicated in Table 1.

Experimental design for the response surface procedure

The RSM used a four numeric factor, five level and rotatable central composite design (CCD) consisting of 30 experimental runs with 6 centre points. The different levels of the variables as described in Table 1 were used to generate the CCD design matrix. The response surface regression was analysed by Design Expert Software V.8.0.6 (Stat-Ease, Minneapolis, USA). Experimental data were fitted to a second-order polynomial as follows:

$$Y = \beta_0 + \beta_1 X_1 + \beta_2 X_2 + \beta_3 X_3 + \beta_4 X_4 + \beta_{12} X_1 X_2 + \beta_{13} X_1 X_3 + \beta_{14} X_1 X_4 + \beta_{23} X_2 X_3 + \beta_{24} X_2 X_4 + \beta_{34} X_3 X_4 + \beta_{11} X_1^2 + \beta_{22} X_2^2 + \beta_{33} X_3^2 + \beta_{44} X_4^2$$

Where Y is the predicted response, β_1, β_2, β_3, β_4 are the coefficients for the linear terms, β_{11}, β_{22}, β_{33}, β_{44} are the coefficients for the quadratic and β_{12}, β_{13}, β_{14}, β_{23}, β_{24}, β_{34} are the coefficients for interaction terms respectively. X represents the coded values for the independent process variables.

Determination of the optimum conditions and validation of the model

Optimum desirability of the response variables, *i.e.* the maximum yield for total antioxidant activity based on the values of TPC and FRAP were predicted by the model to determine the region of response surface where it should reach its optimum value. The validity and adequacy of the predictive extraction model was verified by performing three experimental replicates at the predicted optimized conditions and the experimental and predicted values were compared.

Analyses of the response variables

Determination of total polyphenolic content (TPC)

TPC of the extracts were determined by the method described by Malik and Singh (1980) with some changes. Briefly, 0.75 ml of different concentrations of the extracts were taken, to which 3 ml of distilled water and 0.5 ml of Folin-Ciocalteu reagent (diluted to 1:1 with water) and 1 ml of 20% Na_2CO_3 were added. The absorbance was read after 2 hours of incubation by spectrophotometer (Hitachi U-2000) at 760 nm wavelength and plotted in a standard calibration curve of gallic acid. These results are expressed as milligram gallic acid equivalents per gram of dry sample (mg GAE/g).

Determination of total antioxidant activity (FRAP assay)

The FRAP assay was carried out according to the method of Benzie & Strain (1996) with minor modifications. Briefly, sodium acetate buffer (300 mM, pH 3.6), 10 mM TPTZ solution (dissolved in 40 mM HCl) and 20 mM iron(III) chloride solution were mixed in a ratio (v/v) of 10:1:1, respectively, to prepare the FRAP reagent. The freshly prepared reagent was warmed to 37 °C in a water bath before use and 3 ml of this was added to 100 µl of the sample solution. The absorbance was measured at 593 nm after 4 min and plotted in a standard calibration

curve of $FeSO_4$ solution. The results are expressed as µmol Fe(II)/g dry sample.

Statistical analysis

Results of the analyses are expressed as mean ± standard deviation of triplicate assays and analysed by Microsoft Excel 2007. Correlations between variables are established by Pearson correlation values using Minitab Statistical Software (Version 17).

Results and Discussions

Selection of suitable extraction medium

Antioxidant extract of the sample by methanol (ME) was found to have the highest FRAP and TPC values

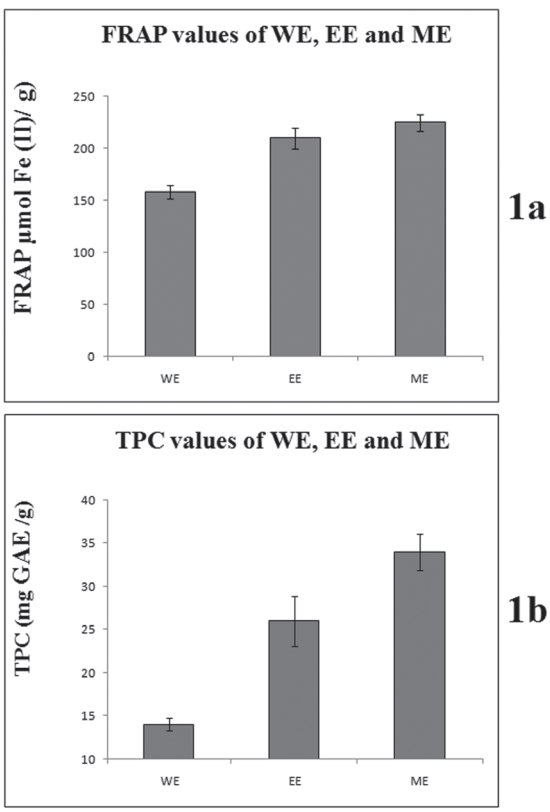

Figure 1. Ferric reducing antioxidant power (FRAP) (1a) and total polyphenol content (TPC) (1b) of boiling water extract (WE), ethanolic extract (EE) and methanolic extract (ME) of tamarind seed.

followed by ethanol (EE) and aqueous extract (WE) (Figs. 1a, b). There was comprehensible, but no significant ($p<0.05$) difference in TPC and FRAP values between the methanol (ME) and ethanol extracts (EE), but a significant difference was observed between aqueous (WE) and alcoholic extracts (ME and EE). A strong correlation of 0.98 between FRAP and TPC values of different extracts indicated that the antioxidant activity of the sample may owe to the polyphenols present in the sample. However, an extracting solvent in food system is selected not only for the purpose of acquiring maximum extractives, but health hazard and safety are also considered.

The toxicity of methanol is well-known (McMartin et al. 1980; Clay et al. 1975) in contrast to ethanol which has "Generally Recognized as Safe" (GRAS) status.

The discrepancy in antioxidant activity between extracts from different solvent can be addressed to the different diffusivity, solubility and partition coefficient. Many investigations (Valgimigli et al. 1996; MacFaul et al. 1996) have reported hydrogen bonding and electron donor-acceptor interaction between the solute and solvent as the reason of variation in antioxidant activities of dif-

Table 2. CCD design with experimental responses.

Run		Independent variables[a]				Responses[a]	
Std. order	Run no.	X_1	X_2	X_3	X_4	Y_1	Y_2
13	1	0.04	2.5	45	55	201	28.34
24	2	0.05	3	40	60	200	32.44
8	3	0.06	3.5	45	45	199.05	32
20	4	0.05	4	40	50	181.89	35.33
5	5	0.04	2.5	45	45	200.03	28
6	6	0.06	2.5	45	45	197.34	29
3	7	0.04	3.5	35	45	192	32.98
12	8	0.06	3.5	35	55	184	29
22	9	0.05	3	50	50	212.78	35.87
4	10	0.06	3.5	35	45	189.45	28.79
16	11	0.06	3.5	45	55	191.54	32
30	12	0.05	3	40	50	227.72	32.87
23	13	0.05	3	40	40	202	32
25	14	0.05	3	40	50	225.54	32.56
26	15	0.05	3	40	50	227.15	32.53
18	16	0.07	3	40	50	179.98	20
28	17	0.05	3	40	50	227	32.65
17	18	0.03	3	40	50	194	22.54
7	19	0.04	3.5	45	45	200.42	30
1	20	0.04	2.5	35	45	200.67	30
19	21	0.05	2	40	50	191	30.12
11	22	0.04	3.5	35	55	193.87	33
9	23	0.04	2.5	35	55	198	30.65
27	24	0.05	3	40	50	227.12	32
15	25	0.04	3.5	45	55	203	31.94
29	26	0.05	3	40	50	227.65	32.65
10	27	0.06	2.5	35	55	191.87	26
2	28	0.06	2.5	35	45	199	26
21	29	0.05	3	30	50	206.65	32.56
14	30	0.06	2.5	45	55	192.55	29

[a]Experiments were run in triplicate.
X_1 = concentration of extractable solids in solvent (m:v, g/ml); X_2 = extraction time (h); X_3 = extraction temperature (°C), and X_4 = solvent concentration (%, v:v). Y_1 = FRAP, and Y_2 = TPC.

ferent extracts. Greater FRAP and TPC values of alcoholic extracts (ME and EE) may be ascribed to the less polarity of the alcohol solution which makes it more efficient than water to break the cell wall structure and leach out the soluble antioxidants in the solution. Hence, in this study ethanol in different dilutions with water was chosen as medium for phenolic extraction from tamarind seed.

Table 3. Analysis of variance (ANOVA) for the quadratic polynomial model.

Source	Sum of squares	DF[a]	Mean square	F-value	P-value Prob>F
FRAP[b]					
Model	5968.866	14	426.3475	275.013	<0.0001**
X_1	217.3822	1	217.3822	140.2211	<0.0001**
X_2	85.6926	1	85.6926	55.27551	<0.0001**
X_3	97.32454	1	97.32454	62.77862	<0.0001**
X_4	28.44904	1	28.44904	18.35088	0.0007*
X_1X_2	2.488506	1	2.488506	1.605196	0.2245
X_1X_3	0.878906	1	0.878906	0.566933	0.4631
X_1X_4	47.71356	1	47.71356	30.77735	<0.0001**
X_2X_3	69.34726	1	69.34726	44.73204	<0.0001**
X_2X_4	1.632006	1	1.632006	1.052716	0.3211
X_3X_4	1.339806	1	1.339806	0.864234	0.3673
X_1^2	2764.442	1	2764.442	1783.187	<0.0001**
X_2^2	2839.988	1	2839.988	1831.917	<0.0001**
X_3^2	520.9329	1	520.9329	336.0247	<0.0001**
X_4^2	1172.006	1	1172.006	755.9953	<0.0001**
Residual	23.25423	15	1.550282		
Lack of fit	20.15023	10	2.015023	3.245848	0.1029[NS]
Pure error	3.104	5	0.6208		
Cor total	5992.12	29			
TPC[c]					
Model	338.1326	14	24.15233	91.70318	<0.0001**
X_1	13.80167	1	13.80167	52.4031	<0.0001**
X_2	45.76082	1	45.76082	173.7478	<0.0001**
X_3	4.576267	1	4.576267	17.37548	0.0008*
X_4	0.680067	1	0.680067	2.582123	0.1289
X_1X_2	0.046225	1	0.046225	0.17551	0.6812
X_1X_3	26.4196	1	26.4196	100.3117	<0.0001**
X_1X_4	0.469225	1	0.469225	1.781585	0.2019
X_2X_3	0.0144	1	0.0144	0.054675	0.8183
X_2X_4	0.087025	1	0.087025	0.330422	0.5739
X_3X_4	0.1225	1	0.1225	0.465116	0.5056
X_1^2	226.0248	1	226.0248	858.1863	<0.0001**
X_2^2	0.001296	1	0.001296	0.004922	0.9450
X_3^2	3.666696	1	3.666696	13.92196	0.0020*
X_4^2	0.486096	1	0.486096	1.845644	0.1944
Residual	3.950625	15	0.263375		
Lack of fit	3.525492	10	0.352549	4.146336	0.0650[NS]
Pure error	0.425133	5	0.085027		
Cor total	342.0832	29			

a: Degrees of freedom.
b: Standard deviation = 1.245; Mean = 202.14.
c: Standard deviation = 0.51; Mean = 40.42.
**: Significance values of "Prob>F" are less than 0.0001.
*: Significance values of "Prob>F" are less than 0.05.
NS: Non significant.

Optimisation of the extraction parameters

Fitting the models

Table 2 shows the design matrix generated by Design Expert Software (Version 8.0.6). It is composed of 30 experimental runs arranged in randomised order of experiments to minimise the effects of unexplained variability in the response due to extraneous factors. The Analysis of Variance (ANOVA) was done to examine the statistical significance of the quadratic model. The summary of ANOVA analysing of the experimental results are indicated in Table 3. The *F*-value is indicative of whether the quadratic model is significant and the *P*-value indicates the significance of each coefficient. Table 3 shows the *F*-values for the response surface quadratic model for FRAP and TPC to be 275.01 and 91.70, respectively, with the *P*-values <0.0001 indicating only a 0.01% chance that the model *F*-values may occur due to noise. In other words this result implies the model to be statistically significant and suitable for use. The *F*-values of "lack of fit" as 3.24 and 4.14 for the responses FRAP and TPC have *P*-values insignificant, 0.1029 and 0.0650, respectively, indicating the "lack of fit" was insignificant in relation to the "pure error". Values of Prob>F less than 0.0500 indicate the model terms are significant. The "Pred *R*-Squared" for the response FRAP and TPC are 0.9798 and 0.9388, respectively, which are in reasonable agreement with their respective "Adj R-Squared" values of 0.9925 and 0.9776. The high "Adeq Precision" ratio of 52.44 and 43.35 for the models of FRAP and TPC, respectively, are indicative of adequate signal and minimal noise and hence suitable for navigating the design space. The low coefficients of the variation (CV %) of 0.6159 for FRAP and 1.6866 for TPC confer very high reliability and degree of precisions to the models.

Optimisation of the extraction conditions

The predicted response (Y_1, FRAP) was achieved by the following second order polynomial equation:

$$Y_1 = 227.03 - 3.10X_1 - 1.89X_2 + 2.01X_3 - 1.09X_4 - 0.40X_1X_2 - 0.23X_1X_3 - 1.73X_1X_4 + 2.08X_2X_3 + 0.32X_2X_4 + 0.29X_3X_4 - 10.04X_1^2 - 10.18X_2^2 - 4.36X_3^2 - 6.54X_4^2$$

When the response was FRAP, it was observed that interaction effects of extraction time and extraction temperature (X_2, X_3) along with concentration of extractable solids in solvent and solvent concentration (X_1, X_4) played significant roles, while all the four factors individually (X_1, X_2, X_3, X_4) were found to significantly affect the response. Figs. 2a and b show 3D response surfaces with contour plots revealing significant effects of con-

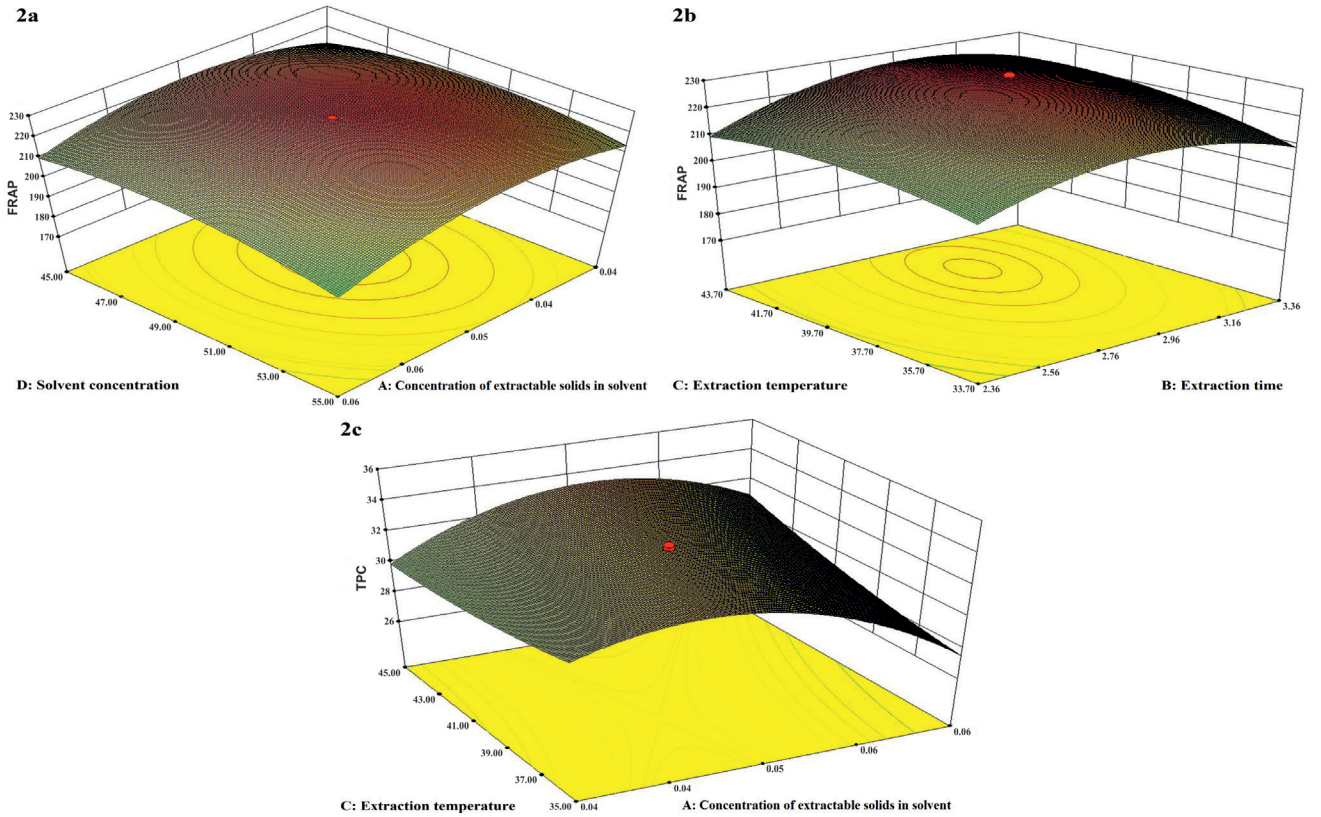

Figure 2. 3D response surface graphs showing the interaction effects of solvent concentration and concentration of extractable solids in solvent for the response of FRAP (2a), extraction temperature and extraction time for the response of FRAP (2b), and extraction temperature and concentration of extractable solids in solvent for the response of TPC (2c)

centration of extractable solids in solvent and solvent concentration (X_1, X_4) along with extraction time and extraction temperature (X_2, X_3) in maximizing yield of FRAP with the other factors being held at a fixed level (zero level, X_1 = 0.05 g/ml, X_4 = 50% and X_2 = 2.97 h, X_3 = 40 °C, respectively). The yield of FRAP value in *T. indica* seed extracts of various experiments (represented in Table 2) ranged from 179.98 to 227.72 μmol Fe(II)/g of dry sample. The highest FRAP content was obtainable at a concentration of extractable solids in solvent of 0.05 g/ml, 50% ethanol as solvent, extraction temperature of 40 °C and extraction time of 3h. The quadratic surface in Fig. 2a describes too low and too high concentration of extractable solids in solvent and solvent concentration (X_1, X_4) to have negative impact on antioxidant extraction. Fick's second law states that a final equilibrium between the solute concentrations in the solid matrix and in the extraction medium is achieved after a certain time. This describes the nature of the 3D plot (Fig. 2b) where the initially increasing yield of FRAP drops after a certain time. The fall in FRAP at high temperature may be attributed to the degradation of heat labile antioxidant compounds. Earlier ethanol had been reported to be an efficient solvent for antioxidant extraction (Pompeu et al. 2009) and by varying its concentration antioxidant yield also varied (Kiassos et al. 2009). The current findings of the study are in agreement with the previous reports (Liyana-Parthirana and Shahidi 2005) where 50% ethanol was found to be optimal concentration for extraction purpose. Concentration of extractable solids in solvent greater than 0.05 g/ml showed a fall in FRAP value indicating this value to be the equilibrium point (Zhang et al. 2007) beyond which no rise in extraction was possible. The regression coefficient (R^2>0.8) between predicted and experimental results indicated a good fit.

The predicted response (Y_2, TPC) was achieved by the following second order polynomial equation:

$$Y_2 = 32.54 - 0.75X_1 + 1.38X_2 + 0.43X_3 + 0.16X_4 + 0.054X_1X_2 + 1.29X_1X_3 - 0.17X_1X_4 + 0.03X_2X_3 + 0.09X_2X_4 + 0.09X_3X_4 - 2.87X_1^2 - 0.006X_2^2 + 0.37X_3^2 - 0.13X_4^2$$

When the response was TPC, it was observed that interaction effect of concentration of extractable solids in solvent and extraction temperature (X_1, X_3) along (Fig.

2c) with individual independent variables of concentration of extractable solids in solvent (m:v, g/ml; X_1), extraction time (h; X_2), extraction temperature (°C; X_3) played significant roles. The yield of TPC in *T. indica* seed extracts of various experiments (represented in Table 2) ranged from 20 to 35.87 mg GAE/g. The highest TPC content was obtainable at a concentration of extractable solids in solvent (X_1) of 0.05 g/ml, 50% ethanol as solvent, extraction temperature of 50 °C and extraction time of 3 h. While concentration of extractable solids in solvent was found optimal at 0.05 g/ml, increasing extraction temperature showed an increasing trend in TPC yield. Higher temperature might have increased phenolic solubility by increasing the diffusion rate, extraction rate (Ju and Howard 2003) and also breaking the cell wall of plant material resulting in greater solubility. The regression coefficient (R^2>0.8) indicated a good fit between predicted and experimental results.

Validation of the model

The optimal extraction parameters were verified for the highest polyphenolic antioxidant content (TPC, FRAP) based on the values obtained using RSM. The optimal condition was established by using maximum desirability for TPC and FRAP. The optimised condition predicted by the model was recorded to be concentration of extractable solids in solvent of 0.049 g/ml, extraction time for 3.24 h, extraction temperature of 45 °C and a solvent concentration of 50% which predicted to yield 222.58 μmol Fe(II)/g FRAP and 33.98 GAE/g TPC. Experiment was carried out to compare the results of experimental and predicted data. At the optimal conditions 223 μmol Fe(II)/g FRAP and 34.15 GAE/g TPC were obtained. The experimentally obtained values fall within a 95% mean confidence interval of the predicted value for FRAP and TPC. These results confirm the validity and predictability of the model for the extraction of phenolic antioxidant from *T. indica* seeds.

Conclusion

The findings of the study suggested aqueous ethanol to be the most suitable solvent for antioxidant extraction from tamarind seed and a strong correlation between TPC and FRAP values led to the conclusion that phenolic compounds were responsible for the overall antioxidant activity of tamarind seed. The response surface methodology was successfully utilised to optimize the phenolic extraction from *T. indica* seeds. The second-order polynomial model gave a satisfactory description of the experimental data. Under optimized conditions the experimental values agreed with the values predicted by the model. The experimental conditions allow a fast, quantitative and maximum extraction of phenolic antioxidants from *T. indica* seeds.

Acknowledgement

The financial support by Department of Science and Technology under Ministry of Science and Technology, Government of India in the form of INSPIRE fellowship for doctoral studies (sanction order no. DST/INSPIRE Fellowship/2015/IF 150107) is acknowledged.

References

Akowuah GA, Ismail, Z, Norhayati I, Sadikun A (2005) The effects of different extraction solvents of varying polarities on polyphenols of *Orthosiphon stamineus* and evaluation of the free radical-scavenging activity. Food Chem 93(2):311-317.

Anderson MJ, Whitcomb PJ (2016) RSM Simplified: Optimizing Processes Using Response Surface Methods for Design of Experiments, Special Indian ed. Taylor & Francis Group, New York.

Benzie IFF, Strain JJ (1996) The ferric reducing ability of plasma (FRAP) as a measure of "antioxidant power": The FRAP assay. Anal Biochem 239:70-76.

Cacace JE, Mazza G (2003) Mass transfer process during extraction of phenolic compounds from milled berries. J Food Eng 59(4):379-389.

Clay KL, Murphy RC, Watrins WD (1975) Experimental methanol toxicity in the primate: analysis of metabolic acidosis. Toxicol Appl Pharm 34(1):49-61.

Herodež ŠS, Hadolin M, Škerget M, Knez Ž (2003) Solvent extraction study of antioxidants from Balm (*Melissa officinalis* L.) leaves. Food Chem 80(2):275-282.

Ju ZY, Howard LR (2003) Effects of solvent and temperature on pressurised liquid extraction of anthocyanins and total phenolics from dried red grape skin. J Agric Food Chem 51:5207-5213.

Kiassos E, Mylonaki S, Makris DP, Kefalas P (2009). Implementation of response surface methodology to optimise extraction of onion (*Allium cepa*) solid waste phenolics. Innov Food Sci Emerg Technol 10:246-252.

Laroze LE, Díaz-Reinoso B, Moure A, Zúñiga ME, Domínguez H (2010) Extraction of antioxidants from several berries pressing wastes using conventional and supercritical solvents. Eur Food Res Technol 231(5):669-677.

Liyana-Parthirana C, Shahidi F (2005) Optimisation of extraction of phenolic compounds from wheat using response surface methodology. Food Chem 93:47-56.

MacFaul PA, Ingold KU, Lusztyk J (1996) Kinetic solvent

effects on hydrogen atom abstraction from phenol, aniline, and diphenylamine. The importance of hydrogen bonding on their radical-trapping (antioxidant) activities. J Org Chem 61(4):1316-1321.

Malik CP, Singh MB (1980) Plant Enzymology and Histoenzymology. Kalyani Publishers, New Delhi, India.

McMartin KE, Ambre JJ, Tephly TR (1980) Methanol poisoning in human subjects: role for formic acid accumulation in the metabolic acidosis. Am J Med 68(3):414-418.

Nakchat O, Meksuriyen D, Pongsamart S (2014) Antioxidant and anti lipid peroxidation activities of *Tamarindus indica* seed coat in human fibroblast cells Indian J Exp Biol 52:125-132.

Pinelo M, Rubilar M, Jerez M, Sineiro J, Núñez MJ (2005) Effect of solvent, temperature, and solvent-to-solid ratio on the total phenolic content and antiradical activity of extracts from different components of grape pomace. J Agri Food Chem 53(6):2111-2117.

Pompeu DR, Silva EM, Rogez H (2009) Optimisation of the solvent extraction of phenolic antioxidants from fruits of *Euterpe oleracea* using Response Surface Methodology. Biores Technol 100:6076-6082.

Sarkar A, Ghosh U (2016) Classical single factor optimisation of parameters for phenolic antioxidant extraction from tamarind seed (*Tamarindus indica*). Plant Sci Today 3(3):258-266.

Spigno G, Tramell L, De Faveri DM (2007) Effects of extraction time, temperature and solvent on concentration and antioxidant activity of grape marc phenolics. J Food Eng 81(1):200-208.

Sudjaroen Y, Haubner R, Würtele G, Hull WE, Erben G, Spiegelhalder B, Owen RW (2005) Isolation and structure elucidation of phenolic antioxidants from Tamarind (*Tamarindus indica* L.) seeds and pericarp. Food Chem Toxicol 43(11):1673-1682.

Treybal RE (1981) Mass-transfer Operations, 4th ed. McGraw-Hill International Editions, Singapore.

Tsuda T, Mizuno K, Ohshima K, Kawakishi S, Osawa T (1995) Supercritical carbon dioxide extraction of antioxidative components from tamarind (*Tamarindus indica* L.) seed coat. J Agri Food Chem 43(11):2803-2806.

Turkmen N, Sari F, Velioglu YS (2006) Effects of extraction solvents on concentration and antioxidant activity of black and black mate tea polyphenols determined by ferrous tartrate and Folin-Ciocalteu methods. Food Chem 99(4):835-841.

Valgimigli L, Ingold KU, Lusztyk J (1996) Antioxidant activities of vitamin E analogues in water and a Kamlet-Taft β-value for water. J Am Chem Soc 118(15):3545-3549.

Yilmaz Y, Toledo RT (2006) Oxygen radical absorbance capacities of grape/wine industry by products and effect of solvent type on extraction of grape seed polyphenols. J Food Comp Anal 19(1):41-48.

Yu J, Ahmedna M, Goktepe I (2005) Effects of processing methods and extraction solvents on concentration and antioxidant activity of peanut skin phenolics. Food Chem 90(1):199-206.

Zhang ZS, Li D, Wang LJ, Ozkan N, Chen XD, Mao ZH, Yang HZ (2007) Optimization of ethanol-water extraction of lignans from flaxseed. Sep Purif Technol 57(1):17-24.

Acta Biologica Szegediensis

Volume 62(1):75-82, 2018
Acta Biologica Szegediensis
http://abs.bibl.u-szeged.hu/index.php/abs
DOI:10.14232/abs.2018.1.75-82

ARTICLE

Characterization of an acidophilic α-amylase from *Aspergillus niger* RBP7 and study of catalytic potential in response to nutritionally important heterogeneous compound

Riddha Mukherjee[1], Tanmay Paul[1], Suman Kumar Halder[1], Jyoti Prakash Soren[1], Amrita Banerjee[1], Keshab Chandra Mondal[1], Bikash Ranjan Pati[1], Pradeep Kumar Das Mohapatra[2]*

[1]Department of Microbiology, Vidyasagar University, Midnapore - 721102, West Bengal, India
[2]Department of Microbiology, Raiganj University, Raiganj - 733134, Uttar Dinajpur, West Bengal, India

ABSTRACT An acidophilic α-amylase from *Aspergillus niger* RBP7 was purified after solid state fermentation on potato peel substrate. Molecular mass of the purified α-amylase was 37.5 kDa and it exhibited 1.4 mg/ml and 0.992 μ/mol/min K_m and V_{max} values, respectively. The enzyme was stable in the pH range from 2.0 to 6.0, at high NaCl concentration (3 M) and at temperatures between 40 °C and 70 °C. The enzyme showed an optimal activity at pH 3.0 and at 45 °C. The enzyme was inhibited by Hg^{2+} and was stable in the presence of different surfactants (Tween 60, Tween 80, and SDS at 1% level) and different inhibitory reagents (β-mercaptoethanol, phenylmethylsulfonyl fluoride, and sodium azide). This acidophilic amylase enzyme can digest heterogeneous food materials, *i.e.* the mixture of rice, fish, bread and curry with comparable activity to the commercial diastase enzymes available. **Acta Biol Szeged 62(1):75-82 (2018)**

KEY WORDS
characterization
digestion of food material
molecular weight determination,
purification

ARTICLE INFORMATION
Submitted
7 December 2017.
Accepted
21 May 2018.
***Corresponding author**
E-mail: pkdmvu@gmail.com

Introduction

α-Amylase is a starch hydrolyzing enzyme generating glucose and maltose as end products. It has high market value in different sectors and the market size of amylase in baking industry was 67476.6 tons in 2015. The use of α-amylase in food and beverage industries is expected to be increased by 1.9% from 2016 to 2024 in North America. Acidophilic amylases are applied in different industries like the glucose and fructose syrup production, bakery industry and fruit juice and digestive syrup producing industries (Souza and Magalhães 2010; Parker et al. 2010).

Various bacterial and fungal isolates can produce acidophilic amylases; most of them are belonging to the genus *Bacillus* and *Aspergillus*. In general, the acidophilic amylases can digest different raw starchy food ingredients (Maity et al. 2010; Mukherjee et al. 2017), therefore, they are frequently used to remove such food materials from various surfaces (*e.g.,* textile). In the starch processing industries, acidophilic amylases are used to produce glucose in high amount from the starch polymer (Konsula and Liakopoulou-Kyriakides 2004; Haq et al. 2010; Khan and Priya 2011; Raghu and Rajeswara 2015). In bakery industry, acidophilic amylases are used to enhance the porosity, flavor and taste of the product (Gupta et al. 2003); amylases are also used for the clarification of beer and fruit juices (Gavrilescu and Chisti 2005; Ghorai et al. 2009).

In the present study, physicochemical characterization of an α-amylase produced by the *Aspergillus niger* RBP7 isolate was evaluated. In addition, the digestion of starchy materials present in nutritionally important heterogeneous foods was also studied comparing the activity of the purified amylase with some commercially available diastases.

Materials and Methods

Microorganism and culture condition

Aspergillus niger RBP7 (GenBank KX100578.1) was isolated from municipal garbage area of Midnapore, West Bengal, India (Mukherjee et al. 2017). The fungal culture was maintained on Czapek Dox agar slants (pH 3) and stored at 4 °C.

Amylase production and enzyme extraction

Enzyme production was carried out using potato peel

as substrate following the method of Mukherjee and co-workers (2017). In the fermentation process, 1.2 g of potato peel was moistened with 1 ml liquid medium ($NaNO_3$ 0.3 g, $MgSO_4$ 0.05 g, KCl 0.05 g, $FeSO_4$ 0.002 g, and K_2HPO_4 0.1 g); pH and temperature were adjusted to 2.7 and 44 °C, respectively (Mukherjee et al. 2017). The flasks were autoclaved at 121 °C for 20 min at 15 psi pressure. The flasks were cooled, inoculated with 1 ml (2×10^2 spores) of *A. niger* RBP7, and incubated at 27 °C for 96 h. After fermentation, 5 ml of sterile distilled water was added to each flask and vigorously agitated in rotary shaker at 100 rpm for 30 min. The mixture was filtered through cheese cloth and centrifuged at 8000 rpm for 10 min. The supernatant was taken as crude enzyme preparation and used for subsequent experiments.

Assay of amylase activity and protein content

α-Amylase activity was determined by incubating 1 ml reaction mixture containing 0.5 ml of enzyme source and 1% soluble starch dissolved in 0.2 M acetate buffer (pH 3.0) at 37 °C for 1 h. The reaction was stopped by 1 ml of 3.5-dinitrosalicylic acid (Merck, India) mixed with the above mixture. Then the mixture was boiled in water bath for 10 min. The produced reducing sugar was measured at 540 nm. One unit (U) of α-amylase activity was determined as the amount of enzyme that releases 1 μmol of reducing sugar as glucose equivalent. The protein content of enzyme solution was estimated according to Lowry et al. (1951) using bovine serum albumin as standard.

Enzyme purification

All purification steps were carried out at 4 °C. After the 96-h fermentation, the crude enzyme was salted out with 80% ammonium sulfate and kept overnight at 4 °C. Then, the solution was centrifuged at 10 000 rpm for 10 min and the precipitate was dissolved in 5 ml acetate buffer (0.2 M, pH 3.0). After dialysis against distilled water (24 h), the dialysate was loaded onto 2.5 cm × 70 cm Sephadex G-100 column (Sigma Aldrich, USA), equilibrated with acetate buffer (0.2 M, pH 3.0) and eluted with the same buffer at a flow rate of 1 ml/min. A volume of 2 ml fractions was collected and the amylase activity and the protein content in each fraction were determined.

Molecular weight determination and zymogram analysis

Sodium dodecyl sulfate-polyacrylamide gel electrophoresis (SDS-PAGE) was carried out by using a 10% (w/v) polyacrylamide gel. Protein bands were detected by staining the gel with Coomassie Brilliant Blue R250 (Laemmli 1970). For zymography, non-denaturing PAGE (10%, w/v) was performed (Halder et al. 2016) at 4 °C and the gel was subsequently washed with deionized water and 0.2 M acetate buffer (pH 3.0) at 40 °C. Then, the gel was incubated in fresh acetate buffer containing 1% (w/v) soluble starch at 40 °C for 30 min. After washing with distilled water, the gel was stained with iodine solution until the clear zone of starch hydrolysis was appeared against the dark blue background.

Determination of the pH and temperature optimum and stability

The effect of pH on the activity was estimated in hydrochloric acid and sodium acetate buffer for pH 2.0 (Uchino 1982) and acetate buffer for pH range of 3.0 - 6.0 using 1% starch as substrate. The pH stability was determined by pre-incubating the enzyme under conditions between pH 2.0 - 6.0 for 1 to 6 hours. The residual activity was measured according to the standard protocol as described above. For determination of optimum temperature, the assay was performed at the temperature range of 20 °C - 60 °C. Temperature stability of the purified α-amylase was measured by incubating the enzyme at different temperatures between 40 °C and 70 °C for different time intervals (20 to 120 min). The residual amylase activity was measured under standard assay conditions described above.

Detection of temperature quotient (Q_{10})

Temperature quotient (Q_{10}) denoted the changes in the rate of the enzymatic catalytic reaction at every 10 °C rise in temperature: $Q_{10} = (R_2/R_1)^{10/(T_2-T_1)}$

Where T_1 and T_2 are the initial and final temperatures at which experiment was conducted. R_1 and R_2 are the amylase activity at T_1 and T_2, respectively.

Effects of additives on enzyme activity

To study the effects of various additives on purified enzyme activity, the enzyme was pre-incubated for 1 h at optimum assay conditions with solutions of the followings additives.

Metal ions: Ca^{2+} ($CaCl_2$), Mg^{2+} ($MgSO_4$), Zn^{2+} ($ZnSO_4$), Mn^{2+} ($MnSO_4$), Cu^{2+} ($CuSO_4$), K^+ (K_2SO_4), Ag^+ ($AgSO_4$), Fe^{3+} (Fe_3SO_4), and Co^{2+} ($CoCl_2$) at final concentration of 1 mM and 5 mM. After 1 h, we added substrate in each reaction mixture containing additives and incubated the reaction under standard assay condition to get the enzyme activity.

For determining the stability with surfactants, SDS, Tween 60, Tween 80 and Triton X-100 with different concentrations (1%, 2% and 3% w/v) were used. Chelating agents like ethylenediaminetetraacetic acid (EDTA) with the concentration of 1, 2 and 3 (%, w/v) were used. Phenylmethylsulfonyl fluoride (PMSF), β-mercaptoethanol, and sodium azide (1%, 2% and 3% w/v) were used as inhibitor for testing the enzyme stability.

Table 1. Purification profile of amylases

Steps for purification	Total activity (U)	Total protein (mg)	Specific activity (U/mg)	Fold purification	Recovery (%)
Crude enzyme	292500	8117.5	36.03	1	100
Ammonium sulfate precipitation	122465	846.9	144.6	4.01	41.86
Sephadex G-100	8812.7	14.34	335.61	9.31	7.19

Solvents (1%, v/v) like acetone, methanol, butanol, propanol, toluene, hexane, ethanol, xylene, acetonitrile were used to estimate their effect on enzyme activity. In all cases, the residual activity was measured.

Halo-stability of purified acidophilic α-amylase

The purified enzyme was incubated with various concentrations of NaCl (0 - 5.0 M) for 1 h at room temperature, and the residual α-amylase activity was measured following the standard protocol.

Storage stability and light sensitivity

For determining the storage stability, the two sets of enzymes were incubated (in acetate buffer, pH 3.0) for 14 days at 4 °C and in room temperature (37 °C) as control. The light sensitivity test was investigated by incubating the enzyme in sun light (40 °C) for 14 days. The enzyme activity was checked following the standard assay protocol after sampling at the 7^{th} and 14^{th} days.

Substrate specificity and enzyme kinetics

Different polysaccharides were used for determination of the spectrum of substrate specificity of the enzyme. The tested substrates were soluble starch (Merck, India), amylose (Merck, India), amylopectin (Merck, India), dextran (HiMedia, India) and pullulan (HiMedia, India) at a concentration of 1.0% (w/v) in 0.2 M acetate buffer (pH 3.0). All assays were performed following the standard protocol for enzyme activity determination.

The kinetic constants (K_m and V_{max}) were estimated by double reciprocal plots of the data according to standard method of Lineweaver and Burk (1934) with Sigma Plot Enzyme kinetics software module 1.3 (Systat Software, USA). Michaelis-Menten plot was also drawn using the same software. Equation of Lineweaver Burk plot: $1/V_{max} = K_m/V_{max} \times 1/[s] + 1/V_{max}$ The turnover number and catalytic efficiency were estimated from the following formula: Turnover number (K_{cat}) = V_{max}/E_t (total enzyme), Catalytic efficiency = K_{cat}/K_m

Study of enzymatic efficiency

Here we used the mixed food materials as substrate to know the activity of purified acidophilic α-amylase and different commercial amylase in heterogeneous condition of food. In this study different commercial alpha amylases were used, e.g., Carmozyme™ (Mendine Pharmaceuticals, India), Unienzyme™ (Unichem Laboratories), Aristozyme™ (Aristo Pharmaceuticals), Vitazyme™ (East India Pharmaceutical). Briefly, a mixed preparation of food materials, *i.e.* rice, fish, bread and vegetable curry, was crushed into small pieces. Then the raw material was smashed with a homogenizer with the addition of acetate buffer (pH 3.0). The whole matter was considered as substrate (1 ml) and was incubated with 1 ml (150 U) of purified enzyme and different commercial enzyme preparations (150 U/ml). After incubation the reducing sugars of each experimental set were determined according to dinitrosalicylic acid method.

Results and Discussion

Enzyme production

The *A. niger* RBP7 produced 1112.25 U/gds of α-amylase in 72 h fermentation period at 40 °C and pH 3.0 (Mukherjee et al. 2017). This crude amylolytic solution was used for the enzyme purification.

Purification of the α-amylase

The α-amylase from *A. niger* RBP7 was purified by ammonium sulfate precipitation followed by a size exclusion chromatography step using Sephadex G100 resin. The purified enzyme had a specific activity of 335.61 U/mg of protein. The molecular weight of enzyme was found to be approximately 37.5 kDa (Fig. 1). The purification procedures are summarized in the Table 1. The isolated enzyme was homogeneous, as seen by a single protein both in native and with reduced and denaturing condition. The protein band of purified α-amylase was confirmed by the zymogram. The purified enzyme (single band) showed clear zone around the single band on starch containing zymogram when the zymogram was flooded with iodine solution (Fig. 1). The microbial α-amylases generally have their molecular weight between 23 and 150 kDa (Krishnan and Chandra 1983; Pandey et al. 2000). Fungal amylases from the *A. niger* JGI 24 and *Monascus sanguineus* have molecular weight of 43 kDa and 56 kDa, respectively (Varalakshmi et al. 2009; Tallapragada et al. 2017).

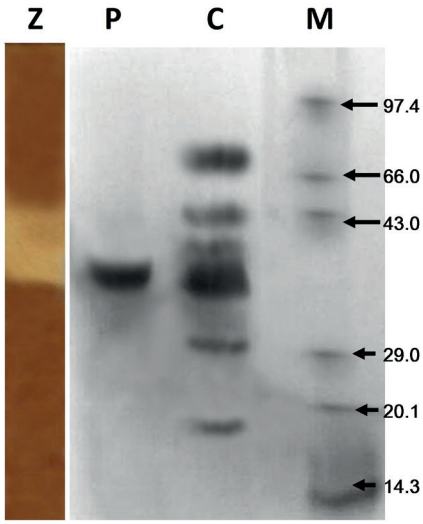

Figure 1. PAGE analysis of each fraction during purification. Z: zymogram; P: purified enzyme; C: crude enzyme; M: molecular weight marker (kD) after column chromatography.

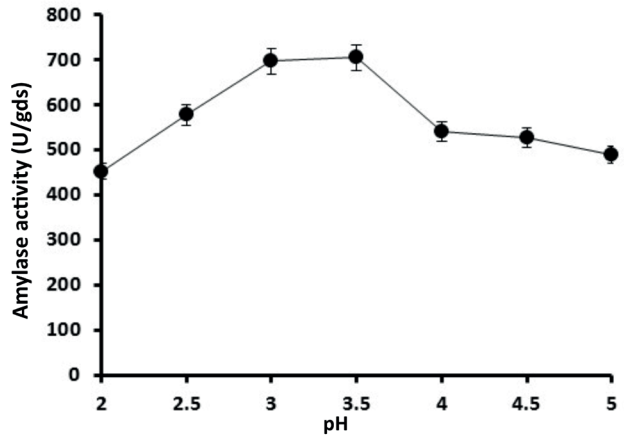

Figure 2. Activity of α-amylase at different pH

Effect of the pH and temperature on the activity and stability of the enzyme

The purified α-amylase exhibited the maximal starch hydrolysis at pH 3.0 (Fig. 2). The enzyme was stable in pHs between 2.0 and 6.0 for 60 to 300 min incubation period (Fig. 3). The purified α-amylase showed maximum amylolytic activity at 45 °C (Fig. 4) and it was stable during incubation at 40 - 70 °C for 20 to 120 min (Fig. 5). Yandri et al. (2012) reported that α-amylase from *Bacillus subtilis* ITBCCB 148 can work between pH 5.0 and 9.0 and maximum activity showed at pH 6.0. The *Streptomyces* sp. MSC702 α-amylase have optimum activity at 60 °C and the enzyme was stable between 20 and 80 °C (Singh et al. 2014). Aygan et al. (2008) reported that the α-amylase obtained from *Bacillus* sp. AB 68 was active in a broad range of temperature (20 to 90 °C), with an optimum of 50 °C. The *Aspergillus terreus* amylase have its optimum activity at pH 5.0, but it is stable at different pHs (pH 3.0 - 10.0) (Sethi et al. 2016).

Temperature quotient (Q_{10})

Temperature quotient (Q_{10}) is mainly used to study the dependence of enzyme catalytic reaction rate on temperature. Results showed that temperature quotient (Q_{10}) of the acidophilic amylase is 1.065 at 45 °C. The temperature coefficient value (Q_{10}) for *Bacillus licheniformis* SKB4 α-amylase was found to be 1.0 (Samanta et al. 2014). This Q_{10} value is calculated in order to know whether temperature is crucial factor for enzymatic reaction or not. For enzymatic catalysis range of Q_{10} value is generally 1-2, and any deviation from that there are other influencing factors which controlling the enzyme activity. In our case the Q_{10} value is 1.065, which indicates that temperature is crucial factor for enzymatic action.

Effect of additives on α-amylase

Metal salts have both enhancing and inhibitory effects on the enzyme activity and stability. Therefore, metal compatibility profiling of an enzyme is very important to find out its optimum catalytic conditions. In this study, it was observed that each metal had inhibitory effect on enzyme activity (Table 2). More than 40% of the activity was lost in presence of all the salt tested in 5 mM concentration. In the presence of 3% EDTA and β-mercaptoethanol, the relative activity of the enzyme decreased by 72% and 82%, respectively. The enzyme activity decreased drastically to about 75% in presence of the solvents tested. This may be due to the amino acid composition as well as three dimensional structures, which endorsed relative resistance of the enzyme against hydrophobic/non-polar micro environment (Halder et al. 2016).

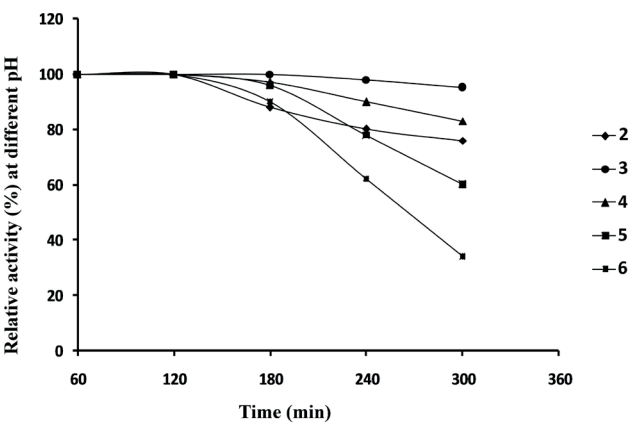

Figure 3. Effect of pH on the stability of purified α-amylase of *A. niger* RBP7

Table 2. Effect of additives on purified α-amylase of *A. niger* RBP7

Metal ion	Concentration	Relative activity (%)
K^+	1 mM	53.53
	5 mM	53.12
Cu^{2+}	1 mM	60.2
	5 mM	58.1
Fe^{3+}	1 mM	56.86
	5 mM	55.61
Mg^{2+}	1 mM	59.35
	5 mM	58.9
Zn^{2+}	1 mM	61.01
	5 mM	59.34
CO^{2+}	1 mM	60.6
	5 mM	53.54
Ca^{2+}	1 mM	60.6
	5 mM	57.6
Ag^+	1 mM	61.8
	5 mM	57.6
Mn^{2+}	1 mM	60.17
	5 mM	58.5
Surfactant		
SDS	1%	34.03
	2%	32.8
	3%	23.24
Tween 60	1%	43.6
	2%	37
	3%	35.7
Tween 80	1%	51.05
	2%	40.7
	3%	40.26
Triton X	1%	40.26
	2%	33.6
	3%	30.7
Solvent		
Acetone	1%	22.8
Methanol	1%	25.31
Butanol	1%	22
Propanol	1%	22.83
Toluene	1%	22
Hexane	1%	23.5
Ethanol	1%	23.65
Xylene	1%	22.4
Acetonitrile	1%	22.83
Chelating agent		
EDTA	1%	32.8
	2%	31.12
	3%	28.21
Inhibitory agent		
PMSF	1%	46.48
	2%	46.48
	3%	44.82
β-mercaptoethanol	1%	20.75
	2%	20.33
	3%	17.84
Sodium azide	1%	45.7
	2%	45.23
	3%	37.8

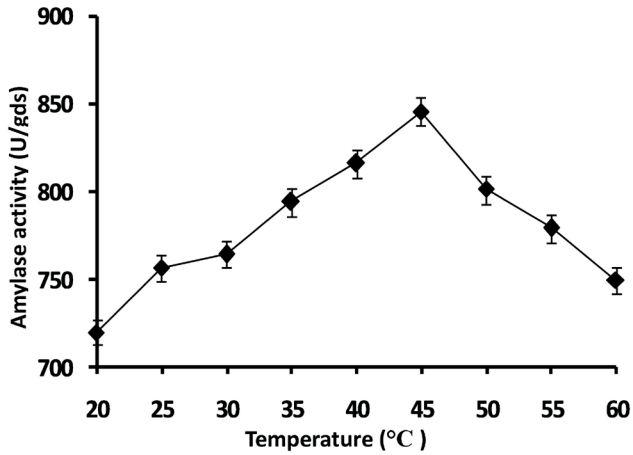

Figure 4. Activity of α-amylase at different temperature

Effect of NaCl on the purified α-amylase

The high salt tolerance capability of enzyme is very important for its commercialization in bioprocess industry. Enzymatic activity of α-amylase was tested in presence of NaCl (0 - 5.0 M). Salt tolerant capacity of acidophilic amylase from *A. niger* RBP7 at various NaCl concentrations shown in Fig. 6. It was found that NaCl was not required for activity; however, maximum starch hydrolyzing activity (808 U/gds) was observed in the presence of 3 M of NaCl. The enzyme was found to be salt-tolerant since the hydrolysis also proceeded well in the presence of 5 M NaCl. Previous study showed that α-amylases produced by *Bacillus* sp MD124 was stable in 1 M NaCl concentration (Jana and Pati 1997). Amylase activity was 0.105 U/ml and inhibited by 44.7% NaCl produced by *Monascus sanguineus* reported by Tallapragada et al. (2017). There was a salt tolerant amylase produced by *Bacillus* sp. MD124 which was found to be retained 75% of its activity in 5.0

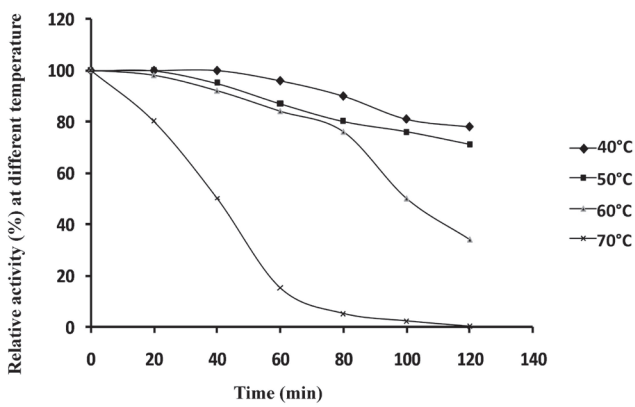

Figure 5. Effect of temperature on the stability of purified α-amylase of *A. niger* RBP7

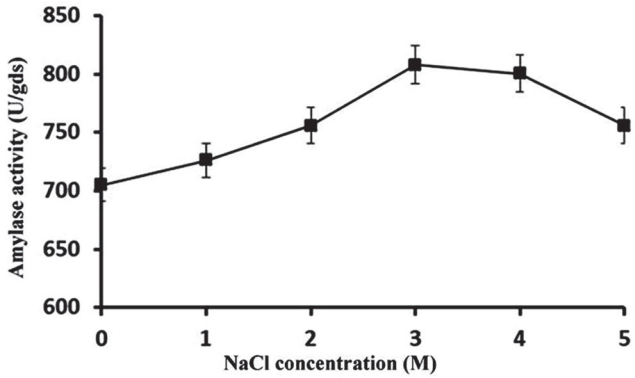

Figure 6. Activity of α-amylase at different concentration of NaCl

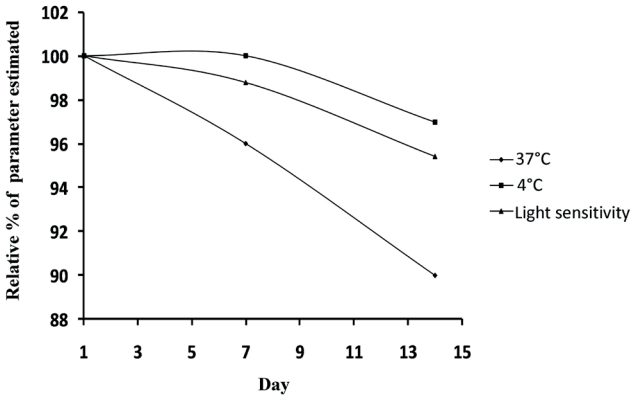

Figure 7. Effect of storage time and light sensitivity on stability of α-amylase of *A. niger* RBP7

M of NaCl concentration (Jana et al. 1997).

Storage stability and light sensitivity

The purified amylase retained about 90% of its activity after 14 days incubation at room temperature (Fig. 7) and retain 97% activity in freezing condition. Enzyme retains its 95.4% activity after 14 days of incubation.

Substrate specificity and enzyme kinetics

The enzyme was active on soluble starch, amylose, amylopectin. It was found that the hydrolytic efficiency was different from substrate to substrate and the descending order of efficiency as follows: soluble starch > amylose > amylopectin. Pullulan was not cleaved by the enzyme. The enzyme showed Michaelis-Menten kinetic on soluble starch applied in various concentrations (Fig. 8). Kinetic parameter (V_{max}, K_m, K_{cat} and catalytic efficiency) values for the hydrolysis of soluble starch by α-amylase were K_m (1.4 mg/ml), V_{max} (0.992 µmol/ min), K_{cat} 2.9796 min^{-1} and catalytic efficiency 5.0693 mg/ml/min (Fig. 8a, b; $V_0 = V_{max}$ [S]/ K_m+ [S]). The result of the relationship between substrate concentration and enzyme activity of substrates reveal that the activity of the enzyme increased concomitantly with an increase in substrate concentration. But the enzyme activity stopped to increase when the concentration exceeded 4 mg/ml indicating that substrate saturation was taking place. Haq et al. (2010) reported that α-amylase with K_m value of 4.11 mg/ml and

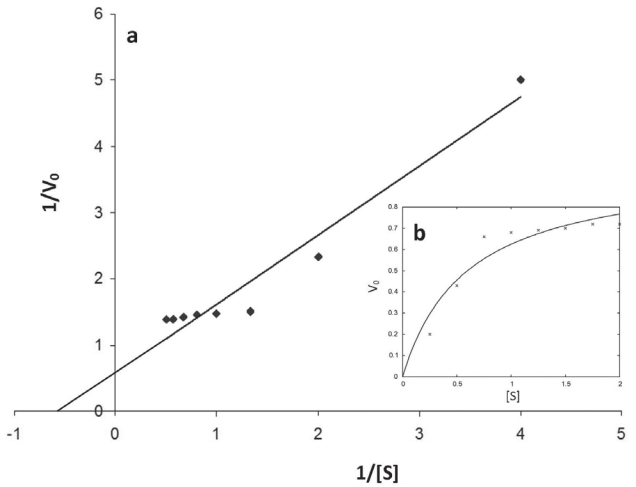

Figure 8. Lineweaver-Burk (a) and Michaelis-Menten (b) plots of enzyme kinetics of purified α-amylase at optimum pH and temperature

V_{max} value 0.45 mg with soluble starch as substrate from *B. licheniformis* EMS-6.

Enzymatic efficiency and bioconversion of heterogeneous nutritionally important compound

In these studies, mixture of food ingredients, *i.e.* rice, bread, fish and vegetable curry were digested with the

Table 3. Comparison of α-amylase from RBP7 with the commercially available Diastase

Enzyme	Enzyme activity (U/ml)	Specific activity (U/mg)	Reducing sugar (µg/ml)
Carmozyme™	157.36	15.73	78.65
Vitazyme™	118.3	29.57	29
Aristrozyme™	121.73	12.17	60.84
Unienzyme™	115.79	17.39	57.88
α-Amylase from *A. niger* RBP7	155.9	5.5	77.91

purified amylase of *A. niger* RBP7 and the performance was compared with some commercially available amylolytic cocktails. Results showed that the reducing sugar concentration after treatment with *A. niger* RBP7 α-amylase was higher than those detected for most of the commercial enzymes tested. Only the Carmozyme cocktail resulted similar digestive capacity (Table 3). Anyway, the α-amylase from *A. niger* RBP7 have the potential to degrade starchy materials present in the mixture of different food ingredients.

Conclusion

Acidophilic α-amylase produced in SSF from *A. niger* RBP7 was purified by ammonium sulfate precipitation followed by gel filtration chromatography. The purified enzyme had molecular weight of 37.5 kDa detected on SDS-PAGE and exhibited active band after zymography. It can hydrolyze starchy materials present in the mixture of rice, bread, fish and vegetable curry food products. The broad pH and temperature stability and the activity remained after long-time storage are also validate the possible application of the *A. niger* RBP7 α-amylase as additive for digestive syrup cocktails.

References

Aygan A, Arikan B, Korkmaz H, Dinçer S, Colak O (2008) Highly thermostable and alkaline α-amylase from a halotolerant-alkaliphilic *Bacillus* sp. AB68. Braz J Microbiol 39(3):547-553.

Gavrilescu M, Chisti Y (2005) Biotechnology - a sustainable alternative for chemical industry. Biotechnol Adv 23(7-8):471-499.

Ghorai, S, Banik SP, Verma D, Chowdhury S, Mukherjee S, Khowala S (2009) Fungal biotechnology in food and feed processing. Food Res Int 42(5):577-587.

Gupta R, Gigras P, Mohapatra H, Goswami VK, Chauhan B (2003) Microbial α-amylases: a biotechnological prospective. Process Biochem 38:1599-1616.

Halder SK, Jana A, Paul T, Das AP, Ghosh K, Pati BR, Mondal KC (2016) Purification and biochemical characterization of chitinase of *Aeromonas hydrophila* SBK1 biosynthesized using crustacean shell. Biocat Agri Biotechnol 5:211-218.

Haq I, Ali S, Javed MM, Hameed U, Saleem A, Adnan F, Qadeer MA (2010) Production of alpha amylase from a randomly induced mutant strain of *Bacillus amyloliquefaciens* and its application as a desizer in textile industry. Pak J Bot 42(1):473-484.

Haq IU, Javed MM, Hameed U, Adnan F (2010) Kinetic and thermodynamic studies of alpha amylase from *Bacillus licheniformis* mutant. Pak J Bot 42(5):3507-3516.

Jana M, Pati B (1997) Thermostable, salt-tolerant α-amylase from *Bacillus* sp. MD 124. J Basic Microbiol 37(5):323-326.

Khan JA, Priya R (2011) A study on partial purification and characterization of extracellular amylases from *Bacillus subtilis*. Adv Appl Sci Res 2(3):509-519.

Konsula Z, Liakopoulou-Kyriakides M (2004) Hydrolysis of starches by the action of an α-amylase from *Bacillus subtilis.* Process Biochem 39:1745-1749.

Krishnan T, Chandra AK (1983) Purification and characterization of α-amylase from *Bacillus licheniformis* CUMC 305. Appl Environ Microbiol 46:430-437.

Laemmli UK (1970) Cleavage of structural proteins during the assembly of the head of bacteriophage T4. Nature 227:680-685.

Lineweaver H, Burk D (1934) The determination of enzyme dissociation constants. Acc Chem Res 56(3):658-666.

Lowry OH, Rosebrough NJ, Farr AL, Randall RJ (1951) Protein measurement with Folin phenol reagent. J Biol Chem 193:265-275.

Maity C, Samanta S, Halder SK, Das Mohapatra PK, Pati BR, Jana M, Mondal KC (2010) Isozymes of α-amylases from newly isolated *Bacillus thuringiensis* CKB 19: production from immobilized cells. Biotechnol Bioprocess Eng 16(2):312-319.

Miller GL (1959) Use of dinitrosalicylic acid reagent for determination of reducing sugar. Anal Chem 31(3):426-428.

Mukherjee R, Paul T, Soren JP, Halder SK, Mondal KC, Pati BR, Das Mohapatra PK (2017) Acidophilic α-amylase production from *Aspergillus niger* RBP7 using potato peel as substrate: a waste to value added. Waste Biomass Valor, https://doi.org/10.1007/s12649-017-0114-8.

Pandey A, Nigam P, Soccol CR, Soccol VT, Singh D, Mohan R (2000) Advances in microbial amylases. Biotechnol Appl Biochem 31(2):135-152.

Parker K, Salas M, Nwosu VC (2010) High fructose corn syrup: production, uses and public health concerns. Biotechnol Mol Biol Rev 5(5):71-78.

Raghu HS, Rajeshwara NA (2015) Immobilization of α-amylase (1,4-α-D-glucanglucanohydralase) by calcium alginate encapsulation. Int Food Res J 22(2):869-871.

Samanta S, Das A, Halder SK, Jana A, Kar S, Das Mohapatra PK, Pati BR, Mondal KC (2014) Thermodynamic and kinetic characteristics of an α-amylase from *Bacillus licheniformis* SKB4. Acta Biol Szeged 58(2):147-156.

Sethi BK, Nanda PK, Sahoo S, Sena S (2016) Characterization of purified α- amylase produced by *Aspergillus terreus* NCFT 4269.10 using pearl millet as substrate. Cogent Food Agric 2(1).

Singh R, Kumar V, Kapoor V (2014) Partial purification and characterization of heat stable α-amylase from a thermophilic actinobacteria, *Streptomyces* sp. MSC 702. Enzyme Res 2014:8, ID 106363.

Souza PMD, Magalhães PDOE (2010) Application of microbial α-amylase in industry - a review. Braz J Microbiol 41:850-861.

Tallapragada P, Dikshit R, Jadhav A, Sarah U (2017) Partial purification and characterization of amylase enzyme under solid state fermentation from *Monascus sanguineus.* Genet Eng Biotechnol J 15(1):95-101.

Uchino F (1982) A thermophilic unusually acidophilic amylase produced by a thermophilic acidophilic *Bacillus* sp. Agric Biol Chem 46(1):7-13.

Varalakshmi KN, Kumudini BS, Nandini BN, Solomon J, Suhas R, Mahash B, Kavitha AP (2009) Production and characterization of α-amylase from *Aspergillus niger* JGI 24 isolated in Bangalore. Pol J Microbiol 58(1):29-36.

Yandri, Susanti D, Suhartati T, Hadi S (2012) Immobilization of α-amylase from locale bacteria isolate *Bacillus subtilis* ITBCCB148 with carboxymethyl cellulose (CM-Cellulose). Modern Appl Sci 6(3).

Acta Biologica Szegediensis

Volume 62(1):83-105, 2018
Acta Biologica Szegediensis
http://abs.bibl.u-szeged.hu/index.php/abs
DOI:10.14232/abs.2018.1.83-105

DISSERTATION SUMMARIES

Circularly permuted variants of two CG-specific prokaryotic DNA-methyltransferases

Pál Albert

Institute of Biochemistry, Biological Research Centre of the Hungarian Academy of Sciences, Szeged, Hungary

The prokaryotic cytosine (C-5) DNA methyltransferases (MTase) M.SssI and M.MpeI share the sequence specificity of mammalian MTases, thus they are excellent research tools for studying certain aspects of mammalian CpG-methylation. Both M.SssI and M.MpeI are amenable to fragment complementation, *i.e.* certain inactive truncated fragments of the proteins can assemble to form active enzyme. Our work with fragment complementation was hindered by the instability and/or low solubility of C-terminal fragments of M.SssI and M.MpeI. We assumed that poor solubility was due to the exposure of the hydrophobic C-terminal α-helix to the solvent. We hypothesized that this problem could be circumvented by using fragments derived from circularly permuted (CP) enzyme variants. Genes encoding CP variants of M.SssI and M.MpeI were created by PCR using tandemly duplicated MTase gene copies as templates. Most of the permutation sites were designed to leave conserved motifs and known secondary structural elements intact. MTase activity of the permutants was tested by a restriction protection assay and by measuring the incorporation of tritiated methyl groups into DNA. Eleven of the fourteen cpM.MpeI and six of the seven cpM.SssI variants were shown to have detectable MTase activity. Based on the linear arrengement of the conserved motifs, the catalitically active permutants were classified in ten topological types (A - J). Type B permutants, in which the new N-termini are located between conserved motifs II and III, had by far the highest activity. A computer search of the C5-MTase sequences available in the REBASE database revealed several MTases with naturally CP sequence. Interestingly, they appear to represent only one of the CP topologies created in this work. To our knowledge this is the first study describing the construction of designed CP C5-MTases. The wide range of CP topologies compatible with detectable MTase activity is a new evidence for the structural plasticity of C5-MTases. The CP variants open new possibilities for enzyme engineering and for testing the available structural models of the two enzymes.

Supervisor: Antal Kiss
E-mail: albert.pal@brc.mta.hu

Functional characterization and subcellular localization of CDPK Related Kinase (CRK) family in *Arabidopsis thaliana* plant

Abu Imran Baba[1,2]

[1]Institute of Plant Biology, Biological Research Centre of the Hungarian Academy of Sciences, Szeged, Hungary
[2]Doctoral School of Biology, University of Szeged, Szeged, Hungary

The CDPK (Ca^{2+}–dependent serine/threonine protein kinases) superfamily existing only in plants consists of several subfamilies like CDPK family and the structurally closely related CRK (CDPK-Related Kinase) family. Within the CDPK superfamily, the CDPK subfamily is widely involved in regulation of several abiotic and biotic stress responses in diverse plant species which is up to now relatively well documented. However, functional role of the CRK subfamily (CRKs) which contains eight members in *Arabidopsis thaliana (At)* are the least characterized until now. Previous studies from one of the members of AtCRKs showed that the plasma membrane localized AtCRK5 is required for proper polar localization of PIN2 in *Arabidopsis* roots. Inactivation of AtCRK5 causes root gravitropic defect; reduced root growth and enhanced lateral root formation. In this study, we performed the functional analysis of T-DNA insertion mutants of *Arabidopsis* CRK family members and over-expressing transgenic lines tagged with Green Fluorescent protein (GFP) and further their characterization of developmental alterations, mostly their response to gravitropic processes in roots/hypocotyls bending and root growth. Studies of the AtCRK family members with C-terminal GFP tag revealed that most of the members exhibit plasma membrane localization in the roots as was predicted by their N-terminal myristolyation sites and thus assumed to be important candidates for study of root gravitropic and other growth responses. Delayed root gravitropic and hypocotyl bending in most of the At*crk* T-DNA insertional mutants was observed when compared to the wild type (Col-0). Furthermore, the in-depth characterization of AtCRK1, which was earlier reported to be thermo-tolerant and salt sensitive member of this family, was found to be photo sensible

Volume 62(1):83-105, 2018
Acta Biologica Szegediensis
http://abs.bibl.u-szeged.hu/index.php/abs

DOI:10.14232/abs.2018.1.83-105

in continuous light growth conditions which lead to its dwarf phenotype and enhanced cell death in leaf tissues revealing its potential regulatory role in maintenance of cellular homeostasis during continuous light conditions.

Supervisor: Ágnes Cséplő
E-mail: baba.abuimran@brc.mta.hu

The biological significance of the nuclear localization of an actin-binding cytoskeletal protein

Csaba Bajusz

Institute of Genetics, Biological Research Centre of the Hungarian Academy of Sciences, Szeged, Hungary

The members of Ezrin-Radixin-Moesin family of proteins play important role in cytoskeletal rearrangements. They act as crosslinkers between membrane proteins and the actin cytoskeleton, thereby function in cell migration and metastasis. The majority of ERM proteins localize in the cytoplasm and to the cell cortex, however the Moesin (Moe) protein of *Drosophila melanogaster*, the only representative of the ERM protein family in the fly, has been detected by our laboratory also in the cell nucleus. The cytosolic role of Moe is well characterized but since its nuclear transport mechanism is unknown, the direct study of its nuclear function is not possible. To overcome this problem and to eliminate the nuclear functions of the Moe protein without affecting its manifold cytoplasmic functions, we aimed to tag the *Moe* gene *in situ* with a nuclear export signal (NES) by applying the genome editing CRISPR-Cas9 method. As a result, the Moe-NES protein would be constantly cleared out from the nucleus while it can still perform its cytoplasmic functions.

To achieve our goal, we designed and tested the efficiency of the guide-RNA (gRNA) constructs in Drosophila embryos and built up the donor construct which served as a template for homologous recombination. Next, we co-injected Cas9 producing embryos with the gRNAs and the donor construct, then screened for succesful recombination. Four *Moe*[NES] mutant lines have been recovered. Mutant adult flies showed dominant grandchild-less phenotype: germline stem cells and germ cells are both missing from the ovaries. We also observed developmental defects in *Moe*[NES] animals: bristle and wing phenotypes, cuticular and bristle malformations and the rotation of genitalia. The grandchild-less phenotype turned out to be of maternal origin while the developmental defects are zygotic effect phenotypes. Besides developmental defects, *Moe*[NES] flies also exhibit decreased heat shock tolerance and climbing capacity. We plan to reveal the molecular mechanisms behind these phenotypes by the detailed examination of the ovary and embryos of the grandchild-less females.

Supervisor: Péter Vilmos
E-mail: csaba.bajusz@gmail.com

A bioarchaeological analysis of horse riding in the Hungarian conquerors

William Berthon[1,2,3]

[1]École Pratique des Hautes Études (EPHE), PSL Research University Paris, Chaire d'Anthropologie biologique Paul Broca, Paris, France
[2]Department of Biological Anthropology, Faculty of Science and Informatics, University of Szeged, Szeged, Hungary
[3]UMR 5199 PACEA, CNRS - Université de Bordeaux, Pessac, France

In certain conditions, some changes observed on the bones can be related to an intense and regular physical activity during the life of individuals. The reconstruction of the activities in past human societies is considered by some scholars as the "Bioarchaeology's Holy Grail". However, due to various biases and the lack of a clear cultural context, the link between skeletal markers and specific activities cannot often be reliably determined. Horse riding, in particular, has already been investigated in bioarchaeology, but what markers should be considered as specific for this activity is still a debated discussion. This study is an attempt to clarify the question, from the analysis of skeletons of archaeologically presumed horse riders.

The Hungarian tribes who conquered the Carpathian Basin from the end of the IXth Century and during the Xth Century CE were composed of powerful armies of archers mounted on horses. In many cemeteries from the Conquest period, we can frequently find archery and horse riding equipment or horse bones, intentionally deposited in the graves.

Volume 62(1):83-105, 2018
Acta Biologica Szegediensis
http://abs.bibl.u-szeged.hu/index.php/abs
DOI:10.14232/abs.2018.1.83-105

We relied on the rich cemetery of Sárrétudvari-Hízóföld (Hungary), with a total of 263 burials, and performed a systematic macromorphological analysis on the adult skeletons, including scoring of joint, muscular insertion, and vertebral changes, as well as morphological variations, traumas, and a large series of infracranial measurements. We present here part of the results, with a special focus on the coxofemoral joint, and we attempt to correlate the observed skeletal changes with the presence of horse riding equipment in the graves.

This study aims to provide a methodological contribution in the field of activities in past populations, for reliable identification of the presence of riders in anthropological collections, as well as to improve our understanding of the societies of Hungarian conquerors in particular.

Supervisors: Olivier Dutour, György Pálfi, Co-supervisors: Hélène Coqueugniot, László Révész
E-mail: william.berthon@etu.ephe.psl.eu

Production of bioactive phenolic compounds from fruit residues by solid state fermentation and carbohydrase treatment

Carolina Lorena Zambrano Carrillo

Department of Microbiology, Faculty of Science and Informatics, University of Szeged, Szeged, Hungary

Application of plant derived phenolics in functional foods has increased on the past years. Though many of these phenolics have antioxidant and antimicrobial capacities, their bioavailability is often limited due to the glycosidic complexes formed. Carbohydrate-cleaving enzymes, however, can hydrolyze these bonds releasing the phenolic aglycone. Fruit residues are excellent substrates for the production, thus, we aimed to mobilize such bioactive phenolic compounds from oven-dried and lyophilized white and black grape, apple, pitahaya (known as dragon fruit), mango, naranjilla and tomato residues via two approaches: i) *in vivo* solid-state fermentation with the cellulolytic fungus *Rhizomucor miehei* NRRL 5282 and ii) *in vitro* enzymatic treatment using *R. miehei* cellulase and *Aspergillus niger* pectinase cocktails.

Positive correlation between the total phenolic content and antioxidant activity was generally found after the fermentation and the enzymatic treatments. However, the antioxidant activity increase depended on the substrate pretreatment technique as well. Concentration of the major individual phenolics determined by HPLC changed by different degrees after the enzymatic treatments depending on the substrate and the pretreatment. In further studies, the antimicrobial and antibiofilm activities of the enzyme treated extracts were evaluated against foodborne pathogens and food spoilage bacteria. Then, we studied the anti-quorum sensing potential of the samples using the model organism *Chromobacterium violaceum*. In general, carbohydrase treatments influenced positively the anti-QS properties of the extracts as well. The effects were strongly depended on the type of the fruit, the pretreatment and the enzymatic treatments. Black and white grapes displayed the highest antimicrobial activity among the residues tested, while the mango samples showed the most significant effect against the bacterial biofilm formation. The tomato and naranjilla samples were outstanding in terms of the anti-quorum sensing activity. For all extracts, the sensitive bacteria were among the *Bacillus*, *Pseudomonas* and *Staphylococcus* strains and the resistant were the *Listeria monocytogenes*, *Salmonella enterica* and *Escherichia coli*.

This work was supported by the Hungarian Government and the European Union within the frames of the Széchenyi 2020 Programme through grant EFOP-3.6.1-16-2016-00008. The infrastructural background was established with the support of GINOP-2.3.3-15-2016-00006 grant (Széchenyi 2020 Programme).

Supervisors: Judit Krisch, Miklós Takó
E-mail: czambranocarrillo@gmail.com

Do maternal smoking during pregnancy alters the morphology, rheology and function of red blood cells?

Payal Chakraborty

Department of Biochemistry and Molecular Biology, Faculty of Science and Informatics, University of Szeged, Szeged, Hungary

Cigarette smoking during pregnancy imposes risks to develop several obstetrics complications like gestational hypertension, preeclampsia, miscarriage and ectopic pregnancy. Present epidemiological data shows approximately 20-30% of women continue to smoke during

Volume 62(1):83-105, 2018
Acta Biologica Szegediensis
http://abs.bibl.u-szeged.hu/index.php/abs

DOI:10.14232/abs.2018.1.83-105

pregnancy which makes it a major health issue. Pregnancy is a physiological state with enhanced metabolism and demand for oxygen. In addition, active smokers during pregnancy get exposed to more than 4 800 harmful compounds present in the particulate and vapor phases of cigarette smoke which causes macromolecular damages. Red Blood cells (RBCs) contain numerous sources of oxidants with well-equipped redox buffering system. Till now RBCs were considered as a sink for nitric oxide (NO) derived from vascular endothelial nitric oxide synthase (NOS3) and limits the bioavailable NO for vasodilation. Recent evidence showed RBCs to have a new "Erythrocrine function" that possess a functional NOS (NOS3 like) which produce and release bioactive NO and can regulate vascular homeostasis. RBCs can mediate hypoxic vasodilation due to decreased oxygen saturation by exporting NO bioactivity. Sustained smoking during pregnancy, lowers oxygen levels, increases the concentrations of transition metal ions that release reactive oxygen species and intervenes with RBCs. The study evaluated the redox state of the RBCs with its morphological, rheological and functional alterations in the heavy smoking pregnant adults compared to control pregnant adults. It showed distinct morphological variations, significant changes in the post translational modification of NOS3, macromolecular damages developed by 4-hydroxy-2-trans-nonenal staining, a product of lipid peroxidation and rheological alterations as indicated by atomic force microscopy. Thereby, smoking during pregnancy causes irreversible changes that leads to macromolecular damages which induces adverse outcomes in the gestation period.

This work was funded by GINOP 2.3.2-15-2016-0040 („MyoTeam")

Supervisor: Edit Hermesz
E-mail: payal96.pharm@gmail.com

Gut region-specific alterations of the endogenous heme oxygenase system and pro-inflammatory cytokines in the enteric neurons of streptozotocin-induced diabetic rat model

Lalitha Chandrakumar

Department of Physiology, Anatomy and Neuroscience, Faculty of Science and Informatics, University of Szeged, Szeged, Hungary

Increase of the hyperglycaemia-induced oxidative stress and decreased effectiveness of the endogenous antioxidant enzymes plays a major role in the initiation of diabetes-related neuronal damage. Nitrergic myenteric neurons in the different gut segments displayed different susceptibilities to diabetes and insulin treatment. Therefore, we aimed to study the gut segment-specific differences in the expression of heme oxygenase (HO) isoforms and their co-localization with neuronal nitric oxide synthase (nNOS) in myenteric neurons as well as the proportion of HO1-immunoreactive (IR), HO2-IR and nNOS-IR submucous neurons in a type 1 diabetic rat model. We also attempted to reveal the gut segment-specific differences in the expression of tumor necrosis factor alpha (TNFα) and interleukin 6 (IL6) in the myenteric ganglia and its microenvironment in type 1 diabetes. Ten weeks after the onset of hyperglycemia, segments from duodenum, ileum and colon of streptozotocin-induced diabetic, insulin-treated diabetic, and control rats were processed for double-labelling fluorescent immunohistochemistry, post-embedding electron microscopic immunocytochemistry and enzyme-linked immunosorbent assay. The number of HO-IR and nNOS-HO-IR myenteric neurons were significantly increased in the diabetic ileum and colon. The proportion of nNOS-IR and HO-IR submucous neurons were highly pronounced in the distal parts of gut in diabetic and insulin-treated diabetic rats. The expression of TNFα and IL6 were strictly gut region-dependent in the myenteric ganglia and supplying capillary endothelium in controls, diabetic and insulin-treated diabetic rats. Based on these results, we suggest that the regional differences in the induction of the endogenous HO system as well as the investigated pro-inflammatory cytokines are strongly correlated with diabetes-related region-specific nitrergic neuropathy.

Supervisor: Mária Bagyánszki
E-mail: lalitha.biochem87@gmail.com

Structural elucidation of bioactive peptaibols and understanding their dynamics

Chetna Tyagi

Department of Microbiology, Faculty of Science and Informatics, University of Szeged, Szeged, Hungary

Amongst the plethora of secondary metabolites produced by fungi from the genus *Trichoderma*, peptaibols deserve special attention

DOI:10.14232/abs.2018.1.83-105

due to their demonstrated anti-bacterial, anti-fungal, anti-viral and anti-helminth properties. These peptides have an acetylated N-terminal and a C-terminal 1, 2-amino alcohol. Non-standard amino acid residues like D-isovaline (Div) and the highly studied residue aminoisobutyric acid (Aib) also constitute their primary structure. They are known to aggregate and form pores across bilayer membranes. The knowledge of their three-dimensional structures and dynamics of channel forming is therefore crucial for understanding their bioactivities.

The non-standard residues of *Trichoderma* peptaibols were first parameterized using RESP charges. Various paracelsins, hypomurocins and peptides from the recently described tripleurin class were simulated under different solvents, starting structures and time periods. The longer peptides like paracelsins show higher propensity to form continuous helix formation. The number of Aib residues in the sequence promotes helicity in the sequence which may fluctuate between left- and right-handedness depending on the neighboring amino acid residues. New tripleurins were seen to conform into a linear helical shape with beta-bend ribbon spirals at the N-terminal and a 3_{10}/alpha-helix at the C-terminal. Peptide folding in methanol solvent promotes stability of the secondary structure more than aqueous solvent. These peptides show a characteristic break from helix continuity at the Aib-Pro bond which confers hinge-like movement to the C-terminal. This movement probably plays a crucial role in channel arrangement.

These results will be used further to model ion channels and visualize their interaction with the membrane. The study of exact mechanism of channel formation and ion expulsion is in the pipeline.

This work was supported by the Hungarian Government and the European Union within the frames of the Széchenyi 2020 Programme through grant GINOP-2.2.1-15-2016-00006. The infrastructural background was established with the support of GINOP-2.3.3-15-2016-00006 grant (Széchenyi 2020 Programme).

Supervisors: Ferenc Ötvös, László Kredics
E-mail: cheta231@gmail.com

High-throughput screening to identify inhibitors of PCNA ubiquitination

Paras Gaur

Laboratory of Mutagenesis and Carcinogenesis, Institute of Genetics, Biological Research Centre of the Hungarian Academy of Sciences, Szeged, Hungary

Cancer is a major disease with a high rate of mortality. According to the worldwide cancer incidence statistics published by Cancer Research UK, there were 14.1 million new cancer patients in 2012 and there will be 23.6 million new cancer cases per year by 2030. In cancer research, major challenges are in early diagnosis and developing highly effective treatments with low toxicity. DNA replication in cells can be stalled by DNA damage, requiring repair through translesion synthesis (TLS), which is an error-prone pathway and can lead to mutations that favor cancer cell growth and metastasis, as well as result in DNA damage tolerance and therapeutic resistance to numerous anticancer agents.

PCNA is a homotrimeric protein complex that serves as a sliding clamp during DNA replication and as a co-factor for TLS polymerases. When replicative DNA polymerases encounter stretches of damaged DNA, the replication fork stalls. In response, PCNA undergoes monoubiquitination on a specific lysine residue, activating the mutagenic TLS pathway. We are interested in discovering small molecules that inhibit the monoubiquitation of PCNA, the trigger for TLS and so downstream interactions of PCNA with TLS polymerases such as Pol eta (η). This process is central to DNA damage tolerance. Pol η-PCNA complexes have been demonstrated in yeast cells by using a novel genetic code expansion system.

We have developed a functional *in vitro* ubiquitination assay that displays virtually 100% PCNA ubiquitination in control samples and have scaled the assay to high-throughput levels. Screening of NCI/DTP Diversity Set IV, Mechanistic Set IV, Approved Oncology Drugs Set VIII, and Natural Products Set IV with AlphaScreen/AlphaLISA system is underway.

Supervisor: Lajos Haracska
E-mail: gaur.paras@brc.mta.hu

Volume 62(1):83-105, 2018
Acta Biologica Szegediensis
http://abs.bibl.u-szeged.hu/index.php/abs

DOI:10.14232/abs.2018.1.83-105

The redundant role of formins during pigment cells development in the *Drosophila* eye

Gabriella Gazsó-Gerhát

Institute of Genetics, Biological Research Centre of the Hungarian Academy of Sciences, Szeged, Hungary

The highly dynamic actin cytoskeleton is one of the structurally and functionally most important cellular constituents. The dynamic assembly and disassembly of the actin filaments is controlled by a large set of regulatory proteins some of which also contribute to the formation of higher-order actin structures, such as bundles and networks of filaments. One of the most important classes of the actin regulatory proteins are designated as actin nucleation factors that promote the formation of new actin filaments. Among the three major types of actin nucleation factor that have so far been identified, we focus our studies on the formin protein family.

Formins are highly conserved cytoskeleton regulatory proteins that act in dimers and support the assembly and elongation of new actin filaments. The major aim of my studies is to examine the potentially redundant role of two formins, DAAM and FRL, during eye development in *Drosophila melanogaster*. We have previously shown that these two actin assembly factors play redundant roles during axonal growth in the mushroom bodies of the adult brain. We also noticed that although dDAAM and FRL are strongly expressed in the developing eye and in axons of the photoreceptor cells, *dDAAM* or *frl* single mutant animals do not exhibit any developmental abnormalities in the eye. On the contrary, *dDAAM; frl* double mutant adult flies exhibit rough eyes and we observed a unique and novel eye phenotype: the pigment cells (also known as interommatidial cells) are often detached from the basal lamina and fail to undergo a typical cell shape change required to properly seal the bottom of the unit eyes. These results suggested that these formins act redundantly during eye development. To determine the cellular role of these two formins, we are currently analysing the changes in cell shape and cytoskeleton organization during eye development in the double mutants, whereas the single mutants are used as controls.

Supervisor: József Mihály
E-mail: gerhat.gabriella823@gmail.com

Functional Analysis of a novel hydrophobic surface binding protein in Mucorales

Amanda Grace Vaz

Department of Microbiology, Faculty of Science and Informatics, University of Szeged, Szeged, Hungary.

Hydrophobic surface binding protein A is a small secreted protein found in eukaryotes. This protein was firstly isolated from *Aspergillus oryzae* culture broth. That protein was found to be able to recruit cutinase 1 (Cult1) to the surface of hydrophobic solid materials and could promote the activity of degradative extracellular enzymes. This protein also participates in fungal resistance to stress that could be caused due to toxicity of some aromatic compound or reactive oxygen species released during the degradation process. During infection of MH-S macrophages, *Lichtheimia corymbifera* expressed an Hsb-A-like protein at high level. Hsb-A protein is functionally uncharacterized in Mucorales and its role in the host-pathogen interactions is yet unknown. The objective of the current study was to characterize Hsb-A proteins and the encoding genes of *Mucor circinelloides*.

We found six *hsb-A* genes in the *M. circinelloides* genome, which are homologous to the *L. corymbifera hsb-A*. Two genes (*hsb-A1* and *hsb-A2*) were found to be highly expressed during the life cycle of the fungus. Hence, these two genes were used for further studies. To analyse the possible role of Hsb-A1 and Hsb-A2 in the pathogenesis of *M. circinelloides*, deletion and overexpression mutants were constructed. For overexpression, the genes were placed under the regulation of the strong *gpd1* promoter. To create *hsb-A* knock out mutants, a recently developed CRISPR-Cas9 system was used. Micro- and macromorphology assays were conducted for the deletion and overexpression mutants. Host-pathogen interaction assay was conducted using *Drosophila* models. Furthermore, *Pichia* expression systems were constructed and the expressed hsb-A1 and hsb-A2 proteins were purified for further analysis.

This study was supported by the Hungarian Government and the European Union within the frames of the Széchenyi 2020 Programme through grant GINOP-2.3.2-15-2016-00035. The infrastructural background was established with the support of GINOP-2.3.3-15-2016-00006 grant (Széchenyi 2020 Programme).

Supervisor: Tamás Papp and Gábor Nagy
E-mail: amanda.grace6vaz@gmail.com

Volume 62(1):83-105, 2018
Acta Biologica Szegediensis
http://abs.bibl.u-szeged.hu/index.php/abs

DOI:10.14232/abs.2018.1.83-105

Endoplasmic reticulum stress: major player in size-dependent inhibition of P-glycoprotein by silver nanoparticles in multidrug-resistant breast cancer cells

Mohana Krishna Gopisetty

Department of Biochemistry and Molecular Biology, Faculty of Science and Informatics, University of Szeged, Szeged, Hungary

Multidrug-resistant (MDR) cancer is strongly associated with P-glycoprotein (Pgp) overexpression and has been a major deterrent to current chemotherapeutic regimens, thus demanding novel approaches to defeat resistance. Silver nanoparticles (AgNPs) have gained significant attention in nanomedicine, owing to their multifaceted biological properties, which largely depend on their composition, shape and size. In this study we examined how would a variation in nanoparticle size affect the MDR phenotype of drug-resistant cancer cells. For this purpose, AgNPs of two different sizes (5 nm and 75 nm) were tested on Pgp overexpressing MCF7/KCR as well as on drug-sensitive MCF7 breast cancer cells. Exposures to 75 nm AgNPs significantly inhibited Pgp efflux activity, whereas treatments with 5 nm AgNP did not affect Pgp function. 75 nm AgNPs were less cytotoxic and generated less reactive radicals compared to 5 nm AgNPs. Importantly, large AgNPs potentiated significantly the cytotoxic and apoptotic activities of doxorubicin. In order to explain the molecular mechanisms underlying Pgp inhibition we investigated Pgp expression levels and endoplasmic reticulum stress following AgNP exposures. We did not observe any changes in Pgp expression upon 5 nm or 75 nm AgNP treatments, however larger AgNPs induced notable ER stress in drug-resistant breast cancer cells. The manifested ER stress, characterized by transcriptional and translational activation of ER stress markers and autophagy, proved to be independent from oxidative stress, however correlated well with depleted ER calcium stores. The results infer that 75 nm AgNPs are more effective than 5 nm AgNPs in Pgp inhibition due to the entrapment of unfolded or misfolded Pgp in the endoplasmic reticulum as a consequence of ER stress. This mechanism also explains the sensitizing effect of 75 nm AgNPs on drug-resistant MCF7/KCR cells to doxorubicin induced apoptosis.

Supervisor: Mónika Kiricsi
E-mail: jaisairam205@gmail.com

Characterisation of Plagl1, a putative downstream target of Rybp

Surya Henry

Institute of Genetics, Biological Research Centre of the Hungarian Academy of Sciences, Szeged, Hungary

Congenital heart disorders (CHD) arise from mutations causing structural and functional anomalies in the developing heart. Embryonic stem (ES) cell based *in vitro* differentiation assays are powerful and unique model systems to investigate the underlying molecular events of normal heart development and CHD conditions.

We have previously shown that ES cells, which are lacking the polycomb Ring1 & YY1 binding protein ($rybp^{-/-}$) could not form beating cardiomyocytes *in vitro*. Importantly, expression of several key cardiac transcription factors was strongly affected in the $rybp^{-/-}$ cultures in comparison to the wild-type ($rybp^{+/+}$) counterparts. One of the most affected gene was the Pleiomorphic adenoma gene like 1 (Plagl1), which was nearly absent in the $rybp^{-/-}$ ES cells. Plagl1 is a key cardiac trancription factor: gene targeting experiments has proven that mice lacking Plagl1 develop arterial and ventricular septum defects with thin ventricular wall formation.

During my PhD work, I have further characterised the Plagl1 gene and established its possible relationship with Rybp. Our findings showed that Plagl1 has a complex genomic locus containing three promoter regions coding at least two isoforms of Plagl1 and two non-coding RNAs (ncRNAs) Hymai & Plagl1 I.T. Gene expression analysis of Hymai and Plagl1 I.T revealed that the mRNA levels of these two ncRNAs were greatly affected in the $rybp^{-/-}$ cells during the time course of *in vitro* cardiac differentiation in comparison to the $rybp^{+/+}$ cultures. I have also shown that Plagl1 protein is mostly abundant in the late phase of, *in vitro* cardiac differentiation. Finally, by using *in vivo* luciferase promoter assays, I demonstrated that Rybp was able to activate the Plagl1 promoter through its P3 promoter.

These data suggests that Rybp may exert its functions partially via by activating Plagl1. Considering that Rybp is a repressor protein, current work broadens our limited knowledge on how repressor complex members may also exert their functions as activators during healthy development or disease conditions, like CHD.

Supervisor: Melinda Pirity
E-mail: surya.henry@brc.mta.hu

Volume 62(1):83-105, 2018
Acta Biologica Szegediensis
http://abs.bibl.u-szeged.hu/index.php/abs

DOI:10.14232/abs.2018.1.83-105

Systematic chemogenomic analysis reveals diverse genetic modulators of bacterial susceptibility to antimicrobial peptides

Pramod K. Jangir

Synthetic and Systems Biology Unit, Biological Research Centre of the Hungarian Academy of Sciences, Szeged, Hungary

Antimicrobial peptides (AMPs) are immune effectors and promising therapeutic agents with diverse mechanisms of bacteria killing. However, a comprehensive understanding of the genetic factors that influence bacterial susceptibility to AMPs is prerequisite to ensure their clinical use and to minimise possible cross-resistance to our immunity peptides.

Here, we performed a chemogenomic analysis to systematically assess the impact of all single genes overexpression on *Escherichia coli* susceptibility to 15 different AMPs, including 2 major types of human host defense peptides. We found that multiple genetic determinants influence bacterial resistance and notably, these resistant determinants largely differ to AMPs with different modes of action. Chemogenomic profiles classified the AMPs according to their physicochemical similarities and outlined their broad modes of action. We demonstrated that human AMPs had a very similar chemogenomic profile to a specific class of membrane disruptive AMPs but largely dissimilar to intracellular targeting AMPs. These differences between AMPs facilitated the identification of a compendium of genes showing collateral sensitivity interactions between the AMPs. We confirmed these findings through a laboratory evolutionary experiment and showed that bacterial adaption to human beta-defensin-3 results in cross-resistance to the membrane disruptive AMPs, but collateral sensitivity to intracellular targeting AMPs. Functional analysis of the gene sets that underlie this collateral sensitivity interaction highlighted a clinically relevant molecular pathway that controls outer membrane asymmetry. Overall, these findings have important implications for the therapeutic development of AMPs.

Supervisor: Csaba Pál
Email: jangirk.pramod@gmail.com

Functional characterization of RLCK VI_A kinases with usage of a miRNA-induced gene silencing system

Shyam Jee[1,2,3]

[1]Institute of Plant Biology, Biological Research Centre of the Hungarian Academy of Sciences, Szeged, Hungary
[2]Department of Plant Biology, Faculty of Science and Informatics, University of Szeged, Szeged, Hungary
[3]Doctoral School of Biology, University of Szeged, Szeged, Hungary

The Rho-of-plants (ROP) G-proteins are involved in regulation of cell growth, cell polarity, hormonal and pathogen responses but downstream components of ROP mediated signalling are poorly known. A small subgroup of plant specific receptor-like cytoplasmic kinases (RLCK VI_A) shows ROP-binding-dependent in vitro kinase activity. Our aim was to characterize the function of RLCK VI_A kinases in *Arabidopsis* plants.

In order, to investigate the effects of the loss of RLCK VI_A kinase function, we used a trans-acting micro-RNA-induced gene silencing system (MIGS). This system uses a short (22 nc) *Arabidopsis* specific miRNA (miR173) recognition fragment, which can trigger the production of trans-acting small interfering RNAs (tasiRNA) of adjacent sequences. We fused RLCK VI_A1 and A2 kinase specific gene fragments upstream to miR173 recognition sites in tandem organisation. Agrobacterium mediated plant transformation of Col-0 wild type and *rlck vl_a3* T-DNA insertional mutant plants were performed with the MIGS construct.

The silenced gene expression resulted reduction of rosette size and alteration in the phyllotactic pattern of shoots. Pollen tubes of the transgenic plants also exhibited altered growth characteristics. We found that reduced expression of A1, A2 and A3 kinases caused branching and abnormal pollen tube growth. These results indicate the potential role of the kinases in plant growth and development as well as pollen tube polarity in agreement with their expression pattern.

Supervisor: Attila Fehér
E-mail: shyamhg.yadav@brc.mta.hu

Volume 62(1):83-105, 2018
Acta Biologica Szegediensis
http://abs.bibl.u-szeged.hu/index.php/abs

DOI:10.14232/abs.2018.1.83-105

Analysis of autophagy-related (*Atg*) genes in *Drosophila melanogaster*

András Jipa

Institute of Genetics, Biological Research Centre of the Hungarian Academy of Sciences, Szeged, Hungary

Autophagy is a conserved intracellular degradation process in eukaryotic organisms. This catabolic pathway plays a very important role in cells: the continuous turnover of macromolecules and cell organelles is important for longevity, and it is essential in adaptation to nutrient-poor conditions during starvation. As the autophagy-related (Atg) genes were first described only about 26 years ago in yeast, we still have only limited information about their functions. Via molecular genetic, cell and developmental biology investigations of the *Drosophila* autophagy-related genes (*Atg*), we can clarify their roles.

During my work, I created null mutant alleles for the *Drosophila Atg5*, *Atg9*, *Atg14* and *Atg8b* genes using the CRISPR-CAS9 method and, also for the *Atg8a* gene by gene trapping. These mutants were used both in our own research projects and in an international collaboration as well. The main focus of my work is the investigation of *Atg8* genes in *Drosophila*. Atg8 is an ubiquitin-like protein that is conjugated to the lipid phosphatidylethanolamine (PE) on the phagophore membrane during autophagy. This process is mediated by factors analogous to the ubiquitylation reaction: the Atg8 conjugation machinery also includes factors with E1, E2, and E3-like functions. Only two Atg8 homologs are found in *Drosophila*: the *Atg8a* and *Atg8b* genes. To generate a null mutant allele of *Atg8a* we modified an intronic Minos element of the *Atg8a* locus by inserting a Trojan-Gal4 cassette, which is designed to function as a gene trap. During the characterization of this new allele - based on anti-Atg8 and anti-p62 western blots and somatic mutant clones in the larval fat body - we proved that the created allele functions as an *Atg8a* null mutant, and all homozygotes die during the pharate adult stage. Additionally, we used CRISPR gene editing to generate a nonsense mutant *Atg8a* allele encoding a truncated (G116stop) protein defective in PE conjugation. Animals expressing this non-lipidatable Atg8a are autophagy defective, but viable and fertile. As for *Atg8b*, it is not required for autophagy, and animals homozygous for this allele are adult viable and female fertile but nearly completely male sterile. *Atg8b* mutant sperm cells can develop until the latest stages of spermatogenesis but they are immobile, which explain the male sterility.

Supervisor: Gábor Juhász
E-mail: jipaandras@gmail.com

Investigating the role of Wnt/PCP proteins in axon growth and the regulation of neuronal cytoskeleton

Péter Kaltenecker[1,2]

[1]Institute of Genetics, Biological Research Centre of the Hungarian Academy of Sciences, Szeged, Hungary
[2]Institute of Translational Medicine, University of Liverpool, Liverpool, United Kingdom

In *Drosophila melanogaster* there are 6, evolutionary highly conserved, core Planar Cell Polarity (PCP) proteins that are essential in the formation of planar polarity in epithelial tissues. Besides this function, these proteins are also known to play multiple roles in neuronal development. Neurons are highly polarised cells with extended neuronal protrusions, during the growth and maintenance of which the neuronal cytoskeleton plays a crucial role. The aim of my project is to study how the core PCP proteins regulate the neuronal cytoskeleton, and to understand how they contribute to axon growth in *Drosophila melanogaster*.

To this end two strategies were applied: I used primary embryonic cell cultures which provide powerful subcellular readouts to determine the state of the neuronal cytoskeleton; in addition, I studied the embryonic and the adult central nervous system in order, to assess the *in vivo* relevance of my findings.

My results showed that, the loss of some PCP components affected axon growth in the embryonic central nervous system. This was in accordance with my findings in primary neuronal cell cultures. Furthermore, I found that the lack of PCP components led to changes in microtubule (MT) organisation in cultured neurons. In order, to investigate the mechanism by which PCP proteins can regulate the MT cytoskeleton I also studied Daam, a formin type protein which is a known cytoskeleton regulator and has been linked to PCP signalling previously. In the absence of Daam MT organisation was strongly affected, moreover, I found that Daam has an important role in regulating MT dynamics and stability as well. Further ongoing experiments show that PCP proteins, as well as Daam, control

Volume 62(1):83-105, 2018
Acta Biologica Szegediensis
http://abs.bibl.u-szeged.hu/index.php/abs

DOI:10.14232/abs.2018.1.83-105

axon growth and guidance in the ventral lateral neurons (LNv) of the adult brain. Together these findings suggest that PCP proteins are necessary to properly regulate MTs, presumably by controlling Daam, and contribute to axon growth *in vivo*.

Supervisors: József Mihály, Natalia Sanchez-Soriano
E-mail: kalter888@gmail.com

The anti-amyloidogenic effect of natural product extracts on amyloid-like fibril formation of trypsin in aqueous organic solvents

Phanindra Babu Kasi

Department of Biochemistry and Molecular Biology, Faculty of Science and Informatics, University of Szeged, Szeged, Hungary

The formation of amyloid fibrils has been associated with several human diseases. The appearance of amyloid aggregation is an indicator of different central nervous system neurological disorders and neurodevelopmental diseases, which affect the brain and peripheral tissues. The misfolding and aggregation of proteins cause a large number of different neurodegenerative diseases. Amyloid is a generic structural form of the polypeptide chain and most proteins can form amyloid-like fibrils under proper conditions.

Natural product extracts contain important bioactive compounds without undesirable side effects, which are necessary for the prevention and cure of various diseases. Fifty-two phenolic compounds were identified in culinary herbs and spices. The aromatic rings of polyphenols may competitively interact with aromatic residues in amyloidogenic proteins, prevent the π-π interaction and block the self-assembly process. The phenolic hydroxyls of polyphenols may inhibit amyloid fibril formation via binding the hydrophobic residues in amyloidogenic proteins. Here we report the inhibitory effect of some natural product extracts on the formation of amyloid fibrils using trypsin as a model protein, in aqueous ethanol. Inhibition of aggregation and fibrillation of trypsin was determined based on turbidity measurement, aggregation kinetics assay, amyloid specific dye Congo red (CR), fourier-transformed infrared (FTIR) spectroscopy, electronic circular dicroism (ECD) and transmission electron microscopy (TEM). The experiments revealed that great anti-fibrillation activity was exerted by chili extract, *P. ginseng* extract, grapefruit seed extract, peppermint extract, Eduscho coffee extract and Egri bikavér red wine. It was found that the amount of fibril formation was greatly reduced with increasing concentration of extracts and the inhibitory effect is dose dependent.

This work was funded by EFOP-3.6.1-16-2016-00008.

Supervisor: Márta Kotormán
E-mail: phansi93@gmail.com

Studies on the sexual development of *Aspergillus nidulans*

Kabi Chandra Singh Keisham

Department of Microbiology, Faculty of Science and Informatics, University of Szeged, Szeged, Hungary

Studies on the sexual development of *Aspergillus nidulans* revealed more than 50 regulatory elements involved in the activation or repression of sexual development. In our previous studies we had identified three, architectural chromatin associated HMGB proteins in *A. nidulans* (HmbA, HmbB and HmbC) and developed deletion mutants. We noted that viability of ascospores is dramatically reduced in *hmbBΔ* and *hmbAΔ* and *hmbCΔ* mutants are self-infertile. Accordingly, we suppose that HMGB proteins play crucial role in the sexual development at chromatin level. We aimed to study the sexual development in the deleted mutants and compare to that of wild type. Through the microsopic analysis of the sexual structures we characterized the sexual impairments of the *hmbAΔ*, *hmbBΔ* and *hmbCΔ* strains. In order, to shed light on the molecular basis of the mutant phenotypes and evaluate the governing role of HmbA/B/C proteins on sexual development, we carried out gene expression analysis on 36 transcription factors involved in sexual development.

A. nidulans produces the carcinogenic sterigmatocystin (STC) toxin, which is thought to be a protective compound for the protection of the fungal reproductive structures. Studies on the sexual development and secondary metabolite biosynthesis have revealed the association of these two processes in time at regulatory level. We aimed to study the spatial distribution of STC production within the colony and assess its association with sexual development by employing a yCFP reporter system. We developed an *stcO* reporter strain by substituting the ORF of *stcO* with nucleus targeted yCFP. We proved that *stcO* has essential role in STC biosynthesis and

Volume 62(1):83-105, 2018
Acta Biologica Szegediensis
http://abs.bibl.u-szeged.hu/index.php/abs
DOI:10.14232/abs.2018.1.83-105

activation of gene expression is restricted to the third day of incubation. We demonstrated that the *stcO* promoter is active only in vegetative hyphae that surround groups of hülle cells and the activity decreases and eventually ceases as the distance between the hypha and the hülle cells increases. This phenomenon indicates that the vegetative mycelium might consist of morphologically uniform, but functionally different hyphae.

This work was supported by the Hungarian Government and the European Union within the frames of the Széchenyi 2020 Programme through grant GINOP-2.3.2-15-2016-00012. The the infrastructural background was established with the support of GINOP-2.3.3-15-2016-00006 grant (Széchenyi 2020 Programme).

Supervisor: Zsuzsanna Hamari
Email: kabinature@gmail.com

Dynamic gene duplication/loss history marks the unique evolutionary route to fungal multicellularity

Enikő Kiss

Biochemistry Institute, Biological Research Centre of the Hungarian Academy of Sciences, Szeged, Hungary

Multicellularity has evolved numerous times during eukaryote evolution, yet the genetic prerequisites for these transitions are hardly known. In contrast to other organisms fungi used their own unique evolutionary route to achieve multicellularity with different physiological bases. This raises the question whether the genetic-mechanistic principles of the evolution of multicellularity are common to both fungi and animals and how fungal multicellularity-related gene families evolved during the history of life. Here we reconstruct the evolution of the genetic background of fungal multicellularity based on both known multicellularity-related genes from the literature and genome-wide identification of gene families that evolve in a correlated fashion with multicellularity. Based on literature surveys, we identified 493 genes involved in the establishment and maintenance of cell polarity, vesicular transport and cytoskeletal rearrangement. The evolutionary origins of these genes were examined using complete genomes of 71 unicellular and multicellular eukaryotes. We implemented phylostratigraphic analyses using a custom pipeline, which uncovered the evolutionary origins of multicellularity-related genes, and reconstructed gene duplication and loss histories by COMPARE analysis. This study yielded a high-resolution view of the dynamics of these known fungal multicellularity-related gene families. Further we could identify 316 gene families, including certain cytochrome P450 families, monocarboxylate permeases and vacuolar aspartyl proteases that show strong correlated evolution with multicellularity, providing candidates for future functional studies. Our results indicate that part of the genetic toolkit behind fungal multicellularity was already present in ancestral unicellulars and that some of the hyphal morphogenesis related gene families show diversification before the emergence of the first filamentous fungi. These results would suggest that beside the *de novo* gene family birth and gene duplication events, hitherto unknown gene regulatory mechanisms could also have had a crucial role in the evolution of multicellular fungi.

Supervisor: László Nagy
E-mail: kisseni90@gmail.com

Characterization of lytic bacteriophages against biofilm-forming multi drug resistance *Pseudomonas aeruginosa*

Sarshad Koderivalappil

Department of Biotechnology, Faculty of Science and Informatics, University of Szeged, Szeged, Hungary

Pseudomonas aeruginosa is a most common opportunistic multi-drug-resistant (MDR) pathogen that is poised to become a widespread problem. Recently some strains even show additional evolved resistance to 'drugs of last resort', resulting in emergent strains that are pan-drug-resistant (PDR). The bacterium has high endogenous resistance to many antibiotics, because of its outer membrane barrier, multidrug efflux pumps, endogenous antibiotic inactivation and biofilm-formation. Biofilm mediated infections including catheter-associated urinary tract infections and ventilator-associated pneumonia. One alternative treatment for MDR bacterial infections is phage therapy: the use of lytic bacteriophages as in situ self-amplifying 'drugs' that specifically target and kill bacteria. Phages also have

Volume 62(1):83-105, 2018
Acta Biologica Szegediensis
http://abs.bibl.u-szeged.hu/index.php/abs

DOI:10.14232/abs.2018.1.83-105

several properties allowing them to act on biofilms. They might produce enzymes that disintegrate the extracellular matrix. The high numbers of bacteria in the biofilms facilitate the action of phages by allowing rapid and efficient infection. In my study, I focused on *P. aeruginosa*, more than Twenty strains belonging various serotypes and 13 lytic phages were isolated and characterized. The morphology of phages was analyzed by electron microscopy, the genomes of the phages and few hosts were studied by NGS technologies. The serotype and the host specificity of the phages were studied in liquid cultures and on biofilms. A major limitation of phage therapy is the potentially narrow host range of the phages; a specific phage is often capable of lysing only one or a small number of strains within a species. To overcome this limitation, we used phage cocktails and also performed co-cultured study harboring phage-resistant and sensitive bacteria. The effectivity of phage cocktails on recalcitrant biofilm architecture was examined by confocal laser scanning microscope. A defined cocktail composed of 5 phages with distinct serotype specificity was effective against any biofilm-formers which clearly indicates the applicability of phages against *P. aeruginosa* infections.

Supervisor: Gábor Rákhely
E-mail: way2sarshad@gmail.com

The role of chloramphenicol in enhancing photodamage of Photosystem II in *Synechocystis* 6803

Sandeesha Kodru[1,2]

[1]Department of Plant Biology, Biological Research Centre of the Hungarian Academy of Sciences, Szeged, Hungary
[2]Doctoral School in Biology, University of Szeged, Szeged, Hungary

Photoinhibition is light induced reduction of photosynthetic capacity in plants algae, and cyanobacteria. Light damages primarily the structure and function of the PSII complex, and the damage is repaired by the re-synthesis of the D1 protein subunit. The rate of photodamage can be monitored in the presence of photosynthetic inhibitors like lincomycin and chloramphenicol, which block the repair. It has been reported earlier that chloramphenicol serves as an electron acceptor of PSI and its reduction intermediate transfers the electrons to molecular oxygen to produce superoxide. We have studied the effect of chloramphenicol on the rate of photodamage in isolated PSII membrane particles and in *Synechocystis* 6803 cells. By using the isolated PSII membranes we have demonstrated that chloramphenicol can accept electrons and mediate superoxide production not only in PSI but also in PSII. We have also shown that the chloramphenicol mediated superoxide production is responsible for accelerated photodamage of PSII in isolated PSII membrane particles.

We have also studied the effect of chloramphenicol on the rate of photoinhibition, as well as on superoxide production in intact *Synechocystis* 6803 cells. In order, to obtain the net rate of photodamage without the effect of the ongoing repair of PSII the light treatment was performed in the presence protein synthesis inhibitors, either chloramphenicol or lincomycin. Our results showed that the rate of photodamage was enhanced in the presence of chloramphenicol as compared to that in the presence of lincomycin. By using oxygen uptake measurements in the presence and absence of superoxide dismutase (SOD) we could show that chloramphenicol mediates the production of superoxide in *Synechocystis* 6803 cells which only PSII complexes and lack PSI. These data indicate that superoxide, which is produced via interaction of chlorampehicol with PSI and PSII in WT cell, or with PSII in the PSI-less mutant *Synechocystis* 6803 is responsible for the enhanced photodamage.

Supervisor: Imre Vass
E-mail: kodru.sandeesha@brc.mta.hu

Development of targeted DNA methylation tools for breast cancer research

Mihály Koncz

Institute of Biochemistry, Biological Research Centre of the Hungarian Academy of Sciences, Szeged, Hungary

In estrogen receptor alpha positive (ER+) breast cancer anti-estrogen endocrine therapy is a standard treatment. Unfortunately, many initially responsive patients develop resistance to the therapy. There are data suggesting that epigenetic changes such as DNA methylation and histone modifications play crucial roles in endocrine resistance. As a member of a Marie Skłodowska-Curie Innovative

Volume 62(1):83-105, 2018
Acta Biologica Szegediensis
http://abs.bibl.u-szeged.hu/index.php/abs
DOI:10.14232/abs.2018.1.83-105

Training Network focusing on epigenetic regulation of endocrine therapy resistance in breast cancer, we develop research tools for targeted DNA methylation. Our goal is to identify genes which have a role in resistance acquisition.

We have constructed a CRISPR/dCas9-guided DNA methyltransferase (MTase) tool set by creating genetic fusions between the catalytically deficient dCas9 protein and the CpG-specific prokaryotic C5-MTase M.SssI. To improve the specificity of methylation, we used mutant forms of M.SssI. Initial testing of the targetable chimeric MTases in *E. coli* indicated that the fusion construct involving the Q147L mutant of M.SssI provided the highest specificity. Targeted DNA methylation experiments in cultured breast cancer cells were performed in collaboration with M. G. Rots' laboratory at Groningen University. Promoter regions of the HesI, YYI, SLC9A3R1 and CD44 genes implicated in endocrine therapy resistance were targeted by transiently expressing the dCas9-MSssI protein. Analysis of gene expression by qPCR showed that CD44 expression could be repressed by methylation of the CD44 promoter. To be able to select transfected cells by cell sorting, a plasmid expressing the dCas9-M.SssI-P2A-mCherry fluorescent fusion protein was constructed.

We have constructed plasmid vectors and developed a method facilitating combination of approaches involving transient expression as well as stable expression of epigenetic effectors in mammalian cells.

Supervisor: Antal Kiss
E-mail: koncz.mihaly@brc.mta.hu

Functional characterization of the mevalonate-isoprenoid biosynthesis pathway genes in *Mucor circinelloides*

Dileep Kumar

Department of Microbiology, Faculty of Science and Informatics, University of Szeged, Szeged, Hungary

Members of the subphylum Mucoromycotina, order Mucorales (such as *Lichtheimia, Mucor, Rhizomucor* and *Rhizopus* species) are saprotrophic fungi, which also have industrial and agricultural importance. Several species belonging to this fungal group are also considered to opportunistic pathogens, which can cause fatal systemic infections (so-called mucormycosis) in immunocompromised patients.

Metabolites synthesised via the mevalonate-isoprenoid pathway (such as sterols, functional groups of proteins and carotenoids) play an important role in signal transduction, morphogenesis, adaptation to environmental change and protection against free radicals. Nowadays ergosterol and its biosynthesis is the major target of the antifungal agents used in clinics. The therapy of mucormycosis is still limited because of the intrinsic resistance of these fungi to the majority of the currently used antimycotics. To date little is known about the function and regulation of the mevalonate-isoprenoid biosynthesis pathway genes in Mucoromycotina fungi. Our aim was to characterize six genes of that pathway in *Mucor circinelloides*, encoding the HMG-CoA synthase (*hmgS*), mevalonate kinase (*mvk*), diphosphomevalonate decarboxylase (*dmd*), isopentenyl pyrophosphate isomerase (*ipi*), farnesyl pyrophosphate synthase (*isoA*) and geranylgeranyl pyrophosphate synthase (*carG*).

Effect of different cultivation conditions on the gene transcriptions was analyzed. Plasmids were constructed for silencing and overexpression of the genes and the micromorphology of the mutants was analyzed. Silencing of the mevalonate-isoprenoid genes led to significant reduction in the ergosterol content in comparison with the wild-type strain, furthermore increased carotenoid content was determined in the transformants harbouring the *mvk*, *ipi* or *carG* gene in extra copies. Overexpression and silencing of the *hmgS*, *dmd* and *ipi* genes led to significant change in the susceptibility to azoles and statins. Phagocytosis assay with the mutants and MH-S macrophages was also performed.

This work was supported by the Hungarian Government and the European Union within the frames of the Széchenyi 2020 Programme through grant GINOP-2.3.2-15-2016-00012: The infrastructural background was established with the support of GINOP-2.3.3-15-2016-00006 grant (Széchenyi 2020 Programme).

Supervisors: Csaba Vágvölgyi, Árpád Csernetics
Email: deepmicro88@gmail.com

Volume 62(1):83-105, 2018
Acta Biologica Szegediensis
http://abs.bibl.u-szeged.hu/index.php/abs

DOI:10.14232/abs.2018.1.83-105

A novel pathophysiological evidence for HCN channels in absence seizures and role of brain pericytes in inflammatory responses induced by bacterial-derived agents *in vivo*

Ádám Mészáros[1,2]

[1]Department of Physiology, Anatomy and Neuroscience, University of Szeged, Szeged, Hungary
[2]Institute of Biophysics, Biological Research Centre of the Hungarian Academy of Sciences, Szeged, Hungary

Hyperpolarization-activated cyclic nucleotide-gated (HCN) channels and the I_h current they generate contribute to the pathophysiological mechanisms of absence seizures (ASs), but their precise role in thalamocortical circuit, the main components of the network underlying AS generation remains controversial. Thus, we showed that the pharmacological block of HCN channels with the antagonist ZD7288 applied via reverse microdialysis in the ventrobasal thalamus (VB) of freely moving GAERS decreases TC neuron firing and abolishes spontaneous ASs. Moreover, thalamic knockdown of HCN channels via virally-delivered shRNA into the VB of Stargazer mice decreases spontaneous ASs and I_h-dependent electrophysiological properties of TC neurons. These findings provide the first evidence that block of TC neuron HCN channels prevents ASs and suggest that any anti-absence therapy that targets HCN channels should consider the opposite role for cortical and thalamic I_h in the modulation of ASs. Cerebral pericytes are perivascular cells involved in the formation and control of the neurovascular unit (NVU). Growing evidence suggests that they also play definitive role in neuroinflammation. Among the pattern recognition receptors common to the innate immune system, we previously detected *in vitro* expression of several NOD-like receptors both basally and, in response to inflammatory mediators. Upon inflammatory stimuli, these receptors with other inflammasome components recruit and activate caspases via canonical or non-canonical routes, resulting in cleavage of precursor cytokines or pyroptosis. To assess the inflammasome activation *in vivo*, either outer membrane vesicles (OMVs) isolated from *E. coli* bacteria or lipopolysaccharide are administered into the common carotid artery of transgenic mice that express red fluorescent protein (DsRed) in perivascular cells. Two-photon-assisted imaging and immunohistochemical stainings are in progress to elucidate if inflammasome activation can induce changes in the function of the NVU after such an inflammatory challenge.

Supervisors: Magor L. Lőrincz, István Krizbai
E-mail: eubeandroo@gmail.com

Processes of selenium toxicity in different plant species

Árpád Molnár

Department of Plant Biology, Faculty of Science and Informatics, University of Szeged, Szeged, Hungary

Selenium is a non-metal element essential to all living organisms except higher plants. Accumulated selenium is able to damage plants *via* toxic processes, such as: disturbances in carbon and nutrient metabolism, disturbance in hormonal homeostasis, non-specific seleno-amino acid production and nitro-oxidative stress. Nitro-oxidative stress consists of abnormal ROS and RNS homeostasis and changes to macromolecules *via* nitration or nitrosilation. I studied protein tyrosine nitration, which is irreversible in plants and most likely inactivates the protein. The experiments were carried out on plant species with different selenium tolerance. Selenium sensitive Arabidopsis (*Arabidopsis thaliana*) was compared with selenium tolerant indian mustard (*Brassica juncea*); a selenium sensitive medicinal plant, *Astragalus membranaceus* was compared to a selenium hyperaccumulator *Astragalus bisulcatus*. The research was conducted in three different experimental designs and the treatment was with sodium selenite and selenate. We measured total selenium content, morphology, viability, ROS and RNS levels and protein tyrosine nitration.

In all experiments plants have accumulated selenium, which changed the morphology of sensitive plants. Protein tyrosine nitration was most significant in *Astragalus membranaceus* compared to all other plant species, describing a heavy stress and a reduction of the active protein pool. In the experiments where different selenium forms were compared, selenite was more toxic compared to selenate.

According to our data there is a strong correlation between selenium sensitivity and protein tyrosine nitration. The tolerant plants

DOI:10.14232/abs.2018.1.83-105

species can cope better with protein tyrosine nitration compared to the sensitive species, where the nitration is more significant.

This work was supported by the János Bolyai Research Scholarship of the Hungarian Academy of Sciences and by the National Research, Development and Innovation Fund (Grants no. NKFI-6, K120383 and NKFI-1, PD120962).

Supervisor: Zsuzsanna Kolbert
E-mail: molnara@bio.u-szeged.hu

Brain state dependent activity of thalamocortical cells

Benedek Molnár

Department of Physiology, Anatomy and Neuroscience, Faculty of Science and Informatics, University of Szeged, Szeged, Hungary

The mammalian brain exhibits various brain states including focused attention, relaxed wakefulness, sleep etc. These states are associated with altered neural activity in various brain structures and can change on a rapid time scale. Recent results suggest that the activity of the neurons in the somatosensory and the visual cortex correlate with these brain state changes, but whether and how neurons in subcortical regions are involved in this phenomenon has remained elusive. The thalamus relays sensory information to primary sensory cortical areas. In our experiments we focused on the brain state dependent fluctuations of neurons in the visual thalamus, *i.e.* the lateral geniculate nucleus (dLGN) which conveys visual information to the primary visual cortex (V1).

We used electrophysiological methods to record the electrical activity of individual neurons in the dLGN and V1 while simultaneously monitoring the local field potential in the dLGN and V1 and pupil diameter of awake, head restrained mice. Pupil diameter is a well-established indicator of brain states. The pupil of the mouse was recorded using a high frame rate (300 fps) infrared camera and the pupil diameter quantified using custom written routine in ImageJ software. Our results show that the spontaneous electrical activity including extracellular action potential output and the membrane potential of the majority of dLGN neurons is positively correlated with pupil diameter, whereas a minority of neurons negatively correlated and the remainder not correlated. To assess the effects of brain states on thalamic visual information processing we presented moving gratings of 8 different orientations presented on a PC screen 20 cm from the contralateral eye of the mouse. Our data analysis suggests that the orientation tuning of thalamocortical neurons in the dLGN is also varies slightly with brain state dynamics, leading to a further suggestion that brain state modulation also affects visual performance.

Supervisor: Magor Lőrincz
E-mail: molnar.benedictus@gmail.com

Exploring evolutionary processes by targeted *in vivo* mutagenesis

Ákos József Nyerges

Biological Research Centre of the Hungarian Academy of Sciences, Szeged, Hungary

Genome engineering has opened a new avenue of research in biology. By constructing mutations orders of magnitude faster than natural evolution genome engineering made the analysis of long-term evolutionary processes feasible within laboratory timescales.

Since the underlying mutations of such processes are rare, efficient exploration of the sequence space requires maximal control over the position and rate of mutagenesis. Specifically, directed evolution of protein complexes and biosynthetic pathways remains a formidable problem, not least because improvement of such traits frequently demands acquisition of multiple mutations simultaneously, many of which provide little or no benefit individually. Technologies enabling targeted mutagenesis of multiple loci in their native genomic context are needed for these goals to be met, however, current *in vivo* mutagenesis methods suffer from serious limitations.

My research addresses the aforementioned limitations of current mutagenesis methods. We developed a technology that enables *in vivo* targeted mutagenesis and precisely generates vast genetic diversity along the full length of multiple, predefined genomic loci.

We demonstrate the potential of this technology by mutagenizing antibiotic resistance genes and comprehensively analyzing

Volume 62(1):83-105, 2018
Acta Biologica Szegediensis
http://abs.bibl.u-szeged.hu/index.php/abs

DOI:10.14232/abs.2018.1.83-105

mutational processes behind antibiotic resistance in multiple bacterial species. We investigate how resistance develops against existing and novel antibiotics and compare these evolutionary processes across pathogens. Moreover, we analyze previously undetected resistance-conferring mutations and generate sensitive structure-activity relationship maps on drug targets.

Finally, we also demonstrate that our targeted mutagenesis technology can be exploited to analyze the mode-of-action of antibacterial drugs in pathogenic bacteria and develop antibiotics that are less likely to suffer from resistance development. Moreover, it is also ideal for biotechnological applications demanding optimization of multiple genomic loci.

Supervisor: Csaba Pál
E-mail: nyerges.akos@brc.mta.hu

Photoautotrophic H_2 production in *Chlamydomonas reinhardtii*

Anna Podmaniczki

Institute of Plant Biology, Biological Research Centre of the Hungarian Academy of Sciences, Szeged, Hungary

The green alga *Chlamydomonas reinhardtii* is one of the most popular organisms used in the research on the photoproduction of H_2. Its hydrogenase enzyme, located in the chloroplast, is highly active, but very sensitive to O_2. H_2 production can be induced by depriving the algae of sulphur, which results in the loss of photosystem II (PSII), responsible for O_2 evolution. However, sulphur deprivation has disadvantages, namely that its effects are unspecific, and it results in irreversible damage and removing sulphur from the culture is a time-consuming process. A less common method for inducing H_2 production is to prepare dense alga cultures, place them in the dark for a few hours under N_2 atmosphere, during which hydrogenases are expressed. When these cultures exposed to light, an initial burst of H_2 production occurs that is subsequently suppressed by O_2 released during photosynthesis. During my PhD studies, we have discovered that continuous and efficient H_2 production lasting for several days can be achieved by keeping the Calvin-Benson cycle inactive by substrate limitation; the protocol we have developed is also fully photoautotrophic, meaning that the electrons used for H_2 production are derived mostly from water.

Our novel H_2 production protocol was also tested on various photosynthetic mutants, including mutants with truncated antenna (*tla3*), reduced chlororespiration (*NDA1*), reduced cyclic electron transport (*pgrl1*), increased amount of PSII reaction center (L159I-N230Y) and reduced state transition (*stt7*). We found that the *pgrl1* mutant produced about approx. 60% more H_2 than the wild-type. A further improvement in H_2 production was achieved also by employing short regeneration phases every 24 hours, which consist of feeding the cultures with CO_2 followed by a dark period. We have also built a photobioreactor with optimized liquid to gas phase ratio and automated gas removal.

Supervisor: Szilvia Zita Tóth
E-mail: anna.podmaniczki@gmail.com

Arabidopsis glutathione peroxidase-like5 (AtGPXL5) is involved in salt stress response and has a function in both the ethylene evolution and polyamine homeostasis

Riyazuddin Riyazuddin

Department of Plant Biology, Faculty of Science and Informatics, University of Szeged, Szeged, Hungary

Plants contain GPX-like (GPXLs) enzymes and are closely related to animal phospholipid hydroperoxide glutathione peroxidases (PHGPX) which play a very important role in protecting against oxidative damage of membranes. Plant GPXLs are regarded to be less important as peroxide scavengers, but it was suggested that they could take part in H_2O_2-based redox regulation. Reactive oxygen species (ROS) and especially H_2O_2 are important compounds of the oxidative stress responses. There are several regulators of ROS homeostasis, among them polyamines (PA) and the plant hormone ethylene. It came to know that the role of ethylene and PAs in signalling processes rather than their accumulation chiefly influences abiotic stress tolerance. Our aim was to investigate the role of AtGPXL5 isoenzyme in response to salt treatment and the ethylene precursor ACC (1-aminocyclopropane -1-carboxylic acid) using *Atgpxl5* T-DNA insertional mutant plants.

The number of lateral roots, length of roots, superoxide level ($O_2^{\cdot -}$), viability and ROS levels were investigated in shoots and roots

Volume 62(1):83-105, 2018
Acta Biologica Szegediensis
http://abs.bibl.u-szeged.hu/index.php/abs
DOI:10.14232/abs.2018.1.83-105

of 12-day-old *Arabidopsis thaliana* Col-0 (wild type) and *Atgpxl5* seedling after one week of treatments using fluorescent microscopy. In another experimental system the wild type and mutant plants grown for 6 weeks in hydroponic system were treated with 1 μM ACC and 100 mM NaCl for 24 hours. Beside measurements of the H_2O_2, malondialdehyde (MDA), ethylene and free PA levels, the activities of diamine oxidase (DAO), polyamine oxidase (PAO) enzymes were determined. The transcript amounts of selected genes were also investigated by RT-qPCR.

The *Atgpxl5* seedlings had more lateral roots even under control conditions, accumulated higher level of ROS and exhibited lower viability than wild type. According to our results, the PA and ethylene amounts changed inversely in mutants after the used treatments, indicating important role of AtGPXL5 protein in regulation of PA and ethylene levels especially under stress conditions.

Supervisor: Jolán Csiszár
E-mail: riyazkhan24992@gmail.com

Secreted aspartic proteases from *Candida parapsilosis* regulate host complement attack and inflammatory responses

Dhirendra Kumar Singh

Department of Microbiology, Faculty of Science and Informatics, University of Szeged, Szeged, Hungary

Candida parapsilosis is an opportunistic fungal pathogen responsible for approximately 30% of the candidaemia episodes in low birth weight infants, while accounts for 10-15% of *Candida* infections in adults. During the infection, fungal secreted aspartic proteases (Saps) play an important role in evading the first line of host defense including the complement responses. However, no detailed studies have been done to investigate the role of Sapps in impairing the host innate immune response including host complement attack. Thereby, in this study, we sought to delineate the exquisite role of Sapps in *C. parapsilosis* mediated pathogenesis. To examine the effect of complement proteins on the growth of the *C. parapsilosis* GA1 (wild-type) and *sapp* $^{-/-}$ strains, their growth was measured in YPD and YCB liquid medium supplemented with 20% of either normal human plasma Data derived from both colony forming unit (CFU) counting and growth kinetics showed that the *sapp* $^{-/-}$ was hypersensitive to the presence of NHP compared to the wild-type. Deletion of *CpSAPPs* neither affects biofilm formation, nor the morphological attributes of *C. parapsilosis*. Virulence properties of both strains were also tested and showed that *sapp* $^{-/-}$ strain induced less damage to human epithelial cells, THP-1 cells and to PBMC-DMs. THP-1 and PBMC-DM's killed and phagocytosed *sapp* $^{-/-}$ cells more efficiently. Furthermore, when examining host cytokine responses, the wild-type strain induced higher levels of IL-1β, TNF-α and IL-8 than the *sapp* $^{-/-}$ strain. We also found that Sapp1p and Sapp2p proteins efficiently inactivate host complement factors such as C3b, C4b and factor H.

In summary, our results indicate that *SAPPs* are an indispensable factor in *C. parapsilosis* mediated virulence.

This study was supported by the Hungarian Government and the European Union within the frames of the Széchenyi 2020 Programme through grant GINOP-2.3.2-15-2016-00035. The infrastructural background was established with the support of GINOP-2.3.3-15-2016-00006 grant (Széchenyi 2020 Programme).

Supervisor: Attila Gácser
E-mail: dhirendrabhadauria03@gmail.com

Investigation of the archery related skeletal changes in the series of the 10th century AD cemetery of Sárrétudvari-Hízóföld

Balázs Tihanyi[1,2]

[1]Department of Biological Anthropology, Faculty of Science and Informatics, University of Szeged, Szeged, Hungary
[2]Department of Archaeology, Faculty of Arts, University of Szeged, Szeged, Hungary

In this presentation we introduce the preliminary results of an anthropological investigation of archery-induced stress markers on the skeletons of the Hungarian Conquest Period (10th century AD) cemetery of Sárrétudvari-Hízóföld. According to historical and archaeological data the bow was a common weapon in this era and the Hungarian army based on highly skilled mounted archers. In the Sárrétudvari-Hízóföld cemetery the archery equipment is a frequent type of the grave goods- 58 graves contained arrowheads, quivers

Volume 62(1):83-105, 2018
Acta Biologica Szegediensis
http://abs.bibl.u-szeged.hu/index.php/abs

DOI:10.14232/abs.2018.1.83-105

or bow plates, which suggests that archery was one of the main activities of the concerned population. Our main question is whether anthropological data also reflect this fact, or not. We focused on the so called activity related changes that occur on the skeleton as a result of physical stress, such the entheseal changes, the joint changes, metrical data, traumas and certain types of non-metrical variations. Macroscopic analysis was performed on the bones of the upper limb - the scapulas, claviculas, humeruses, radiuses and ulnas of the "archer" graves and the unarmed adult male graves. Among the different types of activity related changes we found hypertrophy at the attachment of a wide scale of muscles of the upper body and a few of them - such as *m. deltoideus, m. pectoralis major, m. latissimus dorsi, m. brachialis and m. biceps brachii* - appear in high frequency. As a preliminary result we can state that the anthropological and archaeological data do support each other concerning the application of archery in the population in question.

Supervisors: György Pálfi, László Révész
E-mail: balazs0421@gmail.com

Characterization of a novel G-quadruplex binding protein

Ágnes Tóth

Institute of Genetics, Biological Research Centre of the Hungarian Academy of Sciences, Szeged, Hungary

The basic criterion for staying alive for any living organism is the preservation of the genomic integrity, therefore the greatest challenge in this process is the correct replication of the genetic information during cell division. In order to create an accessible template for the replication process, single-stranded DNA is formed by the unwinding of the parental double-stranded DNA. Since single-stranded DNA sequences often form stable secondary structures, which represent replication blockades, for complete replication, cell division, and for the prevention of apoptosis and cell death these structures must be resolved.

One of the most studied blocking DNA structure is the G-quadruplex (also called G4), which in the recent years has emerged as a key regulatory cis element in essential cellular processes, like transcription, translation, replication and recombination.

The replicative polymerases are primarily blocked by the stable secondary structure-forming DNA sequences, therefore, the cooperation of DNA helicases and DNA polymerases is needed for replication. Some key players of this process are already known, recently it has been described that the mutation rate of G4 sequences increases in the absence of the yeast Pif1 or human FANCJ protein. In order to gain more information about this complex process we searched for uncharacterized players of G4 replication. Here we report the biochemical characterization of a novel G-quadruplex binding protein, which possible function could be the synchronization of the G4 unwinding helicases and DNA polymerases.

Supervisors: Péter Burkovics, Lajos Haracska
E-mail: toth.agnes@brc.mta.hu

Identification of ascorbate transporters in higher plants and in green algae

Dávid Tóth

Institute of Plant Biology, Biological Research Centre of the Hungarian Academy of Sciences, Szeged, Hungary

Ascorbate (also called vitamin C) is a multifunctional metabolite in plants. It is an antioxidant and coenzyme for a number of metabolic reactions. It also participates in cellular development, cell wall synthesis and regulation of gene expression.

Ascorbate is produced in the mitochondria and for fulfilling its multiple roles in the cell, it must be transported through several membrane systems. Because of its size and negative charge at physiological pH, ascorbate cannot freely diffuse through membranes. In plants until now, there was only one ascorbate transporter identified, a chloroplastic phosphate transporter, with dual function, called PHT4;4. However, this cannot be the only one chloroplastic ascorbate transporter, because the *pht4;4* knockout mutant does not show any alteration in phenotype.

Our approach to identify chloroplastic ascorbate transporters is based on coexpression analysis using the key ascorbate biosynthesis gene, *vtc2* as a bite, against all the chloroplast-localized transporters. We have found several genes showing relatively high coexpression with *vtc2*. Altogether we screened about 120 T-DNA lines for about 30 transporter proteins, and 5 putative ascorbate transporters were found. We started the characterization of these lines and the initial results confirm that we indeed found novel ascorbate transporters.

Volume 62(1):83-105, 2018
Acta Biologica Szegediensis
http://abs.bibl.u-szeged.hu/index.php/abs
DOI:10.14232/abs.2018.1.83-105

We have also started the molecular characterization of these lines.

We have found 3 homologs (PHT3, PHT4, PHT7) of the PHT4;4 protein in the green alga *Chlamydomonas reinhardtii* and the *PHT3* and *PHT7* genes responded strongly to oxidative stress treatment. In order, to study the function of these proteins, the recently developed CRISPR/Cpf1 genome editing technique was used to generate knockout *PHT3* and *PHT7* lines. The mutant lines show a retarded growth phenotype and decreased photosynthetic performance particularly at high light intensities. In order, to study the cellular localization of these proteins, we started generating YFP constructs.

Supervisor: Szilvia Zita Tóth
E-mail: toti86@brc.hu

Lipid biomarkers - a renewed verification method for the better diagnosis and evaluation of ancient TB infection

Orsolya Anna Váradi[1,2]

[1]Department of Biological Anthropology, Faculty of Science and Informatics, University of Szeged, Szeged, Hungary
[2]Department of Microbiology, Faculty of Science and Informatics, University of Szeged, Szeged, Hungary

The research of tuberculosis (TB), the pathomechanism and evolution of its infectious agents is surpassingly important since TB is still the 9th leading cause of death. According to the estimation of the WHO 10,4 million people got ill in 2016. TB is caused by the members of the *Mycobacterium tuberculosis* complex, especially by *M. tuberculosis*. Scholars proved that the disease has been presented as a human pathogen at least for 10000 years, but it is widely known since the beginning of the 20th century for its high mortality. The worldwide spread of the TB related problems (e.g. the spread of MDR strains, co-infections) resulted in fast development of the diagnostics. The traditional methods (e.g., acid-fast staining, histology) are going to be replaced in the clinical practice with faster and more effective diagnostic methods which are based on the DNA and lipid biomarker analysis. Their high sensitivity and their target molecules make them suitable to be adapted to osteoarchaeological purposes, and complement the traditionally used macromorphological investigations.

The key elements are the so-called mycolic acids, because they can be preserved in the bones for ages due to their high representation in the lipid rich mycobacterial cell wall, and their structure. The composition of the mycolic acids is supposed to be characteristic to the different species of the Mycobacteria. Our main task was to establish a lipid biomarker based method by the combination and optimization of two existing methods, which allows us to compare the mycolic acid composition of certain Mycobacterial species, in order to differentiate several Mycobacteria and to exclude the false negative results of the environmental *Mycobacteria*. Our main aim is to make comprehensive paleoepidemiological investigations through the examination of bone samples from different archaeological sites.

The infrastructural background of this research was established with the support of GINOP-2.3.3-15-2016-00006 grant (Széchenyi 2020 Programme).

Supervisors: György Pálfi, András Szekeres
E-mail: varadi.orsolya.90@gmail.com

Examination of potential epigenetical targets of Huntington's disease in *Drosophila melanogaster*

Júlia Varga

Department of Biochemistry and Molecular Biology, Faculty of Science and Informatics, University of Szeged, Szeged, Hungary

Huntington's (HD) disease is a dominantly inherited, late onset, progressive neurodegenerative disorder with characteristic motor, psychiatric and cognitive symptoms. HD is caused by an expansion of a CAG trinucleotide repeat in the first exon of the *huntingtin* gene, which results in an expanded polyglutamine (polyQ) domain in the Huntingtin (Htt) protein. Huntington's disease has a multifaceted molecular pathomechanism that disturbs several cellular processes. Mutant Htt forms intracellular aggregates and participates in abnormal interactions with other proteins. Mutant Htt interacts with histone acetyltransferase enzymes that regulate transcription by modifying lysine (K) residues on histone proteins. These interactions disturb the acetylation balance and lead to transcriptional dysregulation.

Volume 62(1):83-105, 2018
Acta Biologica Szegediensis
http://abs.bibl.u-szeged.hu/index.php/abs

DOI:10.14232/abs.2018.1.83-105

My aim was to characterize the effect of histone acetylation in HD pathogenesis by investigating the influence of the cytosolic acetyltransferase Hat1 and specific histone modifications in a *Drosophila* model of the disease.

To be able to study the role of Hat1 in HD pathogenesis I generated a Hat1 null mutant by P-element remobilization. We found that Hat1 is responsible for the majority of H4K5 and H4K12 acetylation in embryos and influences the transcription of more than 2000 genes, causing a developmental delay. Even though these transcriptional changes, Hat1 mutants are viable and fertile. I found that partial loss of Hat1 moderately ameliorates neurodegeneration in the *Drosophila* HD model. We also studied the effects of histone H4 acetylation marks in the HD model. We generated His4r transgenic lines with substitutions that change specific lysines to glutamine (Q), mimicking acetylated K, or to arginine (R), mimicking not-modified K. Our data show that H4K8Q and H4K16Q substitutions had a positive effect on viability and longevity of the *Drosophila* HD model.

The work was supported by NKFIH grant K112294.

Supervisor: László Bodai
E-mail: sajjul@freemail.hu

Analysis of mitochondrial functions in stress response

Mónika Varga

Laboratory of Arabidopsis Molecular Genetics; Institute of Plant Biology, Biological Research Centre of the Hungarian Academy of Sciences, Szeged, Hungary

Mitochondria, plays central role in the efficient provision of energy for eukaryotic cells by producing adenosine triphosphate and it is also important in production of reactive oxygen species (ROS) which are involved in cellular signalling and stress response in plants. Stabilization of the electron flow in the mitochondrial ETC can protect plants by reducing oxidative damage as well as control of redox balance and support photosynthesis during stress.

Here we describe the *Arabidopsis thaliana cyc1.1* and *cyc1.2* mutants in which T-DNA insertions disrupt the *CYC1-1* and *CYC1-2* genes, respectively. The highly homologous CYC1-1 and CYC1-2 proteins are members of Cytochrome C1 family, and are integral subunits of Complex III, forwarding electrons toward cytochrome c. The two mutants display morphological differences under stress conditions. Phenotype of *cyc1.1* is very similar to the wild type under non-stress conditions. However, under oxidative stress, root growth rate of *cyc1.1* is higher. Measuring rosette size and chlorophyll content also revealed that *cyc1.1* plants are more resistant to oxidative stress. On the other hand, *cyc1.1* is slightly more sensitive to salt stress than *cyc1.2* and wild type. Moreover, *cyc1.2* plants have smaller rosettes and delayed flowering under non-stress conditions and are able to survive for longer time under severe salt stress than wild type or *cyc1.1*. In double mutants with insertions in both *CYC1-1* and *CYC1-2* genes, the electron transport through Complex III presumably strongly reduced, leading to embryo lethality. These observations indicate that CYC proteins have essential function in Complex III.

Although, the studied homologous proteins have very similar structure, our data suggest that they differ from each other in functional properties which influence stress response. Our results suggest that *CYC* genes can be potential targets for engineering in crop plants with aims to improve tolerance to drought or salinity.

Supervisor: Laura Alexandra Zsigmond
E-mail: monika.varga1@gmail.com

The evolution of complex multicellularity in fungi: from megaphylogenies to single cell transcriptomics

Torda Varga

Synthetic and Systems Biology Unit, Institute of Biochemistry, Biological Research Centre of the Hungarian Academy of Sciences, Szeged, Hungary

The Kingdom Fungi is one of the few lineages where complex multicellular structures such as fruiting bodies evolved, however the genetic background of complex multicellularity in fungi is less known. Therefore our aim was to uncover the evolutionary patterns of fruiting body formation and on the genetic toolkit underlying complex multicellularity in fungi.

DOI:10.14232/abs.2018.1.83-105

Majority of the fruiting body forming fungi can be found in the class Agaricomycetes. By analyzing the variation in diversification rates of this class, we examined whether key innovations and mass extinction events have occurred during the evolution of mushroom forming fungi. To test these hypotheses, the most comprehensive phylogeny of Agaricomycetes was constructed to date. The analyses showed more than 100 shifts in diversification rate, and a putative mass extinction event during the course of evolution. We found that changes in diversification rates of lineages coincide with evolutionary innovations in fruiting body morphology. We found that the evolution of cap could be a key innovation which has contributed to the dominance of agaric mushrooms among extant Agaricomycete species. Hence, knowing the genetic background of fruiting body development would help to understand not only the evolution of complex multicellularity, but also cap formation in fungi, for which we chose an Agaricomycete model organism, *Coprinopsis cinerea*. The transition from single to complex multicellularity takes place when the fungal colony differentiates into a primary hyphal knot. To identify genes that involved into this transition and to examine the differentially expressed mRNA of different cell populations we used Laser-Capture Microdissection (LCM) coupled with single cell RNA Sequencing (scRNA-Seq). We developed a protocol for isolating high-quality RNA from fixed and laser micro-dissected cells and in preliminary scRNA-Seq analyses 50-90% of sequenced read could be mapped into exonic regions. In the future, we will further optimize the scRNA-Seq protocol to reveal the genetic toolkit involved in complex multicellularity and fruiting body development.

Supervisor: László G. Nagy
E-mail: varga.torda@gmail.com

Investigation on secondary metabolites of fungal endophytes from medicinal plants

Ramasamy Aruna Vigneshwari

Department of Microbiology, Faculty of Science and Informatics, University of Szeged, Szeged, Hungary

Natural sources are always infinite resources of the new molecules for drug discovery as the novel bioactive molecules or as alternative sources of existing ones. Endophytes are the microorganisms residing in the internal tissues of plants in a symbiotic relationship without causing any apparent diseases to the plants and they are one of the most promising sources of bioactive metabolites. Natural products from fungal endophytes have a broad spectrum of biologically active secondary metabolites and the recent literature is stating that 51% of the drugs isolated from endophytic fungi were previously unknown.

In our project, altogether 707 fungi have been isolated from eight different medicinal plant species in Hungary. The endophytic fungi from the parts of sampled plant were isolated and purified as well as started to identify. Then the individual strains were cultivated in a liquid medium and extracted sequentially with organic solvents for both the targeted and non-targeted screening the bioactive secondary metabolites. During the targeted screening, the endophytic fungi *Epicoccum nigrum* and *Alternaria sp*., isolated from the plant *Hypericum perforatum* has been identified as the producers of the host plant metabolites, hypericin and emodin. The presence of these compounds was qualitative and quantitative analysed using HPLC-UV analysis, which was further confirmed by UHPLC-HRMS and UHPLC-HRMS/MS techniques by comparing them with authentic standards and database entries. In the case of the non-targeted screening, the crude extracts of endophytic fungi isolated from various sources were screened for their antimicrobial activities against different bacterial pathogens for the purposes of the future purification of the active metabolites.

Our results could reveal that the endophytic fungi are one of the potential sources for the compounds, which have remarkable importance for pharmacological application.

This work was supported by the Hungarian Government and the European Union within the frames of the Széchenyi 2020 Programme through grant GINOP-2.3.2-15-2016-00012. The infrastructural background was established with the support of GINOP-2.3.3-15-2016-00006 grant (Széchenyi 2020 Programme).

Supervisor: András Szekeres
E-mail: arunabio2011@gmail.com

Volume 62(1):83-105, 2018
Acta Biologica Szegediensis
http://abs.bibl.u-szeged.hu/index.php/abs

DOI:10.14232/abs.2018.1.83-105

Incompatible symbiotic interactions between *Sinorhizobium meliloti* strain Rm41 and the ecotypes of the host *Medicago truncatula*

Ting Wang

Institute of Plant Biology, Biological Research Centre of the Hungarian Academy of Sciences, Szeged, Hungary

Legumes develop a symbiosis with nitrogen-fixing soil bacteria called rhizobia. In this relationship, legumes provide an optimal environment and energy source for rhizobia. In return, rhizobia fix atmospheric nitrogen into ammonia for the plants.

The legume-rhizobial interaction begins with a molecular dialogue between the two partners. Flavonoid are released into rhizosphere by legume roots, attract rhizobia and induce the synthesis and secretion of Nod factors. Nod factors induce the elongation and curling of the root hairs which trap rhizobial bacteria. Within these trap sites, infection threads are initiated and extended, through which the bacteria are released into new cells formed by the division of cells in the nodule primordium the meristem originated from cortical cells. In *Medicago truncatula*, the meristematic cells keep dividing and the infected cells and the bacteria therein develop into symbiotic cells forming the root nodule.

The nitrogen-fixing symbiotic relationship is highly selective: Particular rhizobial species or strains establish an efficient symbiosis with only a limited set of legume species or genotypes. In nature, *S. meliloti* developes a symbiosis with *Medicago* species like *M. truncatula* and forms root nodules. Interestingly, certain combinations of *S. meliloti* strains and *M. truncatula* ecotypes that otherwise form effective symbiosis with other partners lead to symbiotic incompatibility, i.e. nodule development is arrested.

We have screened more than 100 ecotypes of *M. truncatula* with different *S. meliloti* strains and identified incompatibility between *S. meliloti* strain Rm41 and *M. truncatula* ecotypes F83005 and Jemalong. To find out the reason, we performed random transposon mutagenesis of Rm41 and overexpressed all predicted ORFs of strain Sm1021 in Rm41. In this way, we identified a mutation that restored compatibility with F83005 and isolated a gene that could rescue normal nodule development in Jemalong. At present, we characterize both genes to find out how they contribute to the success of the symbiotic intercation.

Supervisor: Attila Kereszt
E-mail: wangting7336@gmail.com

Characterizing the activity of high fidelity Cas9 nucleases and polymerase III promoters widely used for expressing gRNAs to improve gRNA design

Nóra Weinhardt

Institute of Biochemistry, Biological Research Centre of the Hungarian Academy of Sciences, Szeged, Hungary

Cas9 nucleases are components of the CRISPR system and by making a complex with a small RNA (guide RNA) they can specifically cleave the target DNA, and by this enable editing of complex genomes. The specificity of nuclease is defined by the 5 ,end of the RNA molecule by its complementarity to the DNA sequence and the specificity can be easily reprogrammed by modifying this sequence. This simplicity is why they could make widespread and revolutionary changes in the field of molecular biology and genetic engineering over the past few years.

Last year we found that extending the guide RNA with an extra 5' G nucleotide diminishes the activity of the increased fidelity Cas9 variants (Kulcsár et al. 2017). For making use of the wild type SpCas9, this modification is routinely applied to guide RNAs starting with a non-G nucleotide in order to be effectively transcribed from the U6 promoter.

The U6 promoter is widely used for the expression of small RNAs such as Cas9 guide RNAs. The transcriptional initiation of the human U6 promoter is not precisely defined. It is generally accepted that RNAs are efficiently transcribed only from a starting guanine nucleotide, so that the length of the transcribed RNA molecule is influenced by the occurrence of the first guanine. It is an important issue when exploiting the increased fidelity SpCas9 nucleases to modulate cellular functions, as we just showed in our recent study.

DOI:10.14232/abs.2018.1.83-105

However, the precise nucleotide preference for the transcription initiation of the U6 promoter is not fully understood. Beside getting a more comprehensive picture of the U6 promoter, we aim to learn the preferences of another promoters. To study more systematically the sequence preferences of these promoters for initiating efficient transcription, I created RNA libraries and using next generation sequencing I will determine the sequence specificity of the promoters, thereby enabling more effective guide RNA sequences to be designed.

Supervisor: Ervin Welker
E-mail: nora.weinhardt@gmail.com

Molecular examination of smoking-related endothelial dysfunction in umbilical cord vessels

Szabolcs Zahorán

Department of Biochemistry and Molecular Biology, Faculty of Science and Informatics, University of Szeged, Szeged, Hungary

One of the most typical exogenous stress factors during pregnancy is the smoking. As cigarette smoke is known to contain a large number of prooxidants (*e.g.,* free radicals, heavy metals), many of the adverse effects of smoking may result from oxidative damage to critical biological substances. The effects of smoking on the adult body have been well studied, but the molecular background of the effects on the fetal development is poorly understood. A better understanding of the pathophysiological complications emerging during pregnancy necessitates detailed studies of the umbilical cord (UC).

Therefore, the object of our work was the UC, which is primarily responsible for the transport of oxygen and nourishment to the fetus. The UC vessels can be considered as direct elongation of the fetal vascular system, and particularly exposed to harmful agents that are not filtered out by the placenta. Our aim was to find adequate procedures to detect the impact of maternal smoking on intrauterine life. Our experiments were built around the endothelial nitric oxide synthase (NOS3). Because the UC vessels lack innervation, the endothelial cells (ECs) derived nitric oxide have crucial role in controlling blood flow and maintaining physiologic conditions. UC samples were used for morphological and immunohistochemical analysis. Structurally we found abnormal morphology and unequivocal devastated conditions of the ECs derived from neonates born to smoking mother (Sm). We found that the NOS3 activity was significantly dropped in Sm samples. Furthermore, with classic biochemical approaches on isolated vessels, we found elevated levels of prooxidants such as peroxynitrite, hydrogen peroxide and superoxide radical and, in parallel, inadequate response in antioxidant enzyme defence system's activity. Our results are indicating that the structural changes within the EC layer are closely related to the loss of essential regulatory functions. This effect is markedly driven by the increased oxidative stress and macromolecular damage, as a vicious circle. The long-term harmful exposure and the resulting lack of stress response can ultimately lead to endothelial dysfunction.

This work was funded by GINOP 2.3.2-15-2016-0040 („MyoTeam")

Supervisor: Edit Hermesz
E-mail: zahoran.szabolcs@gmail.com

Acta Biologica Szegediensis

Volume 62(1):107-113, 2018
Acta Biologica Szegediensis
http://abs.bibl.u-szeged.hu/index.php/abs

DOI:10.14232/abs.2018.1.107-113

ABSTRACTS OF UNKP CONFERENCE (MAY 30, 2018, SZEGED)

Antioxidant mechanisms accompanying physical exercise in estrogen depleted rat model

Denise Börzsei

Department of Physiology, Anatomy and Neuroscience, Faculty of Science and Informatics, University of Szeged, Szeged, Hungary

Myocardial extracellular matrix (ECM) plays an important role in the homeostasis of cardiovascular system. Changes in the structure of ECM can cause certain pathological processes, including the disregulation of matrix metalloproteinases (MMP).

The aim of our work was to investigate the cardiovascular effects of voluntary physical exercise against the disregulatory and detrimental consequences of MMP-2, linked with the measurement of ischemia/reperfusion injury.

In our experiment female Wistar rats were underwent either ovariectomy surgery (OVX) or sham operation (SO). After 4 weeks of resting period we divided them into subgroups based on the type of diet (CTRL: standard chow, HT: high-triglyceride diet) and exercise (running or non-running). At the end of the 12-week experimental period, the activity of 64 kDa and 72 kDa MMP-2, the level of total glutathione (GSH), the concentrations of nitrotyrosine (3-NT), tissue inhibitor of matrix metalloproteinase (TIMP-2), and type-I collagen were determined. Following 30 min LAD occlusion and 120 min reperfusion, the ratio of infarct size was also evaluated.

Our results clearly show, that estrogen deficiency and HT diet caused a significant increase in type-I collagen accumulation and in the ratio of infarct size, on the other hand the activity of MMP-2 and the level of TIMP-2, GSH, 3-NT was decreased. 12 weeks of physical activity resulted a significant increase in the level of TIMP-2, 3-NT, GSH as well as in MMP-2 activity, also due to the exercise training the collagen content and the infarcted area significantly reduced in each group.

Voluntary physical exercise can be a potential non-pharmacological strategy to ameliorate the adverse cardiovascular effects by enhancing of MMP-2 activity and reducing the accumulation of type-I collagen and the necrotic extension of heart.

Supervisors: Anikó Pósa, Renáta Szabó
E-mail: borzseidenise@gmail.com

Effects of tunicamycin on photosynthetic activity

Zalán Czékus

Department of Plant Biology, Faculty of Science and Informatics, University of Szeged, Szeged, Hungary

Tunicamycin (Tm) blocks N-linked glycosylation (N-glycans) and induce unfolded protein response (UPR) in plants. The UPR plays an important role in restoring the protein folding capacity of the ER membrane by increasing the levels of molecular chaperones and reducing the protein load into ER. At the same time, Tm can affect the biosynthesis of several components of photosynthetic apparatus. This potential effect can influence the activity of photosynthesis in higher plants. The aims of our work were to study photosynthetic activities after Tm and chemical chaperone treatments in order to reveal their changes upon stress condition.

Tm significantly decreased the maximal (Fv/Fm) and effective [Y(II)] quantum yield of PSII, as well as the effective quantum yield of PSI [Y(I)]. Interestingly, the quantum yield of non-regulated non-photochemical energy dissipation [Y(NO)] did not change significantly upon Tm, but the limitation of the quantum yield of regulated non-photochemical energy dissipation [Y(NPQ)] increased significantly under stress condition. Application of chemical chaperon could modulate the effects of Tm on photosynthetic activity. Not only parameters of photosynthetic activity, but also the product of photosynthesis (sugar and starch contents) were also analyzed, which contents changed significantly upon Tm treatments.

In conclusion, the effects of exogenous Tm application on photosynthetic activity can be significant, which can play a crucial role in UPR and plant defense under stress condition.

This work was supported by the UNKP-17-3 New National Excellence Program of the Ministry of Human Capacities.

Supervisor: Péter Poór
E-mail: czekuszalan@gmail.com

Volume 62(1):107-113, 2018
Acta Biologica Szegediensis
http://abs.bibl.u-szeged.hu/index.php/abs

DOI:10.14232/abs.2018.1.107-113

Molecular identification and characterization of mycoviruses of different filamentous fungi

Tünde Kartali

Department of Microbiology, Faculty of Science and Informatics, University of Szeged, Szeged, Hungary

Detection of double-stranded RNA (dsRNA) elements in fungal isolates suggests the presence of mycoviruses. More than 90 mycoviruses have been described and some of them can cause smaller or greater changes in the phenotype or may cause hypovirulence or hypervirulence. Mycoviruses lack the extracellular route for infection, thus they can be transmitted only intracellularly. All major phyla of fungi contain mycovirus-harboring fungal isolates; however, we have limited information about their distribution and their biological role in the host fungal cells.

The aims of this research were the screening of different fungal isolates for the presence of dsRNA molecules and for the precise identification and characterization of the isolated viruses. Our long-term goal is the examination of the effect of their presence on the host phenotype. We have screened different isolates belonging to *Umbelopsis*, *Mortierella*, *Dissophora*, *Lecanicillium*, *Mycogone* and *Armillaria* genera and we have detected dsRNA elements in 12-23% of more than 200 investigated isolates. We have found a high variability in the numbers and sizes of the detected dsRNA fragments between the genera as well as the isolates of the same genus. We have started the molecular analysis of the detected dsRNA fragments. Four dsRNA fragments were purified from *U. ramanniana* SZMC 11078 and one 6,1 kb size fragment from *Mucor hiemalis* SZMC 12056 strain. The sequence analysis revealed that the identified dsRNA fragments consist of two open reading frames, which are presumably encodes an RNA-dependent RNA polymerase and a capsid protein.

The purification of the virus-like particles (VLPs), polyacrylamide gel electrophoresis and transmission electron microscopy analysis of the purified VLPs are also in progress as well as Northern blot analysis to determine which dsRNA fragment encodes the identified genes.

This work was supported by the Hungarian Government and the European Union within the frames of the Széchenyi 2020 Programme through grant GINOP-2.3.2-15-2016-00052.

The infrastructural background was established with the support of GINOP-2.3.3-15-2016-00006 grant (Széchenyi 2020 Programme).

Supervisors: Ildikó Nyilasi, Tamás Papp
E-mail: kartalit@gmail.com

Signal interaction between nitric oxide (NO) and Rho GTPases during plant growth

Zsuzsanna Kolbert

Department of Plant Biology, Faculty of Science and Informatics, University of Szeged, Szeged, Hungary

Nitric oxide (NO) is a gaseous signal molecule which in cooperation with auxin regulates root developmental processes like primary root or root hair elongation and lateral root formation. Some of these physiological processes take place with the participation of plant-specific regulator Rho of Plants (ROP) proteins which are known to interact with auxin. ROPs act as molecular switches due to conformational changes upon GTP binding and hydrolysis facilitating transient interactions with effector proteins. Although, NO and ROPs as regulators share common interacting partner (auxin) and physiological process (root growth), their crosstalk has not been proven so far. My study aims therefore to examine a suspected ROPs-NO signal interplay in plants. I developed an experimental system, in which the NO sensing of different ROP mutant and reporter *Arabidopsis* lines were evaluated.

Compared to the wild-type (*Col-0*), *rop2-1* and *rop2-2* roots showed significant NO insensitivity, while *rop6* responded to the presence of NO donors similarly to *Col-0* (NO-induced root meristem shortening). In agreement with this, neither the rate nor the pattern of ROP6 *in situ* expression was affected by NO supplementation. The *in situ* expression of ROP2, however, decreased in the presence of NO, as well as the PIN-dependent auxin transport and auxin maximum in the root tip. Moreover, both *rop2* mutants possess elevated endogenous NO level in their root tip compared to *Col-0*, which further support the connection between NO and ROP2 signaling the root meristem.

Based on the results we can strongly suspect that exogenous NO negatively influences ROP2 action thus inhibits polar auxin transport and consequently the generation of auxin maximum leading to root meristem shortening. To confirm this conclusion, my further experiments will focus on providing direct evidence for the involvement of ROP2 in NO-induced root meristem shortening.

E-mail: kolzsu@bio.u-szeged.hu

Volume 62(1):107-113, 2018
Acta Biologica Szegediensis
http://abs.bibl.u-szeged.hu/index.php/abs

DOI:10.14232/abs.2018.1.107-113

Tool use in the ant subfamily Myrmicinae

Gábor Módra

Department of Ecology, Faculty of Science and Informatics, University of Szeged, Szeged, Hungary

The study of tool-using behavior is a rapidly developing part of behavioral ecological studies; however, most of these studies focus on vertebrate tool users. Our aim is, therefore, to widen our knowledge about tool use in insects, particularly in ants. Members of the genus *Aphaenogaster*, and a few other myrmicine species (*e.g., Messor*, *Pogonomyrmex*) use various objects as tools during foraging to transport liquid food sources. In our studies, we investigated the tool-using behavior of various myrmicine species. First, we aimed to detect foraging tool use in species where such behavior is unknown. Second, we aimed to gain more information about the basic mechanisms and possible flexibility of this behavior.

In our research, we successfully identified the following species as novel tool-users: *Aphaenogaster feae, Aphaenogaster beccari, Aphaenogaster iberica, Messor nondentata* and *Messor valentinae*. On the other hand, we failed to detect tool use in *Pheidole noda*. Species of *Aphaenogaster* and *Messor* all belong to a basal myrmicine clade, indicating that foraging tool use might have evolved very early in myrmicine ants. Since the tool-using behavior of *Messor* species seems to be different from that of *Aphaenogaster* species, we aim to compare these species to clarify the differences in their behavior. Furthermore, we are also planning to convey comparative phylogenetic analyses by investigating the foraging behavior of species from other related and unrelated myrmicine genera. In the other part of our study, we investigated in detail the tool-using behavior of *Aphaenogaster subterranea* by examining, how tool-using workers deal with various foraging challenges. We used different liquid baits and different types of tools with varying distances between the baits and the tools piled around them. Our results confirm that tool use in *A. subterranea* exhibits a high degree of flexibility. Ants seem to be able not only to optimize their foraging effort by selecting tools that are best matched to the particular foraging environment, but also to learn how to improve the use of certain tools by modifying them.

Supervisor: Gábor Lőrinczi
E-mail: modragabi@gmail.com

Development of molecular tools to study the virulence of the human fungal pathogen *Candida parapsilosis*

Tibor Mihály Németh

Department of Microbiology, Faculty of Science and Informatics, University of Szeged, Szeged, Hungary

Candida species are responsible for the majority of systemic fungal infections in humans. This is a life-threatening condition associated with high mortality rate affecting predominantly immunocompromised individuals. *Candida albicans* is considered as the predominant and therefore the most studied *Candida* species. Although other members of the genus also gained importance in the last decade, still much less effort has been made to study their patomechanism mostly due to the lack of molecular tools and genome editing approaches.

One of these emerging species is *Candida parapsilosis* that endangers low birth weight neonates in the first place. To gain insights into the factors making capable this species of causing such serious infections, we aimed to develop and optimize a set of molecular techniques. We adopted the state of the art Crispr Cas9 approach that has been described as the "bacterial adaptive immune system". Cas9 is an endonuclease that is capable of, introducing double stranded breaks (DSB) into specific sites of the DNA. The exact target site is appointed by an RNA compound called the guide RNA. DSB is a critical damage and therefore it must be repaired in one of two main ways. When an intact template is not present non-homologous end joining (NHEJ) occurs, in the presence of a template though, homology driven repair takes place that provides a more precise genome alteration than NHEJ.

By using this approach, we created deletion, reintegrant and overexpression mutants. It was also suitable for generating a GFP expressing strain. We found this system strain independent as we could create deletion and reintegrant mutants in all the six strains we subjected to genome alterations. Our plan is to use this technique for HIS- and GFP- tagging of proteins.

Supervisor: Attila Gácser
E-mail: narvaltm@gmail.com

Volume 62(1):107-113, 2018
Acta Biologica Szegediensis
http://abs.bibl.u-szeged.hu/index.php/abs

DOI:10.14232/abs.2018.1.107-113

Investigation of dark modulated ER stress

Péter Poór

Department of Plant Biology, Faculty of Science and Informatics, University of Szeged, Szeged, Hungary

Light is one of the most important environmental factors, which is required for optimal growth and development or during the stress responses of plants. Dark can alter the light-dependent activation of plant developmental or defense responses, it can induce new signaling and regulation pathways modulated by various signaling molecules such as reactive oxygen species (ROS). Tunicamycin (Tm) can induce unfolded protein response (UPR) in plants by blocking N-linked glycosylation (N-glycans). At the same time, Tm can induce the production of ROS and cause several changes in the activity of antioxidant enzymes, but ROS production can be dependent on the presence or absence of light in plants. The aims of our work were to study the effects of Tm and chemical chaperone treatments in the leaves of tomato plants in the light and dark.

Based on our result, Tm induced superoxide production was higher in those plants, which were kept in dark. In contrast to this, levels of H_2O_2 were higher in the illuminated leaves of tomato plants after treatment with Tm. The application of the chemical chaperon reduced the H_2O_2 production both in the light and dark environments. The expression of ER stress marker gene, *BiP* was significantly elevated by Tm in the light, but reduced by the application of chemical chaperon and dark. Expression levels of *IRE1α* and *β* were also elevated by the treatment with Tm in the light but did not change under darkness suggesting a specific role of the presence of the light in ER stress response.

In conclusion, the effects of exogenous Tm application on ROS production can be significant, which can be dependent on the presence or absence of light and can play a crucial role in UPR and plant defense under diverse environmental stimuli.

This work was supported by the UNKP-17-4 New National Excellence Program of the Ministry of Human Capacities.

E-mail: poorpeti@bio.u-szeged.hu

The role of exercise training on cardiovascular system in aging animal model

Anikó Pósa

Department of Physiology, Anatomy and Neuroscience, Faculty of Science and Informatics, University of Szeged, Szeged, Hungary

Aging is a major risk factor for cardiovascular diseases, which can be associated with oxidative stress, inflammation, cardiomyocyte death and cardiac morphological changes.

Echocardiography (ECHO), as a non-invasive imaging technique, provides insight into changes in cardiac structure and function related to aging-associated cardiovascular diseases. Exercise is a diagnostic and therapeutic tool, which may improve aging-influenced cardiac physiology and function.

The aim of our work was to study the potential use of voluntary wheel running exercise to prevent or treat the cardiac morphology and function in aged rats.

12-month-old female and male Wistar rats were divided into running and non-running groups.

At the end of 12-week period, echocardiographic measurements of rats were carried out under *i.m.* anesthesia. Following the ECHO examination, infarct size was also evaluated after 45 min LAD occlusion and 120 min reperfusion.

Fractional shortening (FS) and ejection fraction (EF) of running male and female animals were significantly as compared to matched aged control groups. Left ventricle systolic function was also evaluated measuring mitral annular plane systolic excursions (MAPSE), which showed a significant increase in running female rats. As a result of physical exercise, the E/A ratios were significantly elevated in both running genders, while the isovolumic relaxation time (IVRT) and Tei-index were significantly decreased in running males. The ratio of septal E'/A' and septal E/E' revealed a significant increase in running male groups in comparison to aged male rats. Right ventricle diastolic function was improved in running female animals. Moreover, 12 weeks of physical exercise reduced the infarct size in both female and male rats.

This work was supported by the UNKP-17-4 (Anikó Pósa), UNKP-17-3 (Renáta Szabó), and UNKP-17-2 (Denice Börzsei) New National Excellence Program of the Ministry of Human Capacities.

E-mail: paniko@bio.u-szeged.hu

Volume 62(1):107-113, 2018
Acta Biologica Szegediensis
http://abs.bibl.u-szeged.hu/index.php/abs

DOI:10.14232/abs.2018.1.107-113

The effects of voluntary physical exercise on the consequences of isoproterenol-induced myocardial infarction in experimental menopause

Renáta Szabó

Department of Physiology, Anatomy and Neuroscience, Faculty of Science and Informatics, University of Szeged, Szeged, Hungary

The incidence and progression of coronary artery diseases in premenopausal women are lower as compared to age-matched men but increases rapidly after the onset of menopause.

Fertile Wistar females (CTRL) and pharmacologically ovariectomized (POVX, 750 μg/kg triptorelin, *i.m.*, every 4th week) rats were used in our experiment. CTRL and POVX animals were randomly assigned to receive injection of 0.1 g isoproterenol (ISO)/kg. ISO is a synthetic β-adrenocepor agonist, which induces myocardial infarction (MI) in rats. At 24th hours after ISO injection serum markers of myocardial injury, such as LDH and myoglobin were measured. After a 3-week resting period ISO-treated and untreated animals were further divided based on the physical exercise. During a 6-week period, the running animals were placed into cages fitted with a running-wheel. At the end of the experiment the cardiac activity of antioxidative heme oxygenase (HO) enzyme, the expression of HO-1, the level of glutathione (GSH) and the activity of myeloperoxidase (MPO) were detected.

ISO treatment significantly increased the serum levels of LDH and myoglobin, which were more marked in POVX animals. At the end of the experimental period, MI resulted the lowest HO activity and HO-1expression in the heart of POVX animals, whereas 6 weeks of physical exercise significantly improved the HO and GSH values in both CTRL and POVX rats. Furthermore, our training protocol significantly reduced the pathological activity of MPO.

Our findings clearly demonstrate that 6 weeks of voluntary physical exercise is a potential non-pharmacological therapeutic strategy to ameliorate the antioxidative status and inflammatory parameters in women post-MI.

This work was supported by the UNKP-17-3 (Renáta Szabó), UNKP-17-4 (Anikó Pósa), and UNKP-17-2 (Denise Börzsei) New National Excellence Program of the Ministry of Human Capacities.

Supervisors: Anikó Pósa, Csaba Varga
E-mail: szaborenata88@gmail.com

Characterization of bioactive secondary metabolites produced by microorganisms

András Szekeres

Department of Microbiology, Faculty of Science and Informatics, University of Szeged, Szeged, Hungary

The natural products are naturally derived compounds playing a very important role in health care and prevention of diseases. Moreover, it is well established that natural products have been the sources for the development of many of the most effective drugs currently available for the treatment of a variety of human diseases. Natural products could be presented as metabolites from broad range of organisms including fungi and bacteria, which are almost infinite resources for drug discovery to provide new medicinal agents to the human health care and therapy.

In our research work, both the targeted and the activity-guided metabolic seeking were applied. In the case of targeted identifications, firstly unknown members of the known molecular families were identified including peptaibols and surfactins, which are produced mainly by *Trichoderma* and *Bacillus* species, respectively. On the other hand, endophytic fungi were isolated from medicinal plants possessing production of known, already clinically used compounds and production abilities of the host metabolites were tested in fermentation conditions. In these experiments, the taxol, hypericin and emodin were involved as the host metabolites of *Taxus baccata* and *Hypericum perforatum.* In the case of non-targeted screening, endophytic fungi were also isolated from the medicinal plants (*Artemisia asiatica, A. annua, Ononis spinosa, Juniperus communis, Ephedra distachya, Glycyrrhiza glabra, Asclepias syriaca, Calendula officianalis, Ricinus communis*) collected from the Hungarian areas, and bioactivity assays were applied for their crude extracts to find novel molecules showing anti-bacterial or antifungal effects.

Detailed knowledge on the properties of microbial secondary metabolites or discovery of new ones may provide valuable information about their potential applicability as lead molecules in the drug developments.

E-mail: andras.j.szekeres@gmail.com

Volume 62(1):107-113, 2018
Acta Biologica Szegediensis
http://abs.bibl.u-szeged.hu/index.php/abs

DOI:10.14232/abs.2018.1.107-113

The joint development of oral health literacy and critical thinking in the teaching of Biology

Ádám Szívós

Biology Methodology Group, Department of Physiology, Anatomy and Neuroscience, Faculty of Science and Informatics, University of Szeged, Szeged, Hungary

Critical thinking is one of the essential elements of scientific thinking. However, the analysis of Biology textbooks highlighted the lack of those tasks which improve critical thinking. Numerous biological topics are suitable for this purpose, especially the topic of the human anatomy and health. Within the confines of it, the development of students' health literacy is also possible. One of the specific areas of health literacy is the oral health literacy, whose state of development has an influence on oral hygiene and general health condition. Researches show that the oral hygienic condition of Hungarian population is maleficent, more than half of them have restricted health literacy. The joint development of critical thinking and oral health literacy is likely to happen on Biology classes, whose basis is that their common element is the evaluation as cognitive operation.

The goal of our research is to get familiar with the lack of knowledge concerning oral health literacy amongst university and high school students and using this information to create activities that help develop both critical thinking and oral health literacy.

Based on our research, for more than two thirds of the university students it is hard to judge the credibility of the dental information gained from the media, for 54% it is a problem to judge the advantages and disadvantages of different dental treatments. Based on the surveys filled out by high school students, it can be said that just like in the case of university students they cannot judge the credibility of the dental information gained from the media, and for 54% it is a problem to judge the advantages and disadvantages of different dental treatments. In 2018 spring, a task made by our research team was tested.

Later in our research, we plan to measure the developed tasks' efficiency using control groups. Moreover, we see the need for a research that focuses on the correlation between oral health literacy and status.

Supervisor: Erzsébet Antal Lászlóné Nagy
E-mail: szivosadam@gmail.com

The effect of salt stress on the maturity and quality of tomato fruits

Zoltán Takács

Department of Plant Biology, Faculty of Science and Informatics, University of Szeged, Szeged, Hungary

Excessive salinity is one of the most important environmental stress factors which greatly affects the growth, nutrition, and productivity of many plant species. Tomato is one of the most important horticultural crops in the world, which contains many health beneficial factors. However, salt stress can reduce the yield and quality of tomatoes. In this study we would like to detect the role of ethylene under salt stress. We have used the ethylene-insensitive *Never ripe* (*Nr*) tomato (*Solanum lycopersicum* L.) mutant for the experiments, which mutation blocks ethylene perception. Results in this mutant were compared to the wild type Ailsa Craig (WT) cultivar subjected to NaCl.

Aims of the present investigation was to study the effects of salt stress on quality and physiological responses of fruits, including ionic-, osmotic- and oxidative stress components. The changes in some growth parameters; ascorbic acid (AsA) and glutathione (GSH)-; H_2O_2-; malondialdehyde (MDA) content were also followed. Furthermore, we analyzed the activity of different antioxidant enzymes in both tomato genotypes.

Reduced fresh weight and diameter of fruits, as well as decreased width of exocarpium were observer upon salinity stress in both genotypes. WT exhibited higher Na^+ accumulation, dehydroascorbic acid (DHA) and total and reduced GSH content under salt stress. It is well known that, ethylene can regulate the metabolism of reactive oxygen species (ROS) by modulating antioxidant enzymes. Fruit cells showed increased H_2O_2 production, MDA content and enhanced guaiacol peroxidase (POD, EC 1.11.1.7) activity under NaCl treatment. Interestingly, activity of catalase- (CAT, EC 1.11.1.6) and superoxide dismutase (SOD, EC 1.15.1.1) did not change in WT fruits after salt exposure.

DOI:10.14232/abs.2018.1.107-113

Overall, these results indicate that ethylene signaling can modulate the activity of antioxidant enzymes and can influence fruit quality under salt stress.

Supported by the UNKP-17-3-III-SZTE-35 New National Excellence Program of the Ministry of Human Capacities.

Supervisors: Irma Tari, Péter Poór
E-mail: takacszoltan8923@gmail.com

Comparison of neutrophil response to *Curvularia* and *Aspergillus* species

Eszter Judit Tóth[1,2]

[1]Department of Microbiology, Faculty of Science and Informatics, University of Szeged, Szeged, Hungary
[2]MTA-SZTE "Lendület" Fungal Pathogenicity Mechanisms Research Group, Szeged, Hungary

Opportunistic fungal infections represent a continuously increasing problem, because of the growing population with underlying conditions, the difficulties of diagnosis and the high antifungal resistance of certain fungal agents. Members of the genus *Curvularia* (Ascomycota, Pleosporales) are known as plant pathogenic filamentous fungi. Some members of this genus, like *C. lunata*, have been recovered from human infections known as pheaohyphomycoses. These mycotic infections can manifest as fungal keratitis, sinusitis, cutaneous lesions or invasive infections. The aim of this study was to investigate the neutrophil granulocytes' response and killing efficiency to hyphal forms of *Curvularia lunata* in comparison with that to the well-characterized *Aspergillus fumigatus.*

In the present study, *C. lunata* SZMC 23759 and *A. fumigatus* SZMC 23245, both isolated from human eye infection were examined. Release of H_2O_2 from neutrophil granulocytes were measured in the presence and the absence of the supernatant of germinating conidia and after serum treatment. Activation and survival of neutrophils were checked by measuring the myeloperoxidase and LDH release, respectively. After the interaction viability of fungal strains was also measured. Haloperoxidase activity during the infection was gauged as a potential mechanism of fungal defense.

This research was supported by the grants „Lendület" LP2016-8/2016 and GINOP-2.3.2-15-2016-00035. EJT was granted by the UNKP-17-3 New National Excellence Program of the Ministry of Human Capacities.

Supervisors: Tamás Papp, Csaba Vágvölgyi
E-mail: scedobipo@gmail.com